Biophysical and Structural Investigation into the RNA-Binding Properties of TIAR

Henry Sung Il Kim

MSc, Med Sci (University of Auckland, NZ)

Department of Biochemistry and Molecular Biology

Monash University

Melbourne, Australia

This thesis is presented for the degree of Doctor of Philosophy

July 2010

ADDENDUM

(Below are corrections to this thesis made in response to examiners' comments)

p 25 line 7: Add: "A reasonable consistency was observed between the binding affinities of protein-RNA/DNA interactions determined by SPR and those measured by other techniques such as REMSA, UV crosslinking and nitrocellulose filter binding assay. However, differences in affinities between them were also noticed most likely to be due to slight differences in protein constructs and RNA sequences being used (Dember et al., 1996, Park et al., 2000, Katsamba et al., 2002, Suswam et al., 2005, Kim et al., 2007, Fialcowitz_White et al., 2007). Future studies involving direct comparison of a protein-RNA interaction using different methods would be useful ".

p 29 line 7: change from "TIAR12/123 and HuR12" to "TIAR RRM12 (TIAR12), TIAR RRM123 (TIAR123) and HuR RRM12 (HuR12)".

p 31 line 12: Comment: Mass transport limitations are one of the most common problems in kinetic analysis of binding data. This occurs if the rate of transfer of analyte proteins to the surface is significantly slower than the kinetic binding rate thus slowing down both the association and the dissociation phases. This can be avoided or minimized by using high flow rates and low surface densities as we have done in all of our kinetic binding studies. BIAevaluation software (GE Healthcare) can also fit data to models which include mass transport limitations although interpretation of these data needs to be approached more cautiously. More information is available from BIAevaluation Software Handbook (GE Healthcare) and a recent review by Rich and Myszka (Rich and Myszka, 2007).

p 31 line 21: Comment: The quality of every single model-fitted sensorgram presented in this study (and throughout the thesis) has been validated by close examination of the statistical fitting parameter Chi^2 (the closeness of fit between experimental data and the model), standard error for each fitted parameter (sensitivity of the fit to changes in respective parameter) and the shape of the residual plot. An example of the residual plots and Chi^2 values are shown in supplementary figure 1 (chapter 4). As a general guideline, Chi^2 values less than ~10 are acceptable (BIAevaluation Software Handbook, GE Healthcare).

p 36 Table 1: change from "6.02 ± 0.53" to "6.0 ± 0.5", "2.82 ± 0.31" to "2.8 ± 0.3", "15.6 ± 0.74" to "15.6 ± 0.7", "9.01 ± 0.86" to "9.0 ± 0.9", "11.5 ± 1.41" to "11.5 ± 1.4", "27.2 ± 1.02" to "27 ± 1", "36.5 ± 3.56" to "37 ± 4".

p 39 Table 2: change from "6.02 ± 0.53" to "6.0 ± 0.5", "2.82 ± 0.31" to "2.8 ± 0.3", "3.78 ± 0.42" to "3.8 ± 0.4", "65.1 ± 8.14" to "65 ± 8", "1.29 ± 0.1" to "1.3 ± 0.1", "4.41 ± 0.32" to "4.4 ± 0.3", "50.1 ± 4.16" to "50 ± 4".

p 41 Table 3: change from "60.98 ± 0.68" to "61.0 ± 0.7".

p 44 Table 4: change from "33.73 ± 0.50" to "33.7 ± 0.5", "135.2 ± 1.93" to "135.2 ± 1.9", "56.39 ± 0.79" to "56.4 ± 0.8".

p 55: Add at the end of para 1: "It should be noted that Biacore 3000 instrument may still be very useful in early stages of optimization which requires a series of manual testing (injections) of all different variables involved, whereas the more advanced and automated features of Biacore T100 instrument are suitable for more accurate kinetic analysis involving different oligonucleotide ligands and protein analytes to be performed and evaluated efficiently. It should also be pointed out that the kinetics and affinities observed in this study are from isolated and simplified binding events within a SPR flow system. How this occurs in the presence of other specific and / or non-specific elements in different cellular environment is far more complicated and requires further studies both *in vitro* and *in vivo*".

p 56 line 15: Add: "It can be noticed in some cases that the range of concentrations and the RU chosen for data fitting in one binding event are different from the other (lower or higher) even though the K_D values are quite similar to each other. This is perfectly reasonable as K_D is determined from the curves of the sensorgram in the association and dissociation phases. Thus accurate K_D from kinetic data can be achieved as long as there is a sufficient curvature for fitting and the K_D lies preferably within or close to the concentration ranges being used (BIAevaluation Software Handbook, GE Healthcare; Onell and Anderson, 2005)".

p 56: Add at the end of para 2: "The affinities and kinetic parameters obtained from these analyses need to be interpreted carefully and require further investigation".

p 57: para 2: Comment: Previous structural studies involving other RRM-containing proteins and their targets have shown that RRMs can not only interact with their RNA and DNA targets but also interact with themselves and other proteins although specific RRM-RRM contacts between different proteins have not been observed yet (Clery et al., 2008). Thus investigation into TIAR-HuR interactions remains as an exciting prospect given that they are frequently co-expressed in mammalian cells, share similar tissue distribution and RNA specificity, but lead to critically different outcome for the mRNA.

p 85: change from "*Nucleic Acids Research, Submitted May 2010*" to "*Nucleic Acids Research, Accepted Sep. 2010*"

p 104: line 7: Comment: Scattering profiles and their associated parameters (Figure 4) are clear indications of monodispersity of all the samples and there were no signs of heterogeneity and / or multimeric formation. Gel filtration experiment was also conducted to demonstrate the integrity of TIAR12 and its complex formation with the RNA (Supplementary figure 2).

p 119: para 2, line 6: Add: "Park et al. (2000) has shown by SPR and REMSA that isolated RRM1 and RRM2 of HuD protein binds to ARE target with weak micro molar (K_D >100 μM) and milli molar (K_D >1 mM) affinities respectively. However, the combination of RRM1 and 2 dramatically increase the affinity (K_D = 39 nM)".

p 138 Table 2: change from "33.1 ± 1.29" to "33.1 ± 1.3", "506 ± 13.1" to "506 ± 13", "42.5 ± 0.63" to "42.5 ± 0.6".

p 139 Table 3: change from "8.781 ± 0.15" to "8.78 ± 0.15", "4.126 ± 0.031" to "4.13 ± 0.03", "8.657 ± 0.14" to "8.66 ± 0.14", "195 ± 6.3" to "195 ± 6", "1.588 ± 0.47" to "1.6 ± 0.5", "6.319 ± 1.9" to "6.3 ± 1.9".

p 140 Table 4: change from "33.1 ± 1.29" to "33.1 ± 1.3", "2644 ± 82.3" to "2644 ± 82", "21.7 ± 0.38" to "21.7 ± 0.4", "7.80 ± 0.75" to "7.8 ± 0.8", "4.49 ± 0.44" to "4.5 ± 0.4", "3.81 ± 0.74" to "3.8 ± 0.7".

p 157 Table 1: change from "195 ± 6.4" to "195 ± 6".

p 160 Table 2: change from "313.9 ± 2.04" to "314 ± 2", "66.37 ± 2.68" to "66.4 ± 2.7", "7.80 ± 0.75" to "7.8 ± 0.8", "4.49 ± 0.44" to "4.5 ± 0.4", "3.81 ± 0.74" to "3.8 ± 0.7", "7.47 ± 0.33" to "7.5 ± 0.3".

P 170: Add at the end of para 1: "Previous kinetic analysis of a spliceosomal protein U1A binding to its target RNA has led to identification of key residues involved in different phases of binding (Katsamba et al., 2001). Thus, kinetic analyses can provide key insight into the mechanism of action involving dynamic and complex interactions between protein and RNA, therefore more insight into their function".

Table of Contents

Abstract

The RNA-binding protein (RBP) TIAR [related to TIA (T-cell-restricted intracellular antigen)-1] plays a multifunctional role in the regulation of gene expression through binding target mRNA via its RNA recognition motifs (RRMs). TIAR binds to mRNA at AU-rich elements (AREs) in their 3' untranslated regions (UTRs) and is involved in translational repression via the formation of "stress granules", particularly under conditions of cellular stress. TIAR has also been shown to bind to single-stranded DNA (ssDNA) and be involved in splicing. This study aims to better understand the biophysical and structural basis for TIAR binding to its target oligonucleotides.

TIAR has been reported previously to preferentially bind to U-rich sequences. However, a surprising discovery by our collaborators of a cytosine-rich motif targeted by TIAR initiated our investigation of whether TIAR was really capable of binding this C-rich motif. Firstly, we describe the development of a surface plasmon resonance (SPR) protocol for accurate measurements of TIAR-RNA interactions in vitro. The ability of constructs of TIAR, comprising all or some of its 3 RRMs, to bind to the C-rich consensus motif was then verified using the optimized protocol. Through this analysis, TIAR12 and TIAR123 showed low but significant binding to the C-rich sequence which ultimately led to the elucidation of the C-rich motif as a novel TIAR target.

Similar to TIAR, HuR (Hu antigen R) is an RRM-containing ARE-binding protein that is involved in stabilization of the mRNA transcript. It binds to AREs via its RRMs and

with seemingly overlapping specificity with TIAR. Here we show using SPR that TIAR and HuR bind to both U-rich and AU-rich RNA in the nM range, with higher overall affinity for U-rich RNA. However, both proteins show slower dissociation from AU-rich RNA, indicating what may be a truer measure of their binding preference. Differences between TIAR and HuR are observed in their modes of binding to RNA. TIAR is able to bind deoxy-oligonucleotides with nM affinity, whereas HuR affinity is reduced to a μM level. SAXS data for TIAR12/RNA complex are more consistent with a flexible, elongated shape and not the compact shape of HuR12/RNA suggesting that these proteins interact with their targets in fundamentally different ways.

We show using SPR, specific roles of individual TIAR domains for its high affinity binding to oligonucleotide targets. We not only confirm RRM2 as the major binding domain, but also show that the strong affinity binding to U-rich RNA and T-rich DNA only occurs in the presence of RRM1 and the extension region C-terminal to RRM2. On its own, RRM1 shows preferred binding to DNA over RNA. RRM3 makes little contribution to the overall binding affinities to both RNA and DNA targets. We further characterize the interaction between RRM2 with the C-terminal extension and an ARE target using NMR spectroscopy. ^{1}H-^{15}N HSQC titration experiments reveal specific residues involved in RNA binding including those in RNP1, RNP2, beta sheets, and the extension region.

Lastly, we report our attempts at crystallizing TIAR-oligonucleotide complexes. Although crystals for the complex were not obtained from these trials, the efforts serve as a useful guideline for future trials. In summary, the work presented here advances our understanding of biophysical basis for protein-RNA interactions in post-transcriptional gene regulation and provides insight into the mechanism underlying the complex interplay of their interactions leading to different outcomes for the mRNA, and its encoded protein in the cell.

General Declaration

In accordance with Monash University Doctorate Regulation 17/ Doctor of Philosophy and Master of Philosophy (MPhil) regulations the following declarations are made:

I hereby declare that this thesis contains no material which has been accepted for the award of any other degree or diploma at any university or equivalent institution and that, to the best of my knowledge and belief, this thesis contains no material previously published or written by another person, except where due reference is made in the text of the thesis.

This thesis includes 1 original paper published in a peer reviewed journal and 2 unpublished publications. The core theme of the thesis is Biophysical and structural investigation of protein-mRNA interactions involved in post-transcriptional gene regulation. The ideas, development and writing up of all the papers in the thesis were the principal responsibility of myself, the candidate, working within the Department of Biochemistry and Molecular Biology under the supervision of Dr. Jackie Wilce and Assoc. Prof. Matthew Wilce.

The inclusion of co-authors reflects the fact that the work came from active collaboration between researchers and acknowledges input into team-based research.

In the case of chapter 3, 4, and 5 my contribution to the work involved the following:

Thesis chapter	Publication title	Publication status	Nature and extent of candidate's contribution
3	Elucidation of a C-rich signature motif in target mRNAs of RNA-binding protein TIAR	Published	**Co-first author:** Prepared proteins and RNAs required for SPR experiments, developed, optimised, and carried out SPR assays, analysed data, and contributed towards manuscript preparation. **Candidate's contribution: 30 %**
4	Different modes of interaction by TIAR and HuR with target RNA and DNA	Submitted	**Co-first author:** Performed or supervised the preparation of proteins, oligonucleotides, and their complexes used in all experiments, carried out and supervised all SPR experiments and data analysis, designed and assisted in SAXS experiments and analysis, and prepared the manuscript. **Candidate's contribution: 70 %**

| 5 | Characterization of distinct roles of TIAR RRMs and the hinge region in RNA- and DNA-binding using SPR and NMR | In preparation | **First author:** Performed or supervised the preparation of proteins, oligonucleotides, and their complexes used in all experiments, carried out and supervised all SPR experiments and data analysis, designed and assisted in NMR experiments and processing, collated and analysed the NMR data, and prepared the manuscript. **Candidate's contribution: 70 %** |

Signed: …………………………………………………………………

Date: ………………………………

Publications arising from this work

Journal Articles

Kim HS, Kuwano Y, Zhan M, Pullmann R, Jr., Mazan-Mamczarz K, Li H, Kedersha N, Anderson P, Wilce MC, Gorospe M and Wilce JA: Elucidation of a C-rich signature motif in target mRNAs of RNA-binding protein TIAR. Mol Cell Biol 27: 6806-17, 2007

Kim HS, Wilce MC, Yoga YMK, Pendini NR, Gunzburg MJ, Cowieson NP, Wilson GM, Williams BR, Gorospe M, and Wilce JA: Different modes of interaction by TIAR and HuR with target RNA and DNA. Nucleic Acids Research, Submitted 2010

Kim HS, Yoga YMK, Headey S, Scanlon M, Wilce MC, and Wilce JA: Characterization of distinct roles of TIAR RRMs and the hinge region in RNA- and DNA-binding using SPR and NMR. Prepared for publication

Conference Proceedings

H. Kim, K. Mazan-Mamczarz, M. Zhan, M. C.J. Wilce, P. Anderson, M. Gorospe, J. A.Wilce (2007) Identification of a novel mRNA binding motif of the RNA-binding protein TIAR involved in the regulation of translation. *Proc. 32nd Annual Lorne Conf. Protein Structure and Function*, Lorne, VIC. abs #250

H. S. Kim*, Y. Kuwano, M. Zhan, R. Pullmann Jr, K. Mazan-Mamczarz, H. Li, N. Kedersha, P. Anderson, M. C.J. Wilce, M. Gorospe, J. A. Wilce. Elucidation of a C-Rich Signature Motif in Target mRNAs of RNA-Binding Protein TIAR. *Combio2007*, Australia, Pos-TUE-09 *** awardee of a student poster prize**

H. S. Kim, Y. M.K. Yoga, M. C.J. Wilce and J. A. Wilce (2008) A biophysical study of the mRNA binding protein interactions of the translational corepressor TIAR. *Proc. 33rd Annual Lorne Conf. Protein Structure and Function*, Lorne, VIC. abs #338

H. S. Kim, Y. M.K. Yoga, M. C.J. Wilce, J. A. Wilce (2008) Oligonucleotide recognition by the RNA-binding protein TIAR in post-transcriptional regulation of gene expression. *33rd FEBS Congress & 11th IUBMB Conference*, Athens, Greece, abs #PP2A-33

H. S. Kim et al. (2008) Oligonucleotide recognition by the RNA-binding protein TIAR in post-transcriptional regulation of gene expression. *Melbourne Protein Group Meeting*, Melbourne, VIC abs #003 **(student prize awarded for this presentation)**

H. S. Kim, N. P. Cowieson, Y. M.K. Yoga, N. R. Pendini, M. C.J. Wilce, J. A. Wilce (2009) Structural and biophysical investigation into the RNA-binding properties of TIAR. *Proc. 34th Annual Lorne Conf. Protein Structure and Function*, Lorne, VIC. abs #232

H. S. Kim, Y. M.K. Yoga, M. C.J. Wilce, J. A. Wilce (2009) Oligonucleotide recognition by the RNA-binding protein TIAR in post-transcriptional regulation of gene expression. *BDI (Biomolecular Dynamics & Interactions Symposium) 2009 Satellite*, Bio21, Melbourne, VIC. abs #P7

Acknowledgements

I would like to take this opportunity to thank my supervisor Dr. Jackie Wilce for her vision in this project, enthusiasm, support, and kindness. She has inspired and motivated me with her bright ideas and enthusiasm throughout the whole project and my interest and enthusiasm in the project and in the area of research has also grown as the project progressed. I have learned tremendously from her and it was a real joy working with her which I am grateful for. I also would like to thank my co-supervisor Assoc. Prof. Matthew Wilce for all his support, ideas, discussions, and kindness. It was a pleasure working with him too and special thanks for his part in SAXS analysis.

I would like to thank all my past and present friends and colleagues in the Wilce lab for their support, friendship, and kindness. It was fun working with all of you! Special thanks to Nathan Cowieson, Edward Cummings, Menachem Gunzburg, Nicole Pendini, and Yano Yoga for their assistance and contribution to the TIAR project. I also would like to thank our collaborators Paul Anderson, Myriam Gorospe, Stephen Headey, Martin Scanlon, Gerald Wilson and their colleagues for their invaluable assistance, insights, and feedbacks throughout my whole project.

Lastly, I would like to dedicate this work to my parents for their unconditional support, patience, and love.

Abbreviations

2D	two dimensional
ARE	AU-rich element
A-rich	adenine-rich
AUF1	AU-binding factor 1
BD2	binding domain 2
BSA	bovine serum albumin
COX-2	cyclooxygenase-2
C-rich	cytosine-rich
C-terminal	carboxyl-terminal
Dmax	maximum dimension
DNA	deoxyribonucleic acid
DTT	dithiothreitol
E. coli	*Escherichia coli*
EDTA	ethylenediaminetetraacetic acid
EGFP	enhanced green fluorescent protein
ELAV	embryonic lethal, abnormal vision
EOM	ensemble optimization method
fc	flow cell
GM-CSF	granulocyte macrophage colony-stimulating factor
G-rich	guanine-rich
GSH	glutathione

GST   glutathione-S transferase

HEPES   4-(2-hydroxyethyl)-1-piperazineethanesulfonic acid

HNS   HuR nucleocytoplasmic shuttling sequence

HSQC   heteronuclear single quantum coherence

HuR   human antigen R

IFC   integrated micro fluidic cartridge

IL-1β   interleukin 1 beta

IPTG   isopropyl-β-D-thiogalactopyranoside

IRES   internal ribosome entry site

I(s)   scattered intensity

ITC   isothermal titration calorimetry

k_a association rate constant

k_d dissociation rate constant

K_D equilibrium dissociation constant

kDa   kilo Daltons

KSRP   KH-type splicing regulatory protein

mRNA   messenger RNA

μM   micro-molar

MW   molecular weight

nM   nano-molar

NMR   nuclear magnetic resonance

NSD   normalized spatial discrepancy

N-terminal   amino-terminal

OD   optical density

PEG   polyethylene glycol

PMSF   phenylmethylsulfonyl fluoride

$P(r)$ distance distribution function

RBP   RNA-binding protein

REMSA   RNA electrophoretic mobility shift assay

Rg radius of gyration

RI   refractive index

R_{max} maximum analyte binding capacity

RNA   ribonucleic acid

RNP   ribonucleoprotein

RRM   RNA-recognition motif

RU   resonance unit

SA   streptavidin

SAXS   small angle X-ray scattering

SDS-PAGE   sodium dodecyl sulfate polyacrylamide gel electrophoresis

SELEX   systematic evolution of ligands by exponential enrichment

SG   stress granule

SPR   surface plasmon resonance

ssDNA   single-stranded DNA

ssRNA   single-stranded RNA

TIA-1   T-cell restricted intracellular antigen 1

TIAR   TIA-1 related protein

TNFα   tumor necrosis factor alpha

T-rich   thymine-rich

tRNA   transfer RNA

TTP   tristetraprolin

TZF   tandem zinc finger

U2AF65   U2 small nuclear RNA auxiliary factor

U-rich   uracil-rich

UTR   untranslated region

WAXS   wide angle X-ray scattering

ZF   zinc-finger

Literature Review

TIAR and other ARE-binding proteins: Regulators

of mRNA stability and translational efficiency

Overview: Regulation of mRNA translation at the level of mRNA

Protein-RNA interactions are extensively involved in every stage of posttranscriptional gene expression including the splicing, nucleo-cytoplasmic transport, translation and degradation of mRNA (Figure 1). Each of these steps serves as a checkpoint at which the ultimate production of encoded protein can be regulated. Such post-transcriptional events are proving to be of enormous importance in the rapid flux of gene expression in response to signalling events. In particular, the mRNA stability and translational efficiency is regulated so that in vertebrates, mRNA half-lives range from 20 mins to more than 24 hrs (Brennan and Steitz 2001). This results in 1000-fold differences in their cellular abundance, and consequent differences in the amount of gene product that is produced.
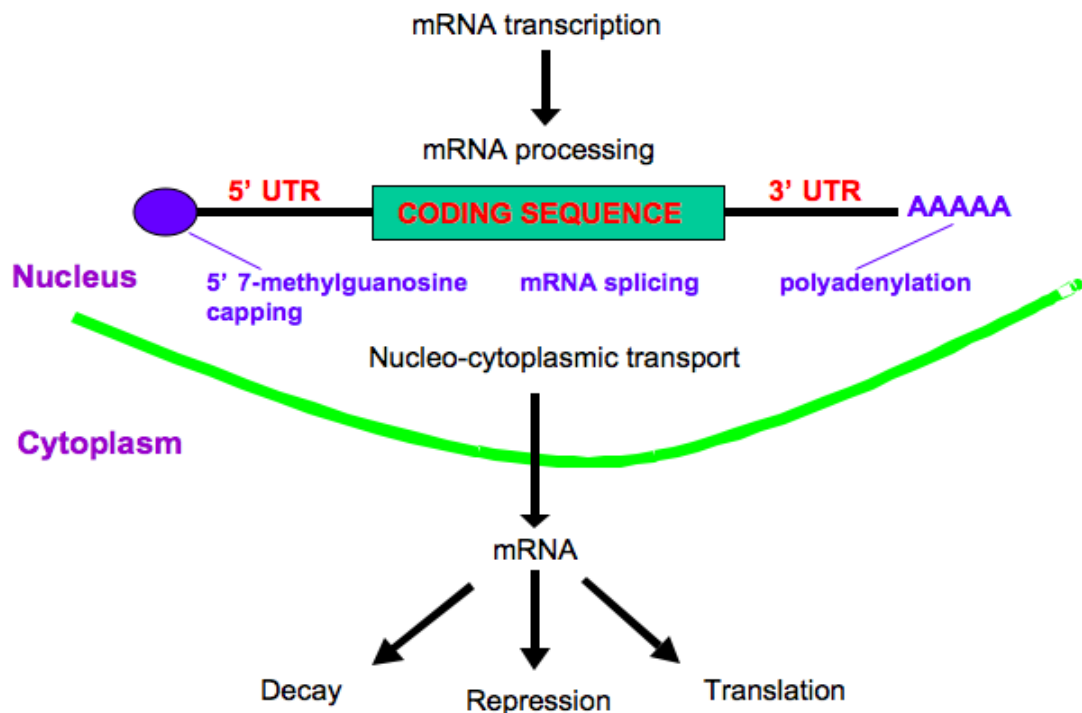
Figure 1. Stages of post-transcriptional gene regulation at which protein-RNA interactions occur. Post-transcriptional events in the lifetime of mRNA in the eukaryotic cell are shown. Each of the events is affected and regulated by protein-RNA interactions (reproduced with permission from JWilce).

Post-transcriptional regulation of gene expression and the occurrence of AREs

The regulation of mRNA stability and translational efficiency is a major control point in gene expression, particularly under conditions of stress, immune response or proliferation (Guhaniyogi and Brewer 2001; Hollams et al. 2002; Ross 1995). Under such conditions mRNA stability and translation are tightly controlled by the association of RNA-binding proteins (RBPs), which specifically recognize elements in the mRNA sequence (Auweter et al. 2006; Guhaniyogi and Brewer 2001; Hollams et al. 2002; Ross 1995; Wilkie et al. 2003). One of the best-characterized regulatory elements, found predominantly in the 3' UTR of mRNA transcripts encoding high turnover proteins such as cytokines, lymphokines, onco-proteins, and inflammatory mediators, are AU-rich elements (AREs) (Barreau et al. 2005; Caput et al. 1986; Chen et al. 1995). AREs are specific regulatory sequences often comprising uridine- or adenine/uridine-rich stretches and have been grouped into three classes, although precise consensus sequences are yet to be clarified (Barreau et al. 2005; Chen et al. 1995). Class I AREs consist of 1-3 copies of scattered AUUUA motifs with a nearby U-rich region. Class II AREs consist of at least two overlapping UUAUUUA (U/A)(U/A) nonamers in a U-rich region and class III AREs, which are less well characterized, have U-rich regions without the AUUUA motif. More than 4000 AREs have been mapped to the human genome, and exist within 5-8% of human genes (Bakheet et al. 2006).

The functional outcomes of recognition of AREs by different RBPs

The presence of an ARE in the mRNA results in the association of specific RBPs. Interestingly, several proteins in eukaryotic cells have been shown to bind to mRNAs

by targeting AREs in their 3' UTR and play a role in regulation of mRNA stability and translational efficiency. Furthermore, their binding can result in quite different outcomes for the mRNAs (Figure 2). RNA-binding proteins TIA-1 (T-cell restricted intracellular antigen-1) and TIAR (TIA-1 related) bind to AREs and function as translational repressors, sequestering target mRNA into stress granules (SG) following cellular stress (Kedersha et al. 2005; Kedersha et al. 1999; Mazan-Mamczarz et al. 2006). In contrast, AUF1 (AU-binding factor 1), TTP (tristetraprolin), and KSRP (KH-type splicing regulatory protein) binding to AREs leads to the rapid decay of the specific mRNAs (Chen et al. 2001; Loflin et al. 1999; Zhang et al. 1993). Alternatively, the HuR (Hu antigen R) protein has a stabilizing effect when it binds to AREs (Brennan and Steitz 2001; Hinman and Lou 2008).
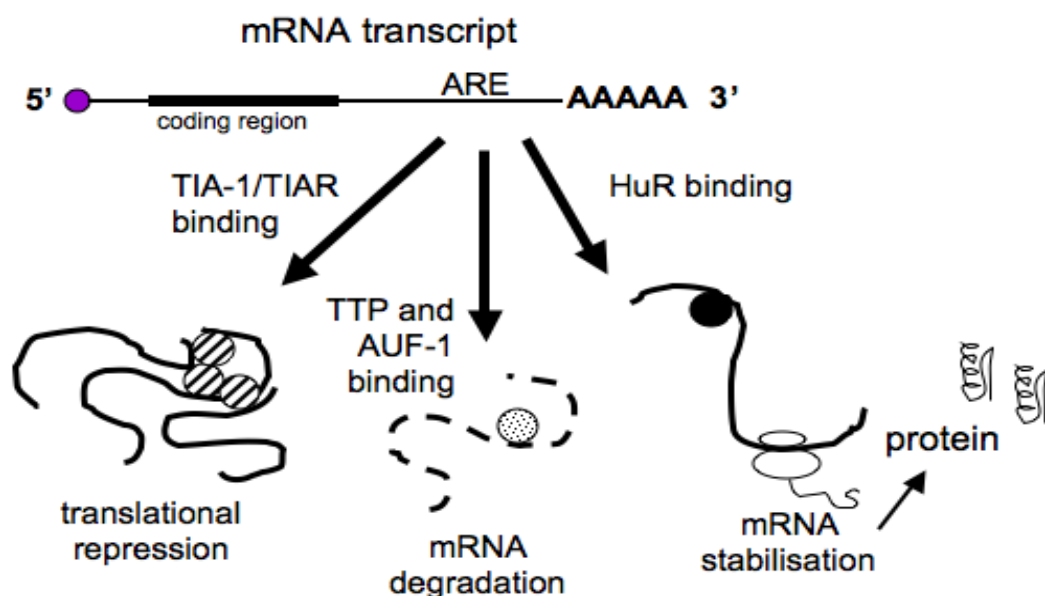
Figure 2. Proteins which bind AREs. mRNA containing AREs are bound by RBPs which dictate whether the mRNA transcript is translationally repressed, degraded, or stabilised (reproduced with permission from JWilce).

But there are also cases where binding by HuR leads to gene silencing and where AUF1 leads to stabilisation of the mRNA transcript (Kim et al. 2009; Liao et al. 2007). In the first case, it is likely to be due to the proximity of the HuR binding site to a miRNA binding site and in the case of AUF1 which includes 4 isoforms (p37, p40, p42, p45), the balance of AUF1 isoform expression seems essential for dictating the fate of at least some ARE-containing mRNAs although the exact mechanism of this is unclear (Lal et al. 2004). Thus AREs appear to be the target of proteins with diverse functions leading to critically different outcomes for the mRNA. The complex interplay of protein-RNA interactions as described here are of particular significance in fine-tuning the innate immune response, for example, where the slightly prolonged expression of inflammatory genes (in the absence of TTP and TIA proteins) leads to chronic inflammation (Phillips et al. 2004). TIAR could prevent the pathological over expression of inflammatory mediators such as TNFα, IL-1β and COX-2 as occurs in rheumatoid arthritis (Phillips et al. 2004).

Classical ARE-BPs: TIAR and HuR

This project involves an in depth investigation of two of the best-characterized ARE-binding proteins, TIAR of the TIA protein family and HuR of the Hu protein family (which includes the neuronal proteins HuB, HuC, and HuD) (Anderson and Kedersha 2002; Brennan and Steitz 2001; Kedersha et al. 1999). These classical RNA-recognition motif (RRM)-containing proteins are ubiquitously expressed in mammalian cells and particularly highly expressed in brain, spleen, thymus, and testes.They bind to several important mRNA targets which requires tight control such as TNF-α and GM-CSF (Beck et al. 1996; Grosset et al. 2004; Gueydan et al.

1999; Lu and Schneider 2004; Masuda et al. 2009; Piecyk et al. 2000). They are both nucleo-cytoplasmic shuttling "multi-functional" proteins performing a variety of roles at different stages of gene expression including splicing, nucleo-cytoplasmic transport, translation and degradation of mRNA (Anderson and Kedersha 2002; Brennan and Steitz 2001; Forch and Valcarcel 2001).

TIA proteins are involved in the control of alternative pre-mRNA splicing, binding to U-rich RNA sequences mostly in introns and promoting the recognition of atypical 5' splice sites (Aznarez et al. 2008; Forch and Valcarcel 2001; Izquierdo and Valcarcel 2007; Le Guiner et al. 2001; Shukla et al. 2004; Zhu et al. 2003). TIAR has also been reported to be able to bind strongly to a single-stranded, but not double-stranded, T-rich DNA which may position TIAR to modulate transcription and help to localise TIAR to U-rich RNA at the time of transcription (Suswam et al. 2005). In the cytoplasm TIA proteins are capable of binding target sequences in the 3'-UTR of mRNA and regulating translation (Anderson and Kedersha 2002; Mazan-Mamczarz et al. 2006). TIAR's glutamine-rich C-terminal region shares sequence similarity to human prion protein (Prusiner 1989). When expressed alone in cells, TIAR forms spontaneous cytoplasmic microaggregates that coaggregate other TIA proteins. It can self-oligomerize in vivo like prion proteins and is thought to be crucial for SG formation when cells are under stress (Eisinger-Mathason et al. 2008; Kedersha et al. 1999). When this occurs, mRNA that is bound by TIA proteins is sequestered into the SGs (Figure 3). It has been proposed that the mRNA remains in this "holding zone" protected from degradation until the stress is relieved and then the mRNA is

either directed towards further translation or degradation (Anderson and Kedersha 2007; Kedersha and Anderson 2002; Kedersha et al. 2005).
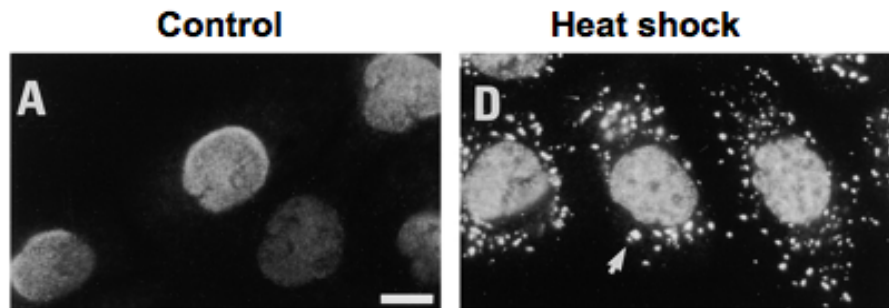
Figure 3. Stress granule formation. TIAR co-localizes at SGs in cytoplasm when cells are under stress (right) whereas it concentrates in the nuclei of unstressed cells (left) (taken from Kedersha et al., 1999).

HuR is a member of the embryonic lethal, abnormal vision (ELAV) family of RBPs. It is best known for its nuclear-cyctoplasmic shuttling and its stabilising effect on many target mRNAs (Brennan and Steitz 2001). HuR can also increase the translation of other associated mRNAs (reviewed by Hinman and Lou, 2008), and repress the translation of other targets via miRNA recruitment (Kim et al. 2009) and by proposed interference with internal ribosome entry sites (IRESs) (Kullmann et al. 2002; Meng et al. 2005; Rivas-Aravena et al. 2009). The fate of the mRNA transcripts is thus very dependent on their interactions with TIAR and/or HuR proteins.

Target specificity of ARE-RBPs

Whether, in fact, these ARE-binding proteins compete for the same mRNA target sites is still not clearly understood. It is conceivable that the same sites are targeted,

and that factors such as the relative local concentration, or activation state of each of these RNA-binding proteins dictate the alternative possible fates of the mRNA transcripts. Liao and colleagues have shown that competitive binding of TIAR and AUF1 determines the translation of the proto-oncogene myc where TIAR represses and AUF1 promotes the mRNA translation via ARE (Liao et al. 2007). Alternatively, the RNA sequence preferences and or RNA-binding modes could differ between these RNA-binding proteins and a more complex interplay of protein-RNA interactions underlies their translational regulation. Indeed, co-immunoprecipitation of ARE-binding proteins and identification of their bound mRNA by microarray has revealed distinctly different populations of target mRNA *in vivo* (Lopez de Silanes et al. 2005; Lopez de Silanes et al. 2004; Mazan-Mamczarz et al. 2009; Mazan-Mamczarz et al. 2006). This is consistent with the existence of distinct binding preferences rather than simple competition for the same pool of ARE-bearing mRNA transcripts. Gorospe and colleagues have proposed different consensus sequences for each of TIAR, TIA-1, HuR, and AUF1 (Lopez de Silanes et al. 2005; Lopez de Silanes et al. 2004; Mazan-Mamczarz et al. 2009; Mazan-Mamczarz et al. 2006) and demonstrated cases where these proteins bind at overlapping as well as distinct places on the same mRNA transcript and together modulate translation (Kawai et al. 2006; Lal et al. 2004). In some cases these proteins have even been shown to interact with non-ARE consensus sequences and it was shown that HuR and TIA-1 binding motifs are U-rich rather than AU-rich (Lopez de Silanes et al. 2005; Lopez de Silanes et al. 2004). Therefore, it is likely that ARE-binding proteins interact with their target RNA sequences with differences in their modes of binding, degree of stringency or even specificity underlying the ultimate fate of the mRNA transcript.

Comparison of ARE recognition by different ARE-BPs

Structural Biology of RBPs - The RBPs that are the subject of this review are all multi-domain proteins of between 306-375 residues in size. They interact with specific sequences of single-stranded RNA (ssRNA) belonging to ARE and single-stranded DNA (ssDNA) in some cases via their RNA-binding domains. These include the RNA-recognition motif (RRM) and the zinc-finger (ZF) (Figure 4).

(E) RRM
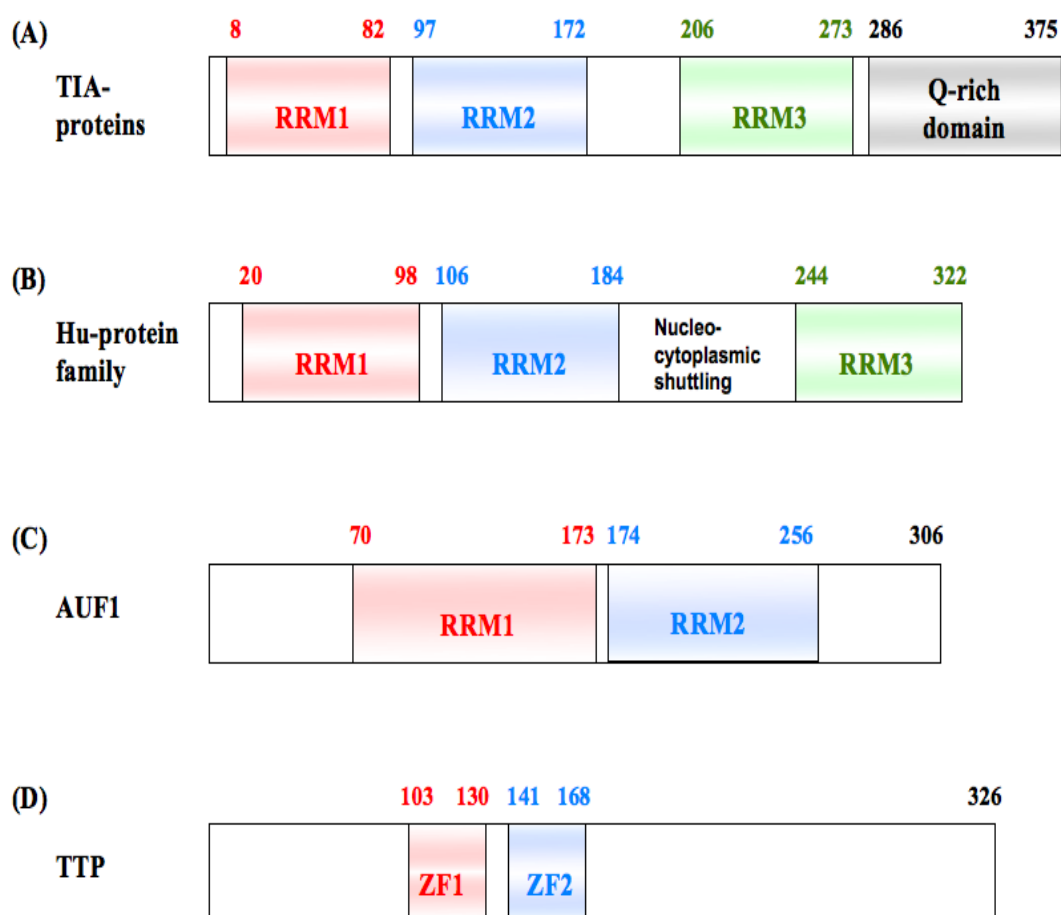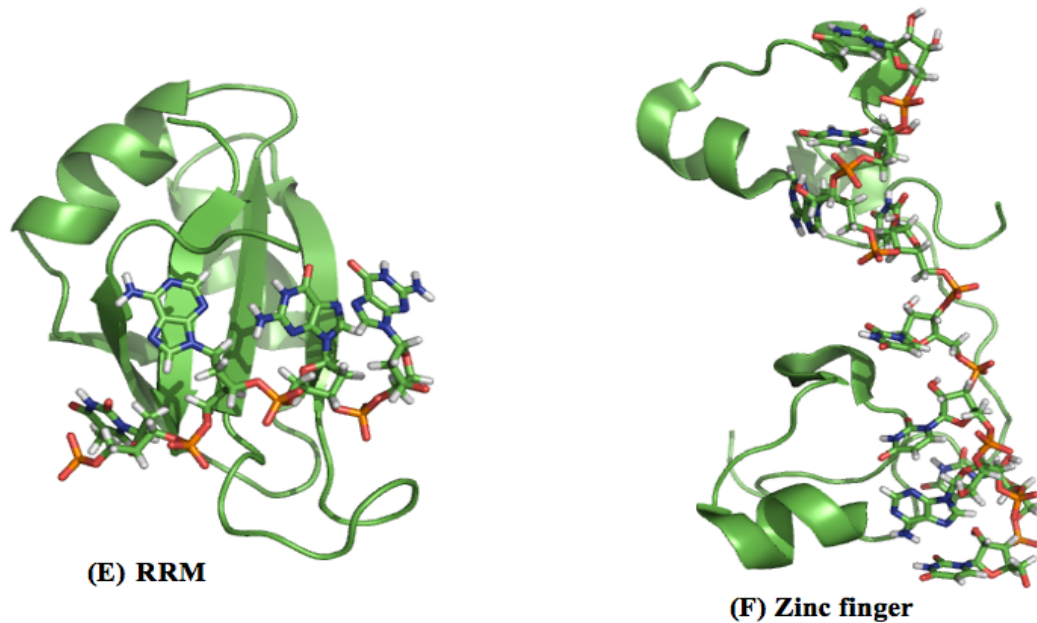
(F) Zinc finger

Figure 4. RRM and zinc-finger motifs of mRNA binding proteins. (A, B, C) A schematic representation of RRM structures of TIAR, HuR, and AUF1 proteins showing RRM1 (red), RRM2 (blue), hinge region involved in nucleocytoplasmic shuttling (HuR), RRM3 (green), and a glutamine-rich C-terminal region (TIAR): RNA/DNA recognition occurs against the surface of the four-stranded β-sheet through stacking, electrostatic, and hydrogen bonding. (D) TZF Domain structure of TTP showing ZF1 (red) and ZF2 (blue): RNA binding occurs via hydrophobic binding pockets formed by aromatic side chains with the help of specific hydrogen bonding. (E) RRM β-sheet interaction with the ssDNA: AUF1 RRM2 (BD2) in complex with telomere DNA (5'-TAGG-3') (Enokizono et al. 2005). PDB ID: 1WTB (F) TZF domains ZF1 and 2 of TIS11d protein in complex with ARE (5'-UUAUUUAUU-3') (Hudson et al. 2004). PDB ID: 1RGO. The RNA-binding domains are shown as cartoons and ssRNA/DNA shown as sticks. The image was generated from PyMOL (Abbreviations: BD2-binding domain 2; TZF-tandem zinc finger).

Each of these types of domains is utilized widely in the human genome for interacting with RNA and DNA (Chen and Varani 2005). The general structural architecture of each class is well described, and has been adapted through evolution for recognizing quite distinct oligonucleotide sequences (Auweter et al. 2006; Clery et al. 2008). The rules for RBP-RNA/DNA recognition, however, are only just beginning to be teased out. For instance, a RRM, which is about 70-90 amino acids

long, consists of four-stranded β-sheet packed against two α-helices with β1α1β2β3α2β4 topology. It has been observed that the RRM, for which fifteen complexes with RNA or DNA are reported, specifically recognizes between two and eight single-stranded nucleotides against the surface of its four-stranded beta sheet. Most RRMs contain three conserved aromatic residues found within the ribonucleoprotein (RNP) consensus domains known as RNP1 and RNP2 of β3 and β1 strand respectively that accommodate two bound nucleotides via ring-stacking interactions and a network of specific hydrogen bonds that dictate molecular specificity. Zinc-fingers, for which four are solved with ssRNA, are small domains (often a three-helical bundle) held together via coordination of zinc. They utilize aromatic interactions as a primary driving force for binding, reinforced by specific hydrogen bonding networks. Importantly, each of these motifs interacts with a linearly structured stretch of RNA, suggesting that RNA secondary structure motifs are not a factor in their molecular recognition. These interactions are summarized in recent reviews (Auweter et al. 2006; Clery et al. 2008).

Multiple domains of RBPs confer additional binding affinity and specificity - The presence of multiple RNA-binding domains increases the potential for RBP specificity, with each domain capable of recognizing the same or distinct consensus sequences. Structural studies conducted for TTP binding to an UUAUUUAUU consensus ARE sequence showed that each of the two zinc-fingers bound an adjacent 5'-UAUU-3' sequence with high specificity (Hudson et al. 2004). In some cases the multiple domains appear to add to the overall affinity of the protein, whilst not necessarily adding to the specificity of the interaction. TIA-1 and TIAR proteins

appear to recognize U-rich sequences via their second RRM with the first and third RRMs contributing towards the overall affinity of the interaction (Dember et al. 1996). Interestingly however, the first RRM of TIAR also confers additional DNA binding specificity by interacting with T-rich ssDNA sequences (Suswam et al. 2005). And HuD (a homologue of HuR) can bind AREs via its first two RRMs, with the third RRM enhancing the overall affinity of the interaction (Park et al. 2000; Wang and Tanaka Hall 2001).

The RNA-binding by these proteins is not always limited to their RNA-binding domains. More recent studies are showing deviations from the classic mode of binding where the hinge region between RRMs, the loops between secondary structure components, or the C-terminal extension of the RRM also contributes significantly towards RNA-binding specificity and affinity (Fialcowitz-White et al. 2007; Kuwasako et al. 2008; Maris et al. 2005).

Translational repressor

TIAR (T-cell restricted intracellular antigen-1 related protein)

TIAR is a 375-amino acid protein belonging to the RRM containing family of RNA-binding proteins (Figure 5). It contains 3 RRMs which share high sequence homology with TIA-1 (RRM1: 79%, RRM2: 92%, RRM3: 91%) and a glutamine-rich carboxyl terminal region which shares 51% homology with TIA-1. Longer isoforms (TIARa and TIA-1a) created by alternative splicing of exon 5 also exist for both TIAR and TIA-1 (Beck et al. 1996) and it was shown that the relative expression of TIAR and TIA-1 isoforms varies in different tissues and cell lines

suggesting distinct functional properties and regulatory mechanisms underlying the

isoform expression (Izquierdo and Valcarcel 2007).
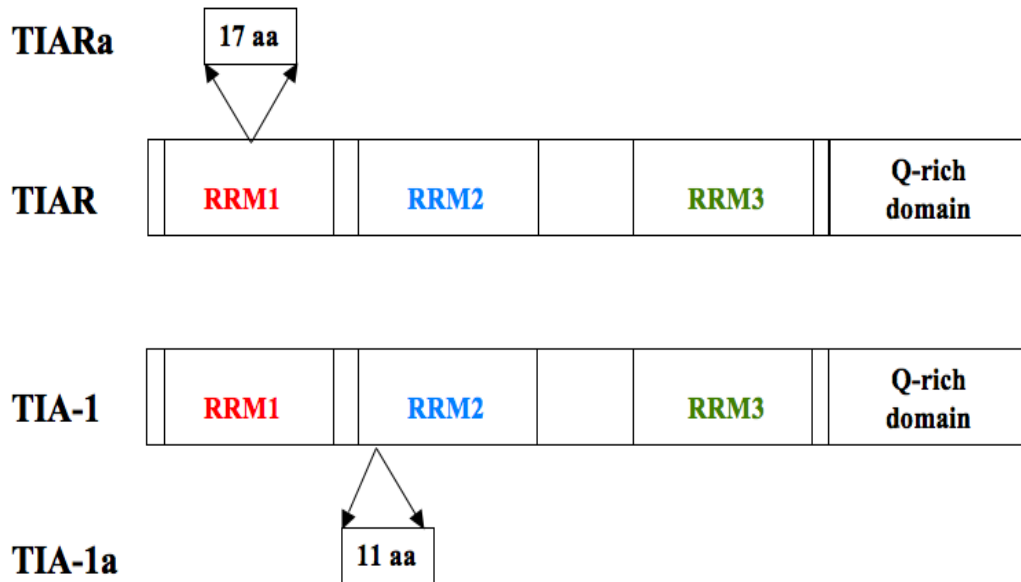
Figure 5. Domain structure of human TIAR and TIA-1 proteins. RRM1, 2, 3, and a glutamine-rich region of TIA-proteins are shown. Longer isoforms (TIARa and TIA-1a) created by alternative splicing are also shown.

SELEX studies by Dember and colleagues showed that TIAR protein preferentially

binds to U-rich sequences (Dember et al. 1996). The three RRMs of TIAR confer

high affinity binding to U-rich RNA sequences with each contributing variously to

the interaction (overall $K_D \sim 20$ nM), while the C-terminal 90-amino acid residue

glutamine-rich sequence is essential for stress-granule formation (Dember et al.

1996; Kedersha et al. 1999; Lopez de Silanes et al. 2005; Tian et al. 1991).

Nitrocellulose filter binding assays were used to show that RRM2 is both sufficient

and necessary for binding to AREs and RRM3 showed binding to RNA but may

have other specificities than AREs. RRM1 showed no binding to U-rich sequences

on its own, although slightly higher affinity by TIAR12 ($K_D = 40$ nM) than by

TIAR2 alone (K_D = 50 nM) was measured suggesting that RRM1 may contribute towards ARE-binding (Dember et al. 1996). Later studies, however, involving affinity measurements using a UV-cross-linking method by Suswam et al. (2005) revealed that TIAR RRM1 bound T-rich ssDNA with significant affinity (K_D = 43 nM) suggesting that the primary role of RRM1 is to interact with DNA. They also showed that TIAR bound T-rich DNA with higher affinity (K_{Dapp} = 1.6 nM) than U-rich RNA (K_{Dapp} = 9.4 nM) (Suswam et al. 2005).

No structural information for TIAR/RNA complexes is yet available, though structures of the individual TIAR RRMs have been elucidated using NMR (PDB ID: 1x4g, He et al., 2005; PDB ID: 2dh7, Imai et al., 2006; PDB ID: 2cqi, Suzuki et al., 2005; Nagai et al., 1990). NMR structures of TIAR RRMs together with the details of amino acid sequence, secondary structure, and RNP motifs of the main RNA-binding domain RRM2 are shown in figure 6. They all share canonical RRM folds of βαββαβ topology although the level of primary sequence homology among themselves is low (< 30 %).
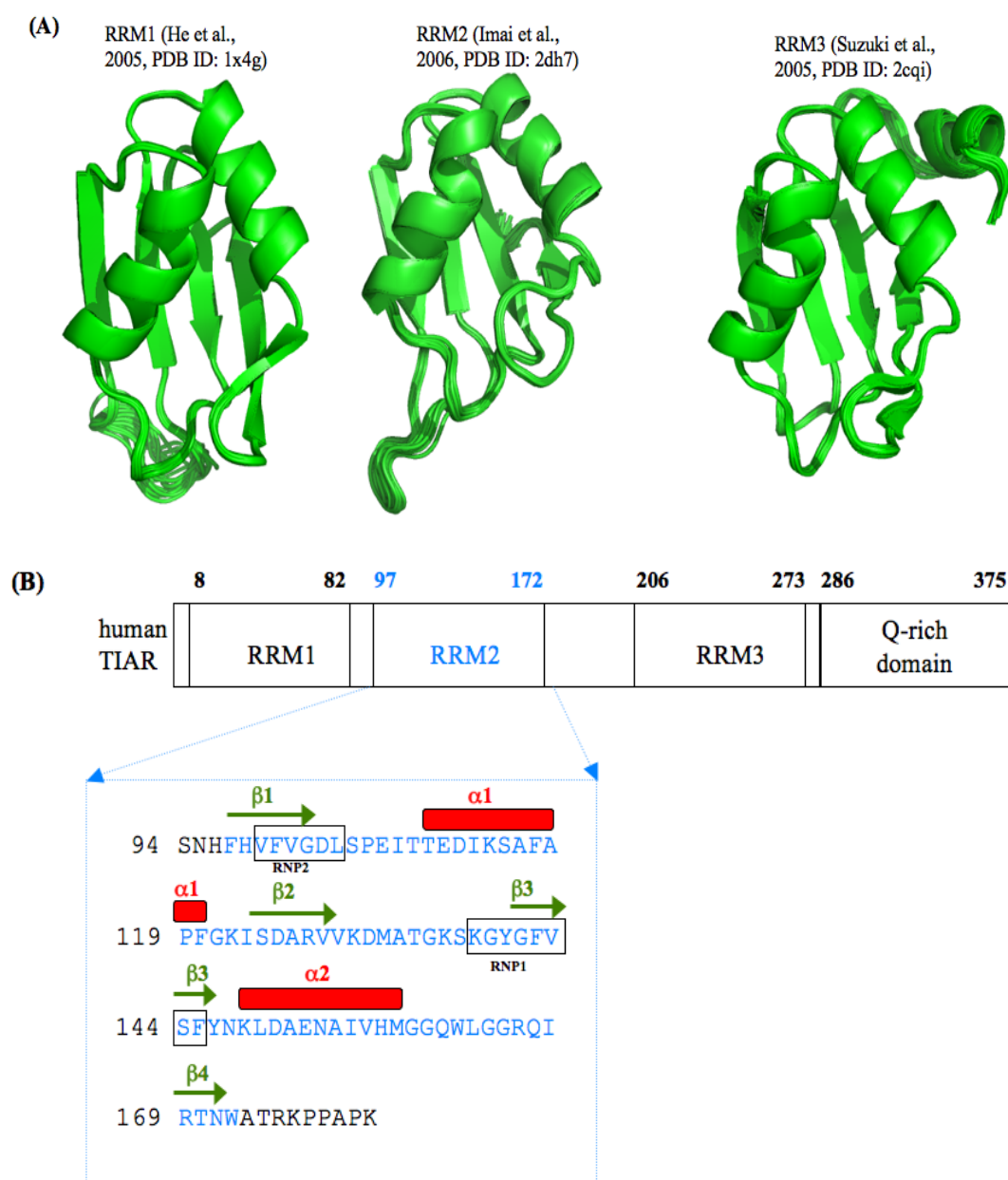
Figure 6. Structures of the human TIAR RRMs showing βαββαβ topology. (A) NMR structures of human TIAR RRMs are shown as cartoons. The images were created using PyMOL. (B) Domain structure of TIAR with the RRM2 (aa 94-181) highlighted and inserted in blue. Secondary structure elements are indicated above the amino acid sequence and the RNP1 and RNP2 are boxed and labelled below the sequence.

The structure of the TIA-1 RRM2 has also been solved by both NMR and x-ray crystallography which showed the canonical RRM fold ($\beta\alpha\beta\beta\alpha\beta$ topology) and its mode of interaction with the target RNA has been investigated (Kumar et al. 2008; Kuwasako et al. 2008). Chemical shift perturbation analyses with pentamer U-rich RNA (5'-UUUUU-3') revealed that most of the β-sheet surface, including those within or adjacent to conserved RNP consensus motifs and β4 C-terminal extension, is involved in the RNA binding. The key amino acid residues perturbed by this binding are also conserved and involved in RNA-binding by other RRM-containing protein such as U2AF65 suggesting that they may have similar modes of interaction (Kuwasako et al. 2008).

mRNA stabiliser

HuR (Hu-antigen R)

The primary structures of the Hu-proteins are well-conserved (RRMs share >70% amino acid sequence identity among family members) and are arranged with two RRMs near the N-terminus, followed by a less conserved basic hinge region and a third RRM near the C-terminus (Hinman and Lou 2008; Ma et al. 1996). This arrangement of three RRM domains is strikingly similar to that seen in the TIA proteins and also confers high-affinity binding to ARE sequences ($K_D \sim$ 1-2 nM) (Fialcowitz-White et al. 2007; Park et al. 2000), although there is less than 30% sequence homology overall and less than 35% homology between any TIA-protein RRM compared to Hu-protein RRM. HuR is predominantly nuclear and it shuttles between nucleus and cytoplasm through the HNS (HuR Nucleocytoplasmic shuttling sequence) found within the hinge region between RRM2 and RRM3 (Fan and Steitz

1998a, b; Keene 1999). In the case of HuD, an *in vitro* selection experiment and gel shift assay by Park-Lee et al. (2003) showed that it preferentially binds a U-rich motif (Park-Lee et al. 2003). HuD shares 80% sequence homology with HuR RRMs and the relative roles of the three RRMs for ARE interactions have been interrogated. RRM1 is essential for RNA-binding, but the high-affinity interaction also requires RRM2 and RRM3 (Park et al. 2000). Kinetic analysis also revealed that the RRM3 as well as the hinge region between RRM2 and RRM3 which shares much less sequence homology (56%) with HuR affect the stability of its ARE binding as the dissociation rate constants (k_d) increase significantly in their absence (Park et al. 2000; Park-Lee et al. 2003). The crystal structures of the first 2 RRMs of HuD protein bound to 11-nt single stranded RNA derived from c-fos (class I ARE: 5'-AUUUUUAUUUU-3') and TNF-α (class II ARE: 5'-UUAUUUAUUUA-3') mRNA transcripts have been reported, providing insight into the mode of interaction of these domains with classical AREs (Figure 7) (Wang and Tanaka Hall 2001). And it is the β-sheet which provides the contact residue surface for binding to specific RNA sequences. It can be seen that the RNA fits into the cleft formed between the β-sheets of the two domains.
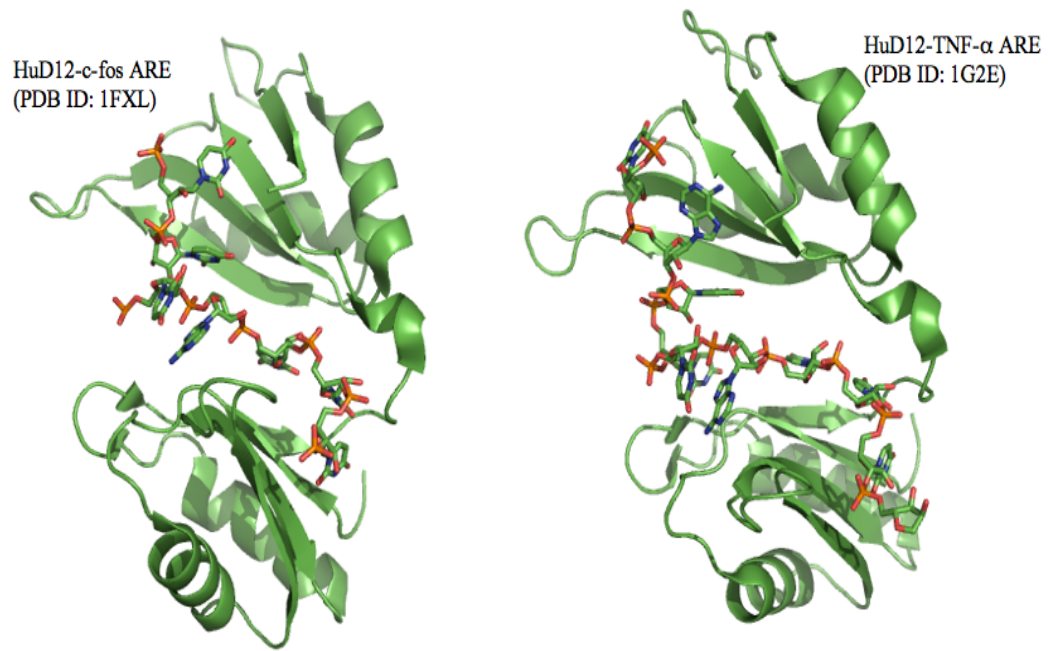
Figure 7. Structures of the HuD12-ARE complexes showing that the target RNAs are sandwiched between the β-sheets of the two RRMs. Schematic representation of the RRM1 and 2 of the HuD protein in complex with c-fos ARE (left) (5'-AUUUUUAUUUU-3') and TNF-α ARE (right) (5'-UUAUUUAUUUA-3'). PDB ID: 1FXL, 1G2E. The RNA-binding domains are shown as cartoons and RNA shown as sticks. The image was generated from PyMOL.

Interestingly, in the case of HuR, the RRM3 as well as the hinge region between RRM2 and RRM3 contribute significantly to ARE-binding in a length-dependent manner by helping to form multimeric HuR-ARE complexes and increasing the RNA-binding affinity respectively (Fialcowitz-White et al. 2007). RRM3 of Hu-proteins has also been suggested to bind to the poly (A) tails of mRNA sequences and contribute towards their stability, or be involved in protein-protein interactions (Beckel-Mitchener et al. 2002; Kasashima et al. 2002; Ma et al. 1997).

Research aims

In this project, we will investigate the interaction of TIAR with target RNA that results in translational repression of target mRNA transcripts. This interaction will be compared to the potentially competing interaction by HuR, which is involved in mRNA transcript stabilization. These interactions are highly significant in understanding the post-transcriptional regulation of high-turnover proteins such as TNF-α involved in the innate immune response. Whilst the downstream effects of many RBPs have been elucidated, there is still little understanding of which mRNA sequences they will selectively bind under particular physiological circumstances. A better understanding of their mRNA targets, their consensus binding sequences, affinity and kinetics of their binding to different target sequences, and the structural features underlying their molecular recognition is required for describing, and potentially predicting, mRNA translational control.

This project is to understand the biophysical and structural basis for RBPs binding to their target oligonucleotides, with a focus on TIAR-ARE interactions that underlie the regulation of mRNA translation. The specific aims of this project are:

1. To develop and optimize a surface plasmon resonance (SPR) system using Biacore instruments investigating the interactions of TIAR and HuR proteins with their target RNA motifs. The optimized system will allow detailed kinetic and affinity analyses of their binding events to be performed.

2. To verify the binding of TIAR RRM domains to a newly discovered C-rich

motif and the kinetic and affinity analysis of their interactions *in vitro* using the optimized SPR system. The detailed kinetic and affinity analyses of their binding events may ultimately lead towards the elucidation of the C-rich signature motif as a novel TIAR target.

3. To directly compare different modes of interaction by TIAR and HuR with target RNA and DNA. This will involve: i) investigation of the binding of TIAR and HuR to an AU-rich motif (class I ARE) compared to the U-rich motif (class III ARE) using SPR. ii) investigation of their ability to bind to DNA compared with RNA and deoxy-U-rich oligonucleotides using SPR. iii) investigation of the potential mode of interaction between these RNA-binding proteins and their target RNA sequences in solution using Small Angle X- ray Scattering (SAXS).

4. To characterize the distinct roles of TIAR RRMs and the hinge region in RNA- and DNA-binding. This will involve: i) Investigation of the binding of separate TIAR domains to a U-rich motif (class III ARE) using SPR. ii) Investigation of the roles of different TIAR domains in DNA-binding compared with RNA using SPR. iii) Identification of the specific TIAR amino acid residues involved in ARE-binding in solution using NMR spectroscopy.

5. To crystallize TIAR in complex with its RNA targets suitable for x-ray crystallographic structure determination. This may lead us to determination of

the molecular structural basis for binding affinity and specificity of TIAR for

its target RNA sequences.

We hypothesize that this study will greatly expand our understanding of the protein-

RNA interactions in post-transcriptional regulation of gene expression and how the

complex interplay of their interactions may underlie critically different outcomes for

the mRNA, and its encoded protein in the cell.

Kinetic and affinity analysis of protein-RNA interactions: Application of Surface Plasmon Resonance (SPR)

Abstract

Multifunctional RNA-binding protein (RBP) TIAR (T-cell restricted intracellular antigen-1-related protein) is an AU-rich element (ARE)-binding protein which acts as a translational repressor when cells are under stress. TIAR proteins have been reported previously to preferentially bind to U-rich sequences. However, a recent in vivo study by our collaborators involving co-immunoprecipitation of TIAR-mRNA RNP (ribonucleoprotein) complexes followed by extraction and identification of the bound mRNA transcripts by microarray led to the discovery of a non-ARE consensus element targeted by TIAR which was predominantly C-rich. The question arose as to whether TIAR was really capable of binding this C-rich motif. Here, we describe the development and optimisation process of surface plasmon resonance (SPR) system using Biacore instruments and demonstrate how the use of instrument (T100), buffer components (tRNA and BSA), and usage of flow cells (pairwise flow cell connections) led to stable, consistent, and accurate measurements of TIAR-RNA interactions *in vitro*. The optimised system was then used for accurate kinetics and affinity measurements of TIAR interacting with its RNA targets which ultimately led to the elucidation of the C-rich motif as a novel TIAR target (Kim et al., 2007 and Chapter 3).

Introduction

TIAR proteins have been reported previously to preferentially bind the U-rich sequences with nanomolar affinities (K_D = 8 nM) (Dember et al. 1996). Surprisingly however, when our collaborators, Gorospe and colleagues, performed co-immunoprecipitation of TIAR-mRNA complexes and identified the bound mRNA by microarray, bioinformatic analysis revealed a distinctly different non-ARE consensus sequence for TIAR. The elucidated common motif present among TIAR-targeted mRNA transcripts was a predominantly cytosine-rich 28-nt long element (Kim et al. 2007). This unexpected finding prompted us to investigate the relative binding affinity and kinetics of TIAR to U-rich RNA compared with the new C-rich motif *in vitro* using a Biacore SPR system.

There are several specialised *in vitro* systems which have been widely applied in studies involving protein-RNA interactions including SPR (surface plasmon resonance), REMSA (RNA electrophoretic mobility shift assay), and ITC (isothermal titration calorimetry). SPR allows intermolecular interactions to be measured in real time within a controlled flow system. It is highly sensitive, being able to measure strong interactions with equilibrium dissociation constants (K_D) ranging between 100 mM ~ 1 pM, only requires small amount of label-free molecules (as little as few ng of RNA and a few µg of protein would be sufficient to measure high affinity protein-RNA interactions), and can provide accurate kinetics as well as affinity information about the binding (Katsamba et al. 2002). REMSA has been used extensively in both qualitative and quantitative measurements of protein-RNA interactions using label-free and labelled

materials respectively. It can provide detailed equilibrium but not kinetic information about the binding within a stationary environment (Hellman and Fried 2007). Thirdly, ITC can provide detailed thermodynamics and equilibrium information about the protein-RNA interactions within a stationary environment (Velazquez-Campoy et al. 2004), although it consumes more materials than required for SPR (µg ~ mg quantity compared to ng ~ µg quantity of label-free molecules as in SPR) and provides no information on kinetics of their binding. Here, an SPR system (Biacore, GE Healthcare Bio-Sciences AB) was applied to be able to obtain detailed kinetics as well as the affinity information about the binding events involving TIAR and its RNA targets in direct comparison with another ARE-binding protein HuR and its targets. HuR is also a multifunctional protein involved in stabilisation of mRNA transcripts and it was used here as a positive control for binding U-rich RNA and negative control for binding C-rich RNA (Brennan and Steitz 2001; Hinman and Lou 2008).

SPR is a physical phenomenon which can be applied to measure bio-molecular interactions and has been used in some instances in studies involving protein-RNA/DNA interactions (Katsamba et al. 2001; Katsamba et al. 2002; Park et al. 2000; Park-Lee et al. 2003). There are several companies producing SPR-based biosensors and Biacore (GE Healthcare Bio-Sciences AB) was the first to produce a commercially available SPR instrument and still is the most widely used commercially available SPR instrument (Myszka 1997, 1999a, b, 2000; Myszka et al. 1998; Rich and Myszka, 2000, 2003, 2005, 2007a, 2008). The basic principle of the system involves a prism on one side of the

transduction surface covered with a thin gold film (50 - 100 nm) and a flow channel on

the other (non-illuminated) side of the surface (Figure 1).
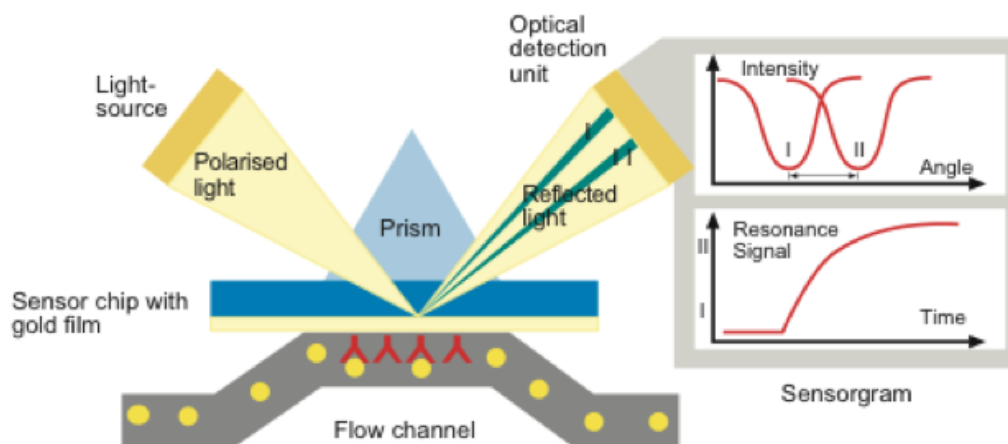
Figure 1. The basic principles of the Biacore system used in our studies of protein-RNA interactions. The system involves a prism on one side of the surface covered with a thin gold film and a flow channel on the other side of the surface. As the light enters the prism it gets reflected over a wide range of incident angles and the intensity of the reflected light is then measured against the incident angle by the optical detection unit. However at one particular angle, the light gets absorbed into the sensor chip surface as plasmons which propagate into the medium in the form of evanescent waves. There are several factors which can influence the angle at which this occurs with RI of the materials in the flow channel close to the surface being one of them. The adsorption of molecules on the sensor chip surface as well as the molecular interactions near the surface lead to change in RI, thus shift in the resonance angle (I to II). This angular change is expressed in RU in a sensorgram (taken from Biacore Technology Brochure, GE Healthcare Bio-Sciences AB).

As the plane polarised light from the light source enters the prism it gets reflected over a

wide range of incident angles and the intensity of the reflected light is then measured

against the incident light angle by the optical detection unit. However at one particular

angle, the light gets absorbed into the sensor chip surface causing a drop in the intensity

of the reflected light. Resonance of surface plasmons is observed at this incidence as the

plasmons propagate into the medium in the form of evanescent waves. There are several factors which can influence the reflection angle at which this occurs with refractive index (RI) of the materials in the flow channel close to the surface (within ~200 nm) being one of them. The adsorption of molecules on the sensor chip surface as well as the molecular interactions near the surface lead to change in RI, thus shift in the resonance angle. This angular change is expressed in resonance unit (RU), which is directly proportional to the change in mass near the surface (Karlsson 2004).

The basic set up of the Biacore sensor chip surface optimised for this study involves immobilisation of the biotinylated RNA molecules onto the streptavidin coated sensor chip surface (SA chip, Biacore) (Figure 2). As the analyte molecules (proteins) injected into the flow system reach the sensor chip surface, the binding occurs leading to a change in the RI of the materials close to the surface, which in turn results in the change in the reflection angle of the incident light. This change is detected by the optical detection unit and gets displayed as sensorgrams (RU vs. time) in the Biacore control software, which can then be used for kinetics or affinity analysis of their interactions (Katsamba et al. 2002) (Figure 3). The sensitivity of SPR allows very small amounts of materials (~pg / mm^2) to be detected on the sensor chip surface.
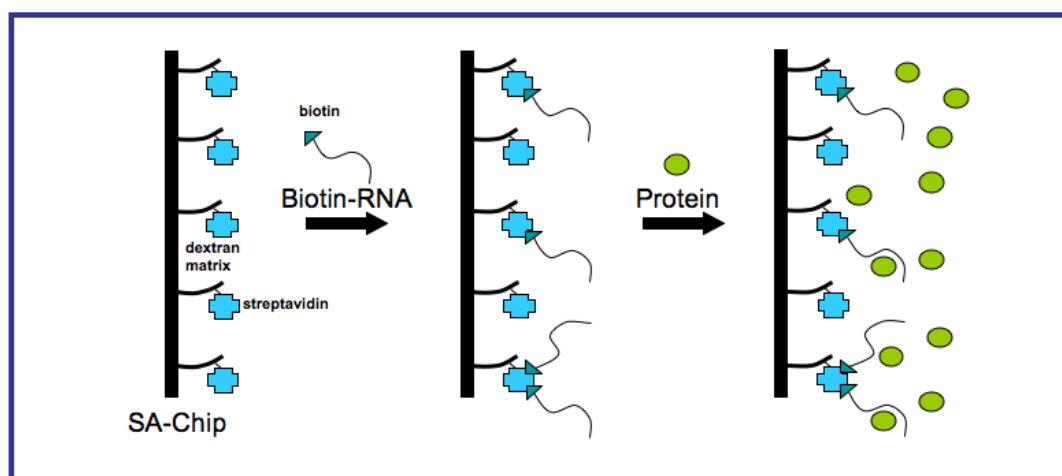
5'-Bi-GGGGGGUUUUUUUUUUUUUUUUUGGGGG-3' (U-rich RNA)

5'-Bi-UUGCCACCUCCUGCUCCUGCCCAGACAG-3' (C-rich RNA)

Figure 2. Protein-RNA interactions at the sensor chip surface. Biotinylated RNA (28mer U-rich and C-rich) was immobilized onto SA-coated sensor chip surface and analyte proteins HuR and TIAR were injected into buffer at a constant flow rate. As the proteins reached the RNA surface, binding occurred leading to refractive index change, which was recorded and displayed as sensorgrams (modified with permission from JWilce).
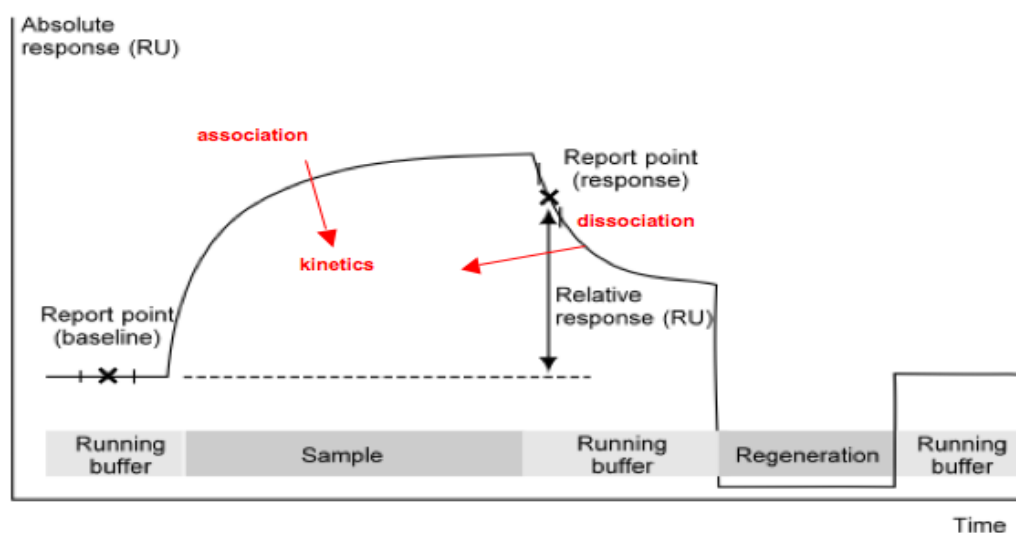
Figure 3. The sensorgram. An illustration of the sensorgram showing different phases of the binding event: the association and dissociation followed by regeneration of the surface to remove any remaining analytes and bring the response back to baseline (modified from Biacore Sensor Surface Handbook, GE Healthcare Bio-Sciences AB).

Despite the basic principle and design of the SPR system being relatively simple, successful SPR experiments and analyses require optimisation of several parameters (Katsamba et al. 2002; Rich and Myszka 2007b, 2008). These include choosing the right instrument (Biacore T100 vs. Biacore 3000), buffer components (+/- tRNA and BSA), and flow cells (pair wise vs. serial run). Here, we show the optimisation process of each of these parameters in developing a system for investigating the interactions of TIAR12/123 and HuR12 proteins with U- and C-rich RNA motifs. The detailed kinetic and affinity analyses of their binding events ultimately contributed towards elucidating the C-rich signature motif as a novel TIAR target (Kim et al., 2007).

Materials and Methods

Plasmid Construction and Protein Purification

Constructs for TIAR RRM123 (residues 1–283) and TIAR RRM12 (residues 1–208) (Dember et al., 1996) were expressed in *E. coli* strain BL21 (DE3). The culture was grown till the desired OD_{600} of ~0.8 was reached, induced with IPTG (0.5 mM) for 2.5 ~ 3 hours and the cells were harvested by centrifugation. The cell pellets were stored at -80 °C overnight, thawed out on ice, and resuspended in lysis buffer (50 mM Tris pH 8.0, 150 mM NaCl, 1 mM EDTA, 1 % Triton X-100, 5 % Glycerol, 1 mM DTT, 0.1 mM PMSF). Cells were lysed by gentle sonication and debris was removed by centrifugation at $15,000 \times g$ for an hour. Supernatant was then incubated with washed glutathione (GSH)-Sepharose beads (GE Healthcare) with gentle mixing at 4 °C for 4~16 hours. After the beads were washed with wash buffer (50 mM Tris pH 8.0, 150 mM NaCl, 1 %

Triton X-100, 5 % Glycerol) for four times or more, the TIAR proteins were cleaved

from the GSH beads by incubating them with thrombin at 4 °C for 16-20 hours and

cleavage confirmed by SDS-PAGE analysis. TIAR123 protein was also treated with

protamine sulfate to remove any bacterial nucleic acid contaminants (evident from

$OD_{260/280}$ ratio). HuR RRM12 (residues 18–184) was cloned into pGEX-4T1, expressed

in *E. coli* BL21 (DE3), and purified according to previously established protocols (Yeap

et al. 2002). The proteins were further purified by size-exclusion and cation-exchange

chromatography. The purified proteins were then dialyzed into the HEPES buffer (10

mM HEPES, pH 7.4, 150 mM NaCl) and concentrated to a final concentration of ~200

μM. The concentration of each protein was determined using the Bradford assay

(BioRad) and by A_{280} measurements using theoretical molar extinction coefficients

(ProtParam). The extinction coefficients were validated for folded protein; A_{280}

measurements were within 10% of measurements made in 6.0 M guanidium

hydrochloride. The purity of each protein was confirmed by SDS–PAGE.

Biosensor Experiments

The dynamics of RNA-protein interactions were characterized by SPR using Biacore

T100 and 3000 instruments (GE Healthcare Bio-Sciences AB). The basic principle of

the sensor surface used in this study is illustrated in Figure 2. The RNA used in the

analyses was: The U-rich RNA [containing poly (U) stretches; 5'-

GGGGGGUUUUUUUUUUUUUUUUUGGGGG-3'] and C-rich RNA (5'-

UUGCCACCUCCUGCUCCUGCCCAGACAG-3'). The RNA was chemically

synthesized carrying a 5'-biotin tag (Dharmacon Research) to facilitate immobilisation of the RNA onto streptavidin-coated sensor chips (SA chip for 3000 and Series S Sensor Chip SA for T100, GE Healthcare Bio-Sciences AB). RNA were diluted to a final concentration of 1 μM in HBS buffer (10 mM HEPES, pH 7.4, 150 mM NaCl) followed by heating at 80 $^{\circ}$C for 10 min, and cooling to room temperature to minimize secondary structure formation. The sample was then diluted 500-fold in running buffer [10 mM HEPES, pH 7.4, 150 mM NaCl, +/- tRNA (125 μg/ml), +/- BSA (62.5 μg/ml), 1 mM DTT, 0.025% surfactant P20; GE Healthcare Bio-Sciences AB] and injected over the sensor chip surface at 10 μl/min at 25 $^{\circ}$C to generate a ~50 response unit (RU) RNA surface (for a low-density surface to maximize simple 1:1 binding events and minimize any mass transport effects where the observed rate of binding is limited by mass transfer). Proteins were serially diluted in running buffer to the concentrations indicated in Figures 5-8 and 11-15, and injected at 25 $^{\circ}$C at a flow rate of 30 or 50 μl/min for 2-3 min. Surface regeneration to remove any protein that remained bound after 3-6 min of dissociation was achieved using a 1 min injection of 2 M NaCl at 20 or 50 μl/min. Analyses of protein concentrations were conducted in duplicate and any background signal from a streptavidin-only reference flow cell was subtracted from every data set. Data were analysed using a simple 1:1 Langmuir interaction model using the Biacore 3000 or T100 evaluation software (GE Healthcare Bio-Sciences AB) to determine the kinetics (association and dissociation rate constants; k_a and k_d) as well as the affinities (K_D) of the protein-RNA interactions.

Results

Choosing the right instrument and buffer components are necessary for the accurate measurements of protein-RNA interactions using SPR.

There are several commonly used Biacore instruments (Biacore X, 1000, 2000, 3000, T100, A100) which can be applied to study detailed kinetics and affinity of protein-RNA interactions (Rich and Myszka 2000, 2007a, b), and Biacore 3000 and T100 were chosen as they were available at the time of this study. They are similar SPR instruments although Biacore 3000 is older and one of the most commonly used Biacore instruments, whereas Biacore T100 is a more recently released model and designed to be more automated, advanced in its liquid handling system, stable and more sensitive - thus ideal for detailed kinetic analysis of systems with small amounts of sample. The four key components of both instruments are the optical detection system (Figure 1) responsible for generating and detecting SPR signals, the IFC (integrated micro fluidic cartridge), the liquid handling system responsible for delivery and precise injections of proteins and buffers to the sensor chip surface, and the sensor chip where molecular interactions occur. The IFC of both instruments have 4 different flow cells (fc1234) over which buffer and proteins can be injected in single, pairwise (fc12/fc34), or serial runs. This could potentially allow maximum of 3 different ligand molecules to be analysed at the same time, with the fourth flow cell as a reference cell (This is described in more detail below). More information on the instruments can be obtained from the manufacturer's instrument handbook (GE Healthcare Bio-Sciences AB).

In optimising the SPR system for accurate measurements of protein-RNA interactions, it is critical to minimise any non-specific interactions and keep the system simple and robust so that the interactions can be best estimated by a simple binding model (Katsamba et al. 2002). Non-specific interactions can often be minimised by adjusting buffer conditions and using blocking agents tRNA and BSA in the running buffer to minimise non-specific binding (Katsamba et al. 2001; Park et al. 2000; Park-Lee et al. 2003). Here we closely examined and compared the effects of the SPR instruments (Biacore 3000 vs. T100) and the presence or absence of blocking agents (tRNA and BSA) in the running buffer on the SPR signals involving protein-RNA interactions.

Biacore 3000

Experiments were conducted to investigate the protein-RNA interactions involving HuR12, TIAR12, and TIAR123 proteins (Figure 4), prepared as described previously (see Materials and Methods) with U-rich (class III ARE) and newly discovered C-rich RNA sequences (Kim et al. 2007) using the method modified from Katsamba et al. (Katsamba et al. 2002) (Figure 5).
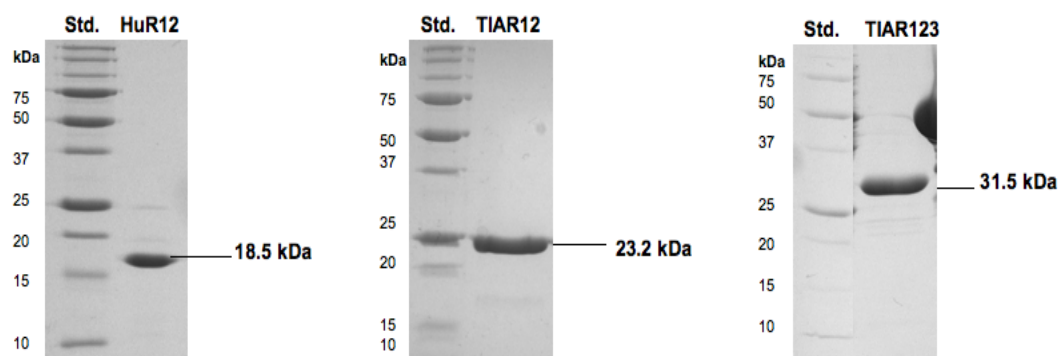
Figure 4. Recombinant proteins used in in vitro binding assays. The construction of plasmids to express recombinant proteins comprising RRM1 and RRM2 or all three RRMs (HuR12, TIAR123, and TIAR12) was previously described (Dember et al., 1996). Proteins were expressed in bacteria and purified to homogeneity (details in Materials and Methods). Std., protein standard, with molecular mass (kDa) indicated

Here we used the Biacore 3000 as our SPR instrument of choice and commonly used blocking agents, tRNA and BSA were included in the standard running buffer to block or minimize any non-specific interactions. The 6 sensorgrams (Figure 5A and 5B) show the binding of a range of concentrations of TIAR123, TIAR12, and HuR12 proteins when injected across the U- or C-rich RNA-coated chip. The association rate constants (k_a), dissociation rate constants (k_d), and overall affinities (K_D) for each protein, as approximated by a simple 1:1 Langmuir binding model, are shown in Table 1.

A U-rich: GGGGGGUUUUUUUUUUUUUUUUUUUGGGGG

B C-rich: UUGCCACCUCCUGCUCCUGCCCAGACAG

Figure 5. Kinetic analysis of the interactions of TIAR12, TIAR123, and HuR12 proteins with U-rich and C-rich RNAs (Biacore 3000). The binding of TIAR123, TIAR12, and HuR12 to a U-rich or a C-rich RNA (28-mer each) is shown. Biotinylated RNA was captured on SA-coated sensor chips and increasing concentrations of protein were injected over the surface. Injections were performed for 120 seconds (association phase), followed by a 180-second flow of running buffer to assess dissociation. The experiments were conducted in duplicate and showed good overlap. The black lines represent the binding responses for injections of protein analyte at specified concentrations (nM) over the RNA surface. The kinetic data was fit by 1:1 Langmuir binding model which describes monovalent analyte binding to a single site on the immobilized ligand. Mass transport effects were not evident. The red curves superimposed on top of the sensorgrams represent the model fitted curves. The rate constant k_a and k_d were determined simultaneously as global fitting parameters from which the K_D was determined. The resulting parameter values are given in Table 1.

Protein	RNA	k_a (1/Ms)	k_d (1/s)	K_D (k_d/k_a, nM)
HuR12	U-rich	$(6.02 \pm 0.53) \times 10^7$	0.17 ± 0.004	2.82 ± 0.31
TIAR123	U-rich	$(7.96 \pm 0.12) \times 10^4$	$(1.24 \pm 0.04) \times 10^{-3}$	15.6 ± 0.74
	C-rich	$(7.82 \pm 0.21) \times 10^4$	$(9.01 \pm 0.86) \times 10^{-4}$	11.5 ± 1.41
TIAR12	U-rich	$(1.12 \pm 0.02) \times 10^5$	$(3.04 \pm 0.06) \times 10^{-3}$	27.2 ± 1.02
	C-rich	$(7.4 \pm 0.23) \times 10^4$	$(2.71 \pm 0.18) \times 10^{-3}$	36.5 ± 3.56

Table 1. Kinetic and affinity constants for the interactions of TIAR123, TIAR12, and HuR12 proteins with U-rich and C-rich RNAs (Biacore 3000). The association and dissociation rate constants (k_a and k_d) were determined as global fitting parameters for a 1:1 binding model. The equilibrium dissociation constant K_D was determined as k_d/k_a.

All 3 proteins bound U-rich RNA with nanomolar affinities, in agreement with the previous findings (Dember et al. 1996; Park et al. 2000). HuR12 however bound with the highest affinity showing both fast association and dissociation rate constants and TIAR proteins showed different kinetics with a lower overall affinity and slower association and dissociation rate constants than HuR12 reflecting a potentially different mode of binding between them. HuR12 showed no binding to C-rich RNA, consistent with its specificity for the ARE targets and proving that there were no non-specific interactions for HuR12 in the SPR system. In contrast, TIAR proteins showed some interactions with the C-rich RNA although at much lower level. Overall however, the signals of these interactions were not very stable and were noisy at times (Figure 5). This was particularly a problem for detecting low RU events and low concentration ranges as it became difficult to distinguish between background noise and the true

binding event. The level of responses for TIAR12 or TIAR123 binding C-rich RNA was very low (~10 RU or lower) and noisy indicating that there was very little detectable binding. HuR12 binding U-rich RNA seems to reach steady state but there is a slight trend in the response during the steady state where the response fluctuates up and down indicating surface instability. Thus it was difficult to fit these data to a binding model and evaluate accurate kinetics from them. Separate kinetic analyses where the association and dissociation phases are fit separately, were also implemented for TIAR binding U- and C-rich RNA in order to improve the accuracy of fitting. This can be useful if there is a problem with one of the phases or if there are inconsistencies between two phases (manufacturer's Biaevaluation software handbook, GE Healthcare Bio-Sciences AB) (Figure 6 – see two separate red fitted lines for each sensorgram).
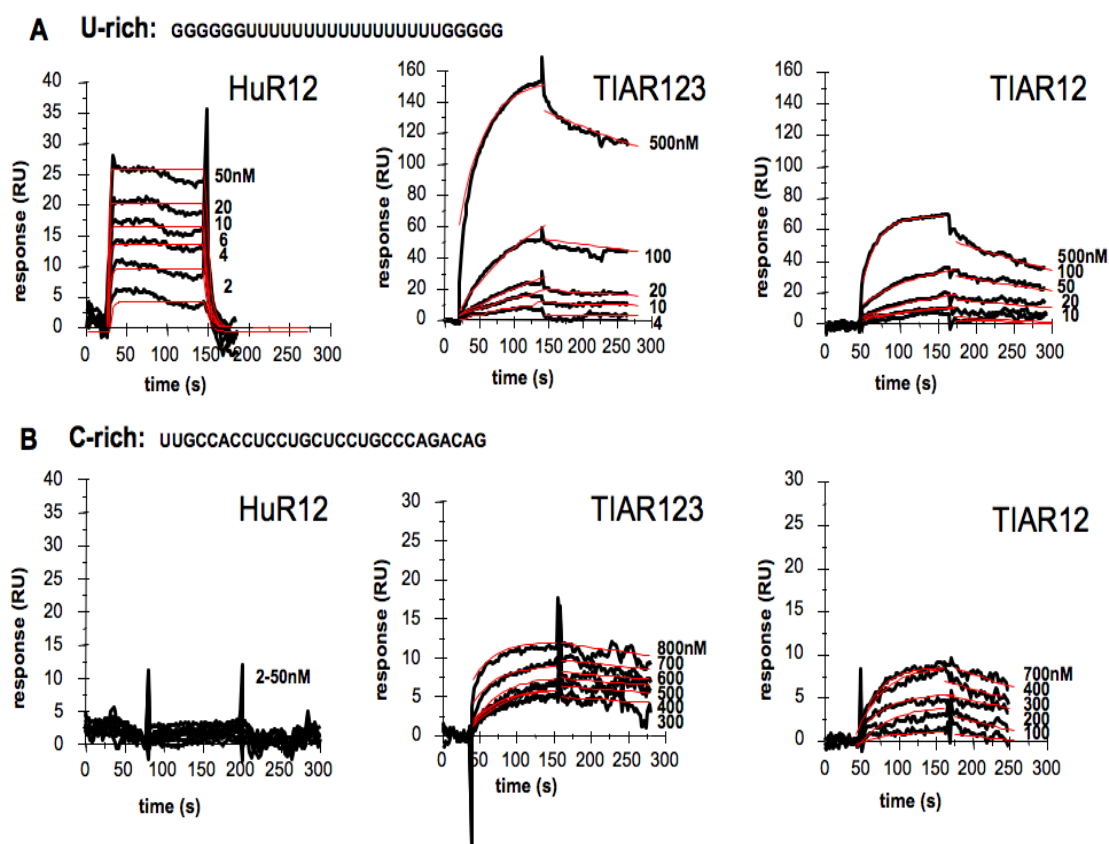
Figure 6. Kinetic analysis of the interactions of TIAR12, TIAR123, and HuR12 proteins with U-rich and C-rich RNAs (Biacore 3000). The same binding as in Figure 5 of TIAR123, TIAR12, and HuR12 to a U-rich or a C-rich RNA is shown. The kinetic data was fit by 1:1 Langmuir binding model. The rate constant k_a and k_d however were determined as separate global fitting parameters from which the K_D was determined. The resulting parameter values are given in Table 2.

The overall K_D values estimated from separate kinetics were generally quite similar (within an order of magnitude) to those obtained from the simultaneous kinetic analyses (Tables 1 and 2) except for the TIAR123 and TIAR12 binding C-rich RNA which were much higher (K_D of ~400 and 1700 nM compared to ~12 and 37 nM for TIAR123 and TIAR12 respectively) in the case of separate kinetics due to estimation of faster

dissociation rate constants. Overall, our confidence in the accuracy of these results was not sufficient to publish the data.

Protein	RNA	k_a (1/Ms)	k_d (1/s)	K_D (k_d/k_a, nM)
HuR12	U-rich	$(6.02 \pm 0.53) \times 10^7$	0.17 ± 0.004	2.82 ± 0.31
TIAR123	U-rich	$(5.81 \pm 0.08) \times 10^4$	$(3.78 \pm 0.42) \times 10^{-3}$	65.1 ± 8.14
	C-rich	$(3.25 \pm 0.16) \times 10^4$	$(1.29 \pm 0.1) \times 10^{-2}$	398 ± 72
TIAR12	U-rich	$(8.79 \pm 0.09) \times 10^4$	$(4.41 \pm 0.32) \times 10^{-3}$	50.1 ± 4.16
	C-rich	$(1.47 \pm 0.17) \times 10^4$	$(2.51 \pm 0.12) \times 10^{-2}$	1710 ± 280

Table 2. Kinetic and affinity constants for the interactions of TIAR123, TIAR12, and HuR12 proteins with U-rich and C-rich RNAs (Biacore 3000). k_a and k_d were determined as separate phases for a 1:1 binding model. K_D was determined as k_d/k_a.

Biacore T100 (+ tRNA and BSA)

In an attempt to improve the stability of SPR signals and minimize the background noise in the system, above experiments involving HuR12, TIAR12, and TIAR123 proteins and U- and C-rich RNA sequences were repeated, but using a different and more advanced SPR instrument Biacore T100 which was launched by Biacore AB in 2005 and became available to us in the department in 2007. Blocking agents, tRNA and BSA were again included in the system. The 6 sensorgrams (Figure 7A and 7B) show the binding of a range of concentrations of TIAR123, TIAR12, and HuR12 when injected across the U- or C-rich RNA-coated chip. k_a, k_d, and K_D for each protein, as approximated by a simple 1:1 Langmuir binding model, are shown in Table 3.

A   U-rich: GGGGGGUUUUUUUUUUUUUUUUUUGGGGG

HuR12 — TIAR123 — TIAR12

B   C-rich: UUGCCACCUCCUGCUCCUGCCCAGACAG

HuR12 — TIAR123 — TIAR12

Figure 7. Kinetic analysis of the interactions of TIAR12, TIAR123, and HuR12 proteins with U-rich and C-rich RNAs (Biacore T100; +tRNA/BSA). The binding of TIAR123, TIAR12, and HuR12 to a U-rich or a C-rich RNA is shown. Injections were performed for 120 seconds (association phase), followed by a 300-second flow of running buffer to assess dissociation. The experiments were conducted in duplicate and showed good overlap. The red lines represent the binding responses for injections of protein analyte at specified concentrations (nM) over the RNA surface. The kinetic data was fit by 1:1 Langmuir binding model. Mass transport effects were not evident. The black curves superimposed on top of the sensorgrams represent the model fitted curves. The rate constant k_a and k_d were determined simultaneously as global fitting parameters from which the K_D was determined. The resulting parameter values are given in Table 3.

Protein	RNA	k_a (1/Ms)	k_d (1/s)	K_D (k_d/k_a, nM)
HuR12	U-rich	$(8.92 \pm 0.05) \times 10^5$	$(5.44 \pm 0.03) \times 10^{-2}$	60.98 ± 0.68
TIAR123	U-rich	$(2.36 \pm 0.003) \times 10^4$	$(7.57 \pm 0.05) \times 10^{-4}$	32.06 ± 0.25
TIAR12	U-rich	$(1.25 \pm 0.005) \times 10^5$	$(1.13 \pm 0.003) \times 10^{-3}$	9 ± 0.06

Table 3. Kinetic and affinity constants for the interactions of TIAR123, TIAR12, and HuR12 proteins with U-rich RNA (Biacore T100; +tRNA/BSA). k_a and k_d were determined as global fitting parameters for a 1:1 binding model. K_D was determined as k_d/k_a.

The change to a more sensitive SPR instrument T100 immediately led to considerable improvements in SPR signals. The background noise, especially, was significantly reduced which resulted in much cleaner signals overall (Figure 7). This in turn made it possible for more accurate measurements of the binding, thus better fitting of the data to the simple 1:1 Langmuir binding model especially for lower level responses. All 3 proteins showed strong nanomolar affinity binding to the U-rich RNA with HuR12 showing both fast association and dissociation rate constants and TIAR proteins showing different kinetics with slower association and dissociation rate constants than HuR12 again indicating a potentially different mode of binding between them as shown previously by using the Biacore 3000 instrument (Figure 5A). However, none of the proteins showed any binding (up to ~1 µM concentrations of the protein) to the C-rich RNA motif (Figure 7B), whereas a low level of responses although with noisy signals had been observed between TIAR proteins and the C-rich RNA when Biacore 3000 was

used (Figure 5B). This was unexpected and the reason for the inconsistency between the two systems is not clear although it is a possible indication of complications in the experimental design and/or non-specific nature of the binding observed when Biacore 3000 was used.

Biacore T100 (- tRNA and BSA)

Finally, having established a stable system (Biacore T100) for looking at protein-RNA interactions, the same set of experiments as above was conducted but this time in the absence of blocking agents, tRNA and BSA in the running buffer. It was possible that these blocking agents were saturating the system to the extent that they were outcompeting physiologically relevant protein-RNA interactions. The 6 sensorgrams (Figure 8A and 8B) show the binding of a range of concentrations of TIAR123, TIAR12, and HuR12 when injected across the U- or C-rich RNA-coated chip (Kim et al. 2007). k_a, k_d, and K_D for each protein, as approximated by a simple 1:1 Langmuir binding model, are shown in Table 4 (Kim et al. 2007).

Figure 8. Kinetic analysis of the interactions of TIAR12, TIAR123, and HuR12 proteins with U-rich and C-rich RNAs (Biacore T100; -tRNA/BSA; Kim et al., 2007). The same binding as described in Figure 7, between TIAR123, TIAR12, and HuR12 proteins and a U-rich or a C-rich RNA is shown but in the absence of the blocking agents (tRNA and BSA). The experiments were conducted in duplicate and showed good overlap. The kinetic data was fit by 1:1 Langmuir binding model. Mass transport effects were not evident. The black curves superimposed on top of the sensorgrams represent the model fitted curves. k_a and k_d were determined simultaneously as global fitting parameters from which the K_D was determined. The resulting parameter values are given in Table 4.

Protein	RNA	k_a (1/Ms)	k_d (1/s)	K_D (k_d/k_a, nM)
HuR12	U-rich	$(1.29 \pm 0.01) \times 10^8$	4.35 ± 0.03	33.73 ± 0.50
TIAR123	U-rich	$(1.58 \pm 0.02) \times 10^6$	$(1.56 \pm 0.01) \times 10^{-3}$	0.99 ± 0.02
	C-rich	$(2.72 \pm 0.03) \times 10^4$	$(36.78 \pm 0.12) \times 10^{-4}$	135.2 ± 1.93
TIAR12	U-rich	$(4.10 \pm 0.11) \times 10^6$	$(2.83 \pm 0.08) \times 10^{-3}$	0.69 ± 0.04
	C-rich	$(3.48 \pm 0.04) \times 10^4$	$(19.64 \pm 0.06) \times 10^{-4}$	56.39 ± 0.79

Table 4. Kinetic and affinity constants for the interactions of TIAR123, TIAR12, and HuR12 proteins with U- and C-rich RNA (Biacore T100; -tRNA/BSA; Kim et al., 2007). k_a and k_d were determined as global fitting parameters for a 1:1 binding model. K_D was determined as k_d/k_a.

A significant increase in RNA binding (for both U- and C-rich RNA) was observed for TIAR proteins but not as much for HuR12 protein compared to the binding observed in the presence of tRNA and BSA (Figure 7; Figure 8). The apparent affinity (K_D) increased by ~2-fold in the case of HuR12-U-rich RNA binding and up to ~30-fold in the case of TIAR-U-rich RNA binding when the blocking agents were excluded from the system (Table 3; Table 4). More interestingly, nanomolar affinity binding was detected between TIAR proteins and C-rich RNA which was not evident in the presence of the blocking agents. The binding events observed here in the absence of tRNA and BSA are stable, concentration-dependent, reproducible, and consistent with the previous findings (Dember et al. 1996; Park et al. 2000). HuR12 showed no binding to C-rich RNA target with or without tRNA and BSA confirming that there is no background interaction in the system. The fact that tRNA was able to interfere significantly with TIAR123 and

TIAR12 binding their target RNAs on the sensor chip surface suggested that TIAR binding is very promiscuous. It did not necessarily indicate that TIAR binding to the C-rich sequence was not physiologically relevant. In fact, later *in vivo* experiments showed that the C-rich sequence is, in fact, physiologically relevent (Kim et al. 2007). Thus, all future experiments were conducted in the absence of BSA and tRNA in the running buffer in order to achieve a simple, robust, and reproducible system to study 1:1 interactions involving RBPs (TIAR and HuR) and their RNA targets. No background interaction was observed between any proteins and the blank sensor chip surface (SA chip, GE Healthcare Bio-Sciences AB).

Biacore T100 flow cells are optimised to be used in pairs (fc2-1 or fc4-3) for kinetic studies involving protein-RNA interactions.

The IFC is one of the key components of the Biacore T100 and consists of 4 inter-connected micro flow channels which form flow cells when the sensor chip is docked onto its surface (Figure 9). It allows the flowing buffer or analyte proteins to flow into designated flow cell(s) in single (fc1, 2, 3, 4), pairwise (fc2-1or fc4-3) with fc2 or 4 as ligand surfaces and fc1 or 3 as reference cells, or in parallel (fc1234) allowing maximum of 3 ligands to be analysed at the same time on fc2, 3, and 4, with fc1 as a reference cell at specified and constant flow rates (Figure 10) (Biacore Sensor Surface Handbook, GE Healthcare Bio-Sciences AB).
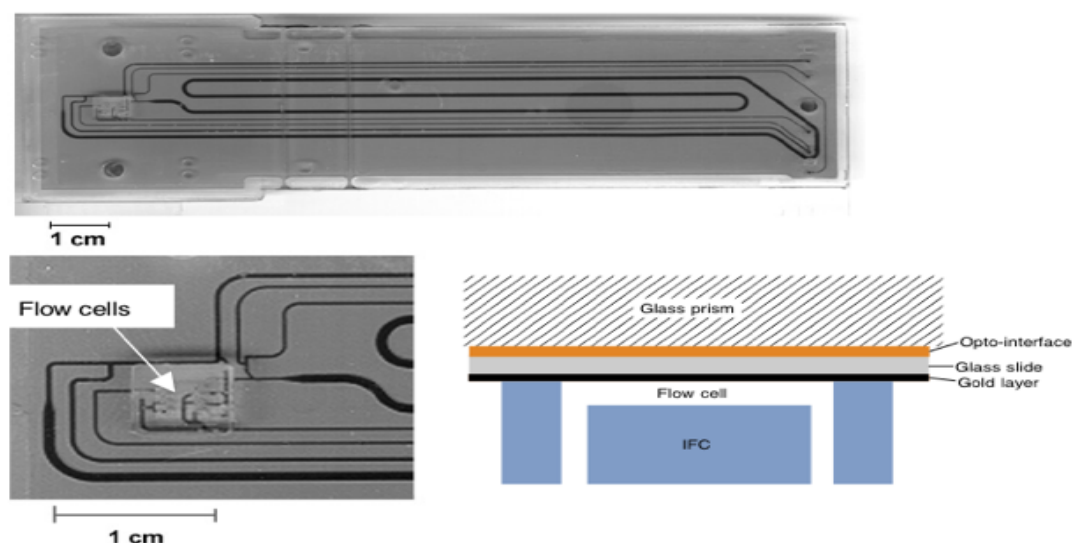
Figure 9. The microfluidic system. Top: Picture of the IFC used in the Biacore instrument. Bottom left: Close up of the flow cell block on the IFC which the sensor chip surface gets docked onto. Bottom right: Schematic representation of the sectional view through the flow cell (taken from Biacore Sensor Surface Handbook, GE Healthcare Bio-Sciences AB).
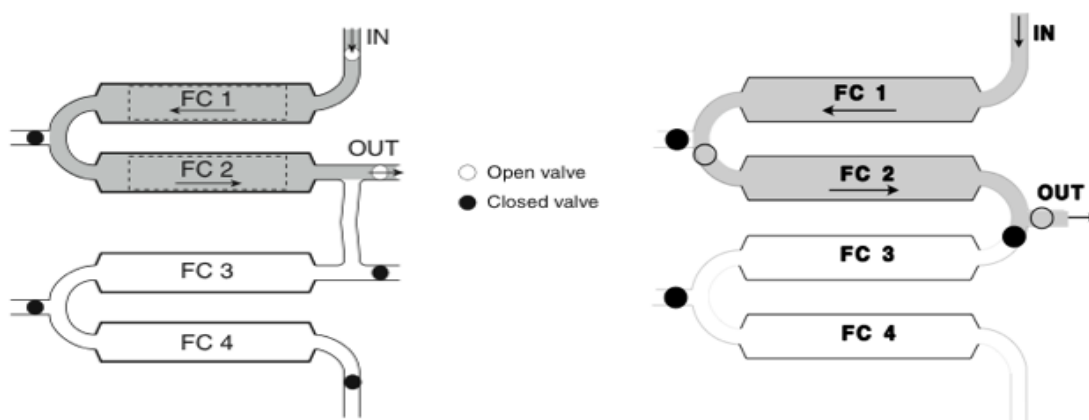
Figure 10. The flow cells. A simplified diagram of the flow cells for Biacore T100 (left) and Biacore 3000 (right) showing sample flow through fc1 and fc2 (taken from Biacore T100 and 3000 Instrument Handbooks, GE Healthcare Bio-Sciences AB).

Thus, we conducted a set of experiments to explore the possibility of simultaneous kinetic analysis of 3 ligands. The same levels (~50 RU) of C-rich RNA were immobilized on flow cells 2, 3, and 4, with flow cell 1 as a blank reference cell and

TIAR12 and HuR12 were injected as analyte proteins. The top 3 sensorgrams (Figure 11) show the binding of a range of concentrations of HuR12 when injected across the 3 C-rich RNA-coated flow cells (fc2, 3, and 4 with reference subtraction).
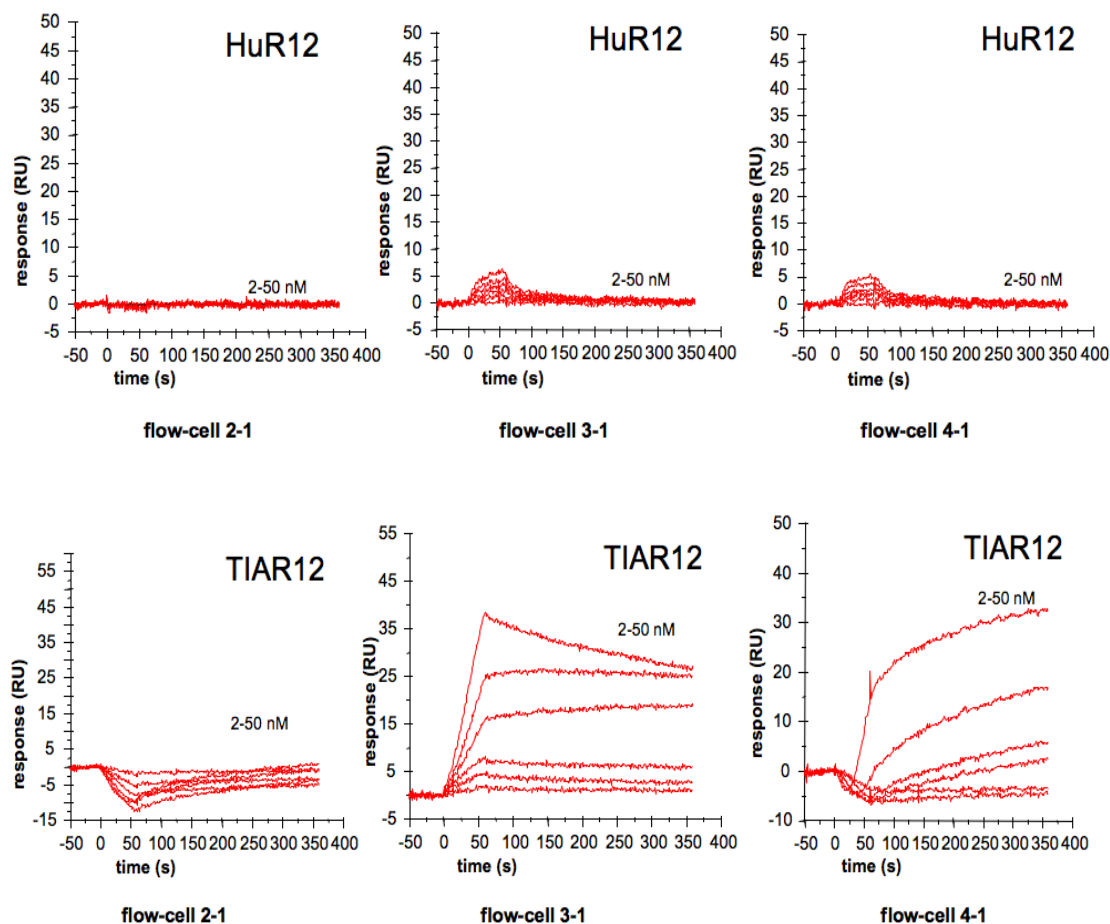
Figure 11. Interactions of HuR12 and TIAR12 proteins with C-rich RNA. The bindings of HuR12 (top) and TIAR12 (bottom) proteins to a C-rich RNA (28-mer) on fc2, 3, and 4 are shown. The same amount of biotinylated RNA (~50 RU) was captured on fc2, 3, and 4 of SA-coated sensor chip and increasing concentrations of proteins were injected over the surface. fc1 was used as a blank reference surface and subtracted from each data set to remove any non-specific responses (denoted as fc2-1, 3-1, and 4-1). Injections were performed for 60 seconds (association phase), followed by a 300-second flow of running buffer to assess dissociation. The experiments were conducted in duplicate. The red lines represent the binding responses for injections of protein analytes at specified concentrations (nM) over the RNA surface.

Firstly, there was no evidence of binding between HuR12 and C-rich RNA on fc2-1 (flow cell 2 with reference subtraction) as expected and consistent with the results from the experiments using a pair of flow cells (fc2-1 or 4-3) (Figure 8B). However, a low level (up to ~5 RU) of non-specific or residual binding was evident in fc3-1 and fc4-1 which was not present when a pair of flow cells was used. The discrepancies between flow-cell 2, 3, and 4 and non-specific responses on them were much more apparent in the case of TIAR12-C-rich RNA interaction (Figure 11). The 3 lower sensorgrams show the binding of a range of concentrations of TIAR12 when injected across the 3 C-rich RNA-coated flow cells. The subtracted flow cells showed inconsistent and unusual responses including negative refractive index in fc2-1 and fc4-1. Surprisingly, detailed examination of the individual flow cells without reference subtractions revealed significant binding on all 4 flow cells including the reference flow cell (fc1) and they resemble one another (Figure 12). These events have not been seen in experiments when we used a pair of flow cells at a time only (Figure 13).
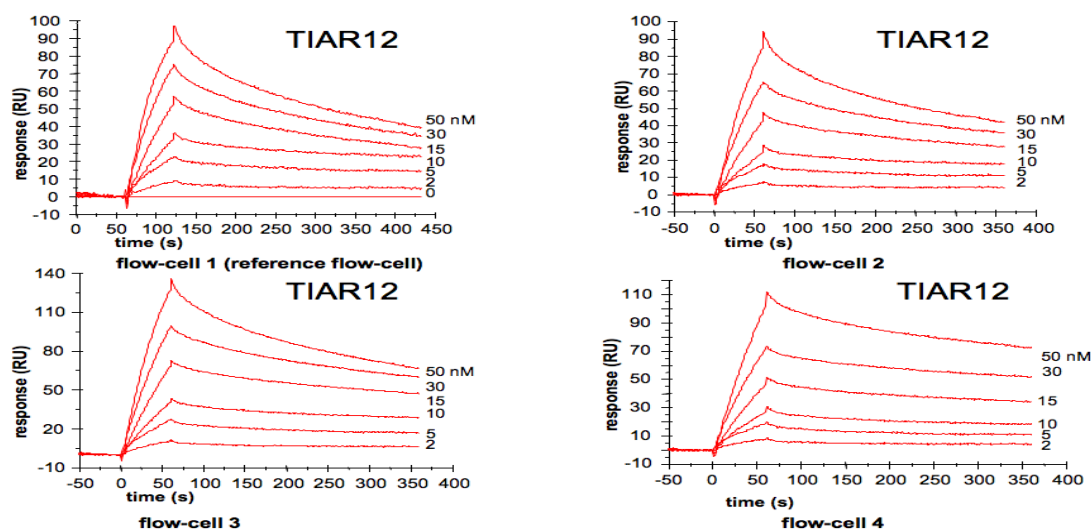
Figure 12. Interaction of TIAR12 protein with C-rich RNA. The 4 sensorgrams represent the non-subtracted original flow cells (fc2, 3, and 4 as well as the reference fc1) for the same binding event of TIAR12 protein to a C-rich RNA immobilized on fc2, 3, and 4 as described in Figure 11.
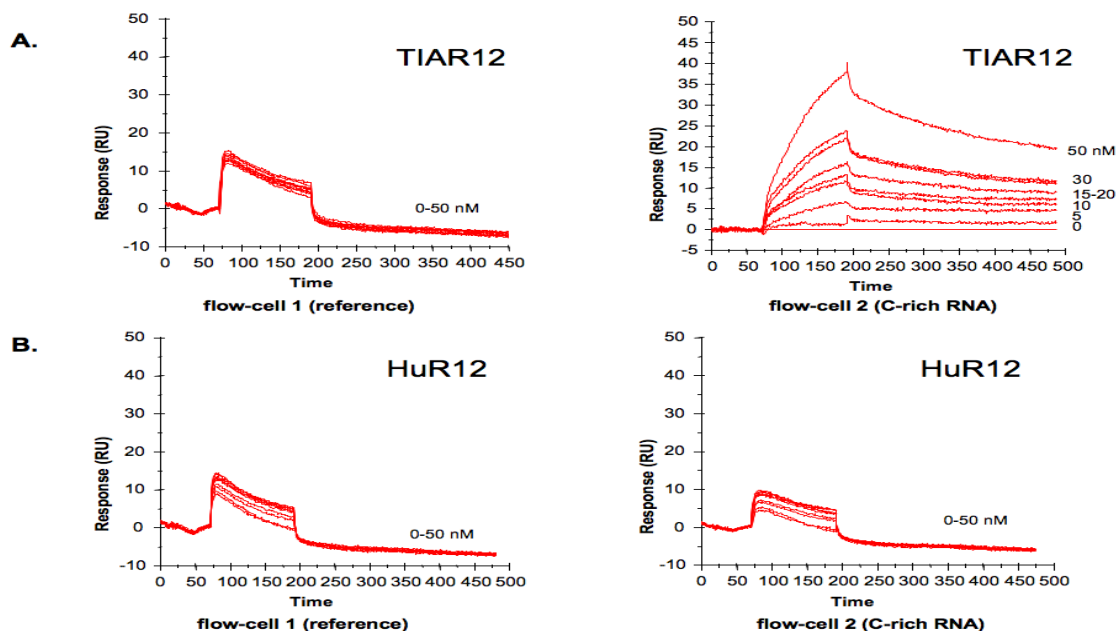
Figure 13. Interactions of HuR12 and TIAR12 proteins with C-rich RNA. The 4 sensorgrams represent the non-subtracted original flow cells (fc1-reference, fc2-C-rich RNA) for the same binding events of TIAR12 (A) and HuR12 (B) proteins to the C-rich RNA immobilized on fc2 as described in Figure 8B.

Overall, simultaneous kinetic analyses of 3 identical RNAs on flow cells 2, 3, and 4, with fc1 as a reference cell using Biacore T100 resulted in: 1) Inconsistency between different flow cells 2) Possible non-specific interactions 3) Binding on the reference flow cell. More thorough investigation is necessary to fully test and understand the maximum kinetic capabilities of using all four flow cells in parallel, although the results presented here are consistent with the manufacturer's recommendations and the design of the Biacore T100 flow system which is optimised for kinetics and best to be used as a pair of flow cells (GE Healthcare Bio-Sciences AB). Thus, simultaneous analysis of multiple ligands was avoided for all our studies of protein-RNA interactions, especially for those involving detailed kinetic and affinity analysis.

TIAR12 interacts with poly-purines with much lower affinity than with U- or C-rich RNA targets.

TIAR thus far has shown binding with nanomolar affinities towards U-rich and C-rich RNA targets. Experiments were conducted here to investigate the possible interactions of TIAR12 with A- and G-rich RNA. These would serve as important negative controls and assure that the low nanomolar affinity binding observed for TIAR above is specific to its U- or C-rich RNA targets. It was important to test G-rich RNA especially to rule out the possibility that the short G-rich sequence used as a linker at the ends of our target U-rich RNA may contribute towards binding. The 2 sensorgrams (Figure 14) show the binding of a range of concentrations of TIAR12 when injected across the A- or G-rich

RNA-coated chip. K_D for each binding was approximated by a simple 1:1 Langmuir

binding model.
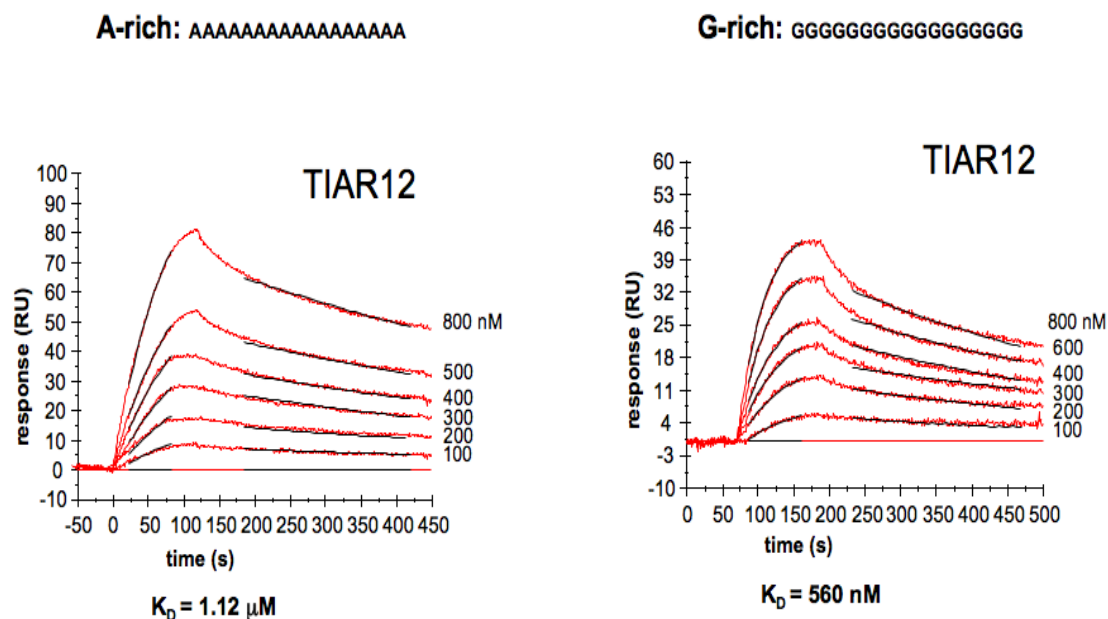
Figure 14. Kinetic analysis of the interactions of TIAR12 protein with G and A-rich RNA. The binding of TIAR12 protein to a G-rich or an A-rich RNA (17-mer each) is shown. Biotinylated RNA was captured on SA-coated sensor chip and increasing concentrations of protein were injected over the surface. Injections were performed for 120 seconds (association phase), followed by a 300-second flow of running buffer to assess dissociation. The experiments were conducted in duplicate and showed good overlap. The red lines represent the binding responses for injections of protein analyte at specified concentrations (nM) over the RNA surface. The kinetic data was fit by 1:1 Langmuir binding model. Mass transport effects were not evident. The black curves superimposed on top of the sensorgrams represent the model fitted curves. k_a and k_d were determined as separate phases from which the K_D was determined.

Despite no interaction being observed between HuR12 and A- or G-rich RNA (data not

shown), some binding was detected between TIAR12 and A- and G-rich RNA although

it was a weaker interaction (20 x and 10 x lower affinity that to the C-rich sequence

respectively). No binding between TIAR12 and A- or G-rich RNA was detected at the

same low nanomolar concentration ranges used for the binding between TIAR12 and U- or C-rich RNA. The binding affinities (K_D) for these interactions could only be approximated by the separate kinetic analyses instead of simultaneous kinetics where the association and dissociation phases were fit separately.

Pre-mixing TIAR12 and HuR12 proteins (at different molar ratios) completely abrogates their ability to bind the U-rich RNA target with nanomolar affinities.

RBPs such as TIAR and HuR target their specific mRNA regulatory elements such as U- or C-rich motifs as shown in the above experiments and play an important role in the regulation of gene expression (Anderson and Kedersha 2002; Brennan and Steitz 2001). Not only do they share some of their mRNA targets, but also they have similar tissue distribution, and are often co-expressed in mammalian cells (Beck et al. 1996; Grosset et al. 2004; Gueydan et al. 1999; Lu and Schneider 2004; Masuda et al. 2009; Piecyk et al. 2000). Nevertheless it is not clear how they would compete with each other for the same mRNA targets in their co-existence. From the above experiments, it would be predicted that TIAR12 would outcompete HuR12 and sensorgrams would reflect the TIAR12 type kinetics. Even though these proteins are not the full length protein, it was of interest to look at the binding of mixtures of these proteins to U-rich RNA. We thus conducted a simple set of SPR experiments by mixing TIAR12 and HuR12 at different molar ratios (1:1, 2:1, and 1:2) and tested their binding with the U-rich RNA, the common target of both proteins. The 3 sensorgrams (Figure 15) show the binding of a range of

concentrations of TIAR12 and HuR12 mixtures at 3 different molar ratios when injected

across the U-rich RNA-coated chip.
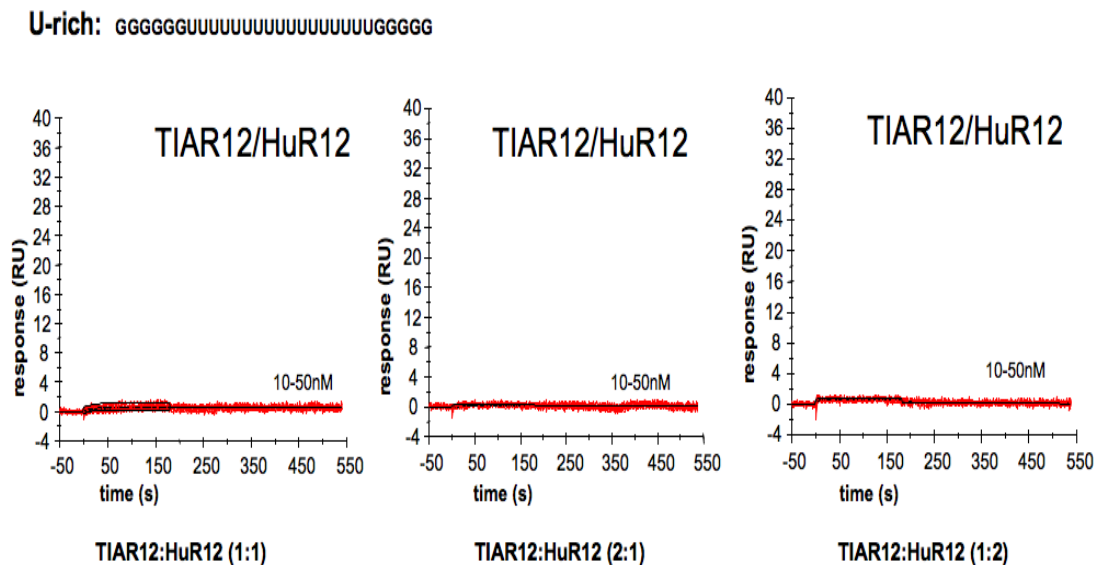
Figure 15. Analysis of the interactions of TIAR12 and HuR12 protein mixtures with U-rich RNA. The binding of HuR12 and TIAR12 protein mixtures to the U-rich RNA (28-mer) is shown. Biotinylated RNA was captured on SA-coated sensor chip and increasing concentrations of protein mixes at different molar ratios (1:1, 2:1, and 1:2) were injected over the surface. Injections were performed for 180 seconds (association phase), followed by a 360-second flow of running buffer to assess dissociation. The experiments were conducted in duplicate and showed good overlap. The red lines represent the binding responses for injections of protein analytes at different concentrations (nM) over the RNA surface.

Our preliminary data here indicates that pre-mixing TIAR12 and HuR12 proteins (at

different molar ratios) completely abolishes their nanomolar binding to target U-rich

RNA. Both proteins were soluble and active, as they showed good binding to U-rich

RNA separately and there was no sign of precipitation after they were combined. The

same observation was also made when we tested TIAR12 and HuR12 premixes with the

AU-rich RNA derived from TNF-α mRNA, also a known target of both TIAR and HuR

proteins (data not shown). One explanation for this surprising observation is that the HuR12 and TIAR12 constructs interact with each other and block their interactions with RNA. Whether these are specific events involving interactions between these two versatile RBPs remains to be seen.

Discussion

Optimisation of the SPR system is essential for accurate measurement of protein-RNA interactions

Here we demonstrated some of the important factors which can influence the quality of SPR data and described how we managed to optimise our SPR system for studying various protein-RNA interactions. Detailed kinetic analyses involving various proteins (TIAR12, TIAR123, and HuR12) and their mRNA targets (U- and C-rich RNA) were performed using the optimised system.

Using the Biacore3000 we showed that all 3 proteins bind U-rich RNA and only TIAR binds the C-rich RNA although at much lower affinities and with noisy signals. Thus it was unclear how accurate the kinetic analyses were for the low-level interactions of TIAR123 and TIAR12 with C-rich RNA. The maximum analyte (TIAR12 and 123) binding capacity (R_{max}) calculated from these interactions is only ~10 RU which is a small fraction (~1/10) of the predicted maximum protein binding capacity (~100 RU) assuming that these are 1:1 binding events and C-rich RNA molecules are fully active and accessible (Biacore Sensor Surface Handbook, Biacore Inc.). This could indicate

that either there is only a small fraction of the C-rich RNA or TIAR proteins available for binding to be measured on the surface of the sensor chip, or there are other complications in the system, or a combination of both. One of the factors which could have contributed to these complications is the presence of tRNA and/or BSA in the flow system. It is certainly possible that TIAR proteins are partially prohibited from reaching the RNA surface, thus only a fraction (~1/10) of protein concentrations (for example, 10 nM instead of 100 nM of TIAR12/123) is available for binding C-rich RNA immobilised on the sensor chip surface. Therefore, the kinetic analyses from these interactions are not likely to be accurate (below detection level with inaccurate protein concentration estimates on the surface) and in fact they were not detectable later on when we used Biacore T100 although the higher protein concentration ranges have not been fully explored (Figure 7). These data raised the question about the use of blocking agents in the system which led us to our further comparison of the Biacore T100 system with and without these agents (Figure 7 and 8). The fact that the ability of analyte protein TIAR to get to the RNA immobilised surface is severely affected by the presence of tRNA in the flow system indicates that this versatile RBP not only interacts strongly with its ARE and C-rich RNA targets, but also interacts non-specifically with the blocking agent such as tRNA (It is not likely that BSA in the buffer blocks the binding on the surface since only TIAR, but not HuR interactions are significantly affected). This is not surprising given the multi-functional and diverse nature of TIAR being able to interact with wide repertoire of RNA and DNA targets as shown previously (Anderson and Kedersha 2002; Dember et al. 1996; Lopez de Silanes et al. 2005; Suswam et al. 2005).

Since the SPR signals are directly proportional to the changes in mass on the surface, the predicted stoichiometry can be estimated as follows assuming that the ligand is fully active:

[Stoichiometry = R (max) / R (Ligand) x MW (Ligand) / MW (Analyte)]

R (max)= Maximum analyte binding capacity (RU); R (Ligand)= Amount of ligand immobilised on the surface (RU); MW (Ligand)= Molecular weight of ligand; MW (Analyte)= Molecular weight of analyte (Biacore Sensor Surface Handbook, GE Healthcare Bio-Sciences AB)

Interestingly most of the binding events described here indicate some variations from the predicted 1 : 1 molar ratio ranging between ~0.5 : 1 and ~1.5 : 1. This could be due to a number of factors including slightly different surface accessibility for different proteins, secondary structure of the RNA, inter-RNA interactions on the surface, and availability of multiple binding registers on the RNA sequence. Most kinetic analyses described here were performed using a simple 1:1 Langmuir binding model with k_a, k_d, and R_{max} all fitted globally and as simultaneous kinetics. However, separate kinetic analysis could only be used in a certain case such as TIAR12 interactions with A- and G-rich RNA (Figure 14), possibly an indication of complexity or non-specificity in their interactions or in the system resulting in inconsistency between the association and dissociation phases.

Simultaneous analysis of multi flow cells as RNA surfaces led to non-specific binding on the blank flow cell and inconsistency between different flow cells (figure 11-12), thus

should be avoided for studies of protein-RNA interactions although more extensive investigation into the accuracy of kinetic data obtained using multi flow cells in parallel is necessary, and pairwise flow cells should be used instead as they are designed and optimised for detailed kinetic and affinity analysis as specified by the manufacturer (more information on the T100 flow cells can be obtained from manufacturer's instrument handbook, GE Healthcare Bio-Sciences AB).

Finally, a simple set of SPR experiments was used to show that pre-mixing RBPs TIAR12 and HuR12 completely abrogates their ability to bind their target RNA with nanomolar affinities. Future investigations using the optimised SPR system with broader concentration ranges and molar ratios of the two proteins as well as other more direct approaches using techniques such as Small Angle X-ray Scattering (SAXS), NMR, and pull-down assays may lead us towards better understand of this interesting phenomena.

The C-rich motif is a novel TIAR target and functions as a translational repressor in the presence of TIAR

Whilst TIAR proteins have been reported previously to preferentially bind the U-rich sequences (Dember et al. 1996), our collaborator's *in vivo* studies and bioinformatic analysis of the mRNA transcripts preferentially bound by TIAR suggested that a 28-nt long motif, predominantly C-rich may be targeted by this protein (Kim et al. 2007). This unexpected finding prompted us to investigate the relative binding affinity of TIAR to U-rich RNA compared with the new C-rich motif in vitro.

The kinetic and affinity results presented here using the optimized SPR system clearly show that both TIAR and HuR proteins bind their U-rich RNA target with nanomolar affinities as reported previously (Dember et al. 1996; Fialcowitz-White et al. 2007; Park et al. 2000). However, only TIAR protein is able to bind the newly discovered C-rich RNA motif with lower but significant nanomolar affinity confirming it as a novel TIAR target (Figure 8). The C-rich motif not only is a target sequence for TIAR but also has a significant functional role as discovered from the functional assays performed by Gorospe and colleagues (Kim et al. 2007). Plasmids were engineered to express EGFP (Enhanced Green Fluorescent Protein) reporter protein with or without the C-rich motif. Insertion of C-rich motif strongly reduced the expression of EGFP and this regulation was TIAR-dependent because silencing of TIAR dramatically increased EGFP expression compared with non-TIAR target control. This further confirms our in vitro findings and strongly supports the view that TIAR can indeed suppress the translation of mRNA containing C-rich motif (Kim et al. 2007).

Conclusion

This study demonstrates the way in which SPR can be used to measure precise binding events involving RBPs and their target RNA sequences. Firstly however the system needs to be optimised and a number of factors need to be taken into consideration to be able to observe the true binding events and obtain meaningful and biologically relevant kinetic and affinity information from them. These include choosing the right instrument,

buffer (blocking agents), monitoring the level of noise and baseline stability, using controls for the RNA surface as well as proteins, using the correct concentration ranges of proteins, considering the RNA immobilisation level, determining the best usage of flow cells, testing binding and fitting models with their associated parameters and errors, and R_{max}. The described optimised SPR system led to identification of the C-rich motif as a novel TIAR target which led to further experiments that ultimately verified the biological effect of the C-rich motif in translational repression (Kim et al. 2007).

References

Anderson P, Kedersha N (2002) Visibly stressed: the role of eIF2, TIA-1, and stress granules in protein translation. Cell Stress Chaperones 7:213-21

Beck AR, Medley QG, O'Brien S, Anderson P, Streuli M (1996) Structure, tissue distribution and genomic organization of the murine RRM-type RNA binding proteins TIA-1 and TIAR. Nucleic Acids Res 24:3829-35

Brennan CM, Steitz JA (2001) HuR and mRNA stability. Cell Mol Life Sci 58:266-77

Dember LM, Kim ND, Liu KQ, Anderson P (1996) Individual RNA recognition motifs of TIA-1 and TIAR have different RNA binding specificities. J Biol Chem 271:2783-8

Fialcowitz-White EJ, Brewer BY, Ballin JD, Willis CD, Toth EA, Wilson GM (2007) Specific protein domains mediate cooperative assembly of HuR oligomers on AU-rich mRNA-destabilizing sequences. J Biol Chem 282:20948-59

Grosset C, Boniface R, Duchez P, Solanilla A, Cosson B, Ripoche J (2004) In vivo studies of translational repression mediated by the granulocyte-macrophage colony-stimulating factor AU-rich element. J Biol Chem 279:13354-62

Gueydan C, Droogmans L, Chalon P, Huez G, Caput D, Kruys V (1999) Identification of TIAR as a protein binding to the translational regulatory AU-rich element of tumor necrosis factor alpha mRNA. J Biol Chem 274:2322-6

Hellman LM, Fried MG (2007) Electrophoretic mobility shift assay (EMSA) for detecting protein-nucleic acid interactions. Nat Protoc 2:1849-61

Hinman MN, Lou H (2008) Diverse molecular functions of Hu proteins. Cell Mol Life Sci 65:3168-81

Karlsson R (2004) SPR for molecular interaction analysis: a review of emerging application areas. Journal of Molecular Recognition 17:151-161

Katsamba PS, Myszka DG, Laird-Offringa IA (2001) Two functionally distinct steps mediate high affinity binding of U1A protein to U1 hairpin II RNA. J Biol Chem 276:21476-81

Katsamba PS, Park S, Laird-Offringa IA (2002) Kinetic studies of RNA-protein interactions using surface plasmon resonance. Methods 26:95-104

Kim HS, Kuwano Y, Zhan M, Pullmann R, Jr., Mazan-Mamczarz K, Li H, Kedersha N, Anderson P, Wilce MC, Gorospe M, Wilce JA (2007) Elucidation of a C-rich signature motif in target mRNAs of RNA-binding protein TIAR. Mol Cell Biol 27:6806-17

Lopez de Silanes I, Galban S, Martindale JL, Yang X, Mazan-Mamczarz K, Indig FE, Falco G, Zhan M, Gorospe M (2005) Identification and functional outcome of mRNAs associated with RNA-binding protein TIA-1. Mol Cell Biol 25:9520-31

Lu JY, Schneider RJ (2004) Tissue distribution of AU-rich mRNA-binding proteins involved in regulation of mRNA decay. J Biol Chem 279:12974-9

Masuda K, Abdelmohsen K, Gorospe M (2009) RNA-binding proteins implicated in the hypoxic response. J Cell Mol Med

Myszka DG (1997) Kinetic analysis of macromolecular interactions using surface plasmon resonance biosensors. Curr Opin Biotechnol 8:50-7

Myszka DG (1999a) Improving biosensor analysis. J Mol Recognit 12:279-84

Myszka DG (1999b) Survey of the 1998 optical biosensor literature. J Mol Recognit 12:390-408

Myszka DG (2000) Kinetic, equilibrium, and thermodynamic analysis of macromolecular interactions with BIACORE. Methods Enzymol 323:325-40

Myszka DG, Jonsen MD, Graves BJ (1998) Equilibrium analysis of high affinity interactions using BIACORE. Anal Biochem 265:326-30

Park S, Myszka DG, Yu M, Littler SJ, Laird-Offringa IA (2000) HuD RNA recognition motifs play distinct roles in the formation of a stable complex with AU-rich RNA. Mol Cell Biol 20:4765-72

Park-Lee S, Kim S, Laird-Offringa IA (2003) Characterization of the interaction between neuronal RNA-binding protein HuD and AU-rich RNA. J Biol Chem 278:39801-8

Piecyk M, Wax S, Beck AR, Kedersha N, Gupta M, Maritim B, Chen S, Gueydan C, Kruys V, Streuli M, Anderson P (2000) TIA-1 is a translational silencer that selectively regulates the expression of TNF-alpha. Embo J 19:4154-63

Rich RL, Myszka DG Grading the commercial optical biosensor literature-Class of 2008: 'The Mighty Binders'. J Mol Recognit 23:1-64

Rich RL, Myszka DG (2000) Advances in surface plasmon resonance biosensor analysis. Curr Opin Biotechnol 11:54-61

Rich RL, Myszka DG (2003) A survey of the year 2002 commercial optical biosensor literature. J Mol Recognit 16:351-82

Rich RL, Myszka DG (2005) Survey of the year 2004 commercial optical biosensor literature. J Mol Recognit 18:431-78

Rich RL, Myszka DG (2007a) Higher-throughput, label-free, real-time molecular interaction analysis. Anal Biochem 361:1-6

Rich RL, Myszka DG (2007b) Survey of the year 2006 commercial optical biosensor literature. J Mol Recognit 20:300-66

Rich RL, Myszka DG (2008) Survey of the year 2007 commercial optical biosensor literature. J Mol Recognit 21:355-400

Suswam EA, Li YY, Mahtani H, King PH (2005) Novel DNA-binding properties of the RNA-binding protein TIAR. Nucleic Acids Res 33:4507-18

Velazquez-Campoy A, Ohtaka H, Nezami A, Muzammil S, Freire E (2004) Isothermal titration calorimetry. Curr Protoc Cell Biol Chapter 17:Unit 17 8

Yeap BB, Voon DC, Vivian JP, McCulloch RK, Thomson AM, Giles KM, Czyzyk-Krzeska MF, Furneaux H, Wilce MC, Wilce JA, Leedman PJ (2002) Novel binding of HuR and poly(C)-binding protein to a conserved UC-rich motif within the 3'-untranslated region of the androgen receptor messenger RNA. J Biol Chem 277:27183-92

Elucidation of a C-Rich Signature Motif in Target

mRNAs of RNA-Binding Protein TIAR

Declaration for Thesis Chapter [3]

Declaration by candidate

In the case of Chapter [3], the nature and extent of my contribution to the work was the following:

Nature of contribution	Extent of contribution (%)
Co-first author: Prepared proteins and RNAs required for SPR experiments, developed, optimized, and carried out SPR assays, analyzed data, and contributed towards manuscript preparation.	**30**

The following co-authors contributed to the work. Co-authors who are students at Monash University must also indicate the extent of their contribution in percentage terms:

Name	Nature of contribution	Extent of contribution (%) for student co-authors only
Yuki Kuwano[2]	Participated in molecular biology experiments and in manuscript preparation	N/A
Ming Zhan[2]	Participated in bioinformatic	N/A

	analysis and in manuscript preparation	
Rudolf Pullmann, Jr. [2]	Participated in molecular biology experiments	N/A
Krystyna Mazan-Mamczarz[2]	Participated in molecular biology experiments	N/A
Huai Li[3]	Participated in bioinformatic analysis and in manuscript preparation	N/A
Nancy Kedersha[3]	Provided the TIAR constructs and contributed to the manuscript	N/A
Paul Anderson[3]	Contributed to the interpretation of the data and the manuscript	N/A
Matthew C. J. Wilce[1]	Contributed to the interpretation of the biophysical data and manuscript preparation.	N/A
Myriam Gorospe[2]	Contributed to the design and interpretation of molecular biology experiments and	N/A

	manuscript preparation.	
Jacqueline A. Wilce[1]	Planned and supervised the SPR experiments and oversaw the reporting of the results.	N/A

Candidate's Signature	████████████████████	**Date: 01/07/2010**

Declaration by co-authors

The undersigned hereby certify that:

(1)   the above declaration correctly reflects the nature and extent of the candidate's contribution to this work, and the nature of the contribution of each of the co-authors.

(2)   they meet the criteria for authorship in that they have participated in the conception, execution, or interpretation, of at least that part of the publication in their field of expertise;

(3)   they take public responsibility for their part of the publication, except for the responsible author who accepts overall responsibility for the publication;

(4)   there are no other authors of the publication according to these criteria;

(5)   potential conflicts of interest have been disclosed to (a) granting bodies, (b) the editor or publisher of journals or other publications, and (c) the head of the responsible academic unit; and

(6)   the original data are stored at the following location(s) and will be held for at least five years from the date indicated below:

Location(s)	1. **Department of Biochemistry and Molecular Biology, Monash University, Clayton, Victoria 3800, Australia** 2. **Laboratory of Cellular and Molecular Biology, National Institute on Aging-Intramural Research Program, National Institute of Health, Baltimore, Maryland 21224, USA**
	3. **Division of Rheumatology and Immunology, Harvard Medical School, Brigham and Women's Hospital, Boston, Massachusetts 02115, USA**

Signatures of co-authors:

Yuki Kuwano		Date:
		July 2, 2010
	on behalf of Yuki Kuwano	
Ming Zhan		July 2, 2010
	on behalf of Ming Zhan	
Rudolf Pullmann, Jr.		July 2, 2010
	on behalf of Rudolf Pullmann, Jr.	
Krystyna Mazan-Mamczarz		July 2, 2010
	on behalf of Krystyna Mazan-Mamczarz	
Huai Li		July 2, 2010
	on behalf of Huai Li	
Nancy Kedersha		7/13/2010

Paul Anderson   7/6/10

Matthew C. J. Wilce   July 1st 2010

Myriam Gorospe   July 2, 2010
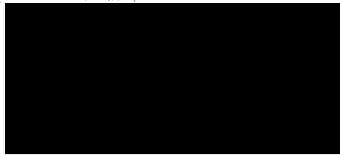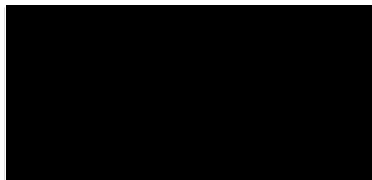
Jacqueline A. Wilce   July 1st 2010

Elucidation of a C-Rich Signature Motif in Target mRNAs of RNA-Binding Protein TIAR[▽][†]

Henry S. Kim,[1][‡] Yuki Kuwano,[2][‡] Ming Zhan,[3] Rudolf Pullmann, Jr.,[2] Krystyna Mazan-Mamczarz,[2]
Huai Li,[3] Nancy Kedersha,[4] Paul Anderson,[4] Matthew C. J. Wilce,[1]
Myriam Gorospe,[2]*§ and Jacqueline A. Wilce[1]§

*Department of Biochemistry and Molecular Biology, Monash University, Victoria 3800, Australia[1]; Laboratory of Cellular and
Molecular Biology, National Institute on Aging-Intramural Research Program, National Institutes of Health, Baltimore,
Maryland 21228[2]; Research Resources Branch, National Institute on Aging-Intramural Research Program,
National Institutes of Health, Baltimore, Maryland 21228[3]; and Division of Rheumatology and
Immunology, Harvard Medical School, Brigham and Women's Hospital,
Boston, Massachusetts 02115[4]*

The RNA-binding protein TIAR (related to TIA-1 [T-cell-restricted intracellular antigen 1]) was shown to associate with subsets of mRNAs bearing U-rich sequences in their 3′ untranslated regions. TIAR can function as a translational repressor, particularly in response to cytotoxic agents. Using unstressed colon cancer cells, collections of mRNAs associated with TIAR were isolated by immunoprecipitation (IP) of (TIAR-RNA) ribonucleoprotein (RNP) complexes, identified by microarray analysis, and used to elucidate a common signature motif present among TIAR target transcripts. The predicted TIAR motif was an unexpectedly cytosine-rich, 28- to 32-nucleotide-long element forming a stem and a loop of variable size with an additional side loop. The ability of TIAR to bind an RNA oligonucleotide with a representative C-rich TIAR motif sequence was verified in vitro using surface plasmon resonance. By this analysis, TIAR containing two or three RNA recognition domains (TIAR12 and TIAR123) showed low but significant binding to the C-rich sequence. In vivo, insertion of the C-rich motif into a heterologous reporter strongly suppressed its translation in cultured cells. Using this signature motif, an additional ∼2,209 UniGene targets were identified (2.0% of the total UniGene database). A subset of specific mRNAs were validated by RNP IP analysis. Interestingly, in response to treatment with short-wavelength UV light (UVC), a stress agent causing DNA damage, each of these target mRNAs bearing C-rich motifs dissociated from TIAR. In turn, expression of the encoded proteins was elevated in a TIAR-dependent manner. In sum, we report the identification of a C-rich signature motif present in TIAR target mRNAs whose association with TIAR decreases following exposure to a stress-causing agent.

Mammalian gene expression is extensively regulated at the posttranscriptional level, via mechanisms such as pre-mRNA splicing, transport, stability, and translation. Prominent among the posttranscriptional *trans*-acting factors that influence these processes are RNA-binding proteins (RBPs) that influence transcript splicing, localization, stability, and association with the translation machinery (11, 17, 42). Many mRNAs encoding stress-response, proliferative, immune, and developmental proteins comprise specific regulatory sequences in the untranslated regions (UTRs), often encompassing uridine- or adenine/uridine-rich stretches (hence termed "AREs"). AREs are bound by a specific subset of RBPs that influence the stability and translation of the ribonucleoprotein (RNP) complex. Many ARE-RBPs decrease the stability of target mRNAs, including AU-binding factor 1 (AUF1), tristetraprolin (TTP),

K homology splicing-regulatory protein (KSRP), and the butyrate response factor 1 (BRF1) (7, 27, 34, 39, 46). Other ARE-RBPs, like the Hu proteins (HuR, HuB, HuC, and HuD), can stabilize target mRNAs instead (4, 6); Hu proteins have also been shown to modulate the translation of several target mRNAs, both enhancing (5, 24, 31) and inhibiting (9, 23, 33) protein synthesis. However, the best-studied ARE-RBPs functioning as translational inhibitors are the T-cell-restricted intracellular antigen 1 (TIA-1) and the TIA-1-related protein TIAR (1, 2, 14, 28, 32).

TIA-1 and TIAR contain three RNA-recognition motifs (RRMs) through which they bind mRNAs (10). In addition to participating in pre-mRNA splicing (12, 26, 38), TIA-1 and TIAR have been proposed to repress translation (1, 2, 32, 37). In unstressed cells, a preinitiation complex (comprising the eukaryotic translation initiation factor 1 [eIF-1], eIF-2, eIF-3, eIF-5, and the 40S ribosomal subunit) forms at the 5′ end of capped mRNAs. Following the recognition of an initiation codon, the 60S subunit assembles, displacing the eIFs and forming a functional ribosome to initiate translation. In cells exposed to damaging agents, phosphorylation of eIF-2α by a family of kinases (PKR, PERK, GCN2, and HRI) reduces the levels of functional preinitiation complex (recently reviewed in

reference 16). Under these conditions, TIAR and TIA-1 have been postulated to function as translational repressors by associating with eIF-4F, eIF-3, and the 40S ribosomal subunit, to form nonfunctional preinitiation complexes (2). The self-aggregating properties of TIA-1 and TIAR were further proposed to facilitate the accumulation of the translationally inactive preinitiation complexes into discrete cytoplasmic foci called stress granules (SGs). Given the presence of RBPs implicated in the regulation of mRNA turnover (such as TTP and HuR) and translation (TIA proteins) at SGs, these foci are believed to function as dynamic sites of mRNA triage during stress, wherein the composition of mRNA RNP complexes and their subsequent engagement with the translation or degradation machineries are decided (20, 21).

While these mechanisms of TIA-1/TIAR action can lead to a general suppression of translation in the cell, they are believed to have a preferential effect upon specific subsets of bound mRNAs, such as ARE-containing mRNAs encoding tumor necrosis factor alpha (TNF-α), matrix metalloproteinase 13 (MMP-13), cyclooxygenase 2 (COX-2), and β2-adrenergic receptor (AR) (8, 14, 19, 37, 44). Accordingly, global searches have been undertaken to identify TIA-1/TIAR target mRNAs systematically. An earlier study in which pools of random RNA sequences were selected/amplified in vitro revealed that both TIA proteins recognized RNAs containing U-rich stretches (10). More recently, a genome-wide search for TIA-1 target mRNAs was carried out by immunoprecipitation (IP) of TIA-1 RNPs followed by the identification of bound transcripts using DNA microarrays (28). A computational analysis of the target mRNAs found by this approach led to the elucidation of a shared signature motif present among mRNAs which was also U rich. TIA-1 was shown to associate with target mRNAs bearing this motif in cells subjected to heat shock and to suppress their translation (28). Using a similar en masse approach, TIAR target mRNAs were found to include many mRNAs encoding translation factors and other proteins involved in translation (32). Further analysis of TIAR RNPs indicated that the association of TIAR with several target mRNAs increased following irradiation with short-wavelength UV light (UVC), thereby helping to suppress their translation (32).

Here, we sought to elucidate a shared motif among TIAR target mRNAs. The starting material was a collection of TIAR-bound transcripts that was isolated from untreated RKO cells (a human colon cancer line) using the RNP IP methodology and was identified by using a microarray (32). Computational analysis of this set of transcripts revealed a shared signature motif that was unexpectedly C rich. The ability of TIAR RRM domains to bind to a representative C-rich sequence was verified in vitro using surface plasmon resonance (SPR). Further validation of this interaction was obtained by studying the binding of mRNAs that were predicted to be TIAR targets because their 3′ untranslated regions (3′UTRs) contained at least one occurrence of the C-rich TIAR motif. Interestingly, the transcripts tested were found to dissociate from TIAR in response to UVC treatment, suggesting that this C-rich TIAR signature motif may occur within mRNAs whose binding to TIAR decreases following stress stimulation.

MATERIALS AND METHODS

Cell culture, treatment, and transfections. Human colorectal carcinoma RKO cells were cultured in minimum essential medium (Invitrogen), and human cervical carcinoma HeLa cells in Dulbecco's modified essential medium, each supplemented with 10% fetal bovine serum and antibiotics. Where indicated, cells were irradiated with 25 J/m^2 of short-wavelength UV light (UVC). Reporter plasmid pEGFP-GAPDH was constructed by inserting a 200 bp of glyceraldehyde-3-phosphate dehydrogenase (GAPDH) 3′UTR (nucleotides 1111 to 1310 of GAPDH [RefSeq accession no. NM_002046]) after the stop codon of pEGFP-N1; reporter plasmid pEGFP-Motif was constructed by inserting the consensus C-rich motif sequence UUGCCACCUCCUGCUCCUGCCCAGACAG within the GAPDH 3′UTR from pEGFP-GAPDH (at nucleotide position 1211 of the above fragment); reporter plasmid pEGFP-APAF1 was constructed by subcloning the 3′UTR of APAF1 (nucleotide positions 5401 to 5825 of NM_013229, including the C-rich motif hit CTGCTCCCTCTTGTTTCTTACATATCAG) immediately after the enhanced green fluorescent protein (EGFP) stop codon. Subconfluent cells were transfected with TIAR-directed (AAGGGCTATTCAT TGTCAGA) or control (TTCTCCGAACGTGTCACGT) small interfering RNAs (siRNAs) (20 nM each) and 24 h later with reporter plasmids (0.2 μg) using Lipofectamine 2000. Cells were subsequently harvested for RNA and protein analyses.

IP assays. IP of [TIAR-mRNA] complexes from RKO cell lysates was used to evaluate the association of endogenous TIAR with endogenous target mRNAs. The assay was performed essentially as described previously (29, 40), except that 100 million cells were used as starting material and lysate supernatants were precleared for 30 min at 4°C using 15 μg of immunoglobulin G (IgG) (Santa Cruz Biotech.) and 50 μl of protein-A Sepharose beads (Sigma) that had been previously swollen in NT2 buffer (50 mM Tris [pH 7.4], 150 mM NaCl, 1 mM MgCl$_2$, 0.05% Nonidet P-40) supplemented with 5% bovine serum albumin. Beads (100 μl) were incubated (16 h at 4°C) with 30 μg of antibody (either goat IgG [Santa Cruz Biotechnology] or goat anti-TIAR [Santa Cruz Biotechnology]) and then for 2 h at 4°C with 1.5 mg of cell lysate. After extensive washes and digestion of proteins in the IP material (40), the RNA was extracted and used either for hybridization of cDNA arrays or for verification of individual TIAR target transcripts. The array analysis was previously reported (32). Briefly, RNA obtained after IP reactions using either an anti-TIAR antibody or IgG was reverse transcribed in the presence of [α-^{33}P]dCTP and the radiolabeled product was used to hybridize cDNA arrays (Mammalian Gene Collection [MGC] arrays, containing ~6,000 individual genes) employing previously reported methodologies (29, 40, 41). All of the data were analyzed using the Array Pro software (Media Cybernetics, Inc.) and then normalized by Z score transformation and used to calculate differences in signal intensities. Significant values were tested using a two-tailed Z test and $P < 0.01$. The data were calculated from three independent experiments. The complete cDNA array data are available from the authors. For the analysis of individual transcripts, RNA in the IP material was used in reverse transcription (RT) reactions followed by quantitative real-time PCR (qPCR) analysis to detect the presence of specific target mRNAs using gene-specific primer pairs (see the supplemental material). qPCR products were visualized after electrophoresis in 1% agarose gels stained with ethidium bromide to verify that single bands were amplified in each reaction.

Computational analysis to identify a TIAR signature motif. Human UniGene records were first identified from the most strongly enriched TIAR targets derived from the array analysis using untreated RKO cells. The top 179 transcripts from which 3′UTRs were available served as the experimental data set (see Table S1 in the supplemental material) for the identification of the TIAR motif. Shared RNA motifs were elucidated from the the 3′UTR sequences; among the top candidate motifs, the motif with the highest statistical enrichment in the experimental 3′UTR data set was considered to be the best TIAR candidate motif (additional description in the supplemental material). The computational analysis was conducted as previously described (28) using the software RNAmotifPro (M. Zhan, unpublished). The motif logo was constructed using WebLogo (http://weblogo.berkeley.edu/). RNAplot was used to depict the secondary structure of the representative RNA motifs. The computation was performed using the NIH Biowulf computer farm. Both UniGene and RefSeq datasets were downloaded from NCBI.

Western blot analysis. Whole-cell protein lysates (10 or 15 μg) were resolved by sodium dodecyl sulfate-polyacrylamide gel electrophoresis (SDS-PAGE), transferred onto polyvinylidene difluoride membranes, and used for Western blot analysis. Primary antibody incubations were performed using mouse monoclonal antibodies recognizing β-actin (Abcam) or c-Myc (BD Pharmingen) or using rabbit polyclonal antibodies recognizing Apaf-1 (Chemicon), eIF5a, PXN,

TABLE 1. Top TIAR target mRNAs identified on MGC arrays after RNP IP[a]

Name	Symbol	RefSeq accession no.	Unigene no.	Z ratio
Nucleolar protein family A3 (H/ACA small nucleolar RNPs)	NOLA3	NM_018648	Hs#S2294033	3.38
ADP-ribosylation factor 3	ARF3	NM_001659	Hs#S1726280	3.13
Metallothionein 1H	MT1H	NM_005951	Hs#S3219010	3.06
Small nuclear ribonucleoprotein D3 polypeptide 18 kDa	SNRPD3	NM_004175	Hs#S1729293	2.90
Metallothionein 1L	MT1L	NM_002450	Hs#S1727187	2.88
Phospholipid scramblase 3	PLSCR3	NM_020360	Hs#S2294612	2.66
Serine hydroxymethyltransferase 2 (mitochondrial)	SHMT2	NM_005412	Hs#S1730829	2.61
Cystatin B (stefin B)	CSTB	NM_000100	Hs#S1730514	2.52
F11 receptor	JAM1	NM_144503	Hs#S4554561	2.42
Laminin, alpha 5	LAMA5	NM_005560	Hs#S3619103	2.40
Adenylosuccinate lyase	ADSL	NM_000026	Hs#S1728269	2.26
H3 histone, family 3B (H3.3B)	H3F3B	NM_005324	Hs#S1730616	2.26
3-Hydroxybutyrate dehydrogenase (heart, mitochondrial)	BDH	NM_004051	Hs#S4001852	2.24
SWI/SNF related, matrix associated, regulator of chromatin	SMARCE1	NM_003079	Hs#S1730834	2.23
Long-chain fatty-acyl elongase	LCE	NM_024090	Hs#S3355556	2.16
H2A histone family, member Y2	H2AFY2	NM_018649	Hs#S2294022	2.16
Non-SMC (structural maintenance of chromosomes) 1	NSE1	NM_145080	Hs#S4554546	2.14
CHK1 checkpoint homolog (*Schizosaccharomyces pombe*)	CHEK1	NM_001274	Hs#S1726468	2.13
Transforming growth factor beta 1-induced transcript 1	TGFB1I1	NM_015927	Hs#S2140275	2.13
MAD1 mitotic arrest-deficient-like 1 (yeast)	MAD1L1	NM_003550	Hs#S1731867	2.12
Amplified in osteosarcoma	OS-9	NM_006812	Hs#S1731315	2.12
Fibrinogen-like 1	FGL1	NM_004467	Hs#S1732393	2.11
Cytochrome *c* oxidase subunit IV isoform 1	COX4I1	NM_001861	Hs#S1730504	2.10
Mevalonate (diphospho) decarboxylase	MVD	NM_002461	Hs#S1731983	2.10
Ubiquitin-conjugating enzyme E2C	UBE2C	NM_007019	Hs#S1731533	2.06
Wiskott-Aldrich syndrome protein-interacting protein	WASPIP	NM_003387	Hs#S4728188	2.02
Dihydropyrimidine dehydrogenase	DPYD	NM_000110	Hs#S1728556	1.98
Small nuclear ribonucleoprotein polypeptide F	SNRPF	NM_003095	Hs#S1727894	1.96
Ribosomal protein L5	RPL5	NM_000969	Hs#S1727704	1.94
Malic enzyme 2, NAD$^+$-dependent, mitochondrial	ME2	NM_002396	Hs#S1727151	1.92
G protein-coupled receptor 56	GPR56	NM_005682	Hs#S1729809	1.91
COX10 homolog, cytochrome *c* oxidase assembly protein	COX10	NM_001303	Hs#S1732347	1.91

[a] Whole-cell lysates prepared from untreated RKO cells were used for IP assays by employing either IgG or anti-TIAR antibodies. RNA was subsequently extracted from the RNP complexes present in the IP material and was reverse transcribed; the resulting radiolabeled molecules were used to hybridize a cDNA array (32). The most enriched transcripts found in association with TIAR (TIAR IP material compared with IgG IP material) are listed. The top 179 enriched transcripts with complete 3′UTR sequences, the experimental dataset (see Table S1 in the supplemental material), were used to derive the TIAR motif. The Z ratio column reflects the differences in signal intensity when comparing TIAR IP with IgG IP array signals (32). Transcripts were deemed TIAR targets if Z ratios are >1.

or TCF3 (Santa Cruz Biotechnology). Following secondary antibody incubations, signals were visualized by enhanced chemiluminescence.

Plasmid construction and protein purification. Constructs to express TIAR RRM123 (residues 1 to 283) and TIAR RRM12 (residues 1 to 208) (10) were transformed into *Escherichia coli* strain BL21(DE3), and the encoded proteins were expressed and purified as described previously (10). HuR RRM12 (residues 18 to 184) was cloned into pGEX-4T1, expressed in *E. coli* BL21(DE3), and purified according to previously established protocols (43). The proteins were further purified by size-exclusion and cation-exchange chromatography. The concentration of each protein was determined using the Bradford assay (Bio-Rad) and by A_{280} measurements using theoretical molar extinction coefficients (ProtParam). The extinction coefficients were validated for folded protein; A_{280} measurements were within 10% of measurements made in 6.0 M guanidium hydrochloride. The purity of each protein was confirmed by SDS-PAGE.

Biosensor analysis. The dynamics of RNA-protein interactions were characterized by SPR using a BIACORE T100 instrument (Biacore Inc.). A U-rich RNA [containing a poly(U) stretch; 5′-GGGGGGGUUUUUUUUUUUUUUU UUGGGGG-3′] and a C-rich RNA (5′-UUGCCACCUCCUGCUCCUGCCC AGACAG-3′) were chemically synthesized carrying a 5′-biotin tag (Dharmacon Research) to allow immobilization of the RNA onto streptavidin-coated sensor chips (series S sensor chip SA; Biacore, Inc.). RNAs were diluted to a final concentration of 1 μM in HBS buffer (10 mM HEPES [pH 7.4], 150 mM NaCl), followed by heating at 80°C for 10 min and cooling to room temperature. The sample was then diluted 500-fold in running buffer (10 mM HEPES [pH 7.4], 150 mM NaCl, 1 mM dithiothreitol, 0.025% surfactant P20 [Biacore, Inc.]) and injected over the sensor chip surface at 10 μl/min at 25°C to generate a 50-response unit (RU) RNA surface (for a low-density surface). Proteins were serially diluted in running buffer to the concentrations indicated in Fig. 3 and injected at 25°C at a flow rate of 50 μl/min for 2 min. Surface regeneration to remove any protein that remained bound after 3 min of dissociation was achieved using a 1-min injection of 2 M NaCl at 50 μl/min. Analysis of each protein concentration was done in duplicate, and samples were run in random order. Any background signal from a streptavidin-only reference flow cell was subtracted from every data set. Data were analyzed using a simple 1:1 Langmuir interaction model using the Biacore T100 evaluation software (Biacore, Inc.) to determine the affinities of the protein-RNA interactions.

RESULTS

Sequence and structure of the predicted TIAR motif. A collection of mRNAs that were TIAR targets was identified using human colorectal carcinoma RKO cells following IP under conditions that preserved the pools of mRNAs bound to TIAR (32). The RNA in the IP materials (associated with TIAR or bound in a nonspecific fashion in the IgG IP samples) was then extracted and reverse transcribed, and the resulting products were hybridized to human cDNA arrays (http://www .grc.nia.nih.gov/branches/rrb/dna/dna.htm#, MGC arrays). Three hundred array spots (~3.1% of the total spots on the array) had Z ratios of >1.00 when comparing the signals in TIAR IP arrays with those in IgG IP arrays and were thus deemed to represent specific TIAR-associated transcripts. Among them, the 179 transcripts for which full-length mRNAs were available (the experimental data set) were selected for further analysis. A subset of transcripts from the experimental data set are
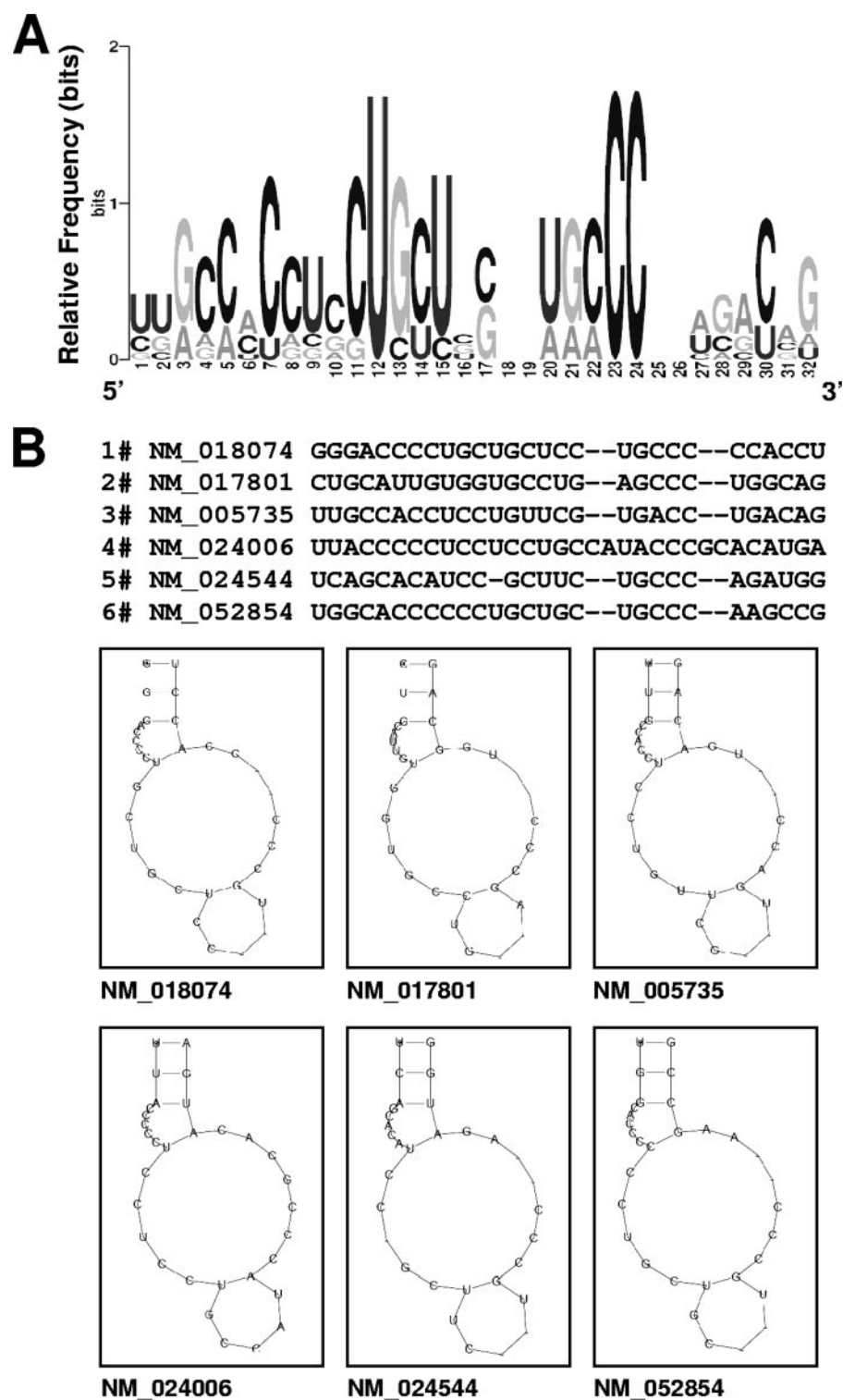
FIG. 1. Sequence and structure of the predicted TIAR motif, as identified among TIAR-bound transcripts. (A) Probability matrix (graphic logo) of the TIAR motif indicating the relative frequency of finding each residue at each position within the motif, as elucidated from the array-derived experimental data set. (B) Secondary structure of six representative examples of the TIAR motif in specific mRNAs; the corresponding RefSeq accession numbers names are shown.

listed in Table 1. The complete experimental data set is provided in Table S1 in the supplemental material, and numerous target transcripts were validated elsewhere (32).

The RNA sequences of the experimental data set were sub-

jected to computational analysis (Materials and Methods) to identify TIAR motifs, based on both primary RNA sequences and secondary structures. Of the 100 possible candidate motifs initially derived from the experimental data set, one motif
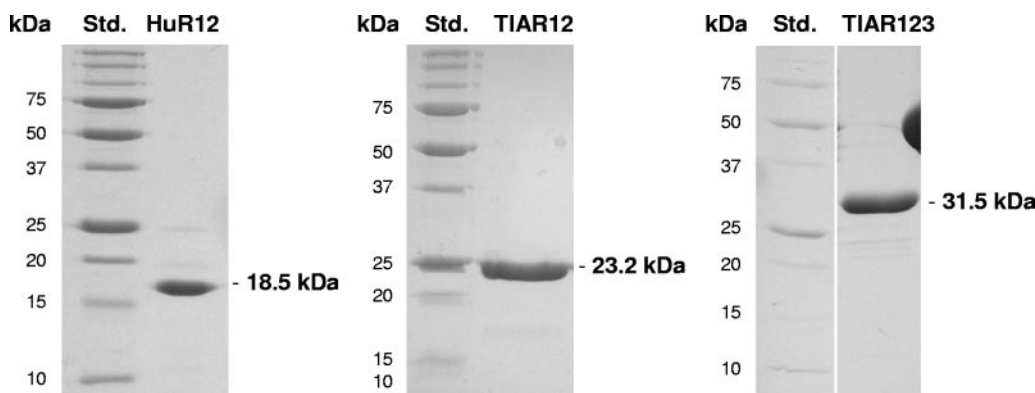
FIG. 2. Recombinant proteins used in in vitro binding assays. The construction of plasmids to express recombinant proteins comprising RRM1 and RRM2 or all three RRMs (HuR12, TIAR123, and TIAR12) was previously described (10). Proteins were expressed in bacteria and purified to homogeneity (details in Materials and Methods). Std., protein standard, with molecular mass (kDa) indicated.

comprising 28 to 32 nucleotides had the highest relative number of hits in the experimental data set compared with the entire UniGene database (as described previously in [28] and in the supplemental material). The sequence alignment, motif logo (graphic representation of the relative frequency of nucleotides at each position), and examples of the secondary structures of this putative TIAR are shown in Fig. 1A and B. The motif was found to be predominantly C rich (46%); U, G, and A nucleotides were significantly less abundant (21%, 18%, and 14%, respectively [Fig. 1A]). The sequence of this motif was unexpected, given our previous finding using SELEX analysis that suggested that TIAR bound to U-rich sequences, although these were often flanked by C residues (10). Figure 1B depicts six examples of the C-rich TIAR motif, with the corresponding mRNAs indicated below.

Both HuR and TIAR proteins bind U-rich RNA. The unanticipated identification of a C-rich RNA motif for TIAR target transcripts prompted us to investigate the relative binding affinity of TIAR to a U-rich [a poly(U) stretch comprising 17 U residues flanked by G residues] RNA compared with this C-rich RNA in vitro. We prepared recombinant TIAR proteins comprising two or three of its N-terminal RRM domains (TIAR12 and TIAR123, respectively), as previously described (10). We also prepared a recombinant protein comprising the N-terminal two RRMs of HuR (HuR12) to serve as a positive control for binding to the U-rich RNA and negative control for binding to the C-rich RNA (Fig. 2).

We investigated the ability of these proteins to bind to the U-rich 28-mer RNA using SPR. This methodology allowed not only a qualitative indication of binding but also a comparative measure of on rates, off rates, and overall affinities to the RNA tethered to a chip via its 5′ end. The sensorgrams in Fig. 3 (top) show the binding of a range of concentrations of HuR12, TIAR123, and TIAR12 when injected across the U-rich RNA-coated chip. The on rates, off rates and overall affinities (equilibrium dissociation constant [K_D]) for each protein, as approximated using a simple Langmuir binding model, are listed in Table 2. As shown, all three proteins bound the U-rich RNA. HuR12 bound with a K_D in the nM range, with both high on and off rates. This finding is in keeping with previous SPR studies of HuD proteins binding to AU-rich sequences,

wherein HuD12 bound with a K_D of 5.4 nM to a 38-mer and a K_D of 15.3 nM to a 13-mer (35, 36).

The TIAR proteins also bound to the U-rich RNA with a K_D in the nM range (TIAR123 K_D, ~1 nM; TIAR12 K_D, ~0.7 nM). These proteins showed slower on and off rates compared with HuR12, reflecting an intrinsically different and potentially more complex process of association and dissociation with the RNA. These findings are also reflected in the imperfect fit of the data by a simple 1:1 Langmuir interaction model and suggest that the K_D values may only be accurate to within an order of magnitude. These affinities are in keeping with those measured previously using nitrocellulose filter-binding assays, which showed binding affinities for poly(U) of 8 nM, 20 nM, and 40 nM by TIAR, TIAR123, and TIAR12, respectively (10). The similar binding properties of TIAR12 compared with TIAR123 also suggest, as previously noted (10), that the primary poly(U) binding contact is made by the first two RRMs of TIAR.

TIAR, but not HuR, binds the C-rich RNA motif. To test if TIAR was able to bind to the newly identified C-rich RNA motif, an RNA sequence was designed by choosing the most frequent nucleotide present at each position within the probability matrix (Fig. 1A). SPR was used to examine the binding kinetics of recombinant HuR and TIAR proteins to this sequence in comparison with the binding seen for the U-rich sequence. The sensorgrams in Fig. 3 (bottom) show the binding of HuR12, TIAR123, and TIAR12 when injected across the C-rich RNA-coated chip. There was no evidence of an interaction between HuR12 and the C-rich RNA, consistent with the known specificity of HuR for U- and AU-rich sequences and demonstrating that the experimental conditions of SPR employed here did not allow the occurrence of nonspecific interactions. In contrast, TIAR proteins were able to bind the C-rich RNA, confirming that this is a bona fide, novel TIAR target sequence. On rates, off rates, and overall affinities (K_D) are indicated in Table 2. TIAR123 and TIAR12 bound the C-rich RNA with nM affinities (~135 and ~56 nM, respectively). These values represent significant binding affinities, although they are approximately 100-fold weaker than TIAR protein binding to the U-rich RNA.
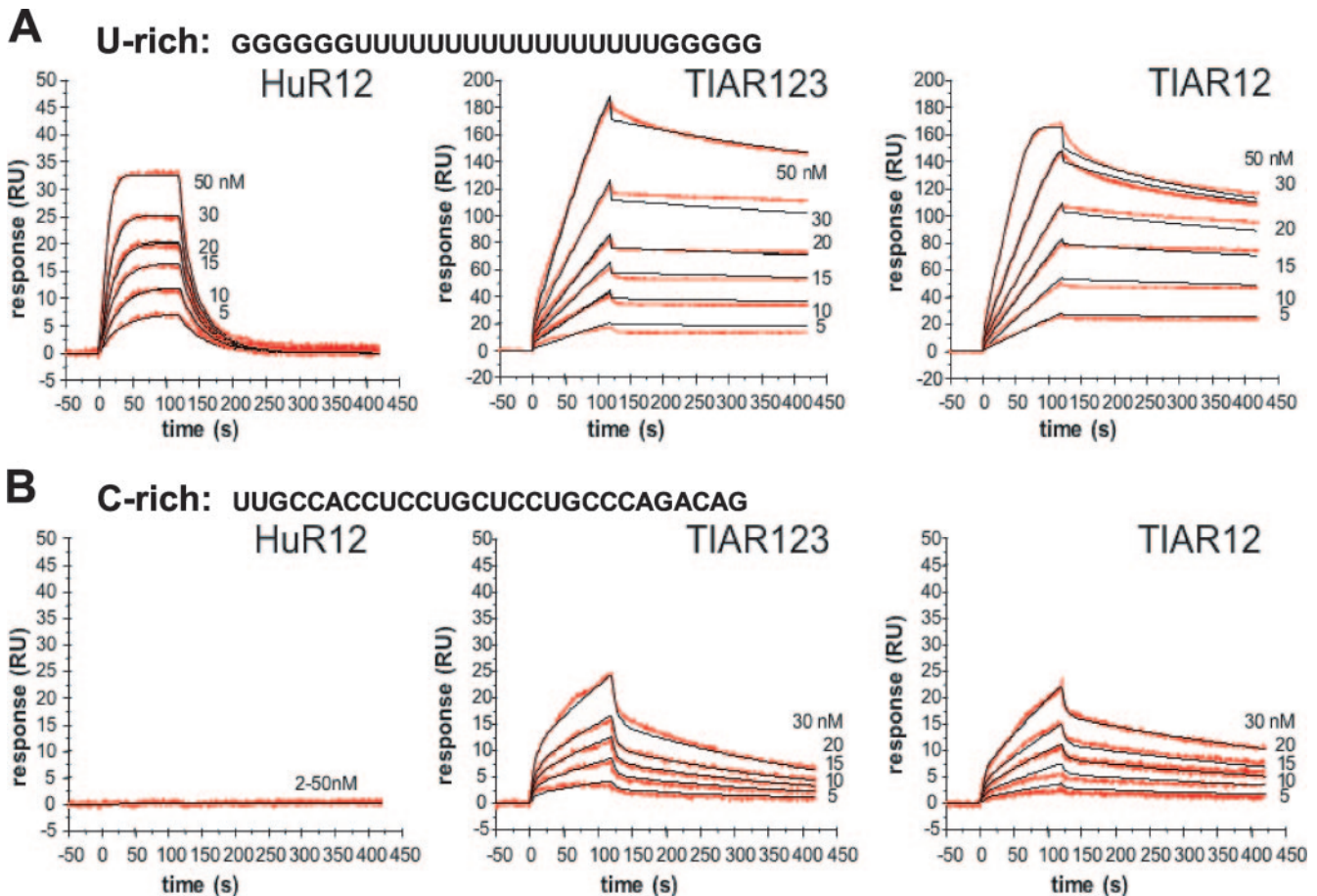
FIG. 3. Kinetic analysis of the interactions of TIAR12, TIAR123, and HuR12 proteins with U-rich and C-rich RNAs. The binding of TIAR123, TIAR12, and HuR12 to a U-rich or a C-rich RNA (28-mer each) is shown. Biotinylated RNA was captured on SA-coated sensor chips, and increasing concentrations of protein were injected over the surface. Injections were performed for 120 s (association phase), followed by a 300-s flow of running buffer to assess dissociation. The experiments were conducted in duplicate and showed good overlap. The red lines represent the binding responses for injections of protein analyte at specified concentrations (nM) over the RNA surface. The kinetic data were fit by a 1:1 Langmuir binding model which describes monovalent analyte binding to a single site on the immobilized ligand. Mass transport effects were not evident. The black curves superimposed on top of the sensorgrams represent the model fitted curves. The association and dissociation rate constants (K_a and K_d, respectively) were determined simultaneously as global fitting parameters from which K_D was determined. The resulting parameter values are given in Table 2.

Functional analysis of the C-rich motif using heterologous reporter assays. The functional role of the C-rich motif present in a given transcript was first tested by using reporter vectors in cells that expressed different levels of TIAR. Depicted in Fig. 4A are three plasmids that were engineered to express the EGFP reporter from chimeric mRNAs that also contained either the GAPDH 3′UTR (pEGFP-GAPDH), the GAPDH 3′UTR with one embedded copy of the consensus C-rich motif (pEGFP-Motif), or the APAF1 3′UTR (one of the TIAR target transcripts), including one hit of the C-rich motif (pEGFP-APAF1). HeLa cells were transfected with siRNAs that effectively silenced the endogenous TIAR (Fig. 4B) and were subsequently transfected with the EGFP reporter constructs. As shown in Fig. 4B, silencing of TIAR potently elevated (~10-fold) EGFP expression from the EGFP reporter bearing the C-rich motif (pEGFP-Motif transfection group) and also induced EGFP expression (approximately threefold) from the EGFP reporter bearing the APAF1 3′UTR and its C-rich motif hit (pEGFP-APAF1 transfection group), but it

did not significantly increase EGFP levels in cells transfected with pEGFP-GAPDH. These changes in EGFP expression did not arise from changes in the levels of the corresponding transcripts, as EGFP mRNA was essentially unchanged in the various transfection groups (Fig. 4C). These data strongly support the view that TIAR suppressed the translation of a transcript bearing the C-rich motif, thereby reducing the expression levels of the encoded protein.

Identification of novel TIAR target transcripts containing the C-rich TIAR motif. We used the C-rich TIAR motif to query transcript databases for additional putative TIAR target mRNAs. A total of 2,209 transcripts were identified from the UniGene database (2.0% of the complete database); a subset of transcripts is presented in Table 3, along with the positions of the individual TIAR motif hits within the 3′UTR. Each motif hit was assigned a score (in parentheses), a value that reflects the degree to which each particular motif matches the TIAR motif model (Fig. 1A).

To test whether the C-rich motif could be used to identify

TABLE 2. Kinetic and affinity constants for the interactions of TIAR123, TIAR12, and HuR12 proteins with U-rich and C-rich RNAs[a]

Protein	RNA	K_a (1/M^{-1} s^{-1})	K_d (1/s)	K_D (K_d/K_a [nM])
HuR12	U rich	$(1.29 \pm 0.01) \times 10^8$	4.35 ± 0.03	33.73 ± 0.50
TIAR123	U rich	$(1.58 \pm 0.02) \times 10^6$	$(1.56 \pm 0.01) \times 10^{-3}$	0.99 ± 0.02
	C rich	$(2.72 \pm 0.03) \times 10^4$	$(36.78 \pm 0.12) \times 10^{-4}$	135.2 ± 1.93
TIAR12	U rich	$(4.10 \pm 0.11) \times 10^6$	$(2.83 \pm 0.08) \times 10^{-3}$	0.69 ± 0.04
	C rich	$(3.48 \pm 0.04) \times 10^4$	$(19.64 \pm 0.06) \times 10^{-4}$	56.39 ± 0.79

[a] The association and dissociation rate constants (K_a and K_d) were determined as global fitting parameters for a 1:1 binding model. The equilibrium dissociation constant, K_D, was determined as K_d/K_a.
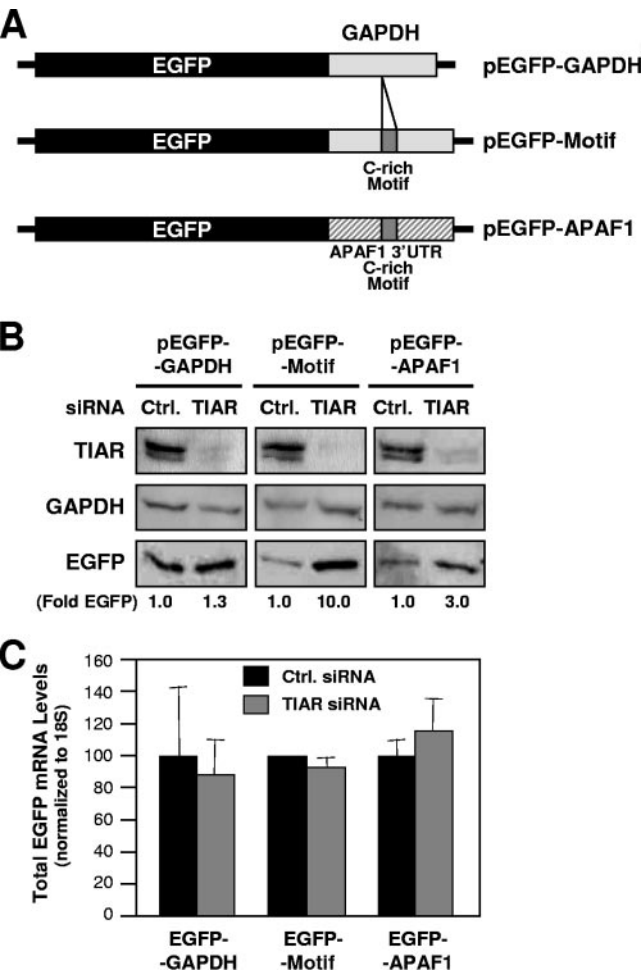

FIG. 4. Functional assessment of the C-rich motif using a heterologous reporter. (A) Plasmid pEGFP-GAPDH contains a 200-bp fragment of the GAPDH 3′UTR after the EGFP coding region; plasmid pEGFP-APAF1 contains nucleotide positions 5401 to 5825 of APAF1 (NM_013229), including one hit of the APAF1 3′UTR C-rich motif (positions 5599 to 5626); plasmid pEGFP-Motif contains a 28-bp insert (the consensus C-rich motif) within the GAPDH 3′UTR (Materials and Methods). (B) Western blot analysis of TIAR, loading control GAPDH, and reporter protein EGFP expression levels in RKO cells that had been transfected 48 h earlier with either control (Ctrl.) or TIAR-directed siRNAs. Signals (representative of five independent experiments) were quantified by densitometry and shown as EGFP levels (fold) in TIAR siRNA compared with control siRNA. (C) The levels of chimeric EGFP-GAPDH, EGFP-APAF1, and EGFP-Motif mRNAs were measured in each transfection group (B) by RT-qPCR analysis. Data are shown as the means and standard errors of the mean of three independent experiments.

TIAR target mRNAs computationally, we monitored the presence of putative target mRNAs in immunoprecipitated TIAR-RNP complexes. Using gene-specific primers, we evaluated the abundance of 12 predicted and randomly selected TIAR target mRNAs by RT followed by qPCR. Indeed, all 12 transcripts (10 shown in Fig. 5A [CAMKK2 and HIP1R not shown]) appeared to be bona fide targets of TIAR, as they were found to be enriched in TIAR IP material compared with IgG IP material (time zero); the degrees of enrichment ranged from just over twofold for RPL34 and MMP25 mRNAs to greater than sevenfold for PABPN1 mRNA. With the same experimental approach, we further sought to determine whether the abundance of such putative RNP complexes would be affected by treatment with short-wavelength UV light (UVC), a genotoxic agent that was previously found to increase binding of TIAR to a subset of mRNAs (32). To our surprise, however, treatment with 25 J/m^2 UVC significantly reduced the association of these mRNAs with TIAR, as their abundance in the TIAR IP material was markedly diminished following exposure to UVC (with few exceptions, such as NK4 at 6 h after UVC). Importantly, negative controls 18S rRNA and housekeeping GAPDH and UBC mRNAs showed negligible enrichment in TIAR IPs relative to IgG IPs; these non-TIAR target RNAs bound the beads and IP reagents in a nonspecific fashion and served to monitor the even input of the samples (Fig. 5A, Neg.). In addition, the binding of MYC mRNA was tested as a positive control, since TIAR-MYC mRNA complexes were previously shown to increase following UVC irradiation (32); in keeping with these earlier findings, MYC mRNA showed strikingly increased binding to TIAR at 1 and 3 h after UVC treatment (Fig. 5A, Pos.).

The reductions in RNPs comprising TIAR and mRNAs bearing the C-rich motif did not simply reflect changes in the total levels of these cellular mRNAs for two reasons. First, by the RNP IP assay, global reductions in mRNA are reflected in binding both in the IgG IP and the TIAR IP, so by measuring mRNA enrichment, such differences would already be accounted for. Second, individual testing of each of the transcripts in whole-cell RNA preparations showed that UVC elicited modest or no changes in the levels of most mRNAs, as shown in Fig. 5B; only whole-cell APAF1 and TCF3 mRNA levels were reduced to about one-third and one-half of their original abundance, respectively.

Finally, we tested the expression levels of proteins encoded by four TIAR target mRNAs. Three of the proteins encoded by dissociation target mRNAs (PXN, EIF5A, and APAF1) were readily detectable (TCF3 could not be detected with the

TABLE 3. Putative TIAR target mRNAs bearing the C-rich signature motif in the 3′UTR[a]

Position(s) in 3′UTR[b]	Name	Symbol	Unigene no.
1445–1472 (0.58), 2180–2207 (3.38), 2630–2659 (1.56)	Sideroflexin 5	SFXN5	Hs#S4546027
1087–1115 (0.85), 1430–1457 (2.60), 1461–1488 (1.50), 1585–1612 (0.24)	Ras-related protein Rab-40C	RAB40C	Hs#S4044974
190–217 (3.95)	Ribosomal protein L34	RPL34	Hs#S3940107
250–277 (3.60)	Calcium-dependent protein kinase IG	CAMK1G	Hs#S3619658
206–235 (1.30)	Homolog of mouse LGP1	LGP1	Hs#S3619636
172–200 (1.14)	Myosin, heavy polypeptide 9, non-muscle	MYH9	Hs#S3220052
1392–1419 (3.55)	Microtubule-associated proteins 1A/1B light-chain 3B	MAP1LC3B	Hs#S3219949
770–797 (3.12)	Matrix metalloproteinase 25	MMP25	Hs#S3219838
683–710 (1.53)	Junctophilin 3	JPH3	Hs#S3219743
135–164 (0.89), 556–583 (2.38)	Phospholysine phospho-His inorganic pyrophosphate phosphatase	LHPP	Hs#S3219695
62–89 (3.63)	Prostate and breast cancer overexpressed 1	PBOV1	Hs#S3219375
140–167 (1.16)	Potassium inwardly-rectifying channel, J11	KCNJ11	Hs#S3218881
828–853 (2.14)	Solute carrier family 2 (facilitated glucose transporter), member 6	SLC2A6	Hs#S2294542
284–308 (2.73)	Sphingosine kinase 2	SPHK2	Hs#S2294536
2014–2041 (3.10)	Ring finger protein 144	RNF144	Hs#S2139432
1472–1501 (0.04), 2649–2677 (0.59), 3189–3216 (2.93)	Protein phosphatase 1F	PPM1F	Hs#S2139385
1308–1335 (3.66)	Apoptotic protease-activating factor	APAF1	Hs#S2138799
1839–1866 (1.31)	ATPase, (Na$^+$)/K$^+$-transporting, beta 4 polypeptide	ATP1B4	Hs#S1824340
431–459 (3.68)	Poly(A) binding protein, nuclear 1	PABPN1	Hs#S1732404
318–345 (4.38)	Interleukin-24	IL-24	Hs#S1732294
194–222 (1.53)	Growth factor, augmenter of liver regeneration (ERV1 homolog)	GFER	Hs#S1732174
975–1002 (3.31)	Mitogen-activated protein kinase kinase kinase 14	MAP3K14	Hs#S1731892
287–314 (4.38)	Polyamine-modulated factor 1	PMF1	Hs#S1731724
1013–1040 (3.21)	Huntingtin-interacting protein 1-related	HIP1R	Hs#S15639035
67–96 (0.38), 276–303 (3.80), 347–372 (0.24), 511–538 (2.12), 745–771 (1.33)	Histamine receptor H3	HRH3	Hs#S1731688
13–40 (1.34)	Neuro-oncological ventral antigen 2	NOVA2	Hs#S1731549
109–136 (3.34), 227–254 (0.17), 956–983 (2.38), 2107–2134 (0.23)	SRY (sex-determining region Y)-box 12	SOX12	Hs#S1731519
1554–1583 (4.23), 2449–2476 (0.27)	Calcium-dependent protein kinase 2	CAMKK2	Hs#S1731273
1218–1246 (1.31), 1960–1985 (0.80)	NK3 transcription factor related, locus 1 (*Drosophila*)	NKX3-1	Hs#S1730286
101–128 (1.05), 859–886 (3.75)	Signal-regulatory protein beta 1	SIRPB1	Hs#S1730130
240–267 (1.12)	Brain-specific angiogenesis inhibitor 1	BAI1	Hs#S1729737
311–337 (0.99), 625–653 (0.78), 4921–4948 (0.95), 5654–5681 (2.12), 5818–5845 (1.25)	Methyl CpG binding protein 2	MECP2	Hs#S1729484
809–836 (3.48)	Vanin 1	VNN1	Hs#S1729359
51–78 (5.63), 660–689 (1.89), 785–812 (0.14), 841–868 (0.21), 3296–3326 (0.02), 3504–3531 (0.06)	Synaptogyrin 1	SYNGR1	Hs#S1729312
1501–1528 (2.31)	Eukaryotic translation termination factor 1	ETF1	Hs#S1729236
155–182 (3.63)	Natural killer cell transcript 4	NK4	Hs#S1729141
357–384 (0.21), 773–801 (1.95), 1094–1125 (0.04)	Paired box gene 2, transcript variant c	PAX2	Hs#S1728525
330–358 (0.76), 2112–2139 (0.62), 2211–2240 (2.46)	Major histocompatibility complex class II transactivator	MHC2TA	Hs#S1728490
55–82 (2.12)	Alpha-L-iduronidase precursor	IDUA	Hs#S1728450
52–82 (3.79)	Tu translation elongation factor	TUFM	Hs#S1728121
663–690 (2.37)	Transforming growth factor, beta receptor III	TGFBR3	Hs#S1728020
290–317 (1.16)	Syntrophin, alpha 1	SNTA1	Hs#S1727897
962–988 (1.34)	Regulator of G-protein signaling 16	RGS16	Hs#S1727647
16–43 (3.16)	RAB3B, member RAS oncogene family	RAB3B	Hs#S1727591
525–552 (0.73), 999–1027 (0.27), 1322–1351 (1.05)	Paxillin	PXN	Hs#S1727580
1734–1761 (1.44), 2017–2042 (1.56)	Oligophrenin 1	OPHN1	Hs#S1727255
464–491 (1.12)	Eukaryotic translation initiation factor 5	EIF5A	Hs#S1726700
782–810 (1.95)	C-terminal PDZ domain ligand of neuronal NOS	CAPON	Hs#S15898574
32–59 (3.12)	Transcription factor 3	TCF3	Hs#S11062708

[a] Shown is a partial list of genes bearing the C-rich signature motif in the 3′UTR of the corresponding transcripts. (The complete list of predicted target transcripts is available from the authors.)
[b] The relative positions of the C-rich TIAR motif within each transcript and the corresponding scores (in parentheses) are indicated.
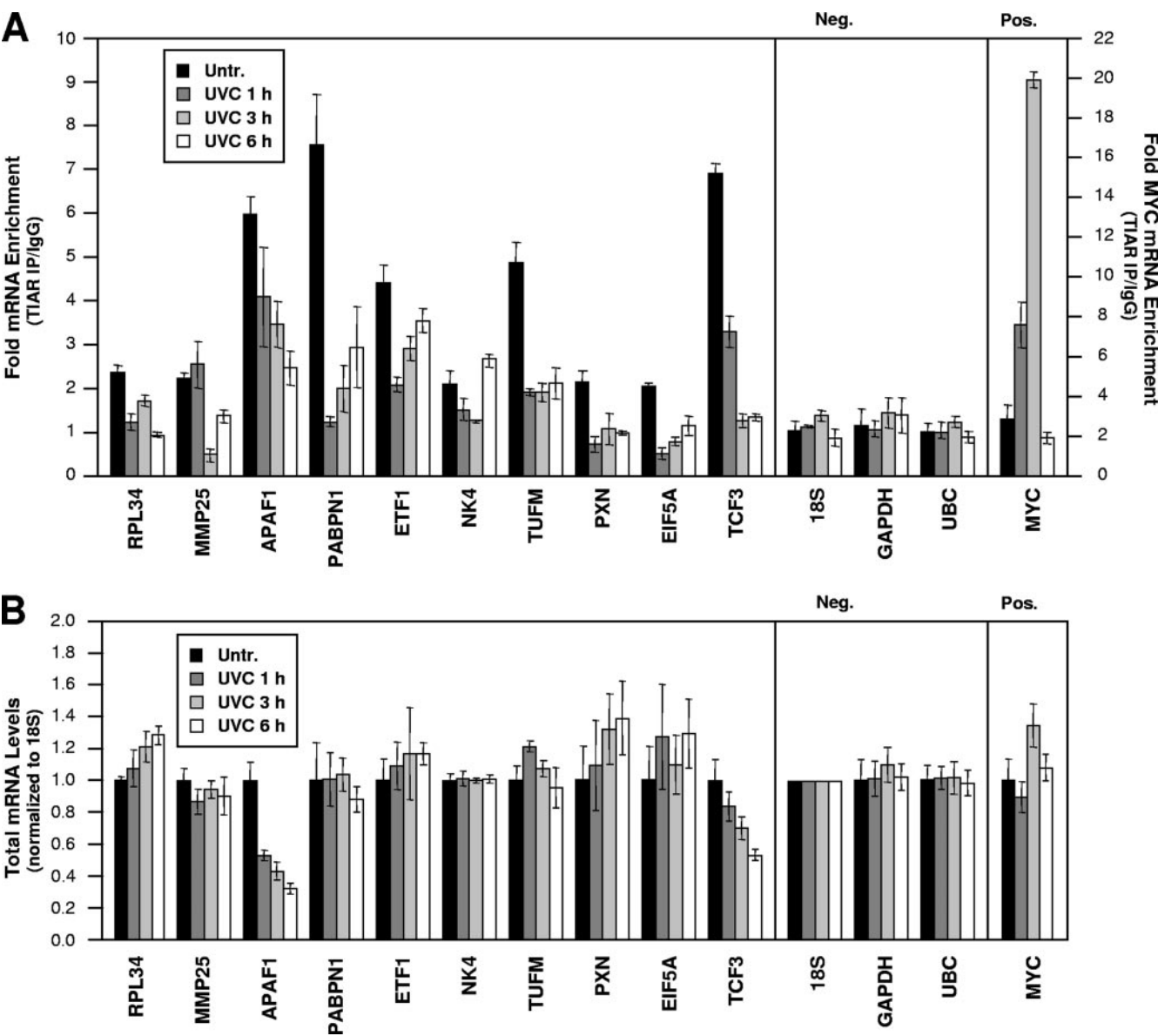
FIG. 5. Analysis of the binding and whole-cell levels of predicted TIAR target mRNAs in untreated and UVC-irradiated cells. (A) The association of endogenous TIAR with endogenous putative target mRNAs was tested using lysates prepared from RKO cells that were either left without treatment (Untr. [0 h]) or were irradiated with 25 J/m² UVC and collected 1, 3, or 6 h afterwards. Anti-TIAR or IgG antibodies were used in IP reactions followed by the analysis of predicted target transcripts by RT-qPCR analysis of the IP material. Neg., negative control transcripts 18S rRNA and housekeeping GAPDH and UBC mRNAs; Pos., positive control MYC mRNA, a known TIAR target (32). Numbers on the right *y* axis indicate MYC mRNA enrichment (TIAR/IgG). (B) Total RNA was extracted from cells that were processed as described for panel A. The whole-cell levels of each mRNA were calculated and normalized to 18S rRNA levels. Data show means and standard deviations (A and B).

antibodies available). While the levels of TIAR itself remained unchanged following UVC irradiation (Fig. 6A), the levels of PXN, EIF5A, and APAF1 were markedly elevated following UVC irradiation, in agreement with the view that TIAR repressed their expression (Fig. 6B). Of note, the steady-state levels of these mRNAs either remained unchanged (PXN and EIF5A) or were actually reduced (APAF1), as shown in Fig. 5B. As a positive control, MYC expression was tested, as UVC stress was previously shown to increase TIAR-MYC mRNA association and to decrease MYC translation and protein lev-

els (Fig. 5A) (32); here, MYC protein abundance was also reduced potently following UVC irradiation (Fig. 6B). Evidence that TIAR contributed to these changes in protein expression was obtained through silencing experiments. As shown by Western blot analysis in Fig. 6C, PXN, EIF5A, and APAF1 abundance increased in RKO cells that expressed reduced TIAR levels (by TIAR siRNA transfection). Combined UVC irradiation and TIAR silencing did not further elevate the expression of these proteins, supporting the view that both interventions shared common mechanisms of action.
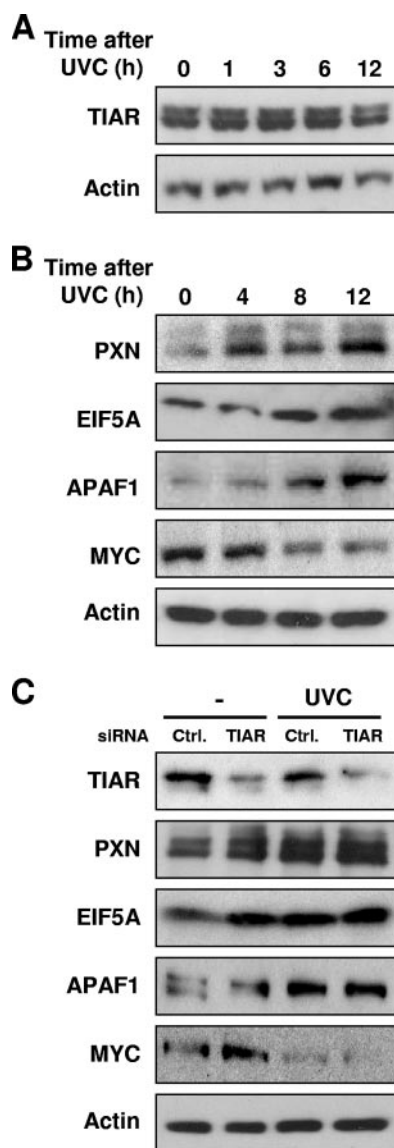
FIG. 6. Expression levels of proteins encoded by predicted TIAR target mRNAs in untreated and UVC-irradiated RKO cells. (A) Western blot analysis of TIAR expression levels in whole-cell lysates (15 μg per lane) that were prepared at the times indicated after UVC irradiation. (B) Western blot analysis of the expression levels of PXN, EIF5A, and APAF1 (encoded by TIAR dissociation target mRNAs), positive control MYC, and loading control β-actin. Whole-cell lysates (10 μg per lane) were prepared at the times shown following UVC irradiation. Shown are representative Western blots from three independent experiments. (C) Western blot analysis of the expression of TIAR, PXN, EIF5A, APAF1, MYC, and β-actin in cells that were transfected with either control (Ctrl.) or TIAR siRNAs. Forty-eight hours later, cells were left untreated or treated with UVC and collected after an additional 8 h. Data are representative of three independent experiments.

DISCUSSION

A C-rich motif is bound by TIAR RRMs in vitro and functions to suppress translation in the presence of TIAR in vivo. We report the identification of a C-rich signature motif present in TIAR target mRNAs. The C-rich motif was unexpectedly distinct from the U-rich target sequence we previously reported for TIAR-bound mRNAs (10). In keeping with these

earlier findings, TIAR proteins containing two or three RRM domains (TIAR12 and TIAR123, respectively) bound with high affinity to a U-rich sequence containing a stretch of 17 uracils; however, they also bound, albeit with 50- to 100-fold-less affinity, to the C-rich motif, as measured by SPR (Fig. 3). TIAR123 and TIAR12 bound to the C-rich sequence with K_Ds in the nanomolar range, representing a significant binding affinity of TIAR for the C-rich motif. These results demonstrate that TIAR binding to RNA may not be restricted to a single class of target motif. Besides serving as a target sequence for TIAR, the C-rich motif had a significant functional role, as revealed by using a chimeric reporter construct that comprised the EGFP coding region linked to the GAPDH 3′UTR. Insertion of the consensus C-rich motif in the GAPDH 3′UTR strongly reduced the expression of the heterologous reporter EGFP (Fig. 4). The C-rich sequence (the consensus motif or the motif hit within the APAF1 3′UTR) specifically suppressed the translation of the reporter construct without affecting reporter mRNA levels; this regulation was TIAR dependent, since silencing of TIAR restored reporter protein production.

Endogenous TIAR forms complexes with endogenous mRNAs. The collection of UniGene transcripts that were predicted to be TIAR targets based on the presence of at least one hit of the C-rich motif was then studied. (A subset of predicted target transcripts is listed in Table 2.) Following TIAR RNP IP analysis and RT-qPCR identification of individual mRNAs present in TIAR RNP complexes, all of the transcripts chosen randomly among this collection were found to be enriched in the TIAR RNP IP material relative to IgG IP; no predicted targets were found not to be enriched (Fig. 5). These observations reveal that in addition to the binding of recombinant purified TIAR to the C-rich motif in vitro, endogenous TIAR was also found in association with endogenous mRNAs bearing the C-rich motif. These results underscore the usefulness of the C-rich motif in predicting TIAR target mRNAs.

It was interesting to discover that UVC irradiation triggered a reduction in binding of TIAR to all of the mRNA targets bearing the C motif (Fig. 5A). This finding suggested that the C-rich signature motif identifies mRNAs which will dissociate from TIAR following UVC treatment and possibly other forms of cell damage. Along with the reduced association of TIAR with C-rich target transcripts (PXN, EIF5A, and APAF1), we documented a sizeable increase in the expression of the encoded proteins following UVC irradiation (Fig. 6). In support of the notion that TIAR contributed to this increase, silencing of TIAR alone similarly elevated the expression levels of these proteins, an effect that recapitulated the regulation of the chimeric reporters (Fig. 4). At this time, the magnitude or kinetics of TIAR-mRNA association/dissociation do not appear to correlate with either score values or the number of motif hits on a given target transcript (not shown), although further analysis of these parameters is warranted. As these studies move forward, it will also be interesting to examine whether the coordinate regulation of subsets of C-rich motif-bearing mRNAs elicits a particular phenotype. This task will be complex, since >2,000 transcripts bearing the C-rich motif have been identified (Table 3 [complete list available from the authors]) and the encoded proteins participate in a broad range of cellular functions. We will first focus our attention on

C-rich motif-bearing targets implicated in the stress response, particularly those that influence cell survival and proliferation.

The reduced binding of TIAR to these target transcripts was in contrast to the results obtained earlier when testing other TIAR target transcripts, particularly those encoding translation-modulatory proteins such as translation regulatory factors EIF4A1, EIF4E2, and EEF1B2, as well as MYC (which transcriptionally upregulates the expression of translation regulatory proteins) (32). In that investigation, binding of TIAR to target mRNAs increased following UVC irradiation, in turn causing a reduction in the expression of those translation regulators and contributing to an overall reduction in protein biosynthesis following UVC treatment. None of the TIAR-bound mRNAs encoding translational regulators was found to have the C-rich motif, in agreement with the idea that the C-rich motif is present in a different subset of mRNAs. Based on these observations, we postulate the existence of a different signature motif on TIAR target mRNAs that would instead signal increased association after cellular stress. Our efforts to identify such a signature motif have led to the preliminary identification of a shared sequence containing a stretch of U residues (see Fig. S1 in the supplemental material) flanked by C residues, similar to what was found by SELEX analysis (10). Studies are under way to test if this U-rich motif is a bona fide recognition sequence for TIAR. Should the U-rich motif be validated by testing recombinant and endogenous target transcripts, then further investigation will assess whether binding of TIAR to mRNAs bearing the U-rich motif increases following exposure to stimuli such as UVC and will examine its influence upon the expression of mRNAs in which it is present.

Multiple RNA target motifs for a given RBP? If indeed the C-rich RNA sequence represents a "TIAR dissociation motif" which signals decreased mRNA association with TIAR after stress, it is conceivable that multiple motifs exist which can direct either increased or decreased TIAR binding to mRNAs after cellular damage. Moreover, signature motifs may exist to guide binding of TIAR (or for that matter, also other RBPs), depending on cellular energy levels, tissue type, proliferation status, subcellular locale, etc. A comprehensive elucidation of the group of TIAR motifs and their functional characteristics will require the development of more sophisticated analysis methods. The TIAR binding properties studied here are also likely to be influenced by UVC-triggered changes, including alterations in its subcellular localization (e.g., stress granules) (2); posttranslational modifications (e.g., by phosphorylation) (18); interactions with chaperones such as heat shock protein 70 (HSP70) (15); or interactions with other proteins that alter its RNA-binding properties, as recently reported for SRC-3, a nuclear transcriptional activator that also functions as a cytoplasmic activator of TIA-1/TIAR (3, 45). Whether UVC affects any of these potential modulators of TIAR activity remains to be addressed experimentally. Other regulatory schemes that merit consideration also await further testing. For example, microRNAs or other RBPs could preferentially facilitate or hinder the binding of TIAR to a target mRNA in cells exposed to stress agents; notably among these, RBPs with preference for C-rich RNA motifs (such as hnRNP K and PCBP1 to -4/αCP1 to -4 [reviewed in references 13 and 30]) might be anticipated to compete for binding, particularly since they have been implicated in regulating the translation of target tran-

scripts and their function is modulated by stress (reviewed in reference 30).

Individual examples of RBPs dissociating from a target mRNA in response to a stimulus have been reported: for instance, TIAR was recently shown to dissociate from GADD45α mRNA following exposure to the alkylating agent methylmethane sulfonate (25). To our knowledge, however, this is the first study to identify an RNA motif that defines a subset of mRNAs which dissociate from an RBP in response to a stimulus. Broadly speaking, our findings illustrate the existence of an additional layer of posttranscriptional gene regulation for a given mRNA, in agreement with the "RNA regulon" model, whereby collections of mRNAs are coordinately regulated at the posttranscriptional level by specific RBPs (recently reviewed in reference 22). In addition to the interplay between *trans* factors (RBPs and microRNAs) acting upon the transcript, the influence of the subcellular environment, and the conditions of cellular growth at a given time, the specific mRNA sequence can also dictate the dynamic association of RBPs and hence the composition of the RNP and its posttranscriptional fate.

REFERENCES

1. **Anderson, P., and N. Kedersha.** 2002. Stressful initiations. J. Cell Sci. **115:**3227–3234.
2. **Anderson, P., and N. Kedersha.** 2002. Visibly stressed: the role of eIF2, TIA-1, and stress granules in protein translation. Cell Stress Chaperones **7:**213–221.
3. **Anderson, P., and N. Kedersha.** 2007. On again, off again: the SRC-3 transcriptional coactivator moonlights as a translational corepressor. Mol. Cell **25:**796–797.
4. **Antic, D., and J. D. Keene.** 1997. Embryonic lethal abnormal visual RNA-binding proteins involved in growth, differentiation, and posttranscriptional gene expression. Am. J. Hum. Genet. **61:**273–278.
5. **Antic, D., N. Lu, and J. D. Keene.** 1999. ELAV tumor antigen, Hel-N1, increases translation of neurofilament M mRNA and induces formation of neurites in human teratocarcinoma cells. Genes Dev. **13:**449–461.
6. **Brennan, C. M., and J. A. Steitz.** 2001. HuR and mRNA stability. Cell Mol. Life Sci. **58:**266–277.
7. **Carballo, E., W. S. Lai, and P. J. Blackshear.** 1998. Feedback inhibition of macrophage tumor necrosis factor-α production by tristetraprolin. Science **281:**1001–1005.
8. **Cok, S. J., S. J. Acton, and A. R. Morrison.** 2003. The proximal region of the 3′-untranslated region of cyclooxygenase-2 is recognized by a multimeric protein complex containing HuR, TIA-1, TIAR, and the heterogeneous nuclear ribonucleoprotein U. J. Biol. Chem. **278:**36157–36162.
9. **Colegrove-Otero, L. J., A. Devaux, and N. Standart.** 2005. The *Xenopus* ELAV protein ElrB represses Vg1 mRNA translation during oogenesis. Mol. Cell. Biol. **25:**9028–9039.
10. **Dember, L. M., N. D. Kim, K. Q. Liu, and P. Anderson.** 1996. Individual RNA recognition motifs of TIA-1 and TIAR have different RNA binding specificities. J. Biol. Chem. **271:**2783–2788.
11. **Derrigo, M., A. Cestelli, G. Savettieri, and I. Di Liegro.** 2000. RNA-protein interactions in the control of stability and localization of messenger RNA. Int. J. Mol. Med. **5:**111–123.
12. **Forch, P., and J. Valcarcel.** 2001. Molecular mechanisms of gene expression regulation by the apoptosis-promoting protein TIA-1. Apoptosis **6:**463–468.
13. **Gamarnik, A. V., and R. Andino.** 2000. Interactions of viral protein 3CD and poly(rC) binding protein with the 5′ untranslated region of the poliovirus genome. J. Virol. **74:**2219–2226.
14. **Gueydan, C., L. Droogmans, P. Chalon, G. Huez, D. Caput, and V. Kruys.**

1999. Identification of TIAR as a protein binding to the translational regulatory AU-rich element of tumor necrosis factor α mRNA. J. Biol. Chem. **274:**2322–2326.

15. **Gilks, N., N. Kedersha, M. Ayodele, L. Shen, G. Stoecklin, L. M. Dember, and P. Anderson.** 2004. Stress granule assembly is mediated by prion-like aggregation of TIA-1. Mol. Biol. Cell **15:**5383–5398.

16. **Holcik, M., and N. Sonenberg.** 2005. Translational control in stress and apoptosis. Nat. Rev. Mol. Cell Biol. **6:**318–327.

17. **Hollams, E. M., K. M. Giles, A. M. Thomson, and P. J. Leedman.** 2002. mRNA stability and the control of gene expression: implications for human disease. Neurochem. Res. **27:**957–980.

18. **Izquierdo, J. M., and J. Valcarcel.** 2007. Fas-activated serine/threonine kinase (FAST K) synergizes with TIA-1/TIAR proteins to regulate Fas alternative splicing. J. Biol. Chem. **282:**1539–1543.

19. **Kandasamy, K., K. Joseph, K. Subramaniam, J. R. Raymond, and B. G. Tholanikunnel.** 2005. Translational control of beta2-adrenergic receptor mRNA by T-cell-restricted intracellular antigen-related protein. J. Biol. Chem. **280:**1931–1943.

20. **Kedersha, N., and P. Anderson.** 2002. Stress granules: sites of mRNA triage that regulate mRNA stability and translatability. Biochem. Soc. Trans. **30:**963–969.

21. **Kedersha, N., G. Stoecklin, M. Ayodele, P. Yacono, J. Lykke-Andersen, M. J. Fitzler, D. Scheuner, R. J. Kaufman, D. E. Golan, and P. Anderson.** 2005. Stress granules and processing bodies are dynamically linked sites of mRNP remodeling. J. Cell Biol. **169:**871–884.

22. **Keene, J. D.** 2007. RNA regulons: coordination of post-transcriptional events. Nat. Rev. Genet. **8:**533–543.

23. **Kullmann, M., U. Gopfert, B. Siewe, and L. Hengst.** 2002. ELAV/Hu proteins inhibit p27 translation via an IRES element in the p27 5′UTR. Genes Dev. **16:**3087–3099.

24. **Lal, A., T. Kawai, X. Yang, K. Mazan-Mamczarz, and M. Gorospe.** 2005. Antiapoptotic function of RNA-binding protein HuR effected through prothymosin alpha. EMBO J. **24:**1852–1862.

25. **Lal, A., K. Abdelmohsen, R. Pullmann, T. Kawai, S. Galban, X. Yang, G. Brewer, and M. Gorospe.** 2006. Posttranscriptional derepression of GADD45alpha by genotoxic stress. Mol. Cell **22:**117–128.

26. **Le Guiner, C., F. Lejeune, D. Galiana, L. Kister, R. Breathnach, J. Stevenin, and F. Del Gatto-Konczak.** 2001. TIA-1 and TIAR activate splicing of alternative exons with weak 5′ splice sites followed by a U-rich stretch on their own pre-mRNAs. J. Biol. Chem. **276:**40638–40646.

27. **Loflin, P., C. Y. Chen, and A.-B. Shyu.** 1999. Unraveling a cytoplasmic role for hnRNP D in the in vivo mRNA destabilization directed by the AU-rich element. Genes Dev. **13:**1884–1897.

28. **López de Silanes, I., S. Galbán, J. L. Martindale, X. Yang, K. Mazan-Mamczarz, F. E. Indig, G. Falco, M. Zhan, and M. Gorospe.** 2005. Identification and functional outcome of mRNAs associated with RNA-binding protein TIA-1. Mol. Cell. Biol. **25:**9520–9531.

29. **López de Silanes, I., M. Zhan, A. Lal, X. Yang, and M. Gorospe.** 2004. Identification of a target RNA motif for RNA-binding protein HuR. Proc. Natl. Acad. Sci. USA **101:**2987–2992.

30. **Makeyev, A. V., and S. A. Liebhaber.** 2002. The poly(C)-binding proteins: a multiplicity of functions and a search for mechanisms. RNA **8:**265–278.

31. **Mazan-Mamczarz, K., S. Galban, I. López de Silanes, J. L. Martindale, U. Atasoy, J. D. Keene, and M. Gorospe.** 2003. RNA-binding protein HuR enhances p53 translation in response to ultraviolet light irradiation. Proc. Natl. Acad. Sci. USA **100:**8354–8359.

32. **Mazan-Mamczarz, K., A. Lal, J. L. Martindale, T. Kawai, and M. Gorospe.** 2006. Translational repression by RNA-binding protein TIAR. Mol. Cell. Biol. **26:**2716–2727.

33. **Meng, Z., P. H. King, L. B. Nabors, N. L. Jackson, C. Y. Chen, P. D. Emanuel, and S. W. Blume.** 2005. The ELAV RNA-stability factor HuR binds the 5′-untranslated region of the human IGF-IR transcript and differentially represses cap-dependent and IRES-mediated translation. Nucleic Acids Res. **33:**2962–2979.

34. **Min, H., C. W. Turck, J. M. Nikolic, and D. L. Black.** 1997. A new regulatory protein, KSRP, mediates exon inclusion through an intronic splicing enhancer. Genes Dev. **11:**1023–1036.

35. **Park, S., D. G. Myszka, M. Yu, S. J. Littler, and I. A. Laird-Offringa.** 2000. HuD RNA recognition motifs play distinct roles in the formation of a stable complex with AU-rich RNA. Mol. Cell. Biol. **20:**4765–4772.

36. **Park-Lee, S., S. Kim, and I. A. Laird-Offringa.** 2003. Characterization of the interaction between neuronal RNA-binding protein HuD and AU-rich RNA. J. Biol. Chem. **278:**39801–39808.

37. **Piecyk, M., S. Wax, A. R. Beck, N. Kedersha, M. Gupta, B. Maritim, S. Chen, C. Gueydan, V. Kruys, M. Streuli, and P. Anderson.** 2000. TIA-1 is a translational silencer that selectively regulates the expression of TNF-α. EMBO J. **19:**4154–4163.

38. **Shukla, S., W. P. Dirksen, K. M. Joyce, C. Le Guiner-Blanvillain, R. Breathnach, and S. A. Fisher.** 2004. TIA proteins are necessary but not sufficient for the tissue-specific splicing of the myosin phosphatase targeting subunit 1. J. Biol. Chem. **279:**13668–13676.

39. **Stoecklin, G., M. Colombi, I. Raineri, S. Leuenberger, M. Mallaun, M. Schmidlin, B. Gross, M. Lu, T. Kitamura, and C. Moroni.** 2002. Functional cloning of BRF1, a regulator of ARE-dependent mRNA turnover. EMBO J. **21:**4709–4718.

40. **Tenenbaum, S. A., P. J. Lager, C. C. Carson, and J. D. Keene.** 2002. Ribonomics: identifying mRNA subsets in mRNP complexes using antibodies to RNA-binding proteins and genomic arrays. Methods **26:**191–198.

41. **Vawter, M. P., T. Barrett, C. Cheadle, B. P. Sokolov, W. H. Wood III, D. M. Donovan, M. Webster, W. J. Freed, and K. G. Becker.** 2001. Application of cDNA microarrays to examine gene expression differences in schizophrenia. Brain Res. Bull. **55:**641–650.

42. **Wilkie, G. S., K. S. Dickson, and N. K. Gray.** 2003. Regulation of mRNA translation by 5′- and 3′-UTR-binding factors. Trends Biochem. Sci. **28:**182–188.

43. **Yeap, B. B., D. C. Voon, J. P. Vivian, R. K. McCulloch, A. M. Thomson, K. M. Giles, M. F. Czyzyk-Krzeska, H. Furneaux, M. C. Wilce, J. A. Wilce, and P. J. Leedman.** 2002. Novel binding of HuR and poly(C)-binding protein to a conserved UC-rich motif within the 3′-untranslated region of the androgen receptor messenger RNA. J. Biol. Chem. **277:**27183–27192.

44. **Yu, Q., S. J. Cok, C. Zeng, and A. R. Morrison.** 2003. Translational repression of human matrix metalloproteinase-13 by an alternatively spliced form of T-cell-restricted intracellular antigen-related protein (TIAR). J. Biol. Chem. **278:**1579–1584.

45. **Yu, C., B. York, S. Wang, Q. Feng, J. Xu, and B. W. O'Malley.** 2007. An essential function of the SRC-3 coactivator in suppression of cytokine mRNA translation and inflammatory response. Mol. Cell **25:**765–778.

46. **Zhang, W., B. J. Wagner, K. Ehrenman, A. W. Schaefer, C. T. DeMaria, D. Crater, K. DeHaven, L. Long, and G. Brewer.** 1993. Purification, characterization, and cDNA cloning of an AU-rich element RNA-binding protein, AUF1. Mol. Cell. Biol. **13:**7652–7665.

Different Modes of Interaction by TIAR and HuR

with Target RNA and DNA

Declaration for Thesis Chapter [4]

Declaration by candidate

In the case of Chapter [4], the nature and extent of my contribution to the work was the following:

Nature of contribution	Extent of contribution (%)
Co-first author: Performed or supervised the preparation of proteins, oligonucleotides, and their complexes used in all experiments, carried out and supervised all SPR experiments and data analysis, designed and assisted in SAXS experiments and analysis, and prepared the manuscript.	**70**

The following co-authors contributed to the work. Co-authors who are students at Monash University must also indicate the extent of their contribution in percentage terms:

Name	Nature of contribution	Extent of contribution (%) for student co-authors only
Matthew C. J. Wilce[1]	Performed repeated SAXS experiments, and interpreted	N/A

	the data using EOM and ab initio analyses.	
Yano M.K. Yoga[1]	Assisted in protein production and SPR experiments.	5
Menachem J. Gunzburg[1]	Prepared TIAR12 protein and showed interaction with RNA using SEC.	N/A
Nicole R. Pendini[1]	Prepared HuR123 protein and performed the SPR experiments.	N/A
Nathan P. Cowieson[2]	Performed SAXS experiments and collected data.	N/A
Gerald M. Wilson[3]	Provided HuR123 construct, advise for its production and assisted with manuscript preparation.	N/A
Bryan R. Williams[4]	Contributed to the manuscript preparation.	N/A
Myriam Gorospe[5]	Provided insight into the biology of HuR and TIAR	N/A

	proteins and assisted with the manuscript preparation.	
Jacqueline A. Wilce[1]	Supervised the SPR experiments, was involved in data interpretation and finalisation of the manuscript.	N/A

Candidate's Signature	████████████████	**Date: 01/07/2010**

Declaration by co-authors

The undersigned hereby certify that:

(1)   the above declaration correctly reflects the nature and extent of the candidate's contribution to this work, and the nature of the contribution of each of the co-authors.

(2)   they meet the criteria for authorship in that they have participated in the conception, execution, or interpretation, of at least that part of the publication in their field of expertise;

(3)   they take public responsibility for their part of the publication, except for the responsible author who accepts overall responsibility for the publication;

(4)   there are no other authors of the publication according to these criteria;

(5)   potential conflicts of interest have been disclosed to (a) granting bodies, (b) the editor or publisher of journals or other publications, and (c) the head of the responsible academic unit; and

(6)   the original data are stored at the following location(s) and will be held for at least five years from the date indicated below:

Location(s)	1. Department of Biochemistry and Molecular Biology, Monash University, Clayton, Victoria 3800, Australia
	2. Centre for Synchrotron Science, Monash University, Victoria 3800, Australia
	3. Department of Biochemistry and Molecular Biology, University of Maryland School of Medicine, Baltimore, MD 21201, USA.
	4. Monash Institute of Medical Research, Monash University, Victoria 3800, Australia
	5. Laboratory of Cellular and Molecular Biology, National Institute on Aging-Intramural Research Program, National Institute of Health, Baltimore, Maryland 21224, USA

Signatures of co-authors:

Matthew C. J. Wilce[1]   July 1st 2010
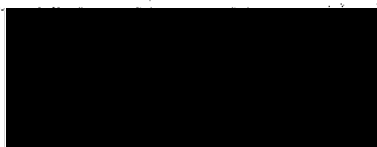
Yano M.K. Yoga[1]   July 20, 2010
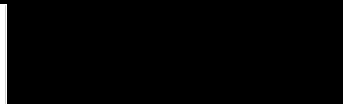
Nicole R Pendini[1]   20/07/2010.
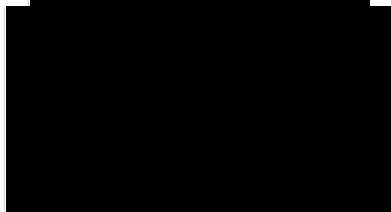
Menachem J Gunzburg[1]   20/07/2010
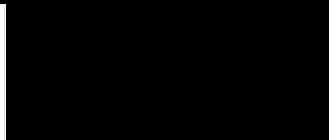
Nathan P. Cowieson[2]   14/07/10
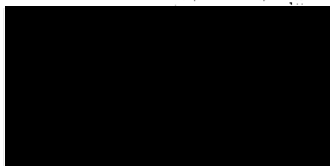
Gerald M. Wilson[3]   July 12, 2010

Bryan R. Williams[4]   July 14 2010

Myriam Gorospe[5]   July 2, 2010

Jacqueline A. Wilce[1]   July 1st 2010

Different modes of interaction by TIAR and HuR

with target RNA and DNA

Henry S. Kim[1#], Matthew C.J. Wilce[1#], Yano M.K. Yoga[1], Nicole R. Pendini[1], Menachem J. Gunzburg[1], Nathan P. Cowieson[1,2], Gerald M.Wilson[3], Bryan R. Williams[4], Myriam Gorospe[5] and Jacqueline A. Wilce[1§]

 # these authors are to be considered co-first authors.

[1]Department of Biochemistry and Molecular Biology, Monash University, Victoria 3800, Australia

[2] Centre for Synchrotron Science, Monash University, Victoria 3800, Australia

[3] Department of Biochemistry and Molecular Biology, University of Maryland School of Medicine, Baltimore, MD 21201, USA.

[4] Monash Institute of Medical Research, Monash University, Victoria 3800, Australia

[5] Laboratory of Cellular and Molecular Biology, National Institute on Aging-Intramural

Research Program, National Institutes of Health, Baltimore, Maryland 21224, USA.

[§] **Corresponding author**:   Postal address: Biochemistry and Molecular Biology

Building 76, Monash University, Wellington Road, VIC

3800, Australia.

E-mail : jackie.wilce@med.monash.edu.au

Phone: +613 9902 9226

Fax: + 613 9902 9500

Abstract

TIAR and HuR are mRNA-binding proteins that play important roles in the regulation of translation. They both possess three RNA recognition motifs (RRMs) and bind to AU-rich elements (AREs), with seemingly overlapping specificity. Here we show using SPR that TIAR and HuR bind to both U-rich and AU-rich RNA in the nM range, with higher overall affinity for U-rich RNA. However, both proteins show slower dissociation from AU-rich RNA, which we propose is a truer measure of their binding preference. Differences between TIAR and HuR are observed in their modes of binding to RNA. TIAR is able to bind deoxy-oligonucleotides with nM affinity, whereas HuR affinity is reduced to a µM level. Studies with U-rich DNA reveal that TIAR binding depends less on the 2'-hydroxyl group of RNA than HuR binding. Finally we show that SAXS data, recorded for the first two domains of TIAR in complex with RNA, are more consistent with a flexible, elongated shape and not the compact shape that the first two domains of Hu proteins adopt upon binding to RNA. We thus propose that these triple-RRM proteins, which compete for the same binding sites in cells, interact with their targets in fundamentally different ways.

Key Words:

RNA-binding protein, AU-rich element, TIAR, HuR, translational regulation, SPR, SAXS.

Copyright licence

In order to make a direct comparison between SPR sensorgrams showing the interaction of TIAR and HuR with U-rich RNA, we have reproduced sensorgrams from a previous publication [from Figure 3 in Kim et al., (2007) Mol Cell Biol 27, 6806-6817]. Permission to re-use these sensorgrams has been granted by the copyright holder, the American Society for Microbiology, under License number 2331741184621.

Introduction

The regulation of mRNA stability is a major control point in gene expression, particularly under conditions of stress, immune response or proliferation (1-3). Under such conditions mRNA stability and translation are tightly controlled by the association of RNA-binding proteins (RBPs) which specifically recognize elements in the mRNA sequence (1-5). One of the best characterised regulatory elements, found predominantly in the 3' UTR of mRNA transcripts encoding high-turnover proteins such as cytokines, lymphokines, onco-proteins, and inflammatory mediators, are AU-rich elements (AREs) (6-8). AREs are specific regulatory sequences often comprising uridine- or adenine/uridine-rich stretches and have been grouped into three classes, although precise consensus sequences are yet to be clarified (7,8). Class I AREs consist of 1-3 copies of scattered AUUUA motifs with a nearby U-rich region. Class II AREs consist of at least two overlapping UUAUUUA(U/A)(U/A) nonamers in a U-rich region and class III AREs, which are less well characterised, have U-rich regions without the AUUUA motif. More than 4000 AREs have been mapped to the human genome, representing 5-8% of human genes (9).

Several proteins have been identified in eukaryotic cells that bind to mRNAs by targeting AREs in their 3' UTR and play a role in regulation of mRNA stability and translational efficiency. Interestingly, their binding can result in quite different outcomes for the mRNAs. RNA-binding proteins (RBPs) TIA-1 (T-cell restricted intracellular antigen-1) and TIAR (TIA-1 related) bind to AREs and function as translational

repressors, sequestering target mRNA into stress granules (SG) following cellular stress (10-12). In contrast, AUF1 (AU-binding factor 1), TTP (tristetraprolin), and KSRP (KH-type splicing regulatory protein) binding to AREs leads to the rapid decay of the specific mRNAs (13-15). Alternatively, the HuR (Hu antigen R) protein generally has a stabilizing effect when it binds to AREs (16,17). Thus AREs appear to be the target of proteins with diverse functions leading to critically different outcomes for the mRNA.

Whether, in fact, these ARE-binding proteins compete for the same mRNA target sites is still not clearly understood. It is conceivable that the same sites are targeted, and that factors such as the relative local concentration or activation state of each of these RNA-binding proteins dictate the alternative possible fates of the mRNA transcripts. Liao and colleagues have shown that competitive binding of TIAR and AUF1 determine the translation of myc (18). Alternatively, the RNA sequence preferences and/or RNA-binding modes could differ between these RBPs and a more complex interplay of protein-RNA interactions underlies their translational regulation. Indeed, co-immunoprecipitation of ARE-binding proteins and identification of their bound mRNA by microarray has revealed distinctly different populations of target mRNA *in vivo* (12,19-22). This is consistent with the existence of distinct binding preferences rather than simple competition for the same pool of ARE-bearing mRNA transcripts. Gorospe and colleagues have proposed different consensus sequences for each of TIAR, TIA-1, HuR, and AUF1 (12,19-22). These studies suggested that HuR and TIA-1 motifs are U-rich rather than AU-rich. They also demonstrated cases where these proteins bind at

overlapping as well as distinct places on the same mRNA transcript and together modulate translation (23,24). In some cases these proteins have even been shown to interact with non-ARE consensus sequences. We have demonstrated in our previous *in vitro* and *in vivo* studies that TIAR can also bind to a C-rich motif in the 3' UTR of target mRNAs, confirming it as a novel TIAR target (19). Therefore, it is likely that ARE-binding proteins interact with their target RNA sequences with differences in their modes of binding, degree of stringency or even specificity underlying the ultimate fate of the mRNA transcript.

Two of the best-characterised ARE-binding proteins are the TIA proteins (TIA-1 and TIAR) and HuR of the Hu protein family (which includes the neuronal proteins HuB, HuC, and HuD) (10,17,25). These classical RNA-recognition motif (RRM)-containing proteins are both ubiquitously expressed in mammalian cells and bind to several common mRNA targets such as TNF-α and GM-CSF (26-31). They are both nucleo-cytoplasmic shuttling "multi-functional" proteins performing a variety of roles at different stages of gene expression including splicing, nucleo-cytoplasmic transport, translation and degradation of mRNA (17,25,32,33). TIA proteins are involved in the control of alternative pre-mRNA splicing, binding to U-rich RNA sequences mostly in introns and promoting the recognition of atypical 5' splice sites (33-39). TIAR has also been reported to be able to bind strongly to a single-stranded, but not double-stranded, T-rich DNA which may position TIAR to modulate transcription and help to localise TIAR to U-rich RNA at the time of transcription (40). In the cytoplasm TIA proteins are

capable of binding target sequences in the 3'-UTR of mRNA and regulating translation (12,25,32). Under conditions of stress TIA proteins play a vital role in SG formation, where untranslated mRNAs accumulate until the stress is passed (11,25,32,41,42). HuR is best known for its nuclear-cyctoplasmic shuttling and its stabilising effect on many target mRNAs (17). HuR can also increase the translation of other associated mRNAs (reviewed by Hinman and Lou, 2008) (16), and repress the translation of other targets via miRNA recruitment (43) and by proposed interference with internal ribosome entry sites (IRESs) (44-46). The fate of the mRNA transcript is thus very different depending on whether it interacts with TIA proteins or HuR.

TIAR, which shares >80% homology with TIA-1, is a 375-amino acid protein belonging to the RRM-containing family of RBPs. The three RRMs located at the N-terminus confer high affinity binding to U-rich RNA sequences ($K_D \sim 1$ nM) (19), while the C-terminal 90-amino acid residue glutamine-rich sequence is essential for stress-granule formation (10,19,21,47-49). RRMs are about 70-90 amino acids long and are able to specifically bind between two and eight sequential single-stranded nucleotides (4,50). TIAR was shown to bind with highest affinity to U-rich RNA sequences, with the three RRMs contributing variously to the interaction (47). It was shown that RRM2 is both sufficient and necessary for binding to AREs and RRM3 showed binding to RNA but may have other specificities than AREs (47). RRM1 showed no binding to U-rich sequences on its own, but was subsequently shown to be able to bind T-rich DNA (40). No structural information for TIAR/RNA complexes is yet available, though structures

of the individual TIAR RRMs have been elucidated using NMR (PDB ID: 2DH7; 2CQI, 1X4G). They all share canonical RRM folds of βαββαβ topology.

TIAR's glutamine-rich C-terminal region shares sequence similarity to human prion protein (51,52). When expressed alone in cells, it forms spontaneous cytoplasmic microaggregates that coaggregate other TIA proteins. It can self-oligomerize *in vivo* like prion proteins and is thought to be crucial for SG formation when cells are under stress (10,53). When this occurs, mRNA that is bound by TIA proteins is sequestered into the SGs. It has been proposed that the mRNA remains in this "holding zone" protected from degradation until the stress is relieved and then the mRNA is either directed towards further translation or degradation (11,41,42).

The primary structures of the Hu-proteins are well conserved (RRMs share >70% amino acid sequence identity among family members) and are arranged with two RRMs near the N-terminus, followed by a less conserved basic hinge region and a third RRM near the C-terminus (54). This arrangement of three RRM domains is strikingly similar to that seen in the TIA proteins and also confers high-affinity binding to ARE sequences ($K_D \sim$ 1-2 nM) (55,56) although there is less than 30% sequence homology overall and less than 35% homology between any TIA-protein RRM compared to Hu-protein RRM. In the case of HuD, the relative roles of the three RRMs for ARE interactions have been interrogated. RRM1 is essential for RNA-binding, but the high-affinity interaction also requires RRM2 and RRM3 (55,57). The crystal structures of the first two RRMs of HuD

protein bound to 11-nt single-stranded RNA derived from c-fos and TNF-alpha mRNA transcripts have been reported and provide insight into the mode of interaction of these domains with classical AREs (58). Interestingly, in the case of HuR, the RRM3 as well as the hinge region between RRM2 and RRM3 contribute significantly to ARE-binding in a length-dependent manner by helping to form multimeric HuR-ARE complexes and increasing the RNA-binding affinity respectively (56).

TIAR and HuR are thus proteins that co-exist in cells and have the capacity to bind specifically to AREs within mRNA in both the nucleus and cytoplasm. They possess analogous RRM architecture and are reported to bind AREs with similar affinity. Here we have determined whether their interactions with target RNA are truly so similar, with the control of mRNA fate potentially dependent on the local availability and activity of these proteins, or whether they have different modes of interaction with RNA. We investigated the binding of TIAR (without the glutamine-rich domain) and HuR to an AU-rich motif, a class I ARE derived from 3'UTR of TNF-α mRNA transcript, compared to a previously established class III ARE, the U-rich motif (19,47) using surface plasmon resonance (SPR). TNF-α mRNA is a known target of TIAR and HuR (28,59) and the mRNA stability and translational efficiency of this key inflammatory mediator has been shown to be regulated by TIAR, HuR, and other RBPs (60). We also investigated their ability to bind to DNA compared with RNA and deoxy-U-rich oligonucleotides. TIAR has been shown to interact with DNA previously (40), but characterisation of this interaction has been very limited to date. Finally, Small Angle X-

ray Scattering (SAXS) was employed to obtain insight into the potential mode of interaction between these RBPs and their target RNA sequences in solution. Together, our data reveal similarities and fundamental differences in the substrate binding activities of these important mRNA binding proteins.

Materials and Methods

Plasmid Construction and Protein Purification

Proteins comprising TIAR and HuR RRM domains were prepared for the current studies. These include proteins with all three RRMs (referred to as TIAR123 and HuR123) and proteins comprising the two N-terminal domains only (referred to as TIAR12 and HuR12). Constructs for the expression of TIAR123 (residues 1–283) and TIAR12 (residues 1–208) were transformed into *E. coli* strain BL21 (DE3) and the encoded proteins were expressed and purified as described previously (47). We discovered, in the course of these studies, that the TIAR12 protein was unstable and consistently degraded to a stable form representing residues 1-181 using mass spectrometry. These residues still encompass the two complete RRMs. HuR12 (residues 18–184) was cloned into pGEX-4T1, expressed in *E. coli* BL21 (DE3), and purified according to previously established protocols (61). A construct for the expression of HuR123 (residues 1–306) was transformed into E. coli ER2566, and purified according to previously established protocols (56). The proteins were further purified by size-exclusion and cation-exchange chromatography. The concentration of each protein was determined using the Bradford assay (BioRad) and by A_{280} measurements using

theoretical molar extinction coefficients (ProtParam). The extinction coefficients were validated for folded protein; A_{280} measurements were within 10% of measurements made in 6.0 M guanidium hydrochloride. The purity of each protein was confirmed by SDS–PAGE.

Biosensor Experiments

The dynamics of RNA/DNA-protein interactions were characterised by SPR using a BIACORE T100 instrument (Biacore Inc.). The oligonucleotides used in the analyses included U-rich and AU-rich RNA, U-rich RNA of varying length, U-rich DNA and T-rich DNA. In the early experiments the U-rich and AU-rich sequences are bounded by G-rich regions (to which the HuR and TIAR have been shown not to interact; data not shown) for the purpose of spacing the binding region from the chip surface and for providing an RNA target of comparable length to other target sequences studied previously (19). Thus the sequences included: U-rich RNA i) 5'-GGGGGGUUUUUUUUUUUUUUUUGGGGG-3', ii) 5'-UUUUUUUUUUUUUUUUU-3', iii) 5'-UUUUUUUUUUUUUU-3', iv) 5'-UUUUUUUU-3'; AU-rich RNA 5'-GGGGGGUAUUUAUUAUUUAUUUAGGGGG-3'; T-rich DNA 5'-TTTTTTTTTTTTTTTTTTTT-3' and U-rich DNA 5'-dUdUdUdUdUdUdUdUdUdUdUdUdUdUdUdUdUdUU-3' (Table 1). The oligonucleotides were chemically synthesized carrying a 5'-biotin tag (Dharmacon Research) to allow immobilization of the RNA/DNA onto streptavidin-coated sensor chips (Series S Sensor Chip SA, Biacore Inc.). RNA were diluted to a final

concentration of 1 μM in HBS buffer (10 mM HEPES, pH 7.4, 150 mM NaCl) followed

by heating at 80 °C for 10 min, and cooling to room temperature. The sample was then

diluted 500-fold in running buffer (10 mM HEPES, pH 7.4, 150 mM NaCl, 1 mM DTT,

0.025% surfactant P20; Biacore Inc.) and injected over the sensor chip surface at 10

μl/min at 25 °C to generate a ~50 response unit (RU) RNA surface (for a low-density

surface). Proteins were serially diluted in running buffer to the concentrations indicated

in Figures 1, 2, and 3, and injected at 25 °C at a flow rate of 50 μl/min for 2-3 min.

Surface regeneration to remove any protein that remained bound after 3-6 min of

dissociation was achieved using a 1- min injection of 2 M NaCl at 50 μl/min. Analyses

of protein concentrations were done in duplicates and any background signal from a

streptavidin-only reference flow cell was subtracted from every data set. Data were

analysed using a simple 1:1 Langmuir interaction model or 2-state (conformational

change) model using the Biacore T100 evaluation software (Biacore Inc.) to determine

the kinetics (association/dissociation rate constants; k_a/k_d) as well as the affinities (K_D)

of the protein-RNA interactions.

SAXS measurements and data reduction

TIAR12 and HuR12 protein samples were subjected to SAXS analysis both in their apo

forms and in combination with a 1:1 molar ratio of a 13-nt U-rich RNA (Dharmacon

Research). SAXS measurements were made using the SAXS-WAXS beamline at the

Australian Synchrotron, Melbourne, Australia, which is equipped with a Pilatus

Detector. The scattering data was collected to provide an *s* range of 0.015-0.3, where *s* is

the magnitude of the scattering vector. Samples were in 1.5 mm quartz capillaries at room temperature. Scattering was collected over a range of five concentrations between 1-4 mg/ml for each sample. The samples and matching buffer solutions were exposed to X-rays for 1, 5, and 1 s as the sample flowed through the capillary. The 2-dimensional scattering images were normalised for sample transmission and radially averaged. In each case the 5 s exposure provided the strongest data with no evidence of radiation damage. Scattering from the buffer and empty capillaries was subtracted after scaling scattering intensities to correspond to incident beam intensities. Data analysis was performed using the ATSAS suite of software. Scattered intensity (I) was plotted against *s*. Extrapolation of the of *I(s)* profiles to zero angle *(I(0))* and comparison with water as a standard indicated a molecular mass for all species consistent with no aggregation. The radius of gyration (*Rg*) did not vary significantly over the concentrations ranges of each molecular species and all Guinear plots were linear for *s.Rg* < 1.3. The scattering data collected at a concentration of 4 mg/ml was used in each case. The program GNOM was used to yield the *P(r)* function via an indirect Fourier transform which provides the relative probabilities of the distances between the scattering centres and the maximal dimension of the scattering molecular species *Dmax* (62). The maximal particle dimensions were computed by constraining the function to 0 at r_{max}, where r_{max} was varied over a wide range of values in 1 Å increments. The value of r_{max} that yielded the highest "total estimate" value as well as a plausible *P(r)* function was taken as the D_{max}. R_g was also calculated from the second moment of the *P(r)* functions. The R_g values calculated from the Guinier approximation or the *P(r)* were favourably comparable.

Ensemble Optimisation Method for SAXS data analysis

The SAXS data were analysed using the ensemble optimization method (EOM) (63), which is suitable for the characterization of flexible proteins in solution. This method allows for the coexistence of different conformations of the protein. A pool of 10,000 random structures of HuR12 (based on the HuD12 structure PDB ID: 1G2E) and TIAR12 (based on RRM1 and RRM2 NMR structures PDB ID: 2CQI, 2DH7) were generated using the EOM method with RRM domains defined as rigid bodies. Scattering curves generated from these structures were filtered using a genetic algorithm against the SAXS scattering curves to select an ensemble of conformers consistent with the experimental data. In order to generate a pool of protein-oligonucleotide complexes, the above process was repeated with HuR12 and TIAR12 structures with a peptide chain insertion to represent the occluded volume of RNA. After the generation of 10,000 structures the peptide was replaced with ssRNA (on the basis of PDB ID:1G2E) from which scattering curves were calculated using CRYSOL (64). These were filtered against the experimental data as described above.

Modelling of SAXS Scattering Data

For the HuR/RNA complex the program DAMMIF (65) was used to generate 15 *ab initio* dummy atoms models from its 4 mg/mL scattering curve. The models were superposed, merged and filtered using the program DAMAVER (66). This program calls a number of programs that superpose the models and also provides the normalised spatial discrepancy (NSD), a measure of how similar the models are to each other.

Models are selected for inclusion for merging and filtering were required to satisfy the criterion NSD < mean NSD + 2 x variation.

Results

TIAR and HuR proteins both show high affinity for U-rich RNA but slow off rates from AU-rich RNA

There has been limited characterisation of HuR and TIAR binding to ARE and C-rich sequences reported previously (19,47,56) but no direct comparison of the binding of these proteins to different classes of AREs, nor a focus on the difference between them. In order to directly compare the RNA-binding of HuR and TIAR to AREs, SPR was used to measure both affinity and kinetics of binding to U-rich (class III ARE) and AU-rich (class I ARE) sequences. TIAR and HuR proteins representing the three RRMs of the proteins (TIAR123 and HuR123) or the two N-terminal RRMs only (TIAR12 and HuR12) were prepared as described previously (see Materials and Methods). These proteins were tested for their affinity for a 17-nt U-rich sequence compared with a 17-nt AU-rich sequence (corresponding to the TNFα 3'UTR region nt 464-480) (28), using SPR (Figure 1). The eight sensorgrams (Figure 1A and 1B) show the binding of a range of concentrations of TIAR123, TIAR12, HuR123, and HuR12 when injected across the U- or AU-rich RNA-coated chip. The association rate constants (k_a), dissociation rate constants (k_d), and overall affinities (K_D) for each protein, as approximated by a simple 1:1 Langmuir binding model, are shown in Table 2 and the residual plots and statistics (χ^2) for the fitting is supplied in Supplementary Figure 1.

All four proteins bound the U- and AU-rich RNA with K_D in the nM range but with quite different affinity and kinetics. HuR123 bound with very low nM affinity to both RNA sequences as expected from previous studies (55,56), and the full-length protein (HuR123) bound with significantly higher affinity (~1000 fold) than HuR12 comprising just the first two domains. Substrate release was the major mechanism contributing to enhanced binding of the full-length protein to both RNA substrates, evidenced by the dramatically slower dissociation rate constants of the full-length HuR123 compared to HuR12. TIAR123 also bound to both U- and AU-rich RNA with nM affinity, though with 20- and 70-fold lower affinity than observed for HuR123 respectively. Here, it is interesting to note that the construct comprising only the first two domains (TIAR12) bound with an affinity similar to full-length (TIAR123) protein. In the case of TIAR, the first two domains alone appear to confer tight binding which is reflected in the TIAR12 sensorgrams showing very slow off-rates compared with HuR12.

In all cases, affinity to the U-rich sequence was higher (~10 fold) than for the AU-rich sequence suggesting that this may be the preferred binding sequence of both HuR and TIAR between the two sequences tested. This higher affinity for U-rich sequence is consistent with a SELEX study by Dember et al. (1996) (47) and *in vitro* selection experiment and gel-shift assay by Park-Lee et al. (2003) (57), which determined that both TIAR and HuD proteins preferentially bind a U-rich motif. However, detailed kinetic measurements reveal that the higher affinities for U-rich sequences are largely due to the faster on-rates to the U-rich sequences. Examination of the dissociation rate

constants reveals that these are, in fact, lower for the AU-rich sequences than the U-rich but, together with the lower association rate constants, an overall higher K_D (lower affinity) is obtained for AU-rich oligonucleotide binding.

HuR12 proteins bind U-rich RNA in a length-dependent manner

Whilst the overall affinity of HuR and TIAR was higher for U-rich compared to AU-rich 17-nt RNA, this was clearly dictated by the much higher on-rates to U-rich RNA compared to AU-rich RNA. On-rates are usually determined by the diffusion of the proteins and their long range electrostatic interactions with the binding partner. These would not be expected to differ between U-rich and AU-rich RNA. The other factor influencing the association rate constant is the probability of a productive interaction occurring. This would be expected to be higher for U-rich RNA as productive binding could take place at any position along the length of the RNA that the RBP encounters. An interaction with the AU-rich sequence, however, may only be productive where the RBP encounters the RNA with adenosine positioned at its adenosine specific site.

In order to verify that this effect could account for the magnitude of the enhanced association rate constant we observed for binding experiments with U-rich RNA, we conducted a series of SPR experiments (with HuR12 for proof of principle) with U-rich RNA of increasing length. The three sensorgrams (Figure 2) show the binding of a range of concentrations of HuR12 when injected across the 8, 13, and 17mer U-rich RNA-coated chip. The association rate constants, dissociation rate constants, and overall

affinities for each binding, approximated by a 1:1 Langmuir binding model, are listed in Table 3 and the residual plots and statistics (χ^2) for the fitting is supplied in Supplementary Figure 1. Notably, as the length of the U-rich sequence was increased (8, 13, 17-mer) we observed increasing affinities, with association rate constants for binding occurring several orders of magnitude faster for the longest oligonucleotide, and dissociation rate constants remaining fairly constant. This is consistent with the increase the probability of a productive interaction with the target RNA.

We therefore propose that the 100-fold faster association rate constants observed for interactions with U-rich 17-nt sequences compared with AU-rich sequence, presented in the previous section, reflect the increased available binding sites for HuR and TIAR. The slower dissociation rate constants of both TIAR and HuR from AU-rich RNA may thus be a truer indication of the "preferred" target sequence for these RBPs.

TIAR and HuR exhibit different binding kinetics and affinity to DNA, suggesting a different mode of interaction

Since TIAR has been reported to bind to DNA as well as to RNA, it was of interest to characterise this oligonucleotide interaction. Both HuR12 and TIAR12 were subjected to binding analysis with 17-nt U-rich DNA and T-rich DNA (to be able to differentiate between effects of removal of the 2'-hydroxyl group and the addition of the methyl group in the thymine base). The four sensorgrams (Figure 3) show the binding of a range of concentrations of HuR12 and TIAR12 when injected across the U-rich DNA and T-

rich DNA-coated chip. The association and dissociation rate constants (k_a and k_d) and overall affinities (K_D) for each binding event were estimated by a 1:1 Langmuir binding model, except for TIAR12 binding T-rich DNA which was best estimated by the 2-state (conformational change) model (Table 4) and the residual plots and statistics (χ^2) for the fitting is supplied in Supplementary Figure 1. Included in the table for comparison's sake are the data obtained for HuR12 and TIAR12 binding to U-rich RNA discussed earlier.

Interestingly, HuR12 binding to DNA was much reduced in affinity compared to RNA. Fast dissociation rate constants were apparent for all interactions by HuR12. The affinity of HuR12 for U-rich DNA was more than 500-fold lower than for U-rich RNA (K_D 20.6 μM from 33 nM; Figure 1A, 3A). HuR12 binding to T-rich DNA was also reduced in affinity, but not as dramatically. Binding to T-rich DNA was approximately10-fold higher in affinity compared with U-rich DNA (K_D 2.6 μM from 20.6 μM; Figure 3B). Together, these results suggest that the 2'-hydroxyl group is important for the interaction of HuR12 with target oligonucleotide, and that, in its absence, the extra methyl in thymine can contribute towards binding.

In contrast, TIAR12 showed strong nM affinities to both U-rich DNA (K_D 21.7 nM; Figure 3A) and T-rich DNA (K_D 3.8 nM; Figure 3B) with K_Ds in the nM range similar to those for U-rich RNA (K_D 0.7 nM; Figure 1A). The kinetics of each interaction are clearly impacted by substrate selection, with the slower dissociation rate constants

observed for the U-rich sequences compared with those for the T-rich DNA sequence. Almost indistinguishable results were obtained for TIAR123 (results not shown). In the case of TIAR12 interactions with oligonucleotides, the absence of the 2'-hydroxyl group results in a 30-fold loss in affinity and the presence of the methyl in thymine impacts on the kinetics of interaction, overall enhancing binding approximately 6-fold. This demonstrates a fundamental difference between the mode of interaction of the first two RRMs of HuR compared with TIAR.

SAXS analysis reveals that TIAR12 bound to RNA maintains an open/flexible conformation whereas HuR12 binds RNA with a closed conformation

SAXS data were collected for HuR12, HuR12/RNA, TIAR12 and TIAR12/RNA in order to obtain low resolution solution structural information. A 13-nt U-rich RNA was used to permit the formation of a simple 1:1 complex. P(r) profiles calculated from the scattering data for the four samples are shown in Figure 4A. Guinier plots calculated from the scattering data for the four samples are shown in Figure 4B and show good linearity. Analysis using the ensemble optimization method (EOM) (63), revealed that, in all cases except for HuR12 in complex with RNA, were not consistent with a single rigid molecular conformation. This is not unexpected for molecules with separate domains that are connected by unstructured linker regions. The SAXS data were therefore analysed using EOM which allows for the coexistence of different conformations of the protein. Sets of conformers are selected using a genetic algorithm from a large number of randomly generated models that best predict the experimental

data. The results of these analyses are shown in Figure 4C which show the Rg and size distribution of the ensemble of randomly generated model structures (in solid line) and the selection of structures from within the ensemble that together give rise to predicted SAXS data consistent with that experimentally obtained. Note that in the cases of protein/RNA complexes models, the analysis was done with (red lines) and without (black lines) the RNA included in the model – with very little effect on the final interpretation.

The data for apo-HuR12 (Figure 4C) (comprised of two RRMs connected by an unstructured linker) were best fit by two populations of HuR12 structures, one more extended (Rg=28 Å, size=74 Å) and one more compact (Rg= 20 Å, size = 56 Å). This is consistent with a flexible protein in which RRMs are positioned at variable distances from each other over time. The SAXS data for the HuR12/RNA complex (Figure 4C), in contrast, were best fitted by a predominantly compact molecular shape (Rg = 16 Å, size= 51Å). This is consistent with the HuR12/RNA complex adopting a stable uniform structure in which both RRMs are held in close proximity. In this case, where predominantly one species exists, *ab initio* reconstruction of the molecular shape can be performed to obtain low resolution information for the molecule or molecular complex (Figure 4D). SAXS data for HuR12/RNA complex were consistent with the structure expected based on the x-ray crystallographically derived HuD12/RNA structure (1G2E; Rg=17.5 Å, size= 60.7 Å).

Similarly to apo-HuR12, the apo-TIAR12 data were best fit by two populations of

TIAR12 structures (Figure 4C), one more extended (Rg=32 Å, size= 90 Å) and one

more compact (Rg= 23 Å, size=64 Å). These greater lengths for apo-TIAR12 structures

may reflect the longer linker region between the RRMs (11 in HuR12 and 14 amino

acids in TIAR12) and the extra residues extending from the TIAR12 construct (5 N-

terminal and 9 C-terminal residues). But unlike the HuR12/RNA complex, the

TIAR12/RNA complex SAXS data were also best fit by two populations, similar to that

seen for apo-TIAR12 (Figure 4C). There was no evidence that the TIAR12/RNA

structure adopts a single compact structure. In order to be certain that the TIAR12

protein and 13mer U-rich RNA used for the SAXS experiments were interacting in

solution, we used size exclusion chromatography to observe complex formation

(Supplementary Data Figure 2). The elution profiles monitored at both A_{260} and A_{280}

show that TIAR12 forms a complex with the RNA of sufficient stability to shift the

RNA peak, verifying the interaction. The SAXS data thus suggest that when TIAR12

interacts with U-rich 13mer RNA, it maintains an extended flexible structure. These data

indicate a fundamental difference in the interaction between the first two domains of

TIAR compared with the first two domains of HuR.

Discussion

Detailed kinetic analyses reveal an accurate measure of RNA-binding specificity by TIAR and HuR proteins: U- vs. AU-rich RNA

In the current study, we demonstrate that TIAR and HuR proteins are able to interact with both U- and AU-rich RNA with K_D values in the nM range, but exhibit different affinities and kinetics of interaction. A simple inspection of K_D suggests that both proteins bind to U-rich RNA sequences with higher affinity than to AU-rich sequences (Figure 1). This is consistent with findings by Park-Lee and colleagues, who reported that HuD protein, a close homologue of HuR, binds U-rich RNA with higher affinity than AU-rich RNA (57). Similarly, SELEX studies by Dember and colleagues showed that TIAR proteins preferentially bind to U-rich sequences (47).

However, the kinetic data reveal that, in fact, both proteins are slower to dissociate from AU-rich sequences than from U-rich sequences, suggesting that the AU-rich sequence is the 'preferred' target sequence for both proteins. The apparently higher affinities for U-rich RNA are a reflection of the much higher association rate constants for U-rich RNA. This may be partly explained by possible secondary structure formation to which the AU-rich sequence could be predisposed (67), but is better explained by the higher number of effective binding positions on the U-rich RNA which would be expected to proportionally increase the association rate constant. Indeed, our comparison of binding to U-rich sequences of increasing length show overall affinities and association rate

constants increasing roughly proportionally to the increase in the number of possible binding sites.

These data help to explain some of the discrepancies between *in vivo* and *in vitro* studies of Hu and TIA protein interactions with target RNA. Whilst there may be a greater probability of these proteins forming a productive interaction at a U-rich site, the interaction with an AU-rich site, once formed, is more stable. Hence, HuR has been shown to bind class I, II and III AREs, but is reported to enhance the stabilisation of messages containing class I and class II (AU-rich) to a greater extent than class III (U-rich) AREs (17). In co-immunoprecipitation experiments, HuR targets identified by microarray were shown to contain a U-rich motif, but with a strong occurrence of adenines at several motif positions (20). Whilst this was considered to be surprisingly more U-rich than AU-rich at the time, it can be argued that the occurrence of adenosine is significant. Immunoprecipitation experiments of TIA-1 targets also revealed a common U-rich motif in which adenosine was also present (21). The equivalent study for TIAR revealed that, under stressed conditions, TIAR bound to mRNA with a consensus motif containing both uridine and adenosine (supplementary data in Kim et al., 2007) (19).

The importance of adenosine in the RNA target of Hu proteins is also apparent from the successful crystallisation of HuD in complex with c-fos and TNF-α RNA, where stability of the complex plays a big role in successful crystallisation. These structures

show that one adenosine is preferentially accommodated at the centre of the RNA-binding site and a second may also be accommodated, though is not critical (58). Structural information for TIA proteins bound to their RNA targets is not yet available. These studies predict that, similarly to HuR, TIAR would form a more stable complex with an AU-rich sequence rather than a U-rich sequence. HuR and TIAR show similar trends in U-rich vs AU-rich preferential binding.

These studies, however, have shown differences between the HuR and TIAR when the hinge region and third RRM are removed. Our studies show that when RRM3 and the hinge region are removed from HuR, there is a dramatic loss in affinity (~1000 fold), particularly apparent in the faster dissociation rate constant. It would thus appear that the hinge region and/or third RRM is very important to ARE binding by HuR. This is consistent with the finding of Fialcowitz-White and colleagues who showed that the hinge region contributes significantly to the HuR interaction with AU-rich RNA (56). In contrast, the affinity difference between TIAR123 and TIAR12 was minimal, suggesting that the hinge region and third RRM of TIAR are of little importance to the interaction with AREs. It must be pointed out that the domain boundaries of the HuR12 and TIAR12 constructs differ slightly. Whilst the HuR12 construct is truncated immediately following the RRM2 structural motif, the TIAR12 construct extends nine residues beyond this. It remains a possibility that this portion of TIAR's hinge region plays a role in the interaction with target RNA. This will be the subject for future investigation. The role of the RRM3 of both proteins remains to be elucidated. It has been speculated that

TIAR RRMs could play a role in binding to other RNA sequences (47) and it was shown that HuR RRM3 is required for cooperative assembly of protein oligomers on RNA substrates (56).

The reported ability of TIAR to bind DNA as well as RNA prompted us to explore this interaction in comparison to that of HuR. TIAR12 and HuR12 interactions with U-rich and T-rich DNA were investigated using SPR and compared with the interactions measured for U-rich RNA. Both proteins were able to interact with DNA, but HuR12 bound with orders of magnitude lower affinity whereas TIAR12 binding remained in the nM range. HuR12 preferentially bound U-rich RNA over U-rich DNA suggesting an important involvement of the 2'-hydroxyl groups. This is consistent with structural information for the HuD12/RNA complex which shows that several 2'-hydroxyl groups from target RNA form intermolecular contacts to HuD12 (58). Interestingly, HuR12 bound T-rich DNA with higher affinity than U-rich DNA. It would appear that in this case, the additional methyl group compensates, to some extent, for the loss in affinity affected by the removal of the 2'-hydroxyl group.

In contrast to HuR12, TIAR12 bound to U-rich and T-rich DNA without such a great loss in affinity compared with U-rich RNA binding. TIAR bound to U-rich DNA with 30-fold reduced affinity compared with U-rich RNA, suggesting that the 2'-hydroxyl group plays a less critical role in the TIAR/RNA interactions than it does in HuR/RNA interactions. TIAR12 also interacted with T-rich DNA with low nM affinity but with

different kinetics (Table 4). This suggests that the addition of methyl groups impacts the

TIAR interaction with oligonucleotides – allowing both the association and dissociation

to occur more readily. These results differ from affinity measurements obtained using a

UV-cross-linking method reported by Suswam et al., (2005) (40) in which it was found

that TIAR bound T-rich DNA with higher affinity (K_{Dapp} = 1.6 nM) than U-rich RNA

(K_{Dapp} = 9.4 nM). These differences are unlikely to be due to the absence of RRM3 in

our experiments, as almost identical SPR results were obtained using the TIAR123

construct (data not shown). Differences in the experimental set up may account for this

reversal in apparent binding preference. In the UV-cross-linking study, the target DNA

was an extended oliogonucleotide of 40 bases, whereas the target RNA was half the

length. It is possible that the selected sequence and length of the oligonucleotide may

have contributed to the apparently higher affinity of TIAR to the DNA sequence. The

current study represents a more direct comparison of binding affinities of TIAR to DNA

and RNA, and suggests that TIAR interacts with U-rich RNA with higher affinity than it

interacts with DNA. Still, both interactions are in the nM range and shuttling between T-

rich DNA and U-rich RNA, as proposed by Suswam et al., (2005) is highly plausible

(40).

TIAR and HuR bind their RNA targets in fundamentally different ways

SAXS (Small Angle X-ray Scattering) was employed to obtain further insight into the

potential mode of interaction of TIAR12 and HuR12 with target RNA sequences in

solution. This revealed a striking difference in the shape of the structure between

TIAR12 and HuR12 upon their complex formation with the 13mer U-rich RNA. SAXS data for TIAR12-RNA complexes are consistent with an elongated shape that is best explained if only one RRM is interacting with the RNA. It is possible that TIAR12 interacts with the RNA via only RRM2. Dember et al., (1996) showed that RRM2 of TIAR is both sufficient and necessary for binding to U-rich RNA and could not detect RNA binding by RRM1 alone (47). They did measure slightly higher affinity by TIAR12 (K_D = 40 nM) than by TIAR2 alone (K_D = 50 nM) using nitrocellulose filter binding assays, suggesting that the RRM1 may contribute to binding to RNA, but the effect is negligible and may not represent a sufficiently stable interaction with the RNA to be observed by SAXS. The current data bring into question the role of RRM1 of TIAR in binding RNA, which will be addressed in future work. It is possible that, as suggested by Suswam et al., (2005) (40), the primary role of RRM1 is to interact with DNA.

The HuR12/RNA complex on the other hand, adopted a globular or more closed conformation (Figure 4B) than TIAR12/RNA, in agreement with the crystal structure of HuD12 in complex with 11mer ARE in which the RNA is sandwiched between the RNA-binding surfaces of two RRMs (58). In the case of Hu proteins it is well documented that primary interactions with RNA occur via RRM1 and that these are augmented by RRM2 (55). Thus overall, these results strongly support the view that the RNA binding proteins TIAR and HuR, though they share a similar triple RRM domain structure, interact with RNA targets in fundamentally different ways.

Conclusion

We have demonstrated that the RNA-binding regions of TIAR and HuR both readily bind AREs with nM affinity, with AU-rich sequences interacting with a greater specificity than U-rich sequences as seen through slower dissociation rate constants. However, the mode of recognition by these two proteins differ however with respect to the contributions to binding made by their different RRM domains and their ability to bind to DNA vs RNA. These distinguishing features would not have been apparent from measurements of affinity alone, but are revealed upon examination of rates of interaction availed by SPR. The fundamental differences in the mode of RNA interaction by these TIAR and HuR may underlie the differences observed in their repertoire of target transcripts, as well as their distinct roles as in the nucleus and cytoplasm. Further studies involving biophysical and higher resolution structural methods will certainly help us to better understand the molecular mechanism underlying their differences, and the basis for the dynamic interplay regulating gene expression in cells.

Funding

Acknowledgments

References

1. Guhaniyogi, J. and Brewer, G. (2001) Regulation of mRNA stability in mammalian cells. *Gene*, **265**, 11-23.
2. Hollams, E.M., Giles, K.M., Thomson, A.M. and Leedman, P.J. (2002) MRNA stability and the control of gene expression: implications for human disease. *Neurochem Res*, **27**, 957-980.
3. Ross, J. (1995) mRNA stability in mammalian cells. *Microbiol Rev*, **59**, 423-450.
4. Auweter, S.D., Oberstrass, F.C. and Allain, F.H. (2006) Sequence-specific binding of single-stranded RNA: is there a code for recognition? *Nucleic Acids Res*, **34**, 4943-4959.
5. Wilkie, G.S., Dickson, K.S. and Gray, N.K. (2003) Regulation of mRNA translation by 5'- and 3'-UTR-binding factors. *Trends Biochem Sci*, **28**, 182-188.
6. Caput, D., Beutler, B., Hartog, K., Thayer, R., Brown-Shimer, S. and Cerami, A. (1986) Identification of a common nucleotide sequence in the 3'-untranslated region of mRNA molecules specifying inflammatory mediators. *Proc Natl Acad Sci U S A*, **83**, 1670-1674.
7. Chen, C.Y., Xu, N. and Shyu, A.B. (1995) mRNA decay mediated by two distinct AU-rich elements from c-fos and granulocyte-macrophage colony-stimulating factor transcripts: different deadenylation kinetics and uncoupling from translation. *Mol Cell Biol*, **15**, 5777-5788.
8. Barreau, C., Paillard, L. and Osborne, H.B. (2005) AU-rich elements and associated factors: are there unifying principles? *Nucleic Acids Res*, **33**, 7138-7150.
9. Bakheet, T., Williams, B.R. and Khabar, K.S. (2006) ARED 3.0: the large and diverse AU-rich transcriptome. *Nucleic Acids Res*, **34**, D111-114.
10. Kedersha, N.L., Gupta, M., Li, W., Miller, I. and Anderson, P. (1999) RNA-binding proteins TIA-1 and TIAR link the phosphorylation of eIF-2 alpha to the assembly of mammalian stress granules. *J Cell Biol*, **147**, 1431-1442.
11. Kedersha, N., Stoecklin, G., Ayodele, M., Yacono, P., Lykke-Andersen, J., Fritzler, M.J., Scheuner, D., Kaufman, R.J., Golan, D.E. and Anderson, P. (2005) Stress granules and processing bodies are dynamically linked sites of mRNP remodeling. *J Cell Biol*, **169**, 871-884.

12. Mazan-Mamczarz, K., Lal, A., Martindale, J.L., Kawai, T. and Gorospe, M. (2006) Translational repression by RNA-binding protein TIAR. *Mol Cell Biol*, **26**, 2716-2727.

13. Loflin, P., Chen, C.Y. and Shyu, A.B. (1999) Unraveling a cytoplasmic role for hnRNP D in the in vivo mRNA destabilization directed by the AU-rich element. *Genes Dev*, **13**, 1884-1897.

14. Chen, C.Y., Gherzi, R., Ong, S.E., Chan, E.L., Raijmakers, R., Pruijn, G.J., Stoecklin, G., Moroni, C., Mann, M. and Karin, M. (2001) AU binding proteins recruit the exosome to degrade ARE-containing mRNAs. *Cell*, **107**, 451-464.

15. Zhang, W., Wagner, B.J., Ehrenman, K., Schaefer, A.W., DeMaria, C.T., Crater, D., DeHaven, K., Long, L. and Brewer, G. (1993) Purification, characterization, and cDNA cloning of an AU-rich element RNA-binding protein, AUF1. *Mol Cell Biol*, **13**, 7652-7665.

16. Hinman, M.N. and Lou, H. (2008) Diverse molecular functions of Hu proteins. *Cell Mol Life Sci*, **65**, 3168-3181.

17. Brennan, C.M. and Steitz, J.A. (2001) HuR and mRNA stability. *Cell Mol Life Sci*, **58**, 266-277.

18. Liao, B., Hu, Y. and Brewer, G. (2007) Competitive binding of AUF1 and TIAR to MYC mRNA controls its translation. *Nat Struct Mol Biol*, **14**, 511-518.

19. Kim, H.S., Kuwano, Y., Zhan, M., Pullmann, R., Jr., Mazan-Mamczarz, K., Li, H., Kedersha, N., Anderson, P., Wilce, M.C., Gorospe, M. *et al.* (2007) Elucidation of a C-rich signature motif in target mRNAs of RNA-binding protein TIAR. *Mol Cell Biol*, **27**, 6806-6817.

20. Lopez de Silanes, I., Zhan, M., Lal, A., Yang, X. and Gorospe, M. (2004) Identification of a target RNA motif for RNA-binding protein HuR. *Proc Natl Acad Sci U S A*, **101**, 2987-2992.

21. Lopez de Silanes, I., Galban, S., Martindale, J.L., Yang, X., Mazan-Mamczarz, K., Indig, F.E., Falco, G., Zhan, M. and Gorospe, M. (2005) Identification and functional outcome of mRNAs associated with RNA-binding protein TIA-1. *Mol Cell Biol*, **25**, 9520-9531.

22. Mazan-Mamczarz, K., Kuwano, Y., Zhan, M., White, E.J., Martindale, J.L., Lal, A. and Gorospe, M. (2009) Identification of a signature motif in target mRNAs of RNA-binding protein AUF1. *Nucleic Acids Res*, **37**, 204-214.

23. Kawai, T., Lal, A., Yang, X., Galban, S., Mazan-Mamczarz, K. and Gorospe, M. (2006) Translational control of cytochrome c by RNA-binding proteins TIA-1 and HuR. *Mol Cell Biol*, **26**, 3295-3307.

24. Lal, A., Mazan-Mamczarz, K., Kawai, T., Yang, X., Martindale, J.L. and Gorospe, M. (2004) Concurrent versus individual binding of HuR and AUF1 to common labile target mRNAs. *Embo J*, **23**, 3092-3102.

25. Anderson, P. and Kedersha, N. (2002) Visibly stressed: the role of eIF2, TIA-1, and stress granules in protein translation. *Cell Stress Chaperones*, **7**, 213-221.

26. Beck, A.R., Medley, Q.G., O'Brien, S., Anderson, P. and Streuli, M. (1996) Structure, tissue distribution and genomic organization of the murine RRM-type RNA binding proteins TIA-1 and TIAR. *Nucleic Acids Res*, **24**, 3829-3835.

27. Grosset, C., Boniface, R., Duchez, P., Solanilla, A., Cosson, B. and Ripoche, J. (2004) In vivo studies of translational repression mediated by the granulocyte-macrophage colony-stimulating factor AU-rich element. *J Biol Chem*, **279**, 13354-13362.

28. Gueydan, C., Droogmans, L., Chalon, P., Huez, G., Caput, D. and Kruys, V. (1999) Identification of TIAR as a protein binding to the translational regulatory AU-rich element of tumor necrosis factor alpha mRNA. *J Biol Chem*, **274**, 2322-2326.

29. Lu, J.Y. and Schneider, R.J. (2004) Tissue distribution of AU-rich mRNA-binding proteins involved in regulation of mRNA decay. *J Biol Chem*, **279**, 12974-12979.

30. Masuda, K., Abdelmohsen, K. and Gorospe, M. (2009) RNA-binding proteins implicated in the hypoxic response. *J Cell Mol Med*.

31. Piecyk, M., Wax, S., Beck, A.R., Kedersha, N., Gupta, M., Maritim, B., Chen, S., Gueydan, C., Kruys, V., Streuli, M. *et al*. (2000) TIA-1 is a translational silencer that selectively regulates the expression of TNF-alpha. *Embo J*, **19**, 4154-4163.

32. Anderson, P. and Kedersha, N. (2002) Stressful initiations. *J Cell Sci*, **115**, 3227-3234.

33. Forch, P. and Valcarcel, J. (2001) Molecular mechanisms of gene expression regulation by the apoptosis-promoting protein TIA-1. *Apoptosis*, **6**, 463-468.

34. Aznarez, I., Barash, Y., Shai, O., He, D., Zielenski, J., Tsui, L.C., Parkinson, J., Frey, B.J., Rommens, J.M. and Blencowe, B.J. (2008) A systematic analysis of intronic sequences downstream of 5' splice sites reveals a widespread role for U-rich motifs and TIA1/TIAL1 proteins in alternative splicing regulation. *Genome Res*, **18**, 1247-1258.

35. Izquierdo, J.M. and Valcarcel, J. (2007) Two isoforms of the T-cell intracellular antigen 1 (TIA-1) splicing factor display distinct splicing regulation activities. Control of TIA-1 isoform ratio by TIA-1-related protein. *J Biol Chem*, **282**, 19410-19417.

36. Izquierdo, J.M. and Valcarcel, J. (2007) Fas-activated serine/threonine kinase (FAST K) synergizes with TIA-1/TIAR proteins to regulate Fas alternative splicing. *J Biol Chem*, **282**, 1539-1543.

37. Le Guiner, C., Lejeune, F., Galiana, D., Kister, L., Breathnach, R., Stevenin, J. and Del Gatto-Konczak, F. (2001) TIA-1 and TIAR activate splicing of alternative exons with weak 5' splice sites followed by a U-rich stretch on their own pre-mRNAs. *J Biol Chem*, **276**, 40638-40646.

38. Shukla, S., Dirksen, W.P., Joyce, K.M., Le Guiner-Blanvillain, C., Breathnach, R. and Fisher, S.A. (2004) TIA proteins are necessary but not sufficient for the tissue-specific splicing of the myosin phosphatase targeting subunit 1. *J Biol Chem*, **279**, 13668-13676.

39. Zhu, H., Hasman, R.A., Young, K.M., Kedersha, N.L. and Lou, H. (2003) U1 snRNP-dependent function of TIAR in the regulation of alternative RNA

processing of the human calcitonin/CGRP pre-mRNA. *Mol Cell Biol*, **23**, 5959-5971.

40. Suswam, E.A., Li, Y.Y., Mahtani, H. and King, P.H. (2005) Novel DNA-binding properties of the RNA-binding protein TIAR. *Nucleic Acids Res*, **33**, 4507-4518.

41. Anderson, P. and Kedersha, N. (2007) On again, off again: the SRC-3 transcriptional coactivator moonlights as a translational corepressor. *Mol Cell*, **25**, 796-797.

42. Kedersha, N. and Anderson, P. (2002) Stress granules: sites of mRNA triage that regulate mRNA stability and translatability. *Biochem Soc Trans*, **30**, 963-969.

43. Kim, H.H., Kuwano, Y., Srikantan, S., Lee, E.K., Martindale, J.L. and Gorospe, M. (2009) HuR recruits let-7/RISC to repress c-Myc expression. *Genes Dev*, **23**, 1743-1748.

44. Kullmann, M., Gopfert, U., Siewe, B. and Hengst, L. (2002) ELAV/Hu proteins inhibit p27 translation via an IRES element in the p27 5'UTR. *Genes Dev*, **16**, 3087-3099.

45. Meng, Z., King, P.H., Nabors, L.B., Jackson, N.L., Chen, C.Y., Emanuel, P.D. and Blume, S.W. (2005) The ELAV RNA-stability factor HuR binds the 5'-untranslated region of the human IGF-IR transcript and differentially represses cap-dependent and IRES-mediated translation. *Nucleic Acids Res*, **33**, 2962-2979.

46. Rivas-Aravena, A., Ramdohr, P., Vallejos, M., Valiente-Echeverria, F., Dormoy-Raclet, V., Rodriguez, F., Pino, K., Holzmann, C., Huidobro-Toro, J.P., Gallouzi, I.E. *et al*. (2009) The Elav-like protein HuR exerts translational control of viral internal ribosome entry sites. *Virology*, **392**, 178-185.

47. Dember, L.M., Kim, N.D., Liu, K.Q. and Anderson, P. (1996) Individual RNA recognition motifs of TIA-1 and TIAR have different RNA binding specificities. *J Biol Chem*, **271**, 2783-2788.

48. Gilks, N., Kedersha, N., Ayodele, M., Shen, L., Stoecklin, G., Dember, L.M. and Anderson, P. (2004) Stress granule assembly is mediated by prion-like aggregation of TIA-1. *Mol Biol Cell*, **15**, 5383-5398.

49. Tian, Q., Streuli, M., Saito, H., Schlossman, S.F. and Anderson, P. (1991) A polyadenylate binding protein localized to the granules of cytolytic lymphocytes induces DNA fragmentation in target cells. *Cell*, **67**, 629-639.

50. Clery, A., Blatter, M. and Allain, F.H. (2008) RNA recognition motifs: boring? Not quite. *Curr Opin Struct Biol*, **18**, 290-298.

51. Prusiner, S.B. (1989) Scrapie prions. *Annu Rev Microbiol*, **43**, 345-374.

52. Prusiner, S.B. (1989) Creutzfeldt-Jakob disease and scrapie prions. *Alzheimer Dis Assoc Disord*, **3**, 52-78.

53. Eisinger-Mathason, T.S., Andrade, J., Groehler, A.L., Clark, D.E., Muratore-Schroeder, T.L., Pasic, L., Smith, J.A., Shabanowitz, J., Hunt, D.F., Macara, I.G. *et al*. (2008) Codependent functions of RSK2 and the apoptosis-promoting factor TIA-1 in stress granule assembly and cell survival. *Mol Cell*, **31**, 722-736.

54.   Ma, W.J., Cheng, S., Campbell, C., Wright, A. and Furneaux, H. (1996) Cloning and characterization of HuR, a ubiquitously expressed Elav-like protein. *J Biol Chem*, **271**, 8144-8151.

55.   Park, S., Myszka, D.G., Yu, M., Littler, S.J. and Laird-Offringa, I.A. (2000) HuD RNA recognition motifs play distinct roles in the formation of a stable complex with AU-rich RNA. *Mol Cell Biol*, **20**, 4765-4772.

56.   Fialcowitz-White, E.J., Brewer, B.Y., Ballin, J.D., Willis, C.D., Toth, E.A. and Wilson, G.M. (2007) Specific protein domains mediate cooperative assembly of HuR oligomers on AU-rich mRNA-destabilizing sequences. *J Biol Chem*, **282**, 20948-20959.

57.   Park-Lee, S., Kim, S. and Laird-Offringa, I.A. (2003) Characterization of the interaction between neuronal RNA-binding protein HuD and AU-rich RNA. *J Biol Chem*, **278**, 39801-39808.

58.   Wang, X. and Tanaka Hall, T.M. (2001) Structural basis for recognition of AU-rich element RNA by the HuD protein. *Nat Struct Biol*, **8**, 141-145.

59.   Dean, J.L., Wait, R., Mahtani, K.R., Sully, G., Clark, A.R. and Saklatvala, J. (2001) The 3' untranslated region of tumor necrosis factor alpha mRNA is a target of the mRNA-stabilizing factor HuR. *Mol Cell Biol*, **21**, 721-730.

60.   Wilson, G.M., Lu, J., Sutphen, K., Sun, Y., Huynh, Y. and Brewer, G. (2003) Regulation of A + U-rich element-directed mRNA turnover involving reversible phosphorylation of AUF1. *J Biol Chem*, **278**, 33029-33038.

61.   Yeap, B.B., Voon, D.C., Vivian, J.P., McCulloch, R.K., Thomson, A.M., Giles, K.M., Czyzyk-Krzeska, M.F., Furneaux, H., Wilce, M.C., Wilce, J.A. *et al.* (2002) Novel binding of HuR and poly(C)-binding protein to a conserved UC-rich motif within the 3'-untranslated region of the androgen receptor messenger RNA. *J Biol Chem*, **277**, 27183-27192.

62.   Svergun, D. (1992) Determination of the regularization parameter in direct-transform methods using perceptual criteria *J. Appl. Cryst.*, **25**, 495-503.

63.   Bernado, P., Mylonas, E., Petoukhov, M.V., Blackledge, M. and Svergun, D.I. (2007) Structural characterization of flexible proteins using small-angle X-ray scattering. *J. Am. Chem. Soc.*, **129**, 5656-5664.

64.   Svergun, D.I., Barberato, C. and Koch, M.H.J. (1995) CRYSOL - a program to evaluate X-ray solution scattering of biological macromolecules from atomic coordinates. *. J Appl Crystallogr*, **28**, 768-773.

65.   Franke, D. and Svergun, D. (2009) *DAMMIF*, a program for rapid *ab-initio* shape determination in small-angle scattering. *J. Appl. Cryst.*, **42**, 342-346.

66.   Volkov, V.V. and Svergun, D. (2003) Uniqueness of ab initio shape determination in small-angle scattering. *J. Appl. Cryst.*, **36**, 860-864.

67.   Fialcowitz, E.J., Brewer, B.Y., Keenan, B.P. and Wilson, G.M. (2005) A hairpin-like structure within an AU-rich mRNA-destabilizing element regulates trans-factor binding selectivity and mRNA decay kinetics. *J. Biol. Chem.*, **280**, 22406-22417.

Figure Legends

Figure 1. Kinetic analysis of the interactions of TIAR and HuR proteins with U and AU-rich RNA using SPR. Sensorgrams of HuR12, HuR123, TIAR12 and TIAR 123 proteins to A) a U-rich or B) an AU-rich RNA (28-mer each) are shown. Biotinylated RNA was captured on SA-coated sensor chips and increasing concentrations of protein were injected over the surface. Injections were performed for 120 seconds (association phase), followed by a 300-second flow of running buffer to assess dissociation. The experiments were conducted in duplicate and showed good overlap. The red lines represent the binding responses for injections of protein analyte at specified concentrations (nM) over the RNA surface. The kinetic data was fit by 1:1 Langmuir binding model that describes monovalent analyte binding to a single site on the immobilized ligand. Mass transport limitation effects were not evident. The black curves superimposed on the sensorgrams represent the model fitted curves. The rate constants k_a and k_d were determined simultaneously as global fitting parameters from which the K_D was determined. The resulting parameter values are given in Table 2. [Note that sensorgrams for HuR12, TIAR12 and TIAR123 are reproduced from Kim et al., 2007 Figure 3 (19) with permission from the American Society for Microbiology to assist visual comparison with other sensorgrams].

Figure 2. Kinetic analysis of the interactions of HuR12 proteins with 8, 13, and 17mer U-rich RNA using SPR. The binding of HuR12 to different lengths of U-rich RNAs (8, 13, and 17-mer) is shown. Biotinylated RNA was captured on SA-coated

sensor chips and increasing concentrations of protein were injected over the surface. Injections were performed for 180 seconds (association phase), followed by a 360-second flow of running buffer to assess dissociation. The experiments were conducted in duplicate and showed good overlap. The red lines represent the binding responses for injections of protein analyte at specified concentrations (nM) over the RNA surface. The kinetic data were fit by 1:1 Langmuir binding model which describes monovalent analyte binding to a single site on the immobilized ligand. Mass transport limitation effects were not evident. The black curves superimposed on top of the sensorgrams represent the model fitted curves. The rate constants k_a and k_d were determined simultaneously as global fitting parameters from which the K_D was determined. The resulting parameter values are given in Table 3.

Figure 3. Kinetic analysis of the interactions of TIAR12 and HuR12 proteins with U-rich and T-rich DNA using SPR. The binding of TIAR12 and HuR12 to A) U- and B) T-rich DNA is shown. Biotinylated DNA was captured on SA-coated sensor chips and increasing concentrations of protein were injected over the surface. Injections were performed for 120 seconds (association phase), followed by a 300-second flow of running buffer to assess dissociation. The experiments were conducted in duplicate and showed good overlap. The red lines represent the binding responses for injections of protein analyte at specified concentrations (nM) over the DNA surface. The kinetic data was fit by the 1:1 Langmuir binding model (except for TIAR12 binding to T-rich DNA which was estimated by the 2-state model). Mass transport limitation effects were not

evident. The black curves superimposed on top of the sensorgrams represent the model

fitted curves. The rate constants k_a and k_d were determined simultaneously as global

fitting parameters from which the K_D was determined.

Figure 4. SAXS analysis of a) HuR12, b) HuR12/RNA, c) TIAR12 and d)

TIAR12/RNA samples. A) P(r) profiles calculated from the scattering data for the four

samples. B) Guinier plots calculated from the scattering data for the four samples.

Intensity (I) is given in arbitary units (au). C) Ensemble optimization analysis: Rg and

Rmax distributions from the best fitting ensembles calculated using EOM (63). The

distribution for the pool of 10,000 conformers (solid line) and the selected best fitting

ensemble (dashed line) are shown for the four samples. Black lines represent ensembles

of protein models only and red lines represent ensembles of protein/RNA models. D)

superposition of the best fitting ensemble from each of the two main peaks shown as

cartoon structures. The total number of structures is shown in brackets. E) *ab initio*

reconstruction of HuR12/RNA complex overlayed with HuD12/RNA structure solved

using x-ray crystallography (1G2E). (Rg (Guinier) = 17.1 Å, Rg (real) = 16.9 Å, Rmax

= 58 Å).

Tables

Table 1. List of oligonucleotides used for the SPR studies. Both 28mer U- and AU-rich RNAs contain poly-G linkers at both ends. The AU-rich sequence represents the HuR target site within the 3' UTR of human TNF-α mRNA transcript (nt 464-480) (28).

Table 2. Kinetic and affinity constants determined for the interactions of TIAR and HuR proteins with U-rich and AU-rich RNA. The association and dissociation rate constants (k_a and k_d) were determined as global fitting parameters for a 1:1 binding model. The equilibrium dissociation constant (K_D) was determined as k_d/k_a. [Note that binding data for HuR12, TIAR12 and TIAR123 to U-rich RNA are reproduced from Kim et al., 2007 (19) with permission from the American Society for Microbiology to assist direct comparison].

Table 3. Kinetic and affinity constants determined for the interactions of HuR12 proteins with 8, 13, and 17mer U-rich RNA. The association and dissociation rate constants (k_a and k_d) were determined as global fitting parameters for a 1:1 binding model. The equilibrium dissociation constant (K_D) was determined as k_d/k_a.
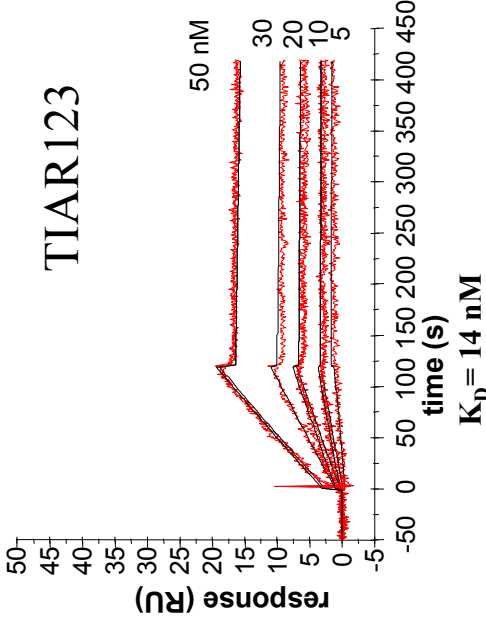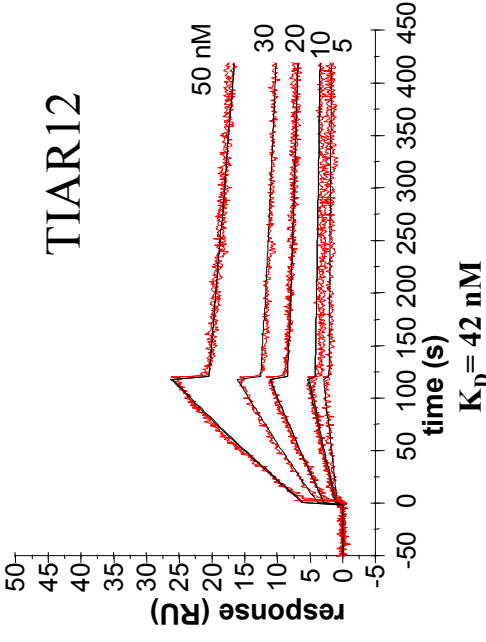
Table 4. Kinetic and affinity constants determined for the interactions of TIAR12 and HuR12 proteins with U-rich RNA, U-rich DNA, and T-rich DNA. The association and dissociation rate constants (k_a and k_d) were determined as global fitting parameters for a 1:1 binding model or a 2-state model in the case of TIAR12 binding T-

rich DNA where k_a and k_d represents k_{a1} and k_{d1} respectively. The equilibrium dissociation constant K_D was determined as k_d/k_a for the 1:1 binding or $1/\{(k_{a1}/k_{d1}) \times (1+ k_{a2}/k_{d2})\}$ for the 2-state binding (k_{a1} and k_{d1}: association and dissociation rate constants; k_{a2} and k_{d2}: forward and reverse rate constants for conformational change; $k_{a2} = 0.0026 \text{ s}^{-1}$, $k_{d2} = 1.84 \times 10^{-4} \text{ s}^{-1}$).

Figure 1A. Kinetic analysis of the interactions of TIAR12, TIAR123, HuR12, and HuR123 proteins with U-rich RNA (SPR)

A   **U-rich:** GGGGGGUUUUUUUUUUUUUUUUUUGGGGG

Figure 1B. Kinetic analysis of the interactions of TIAR12, TIAR123, HuR12, and HuR123 proteins with AU-rich RNA (SPR)

B   AU-rich: GGGGGGUAUUUAUUUAUUUAUUUAGGGGG
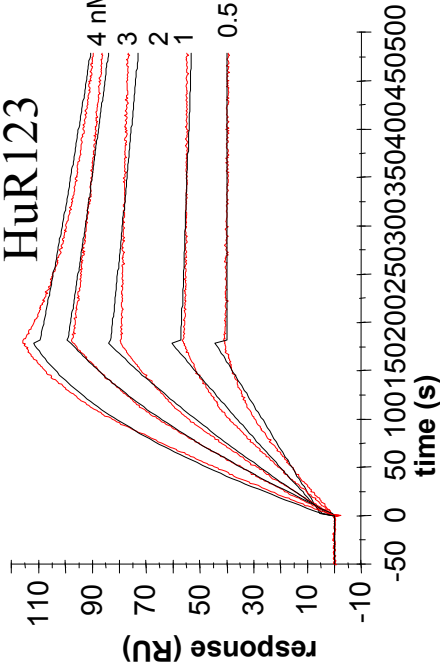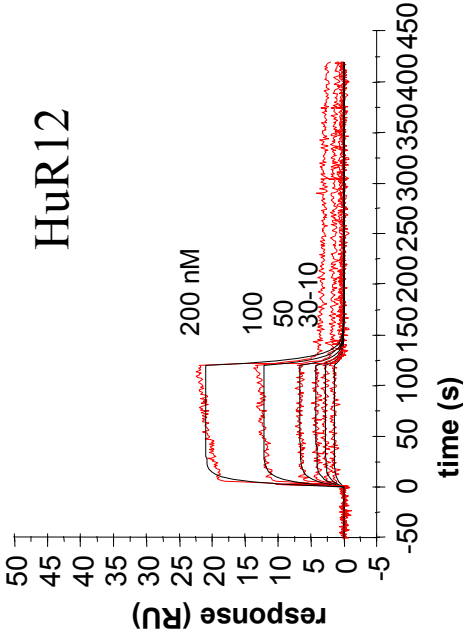
Figure 2. Kinetic analysis of the interactions of HuR12 protein with 8, 13, and 17mer U-rich RNA (SPR)

Figure 3. Kinetic analysis of the interactions of TIAR12 and HuR12 proteins with 20mer U-rich and T-rich DNA (SPR)

A U-rich DNA: aUaUaUaUaUaUaUaUaUaUaUaUaUaUaUaUaUaUaUaU

B T-rich DNA: TTTTTTTTTTTTTTTTTTTT
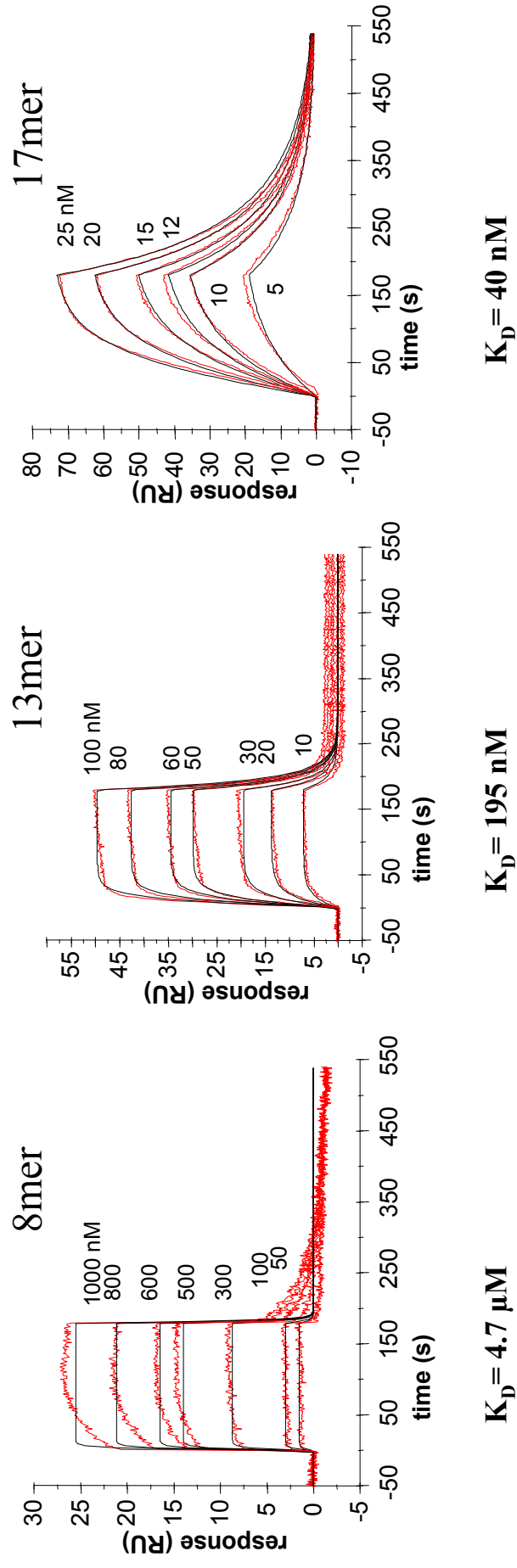
Figure 4. SAXS analysis of a) HuR12, b) HuR12/RNA, c) TIAR12 and d) TIAR12/RNA samples

Figure 4 (A and B)

Figure 4 (C-E)

Table 1. Oligonucleotides used in the SPR analysis

Oligonucleotides	Sequences (5'Biotin - 3')
U-rich	GGGGGGUUUUUUUUUUUUUUUUGGGGG (28mer)
	UUUUUUUUUUUUUUUUU (17mer)
	UUUUUUUUUUUUU (13mer)
	UUUUUUUU (8mer)
AU-rich	GGGGGGUAUUUAUUAUUUAUUUAGGGGG (28mer)
T-rich	TTTTTTTTTTTTTTTTTTTT (20mer)
DeoxyU-rich	dUdUdUdUdUdUdUdUdUdUdUdUdUdUdUdUdUdUdU (20mer)
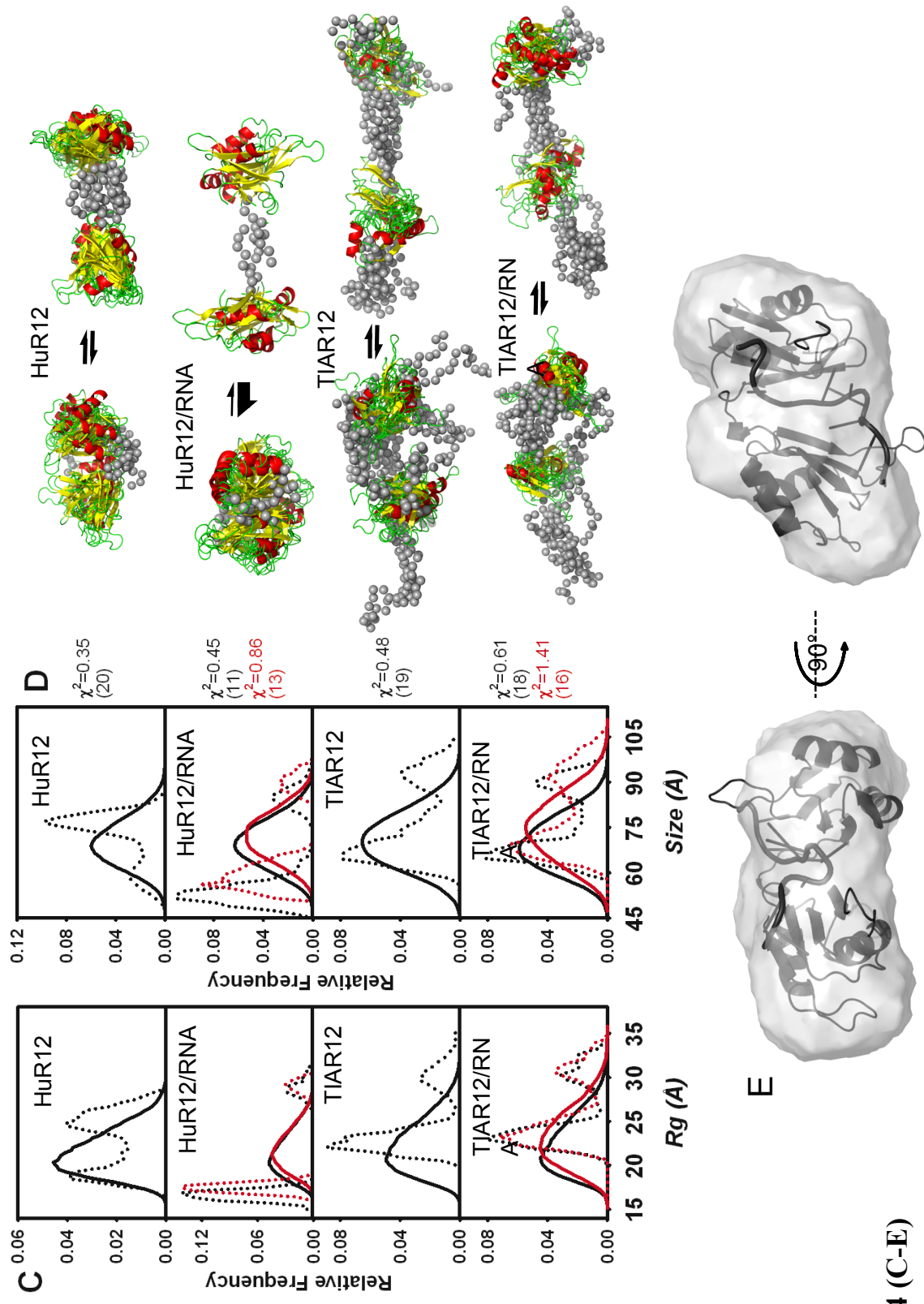
Table 2. Kinetic and affinity constants for the interactions of HuR12, HuR123, TIAR12, and TIAR123 proteins with U- and AU-rich RNA

Protein	RNA	k_a (1/Ms)	k_d (1/s)	K_D (k_d/k_a, nM)
HuR12	U-rich	$(9.66 \pm 0.19) \times 10^6$	$(3.20 \pm 0.06) \times 10^{-1}$	33.1 ± 1.29
	AU-rich	$(3.07 \pm 0.06) \times 10^5$	$(1.56 \pm 0.01) \times 10^{-1}$	506 ± 13.1
HuR123	U-rich	$(1.03 \pm 0.01) \times 10^7$	$(5.15 \pm 0.03) \times 10^{-4}$	0.05 ± 0.001
	AU-rich	$(4.34 \pm 0.1) \times 10^6$	$(8.26 \pm 0.11) \times 10^{-4}$	0.2 ± 0.007
TIAR12	U-rich	$(4.10 \pm 0.11) \times 10^6$	$(2.83 \pm 0.08) \times 10^{-3}$	0.69 ± 0.04
	AU-rich	$(1.71 \pm 0.02) \times 10^4$	$(7.26 \pm 0.04) \times 10^{-4}$	42.5 ± 0.63
TIAR123	U-rich	$(1.58 \pm 0.02) \times 10^6$	$(1.56 \pm 0.01) \times 10^{-3}$	0.99 ± 0.02
	AU-rich	$(1.15 \pm 0.01) \times 10^4$	$(1.63 \pm 0.02) \times 10^{-4}$	14.1 ± 0.22

Table 3. Kinetic and affinity constants for the interactions of HuR12 proteins with 8, 13, and 17mer U-rich RNA

| Protein	U-rich RNA	Kinetic and affinity constants		
	1:1 binding	k_a (1/Ms)	k_d (1/s)	K_D (k_d/k_a, nM)
HuR12	8mer	$(8.781 \pm 0.15) \times 10^4$	$(4.126 \pm 0.031) \times 10^{-1}$	4699 ± 116
	13mer	$(8.657 \pm 0.14) \times 10^5$	$(1.686 \pm 0.027) \times 10^{-1}$	195 ± 6.3
	17mer	$(1.588 \pm 0.47) \times 10^7$	$(6.319 \pm 1.9) \times 10^{-1}$	40 ± 24

Table 4. Kinetic and affinity constants for the interactions of TIAR12 and HuR12 proteins with U-rich RNA, U-rich DNA, and T-rich DNA

Protein	Oligo	k_a (1/Ms)	k_d (1/s)	K_D (k_d/k_a, nM)
HuR12	U-rich RNA	$(9.66 \pm 0.19) \times 10^6$	$(3.20 \pm 0.06) \times 10^{-1}$	33.1 ± 1.29
	U-rich DNA	$(2.93 \pm 0.19) \times 10^4$	$(6.03 \pm 0.07) \times 10^{-1}$	20590 ± 1573
	T-rich DNA	$(1.45 \pm 0.03) \times 10^5$	$(3.84 \pm 0.04) \times 10^{-1}$	2644 ± 82.3
TIAR12	U-rich RNA	$(4.10 \pm 0.11) \times 10^6$	$(2.83 \pm 0.08) \times 10^{-3}$	0.69 ± 0.04
	U-rich DNA	$(2.19 \pm 0.02) \times 10^4$	$(4.77 \pm 0.04) \times 10^{-4}$	21.7 ± 0.38
	T-rich DNA	$(7.80 \pm 0.75) \times 10^6$	$(4.49 \pm 0.44) \times 10^{-1}$	3.81 ± 0.74
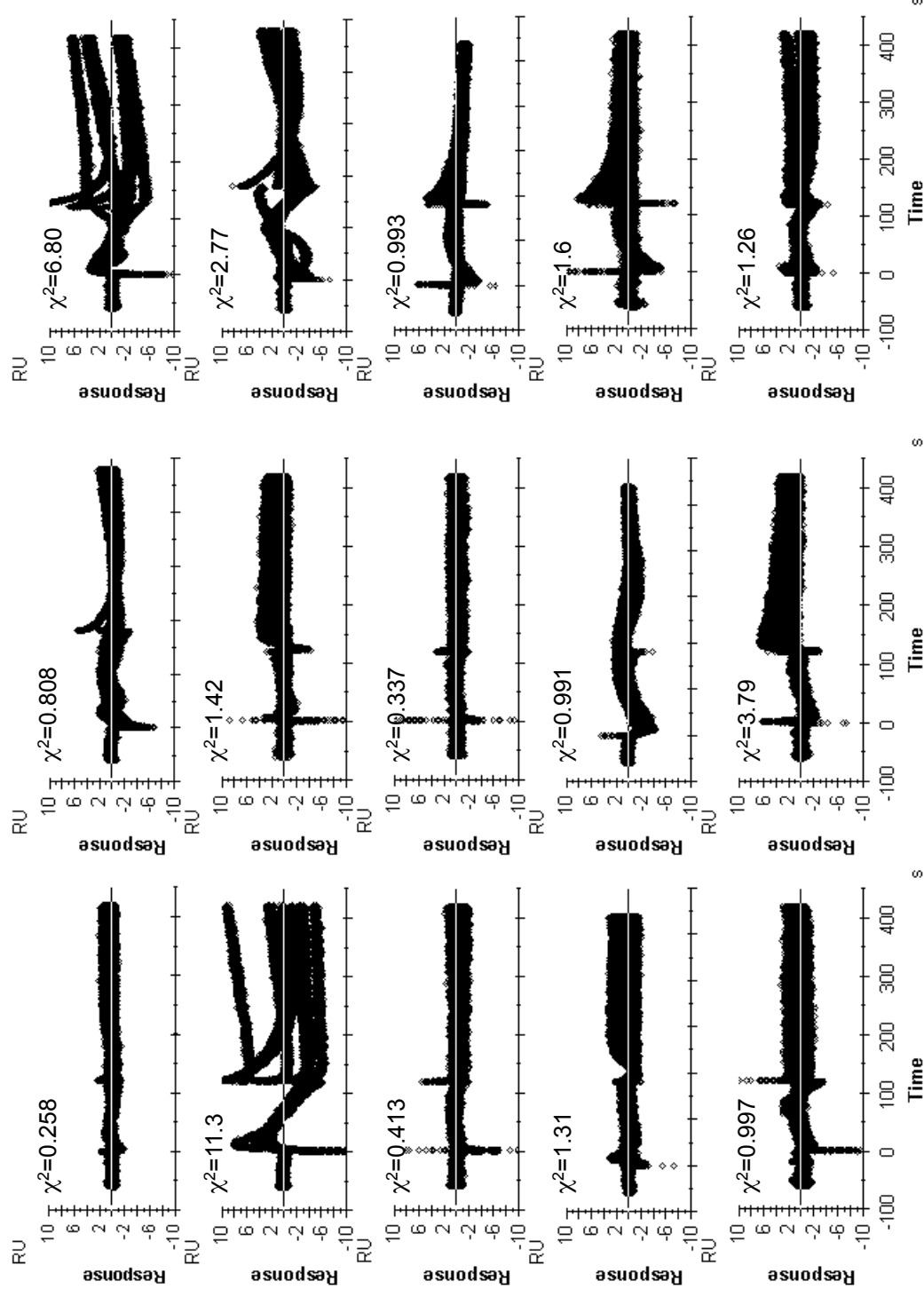
Supplementary Figure 1. Residual plots and corresponding χ^2 values for the fit of models to the SPR data presented in Figures 1, 2 and 3 of the main text. The combined residuals from the fit to the series of sensorgrams are shown. Starting from the **top row (left to right)**, Figure 1A HuR12, HuR123, TIAR12; **Second row**, Figure 1A TIAR123, Figure 1B HuR12, HuR123; **Third row**, Figure 1B TIAR12, TIAR123, Figure2 HuR12-8mer; **Fourth row**, Figure 2 HuR12-13mer and HuR12-17mer, Figure 3A HuR12; **Bottom row**, Figure 3A TIAR12, Figure 3B HuR12 and TIAR12.
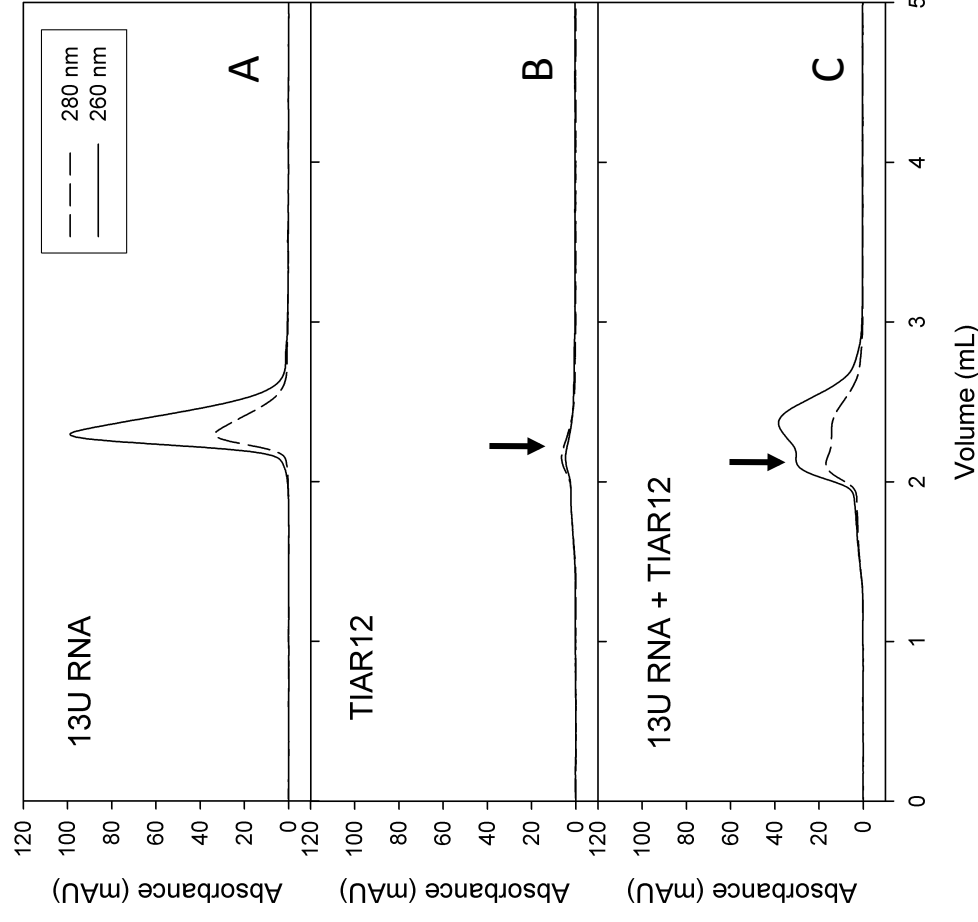
Supplementary Figure 2. Size exclusion chromatography profiles (Superdex™ 200 10/300 GL column from GE Healthcare) showing the interaction of TIAR12 and the 13-nt U-rich RNA used in the SAXS studies . A) 13U RNA alone, B) equimolar TIAR12 alone (shown on the same absorbance scale, its absorption at both wavelengths is much lower than that of the RNA) and C)13U-rich RNA and TIAR12 combined. The early eluting peak (indicated by the arrow) represents the TIAR12/RNA complex, followed by dissociated RNA.

Declaration for Thesis Chapter [5]

Declaration by candidate

In the case of Chapter [5], the nature and extent of my contribution to the work was the following:

Nature of contribution	Extent of contribution (%)
First author: Performed or supervised the preparation of proteins, oligonucleotides, and their complexes used in all experiments, carried out and supervised all SPR experiments and data analysis, designed and assisted in NMR experiments and processing, collated and analyzed the NMR data, and prepared the manuscript.	70

The following co-authors contributed to the work. Co-authors who are students at Monash University must also indicate the extent of their contribution in percentage terms:

Name	Nature of contribution	Extent of contribution (%)

		for student co-authors only
Yano M.K. Yoga[1]	Performed TIAR12s and TIAR2s protein production and assisted in SPR experiments.	7.5
Martin Scanlon[2]	Performed all NMR experiments, processed and assigned the NMR spectra.	N/A
Stephen Headey[2]	Processed and analyzed the HSQC NMR data.	N/A
Matthew C. J. Wilce[1]	Assisted with supervision and manuscript preparation.	N/A
Jacqueline A. Wilce[1]	Supervised the SPR experiments, designed the NMR experiments and oversaw the reporting.	N/A

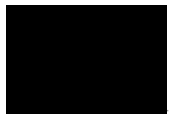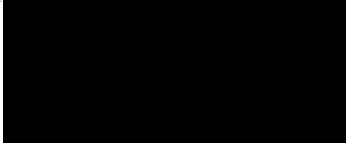| **Candidate's Signature**		**Date: 01/07/2010**

Declaration by co-authors

The undersigned hereby certify that:

(1)   the above declaration correctly reflects the nature and extent of the candidate's contribution to this work, and the nature of the contribution of each of the co-authors.

(2)   they meet the criteria for authorship in that they have participated in the conception, execution, or interpretation, of at least that part of the publication in their field of expertise;

(3)   they take public responsibility for their part of the publication, except for the responsible author who accepts overall responsibility for the publication;

(4)   there are no other authors of the publication according to these criteria;

(5)   potential conflicts of interest have been disclosed to (a) granting bodies, (b) the editor or publisher of journals or other publications, and (c) the head of the responsible academic unit; and

(6)   the original data are stored at the following location(s) and will be held for at least five years from the date indicated below:

Location(s)	1. Department of Biochemistry and Molecular Biology, Monash University, Clayton, Victoria 3800, Australia
	2. Department of Medicinal

	Chemistry, Monash University, Clayton, Victoria 3800, Australia

Signatures of co-authors

Yano M.K. Yoga		Date: 20th July
Martin Scanlon		2nd July 2010
Stephen Headey		13th July 2010
Matthew C. J. Wilce		1st July 2010
Jacqueline A. Wilce		1st July 2010

Characterization of distinct roles of TIAR RRMs and the hinge region in RNA- and DNA-binding using SPR and NMR

Henry Kim, Yano Yoga, *Stephen Headey, *Martin Scanlon, Matthew Wilce, Jackie Wilce

Department of Biochemistry and Molecular Biology, Monash University, Victoria 3800, Australia

*Faculty of Pharmacy and Pharmaceutical Sciences, Monash Institute of Pharmaceutical Sciences, Monash University, Victoria 3052, Australia

Abstract

The RNA-binding protein TIAR [related to TIA (T-cell restricted intracellular antigen)-1] is an mRNA-binding protein that acts as a translational repressor, and is particularly important under conditions of cellular stress. It binds to target mRNA and DNA via its RNA recognition motif (RRM) domains and is involved in both splicing regulation and translational repression via the formation of "stress granules". TIAR has also been shown to bind ssDNA and play a role in the regulation of transcription. Here, we show using surface plasmon resonance and NMR spectroscopy, specific roles of individual TIAR domains for its high affinity binding to RNA and DNA targets. We confirm that RRM2 of TIAR is the major RNA and DNA-binding domain. However, the strong nanomolar affinity binding to U-rich RNA and T-rich DNA only occurs in the presence of the six amino acid residues found in the hinge region C-terminal to RRM2 and presence of RRM1. On its own, RRM1 shows preferred binding to DNA over RNA. RRM3 makes little contribution to the overall binding affinities to both RNA and DNA targets. We further characterise the interaction between RRM2 with the C-terminal extension (TIAR2l) and an AU-rich target sequence (5'-UUAUUU-3') using NMR spectroscopy. ^{1}H-^{15}N HSQC titrations reveal specific residues involved in RNA binding including those in RNP1, RNP2, beta sheets, and the three residues (T174, R175, and K176) in the hinge region. We thus propose that TIAR RRM2, together with its C-terminal extension and presence of RRM1, are the major contributors for the high affinity (nM) interactions of TIAR with AREs.

Introduction

Previous studies have confirmed that TIAR binds with nanomolar affinity to U-rich RNA sequences, with the three RRMs contributing variously to the interaction (Dember et al. 1996; Kim et al. 2007). It was shown that RRM2 is both sufficient and necessary for binding to AREs and RRM3 showed binding to RNA but may have other specificities than AREs (Dember et al. 1996). RRM1 however showed no binding to U-rich sequences on its own. However, these measurements were conducted using nitrocellulose filter binding assays using GST-TIAR fusion proteins and 68-nt U-rich RNA sequences. So here we studied both affinity and kinetics of TIAR domains binding to 17-nt U-rich (class III ARE) RNA sequence using surface plasmon resonance (SPR) to fully and further explore the roles of separate TIAR domains in ARE-binding and understand exactly how they contribute towards the nanomolar interactions being observed. It has been shown previously that TIAR interacts strongly with ssDNA as well as with RNA (Suswam et al. 2005). Thus we further characterized the roles of individual domains of TIAR in DNA binding compared to their RNA binding. Furthermore, we have also explored the possible contribution of the C-terminal extension of TIAR RRM2 towards binding. The unstructured region outside or between the classic RRMs such as the C-terminal extension or the hinge region of other RRM-proteins such as TIA-1, HuR, and HuD has been shown to be significantly involved in ARE-binding (Fialcowitz-White et al. 2007; Kuwasako et al. 2008; Maris et al. 2005; Park et al. 2000; Park-Lee et al. 2003). Thus it was of interest to discover how it affects ARE-binding by TIAR. Finally, NMR spectroscopy was employed to obtain further insight into the involvement

of the specific TIAR RRM2 residues as well as those in the C-terminal extension in ARE-binding in solution.

Materials and Methods

Plasmid Construction and Protein Purification

Constructs for the expression of TIAR RRM123 (residues 1–283), TIAR RRM12l (residues 1–181), TIAR RRM1 (residues 1-94), and TIAR RRM2l (residues 94-181) (Dember et al. 1996) were transformed into *E. coli* strain BL21 (DE3) and the encoded proteins were expressed and purified as described previously (Chapter 2) (Dember et al. 1996). Constructs for the expression of TIAR RRM12s (residues 8–175) and TIAR RRM2s (residues 96-175) were cloned into pGEX-KG2T, expressed in *E. coli* BL21 (DE3), and purified as GST-fusion proteins (Figure 1).
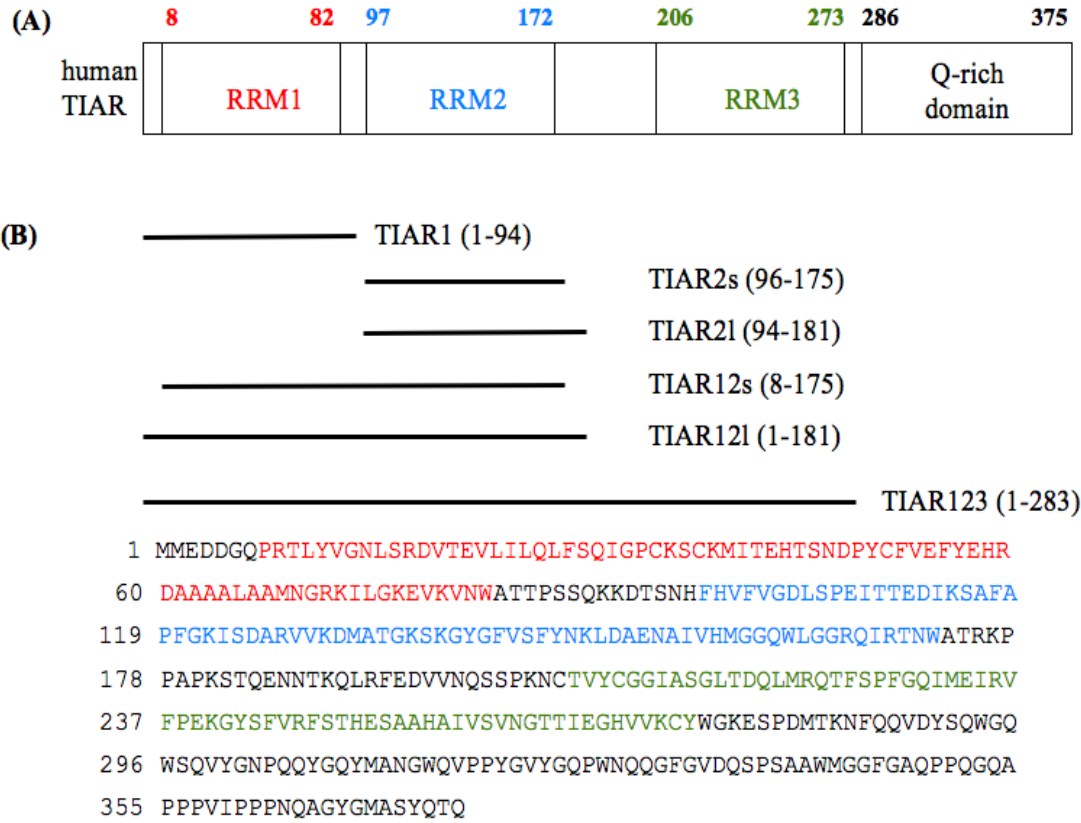
Figure 1. Domain structure, amino acid sequences, and different RRM constructs of human TIAR protein used in our binding assays. (A) Schematic representation of TIAR domain structure showing RRM1 (red), RRM2 (blue), RRM3 (green), and a glutamine-rich C-terminal region. (B) Different TIAR RRM constructs used in our study and the amino acid sequence of TIAR are shown.

The fusion tags were then cleaved by thrombin with gentle mixing at 4 °C for 16-20 hours and cleavage confirmed by SDS-PAGE analysis. The proteins were further purified by size-exclusion and cation-exchange chromatography. The concentration of each protein was determined using the Bradford assay (BioRad) and by A280 measurements using theoretical molar extinction coefficients (ProtParam). The extinction coefficients were validated for folded protein; A_{280} measurements were within

10 % of measurements made in 6.0 M guanidium hydrochloride. The purity of each protein was confirmed by SDS–PAGE.

Biosensor Experiments

The dynamics of RNA/DNA-protein interactions were characterized by surface plasmon resonance (SPR) using a BIACORE T100 instrument (Biacore Inc.). The oligonucleotides used in the analyses were: The U-rich RNA [containing poly (U) stretches; 5'-GGGGGGUUUUUUUUUUUUUUUUUGGGGG-3'] and T-rich DNA (5'-TTTTTTTTTTTTTTTTTTTT-3'). The oligonucleotides were chemically synthesized carrying a 5'-biotin tag (Dharmacon Research) to allow immobilization of the RNA/DNA onto streptavidin-coated sensor chips (Series S Sensor Chip SA, Biacore Inc.). RNA was diluted to a final concentration of 1 µM in HBS buffer (10 mM HEPES, pH 7.4, 150 mM NaCl) followed by heating at 80 ^{o}C for 10 min, and cooling to room temperature. The sample was then diluted 500-fold in running buffer (10 mM HEPES, pH 7.4, 150 mM NaCl, 1 mM DTT, 0.025 % surfactant P20; Biacore Inc.) and injected over the sensor chip surface at 10 µl/min at 25 ^{o}C to generate a ~50 response unit (RU) RNA/DNA surface (for a low-density surface). Proteins were serially diluted in running buffer to the concentrations indicated in Figures 2 and 3, and injected at 25 ^{o}C at a flow rate of 50 µl/min for 2-3 min. Surface regeneration to remove any protein that remained bound after 3-6 min of dissociation was achieved using a 1- min injection of 2 M NaCl at 50 µl/min. Analyses of protein concentrations were done in duplicates and any background signal from a streptavidin-only reference flow cell was subtracted from

every data set. Data were analyzed using a simple 1:1 Langmuir interaction model or 2-state (conformational change) model using the Biacore T100 evaluation software (Biacore Inc.) to determine the kinetics (association/dissociation rate constants; k_a/k_d) as well as the affinities (K_D) of the protein-RNA/DNA interactions.

NMR Experiments and Data Analyses

Preparation of TIAR2l (^{15}N,^{13}C)

Uniformly-labelled TIAR2l (^{15}N,^{13}C) for NMR experiments was expressed in *E. coli* BL21 (DE3) in M9 salt-based minimal media supplemented with ^{15}N NH$_4$Cl (1 g/L) and ^{13}C glucose (3 g/L) (Cambridge Isotope Laboratory, Andover, MA). The culture was grown till the desired OD$_{600}$ of 0.8~1.0 was reached, induced with IPTG (0.5 mM) for 3 hours and the cells were harvested by centrifugation. The cell pellets were stored at -80 ^{o}C overnight, thawed out on ice and resuspended in lysis buffer (50 mM Tris pH 8.0, 150 mM NaCl, 1 mM EDTA, 1 % Triton X-100, 5 % Glycerol, 1 mM DTT, 0.1 mM PMSF), and purified as a GST-fusion protein in the same way as the unlabelled TIAR RRM2l. The purified protein was then dialyzed into the phosphate buffer (50 mM phosphate buffer pH6, 100 mM NaCl) and concentrated to a final concentration of 300 µM with 10 % D$_2$O.

NMR Spectroscopy

The experiments were performed on a Varian Unity AS600 MHz spectrometer at 298 K (25 ^{o}C) with a triple resonance gradient probe. Standard triple resonance experiments as

well as 2D (^{15}N,^{1}H)-HSQC were run to obtain full sequential assignments of backbone resonances for TIAR2l. These include HNCA, HNCACB, HNCACO, HNCO, and CBCA(CO)NH. (^{15}N,^{1}H)-HSQC spectra were recorded for chemical shifts of TIAR2l alone and with the increasing concentrations of RNA. For RNA-titration experiments, 6-nt AU-rich RNA (5' UUAUUU 3') (Dharmacon) was added to TIAR2l at protein:RNA molar ratios of 1:0, 1:0.4, 1:0.8, and 1:1.2. Data were processed using NMRPipe (Delaglio et al., 1995) and analysed with SPARKY (Goddard and Kneller, UCSF, CA).

Results

Different TIAR domains have distinctive roles in ARE-bindng.

The constructs representing one, two and three RRM domains of TIAR (TIAR1, TIAR2, TIAR12, and TIAR123) were prepared as described in Materials and Methods (Figure 1). Their binding to a U-rich [a poly (U) stretch comprising 17 U residues flanked by G residues] RNA sequence was then characterised using SPR (Figure 2).
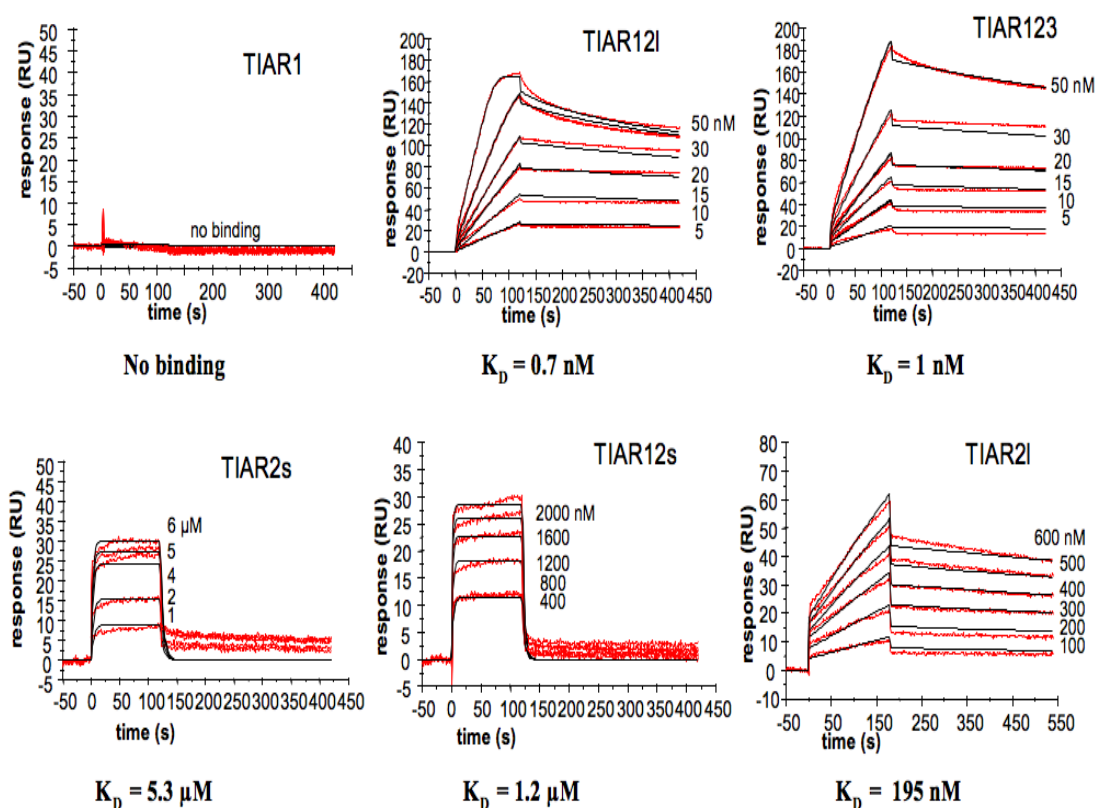
Figure 2. Kinetic analysis of the interactions of different TIAR domains with U-rich RNA (Surface Plasmon Resonance). The binding of TIAR1, TIAR2 (short and long), TIAR12 (short and long), and TIAR123 proteins to a U-rich RNA (28-mer) is shown. Biotinylated RNA was captured on SA-coated sensor chips and increasing concentrations of protein were injected over the surface. Injections were performed for 120 seconds (association phase), followed by a 300-second flow of running buffer to assess dissociation. The experiments were conducted in duplicate and showed good overlap. The red lines represent the binding responses for injections of protein analyte at specified concentrations (nM) over the RNA surface. The kinetic data was fit by 1:1 Langmuir binding model which describes monovalent analyte binding to a single site on the immobilized ligand. Mass transport effects were not evident. The black curves superimposed on top of the sensorgrams represent the model fitted curves. The rate constant k_a and k_d were determined simultaneously as global fitting parameters from which the K_D was determined. The resulting parameter values are given in Table 1 (Note that sensorgrams for TIAR12l and TIAR123 are reproduced from Kim et al., 2007 Figure 3 with permission from the American Society for Microbiology to assist visual comparison with other sensorgrams).

It is of note that the original TIAR12 and TIAR2 constructs (as studied by Dember et al., 1996) extend 36 amino acids C-terminal to RRM2 (amino acids 1-208 and 94-208 respectively). Shorter constructs were therefore cloned that extend only three residues C-terminal to RRM2 domain (amino acids 8-175 and 96-175) and are referred to as TIAR12 short (TIAR12s) and TIAR2 short (TIAR2s) (Figure 1). It became apparent, however, in the course of our studies that the original TIAR12 is susceptible to specific proteolytic cleavage (as are TIAR2 and TIAR123) at residue 181 (as determined by the mass spec-determined molecular weight of the cleaved TIAR2, TIAR12 and TIAR123 which was later confirmed by the full sequential assignments of backbone resonances for TIAR2 by NMR) (Figure 5). For the purpose of this study, the cleaved TIAR12 and TIAR2 are referred to as the TIAR12 long (TIAR12l) and TIAR2 long (TIAR2l) respectively for ease of comparison with the shorter constructs (Figure 1). Interestingly, there was little difference in the binding ability to U-rich RNA between TIAR12l and the original TIAR12 construct (preliminary data). The six sensorgrams (Figure 2) show the binding of a range of concentrations of TIAR1, TIAR2s, TIAR2l, TIAR12s, TIAR12l, and TIAR123 when injected across the U-rich RNA-coated chip. The association rate constants (k_a), dissociation rate constants (k_d), and overall equilibrium dissociation constants (K_D) for each protein, as approximated by a simple 1:1 Langmuir binding model, are shown in Table 1.

| Protein	RNA	k_a (1/Ms)	k_d (1/s)	K_D (k_d/k_a, nM)
TIAR1	U-rich	N/A	N/A	No Binding
TIAR2s	U-rich	$(3.49 \pm 0.09) \times 10^4$	$(1.84 \pm 0.03) \times 10^{-1}$	5268 ± 223
TIAR12s	U-rich	$(2.30 \pm 0.02) \times 10^5$	$(2.77 \pm 0.02) \times 10^{-1}$	1203 ± 20
TIAR2l	U-rich	$(1.84 \pm 0.01) \times 10^3$	$(3.60 \pm 0.1) \times 10^{-4}$	195 ± 6.4
TIAR12l	U-rich	$(4.10 \pm 0.11) \times 10^6$	$(2.83 \pm 0.08) \times 10^{-3}$	0.69 ± 0.04
TIAR123	U-rich	$(1.58 \pm 0.02) \times 10^6$	$(1.56 \pm 0.01) \times 10^{-3}$	0.99 ± 0.02

Table 1. Kinetic and affinity constants for the interactions of different TIAR RRMs with U-rich RNA. The association and dissociation rate constants (k_a and k_d) were determined as global fitting parameters for a 1:1 binding model. The equilibrium dissociation constant was determined as k_d/k_a.

TIAR12l and TIAR123 both bound U-rich RNA with nM affinities (Kd ~ 1nM) and bind with similar association and dissociation rate constants - demonstrating that RRM3 does not contribute detectably to, or impact on, the overall binding affinity to a U-rich RNA sequence (Kim et al. 2007). TIAR1 showed no binding. These data confirm TIAR RRM2 as the major ARE-binding domain and are consistent with the report by Dember et al., (1996) [K_D of 20 nM and 40 nM were reported for TIAR123 and TIAR12 binding to U-rich RNA respectively. No RNA binding was shown for TIAR1]. Having confirmed TIAR RRM2 as the major binding domain, we examined the binding of RRM2 alone (TIAR2s) with U-rich RNA anticipating strong nanomolar binding. But unexpectedly, we observed much less binding with K_D of ~ 5 µM (Figure 2). From this we concluded that either there is a considerable synergistic binding effect of RRM1 N-terminal to RRM2, and/or that the six extra residues at the C-terminus of TIAR RRM2

was also contributing to binding. Thus we examined the binding of TIAR12s and TIAR2l to U-rich RNA to be able to distinguish between the role of RRM1 and the C-terminal extension in contributing to RRM2 binding respectively. Interestingly, TIAR12s binds with 5-fold higher affinity (K_D ~1 μM) than TIAR2s and TIAR2l binds with > 25-fold higher affinity than TIAR2s (K_D = 195 nM). When both RRM1 and RRM2 C-terminal extension are contributing together, TIAR12l results in > 1000-fold increase in affinity (K_D ~1 nM) than TIAR2s. This suggests that not only is the RRM2 domain responsible for U-rich RNA binding, but also the part of the region beyond the classically structured motif as well as the RRM1 synergy contribute strongly towards ARE-binding.

Different TIAR domains also have distinctive roles in DNA binding and exhibit similar kinetics and affinity to their RNA binding

The constructs representing one, two and three RRM domains of TIAR (TIAR1, TIAR2s, TIAR2l, TIAR12s, TIAR12l, and TIAR123) were prepared as described in Materials and Methods (Figure 1). Their binding to a T-rich [a poly (T) stretch comprising 20 T residues] DNA sequence was then characterised using SPR (Figure 3).
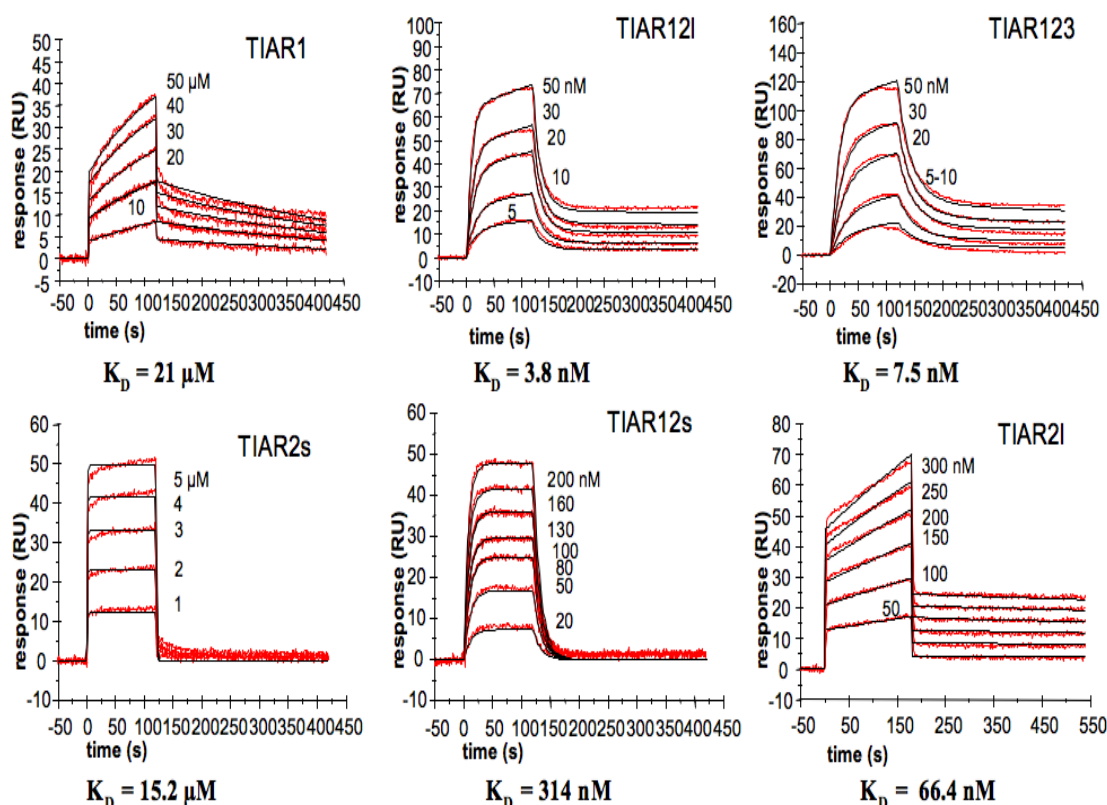
Figure 3. Kinetic analysis of the interactions of different TIAR domains with T-rich DNA (Surface Plasmon Resonance). The binding of TIAR1, TIAR2 (short and long), TIAR12 (short and long), and TIAR123 to T-rich DNA is shown. Biotinylated DNA was captured on SA-coated sensor chips and increasing concentrations of protein were injected over the surface. Injections were performed for 120 seconds (association phase), followed by a 300-second flow of running buffer to assess dissociation. The experiments were conducted in duplicate and showed good overlap. The red lines represent the binding responses for injections of protein analyte at specified concentrations (nM) over the DNA surface. The kinetic data was fit by the 1:1 Langmuir binding model (except for TIAR12l and TIAR123 binding T-rich DNA which were estimated by the 2-state model). Mass transport effects were not evident. The black curves superimposed on top of the sensorgrams represent the model fitted curves. The rate constants k_a and k_d were determined simultaneously as global fitting parameters from which the K_D was determined. The resulting parameter values are given in Table 2 (Note that the sensorgram for TIAR12l is reproduced from Chapter 4 Figure 3 to assist visual comparison with other sensorgrams).

The six sensorgrams show the binding of a range of concentrations of TIAR1, TIAR2s, TIAR2l, TIAR12s, TIAR12l, and TIAR123 when injected across the T-rich DNA-coated chip. The association and dissociation rate constants (k_a and k_d) and overall equilibrium dissociation constants (K_D) for each binding were estimated by a 1:1 Langmuir binding model except for TIAR12l and TIAR123 which were best estimated by the 2-state (conformational change) model (Table 2).

Protein	DNA	k_a (1/Ms)	k_d (1/s)	K_D (k_d/k_a, nM)
TIAR1	T-rich	$(1.12 \pm 0.02) \times 10^2$	$(2.34 \pm 0.02) \times 10^{-3}$	20970 ± 557
TIAR2s	T-rich	$(7.13 \pm 0.1) \times 10^4$	1.09 ± 0.01	15220 ± 353
TIAR12s	T-rich	$(2.54 \pm 0.01) \times 10^5$	$(7.98 \pm 0.02) \times 10^{-2}$	313.9 ± 2.04
TIAR2l	T-rich	$(3.36 \pm 0.06) \times 10^3$	$(2.23 \pm 0.05) \times 10^{-4}$	66.37 ± 2.68
TIAR12l	T-rich	$(7.80 \pm 0.75) \times 10^6$	$(4.49 \pm 0.44) \times 10^{-1}$	3.81 ± 0.74
TIAR123	T-rich	$(1.57 \pm 0.04) \times 10^6$	$(7.61 \pm 0.17) \times 10^{-2}$	7.47 ± 0.33

Table 2. Kinetic and affinity constants for the interactions of different TIAR RRMs with T-rich DNA. The association and dissociation rate constants (k_a and k_d) were determined as global fitting parameters for a 1:1 binding model or a 2-state model in the case of TIAR12l and TIAR123 binding T-rich DNA where k_a and k_d represents k_{a1} and k_{d1} respectively. The equilibrium dissociation constant K_D was determined as k_d/k_a for the 1:1 binding or $1/\{(k_{a1}/k_{d1}) \times (1 + k_{a2}/k_{d2})\}$ for the 2-state binding (k_{a1} and k_{d1}: association and dissociation rate constants; k_{a2} and k_{d2}: forward and reverse rate constants for conformational change; For TIAR12l-T-rich DNA binding, $k_{a2} = 0.0026$ s^{-1}, $k_{d2} = 1.84 \times 10^{-4}$ s^{-1}; For TIAR123-T-rich DNA binding, $k_{a2} = 0.0028$ s^{-1}, $k_{d2} = 5.04 \times 10^{-4}$ s^{-1}).

Figure 3 shows that TIAR1 does bind DNA although with micro molar affinity (21 μM). TIAR12l however shows strong binding with low nanomolar affinity confirming RRM2 as the major DNA-binding domain. TIAR123 shows an affinity similar to that of TIAR12l suggesting that the role of RRM3 in T-rich DNA-binding may be redundant as

in U-rich RNA binding. Having confirmed TIAR RRM2 as the major DNA-binding domain, we examined the binding of RRM2 alone (TIAR2s) to DNA again anticipating strong nanomolar affinity binding. But just as we observed with the RNA binding, we observed a lower affinity with K_D of $\sim$ 15 μM (Figure 3). This suggests that either strong involvement of the C-term extension and/or synergy between RRM1 and 2 is necessary for strong DNA binding. Thus we examined the binding of TIAR12s and TIAR2l to T-rich DNA to be able to distinguish between the role of RRM1 and the C-terminal extension residues in contributing to RRM2 binding respectively. Interestingly, TIAR12s binds with $\sim$50-fold higher affinity ($\sim$300 nM) than TIAR2s and TIAR2l binds with > 100-fold higher affinity than TIAR2s. Together, TIAR12l results in > 1000-fold increase in affinity ($\sim$4 nM) than TIAR2s. These results suggest that different domains of TIAR participate in T-rich DNA binding with quite similar kinetics and affinity to their U-rich RNA binding. TIAR RRM2 is still the major binding domain and the six C-terminal extension residues of RRM2 is heavily involved in binding again. RRM1 however, shows μM binding to T-rich DNA whereas it did not show any binding to U-rich RNA.

Identification of the key residues of TIAR RRM2 and the hinge region involved in ARE-binding by NMR

Having confirmed TIAR RRM2 with its short C-terminal extension of six amino acid residues (KPPAPK) as the key RNA (and DNA) binding domain (Figure 4), it was of

interest to identify the specific regions (residues) involved in ARE-binding, especially in

the extension region.
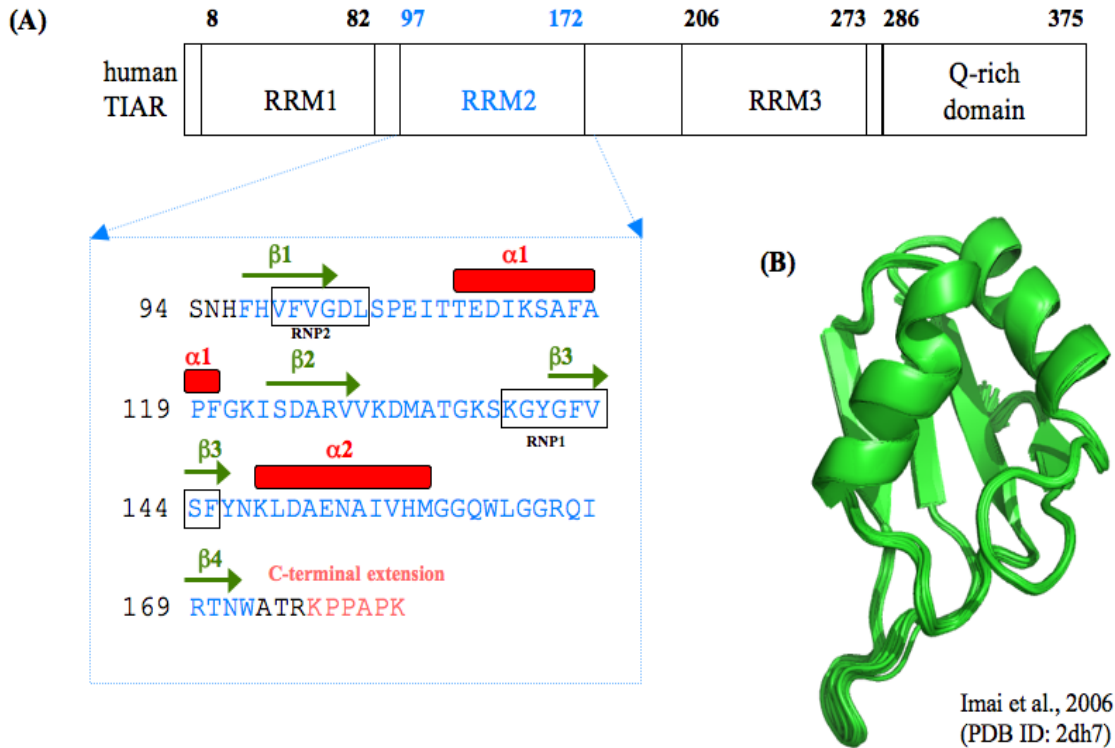
Figure 4. Structure of the human TIAR RRM2 (TIAR2l, AA 94-181). (A) Domain
structure of TIAR with the RRM2 highlighted and inserted in blue. Secondary structure
elements as well as the C-terminal extension region are indicated above the amino acid
sequence and the RNP1 and RNP2 are boxed and labeled below the sequence. (B) NMR
structure of human TIAR RRM2 is shown as a cartoon (Imai et al., 2006; PDB 2dh7).
The image was created using PyMOL.

Thus NMR spectroscopy was employed to examine their interactions in solution. The

involvement of hinge regions in ARE-binding has been reported previously in other

RRM proteins such as TIA-1 and HuR/D (Fialcowitz-White et al. 2007; Kuwasako et al.

2008; Park et al. 2000; Park-Lee et al. 2003), but identification of specific residues

within the region and their direct impact on binding affinity and kinetics to ARE targets

have not been fully explored. The six amino acid residues in the linker region at the C-terminus of RRM2 are well conserved among TIA-proteins but show poor homology with other RRM-containing RBPs such as Hu-proteins, AUF-1, and U2AF[65]. Double-labelled TIAR2l (^{15}N,^{13}C) was prepared from which the full backbone-assignments of entire TIAR2l residues (94-181) were made (data collection and sequential assignments were conducted by Martin Scanlon and Steven Headey). Figure 5 shows the (^{15}N,^{1}H)-HSQC spectra of TIAR2l alone and in complex with different concentrations (protein : RNA molar ratio of 1:0, 1:0.4, 1:0.8, and 1:1.2) of AU-rich RNA (5' UUAUUU 3') from which the effects of ARE-binding on chemical shift perturbation values of main chain amide peaks were quantified. The 6-nt AU-rich RNA was chosen for its length to maximise the interaction while minimising possible multiple binding, and for its sequence to provide a more stable complex with TIAR than U-rich sequence based on our findings from the kinetic studies of TIAR binding U- vs. AU-rich RNA (Chapter 4).
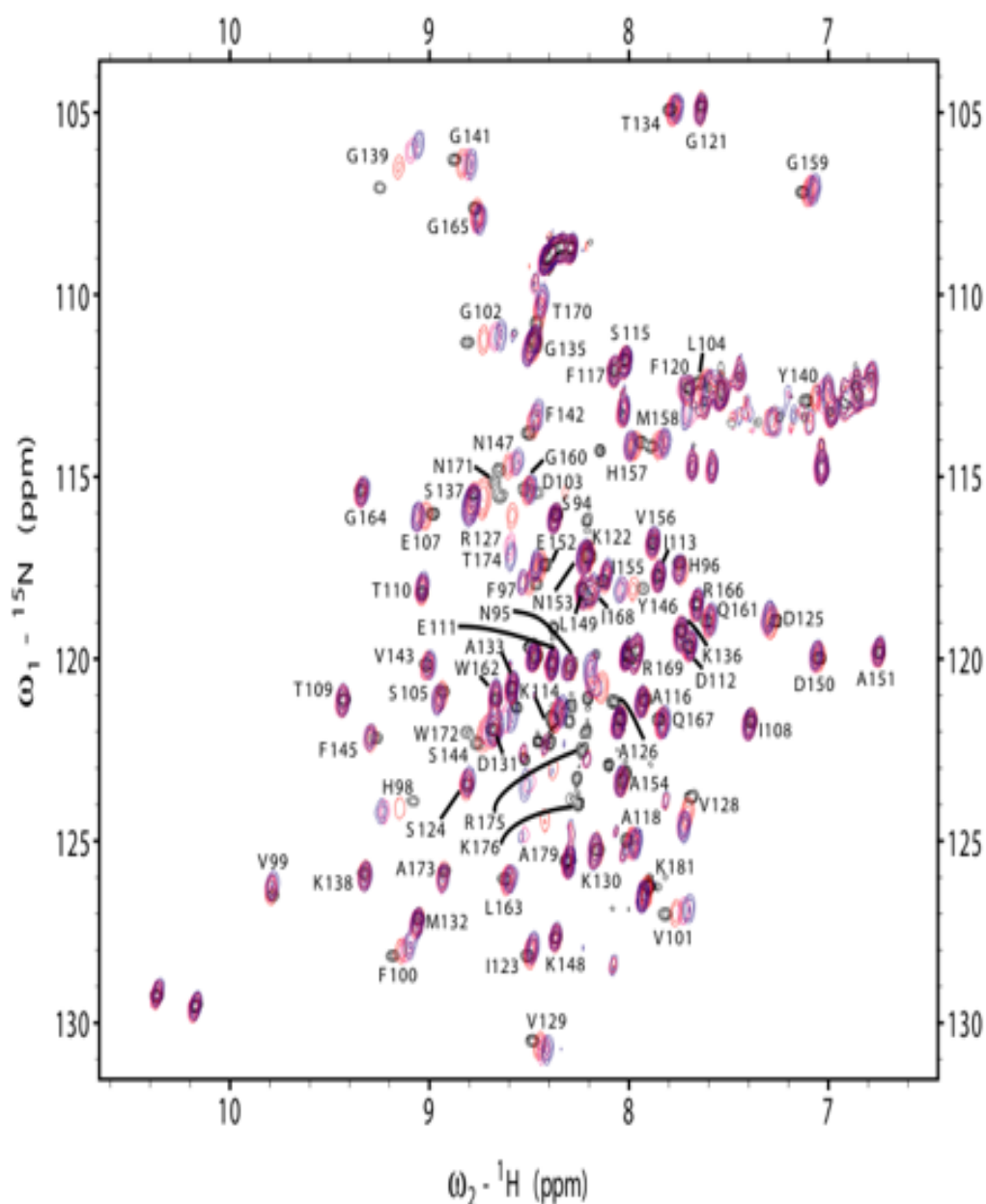
Figure 5. Identification of the key binding sites on TIAR2l involved in AU-rich RNA binding. An overlay of the (^{15}N,^{1}H)-HSQC spectra of TIAR2l alone and in complex with different concentrations of 6nt AU-rich RNA (5' UUAUUU 3'). The molar ratio of TIAR2l to RNA is 1:0 (black), 1:0.4 (red), 1:0.8 (pink), and 1:1.2 (blue).

Upon addition of the RNA, we observed significant chemical shift perturbations of specific ^{15}N,^{1}H peaks almost in a straight line continuously with increasing RNA concentrations which indicates that these are in fast exchange with the RNA compared to NMR time-scale. We also observed disappearance of specific ^{15}N,^{1}H peaks (N171, W172, R175, and K176) after adding the RNA indicating that these are in intermediate exchange with the RNA (Figure 5). Overall, the cross-peaks strongly affected by the ARE-binding include β1 (H98), RNP2 (F100, V101, and G102), β2 (A126, R127, V128, and V129), RNP1 (G139, Y140, G141, F142, and S144), β3-α2 loop (Y146 and N147), β4 (T170, N171 and W172), and the C-terminal extension (Figure 6).
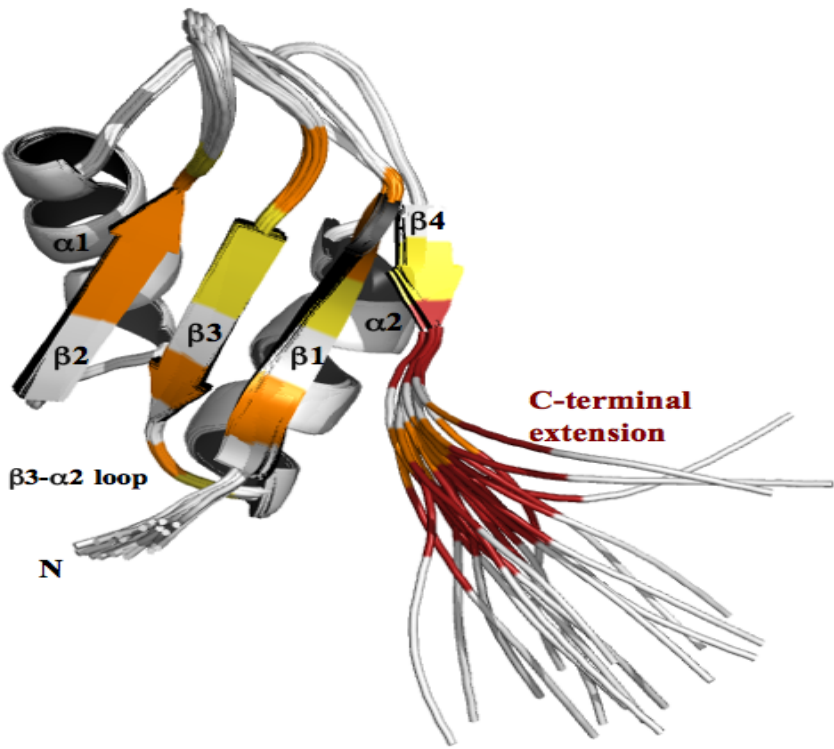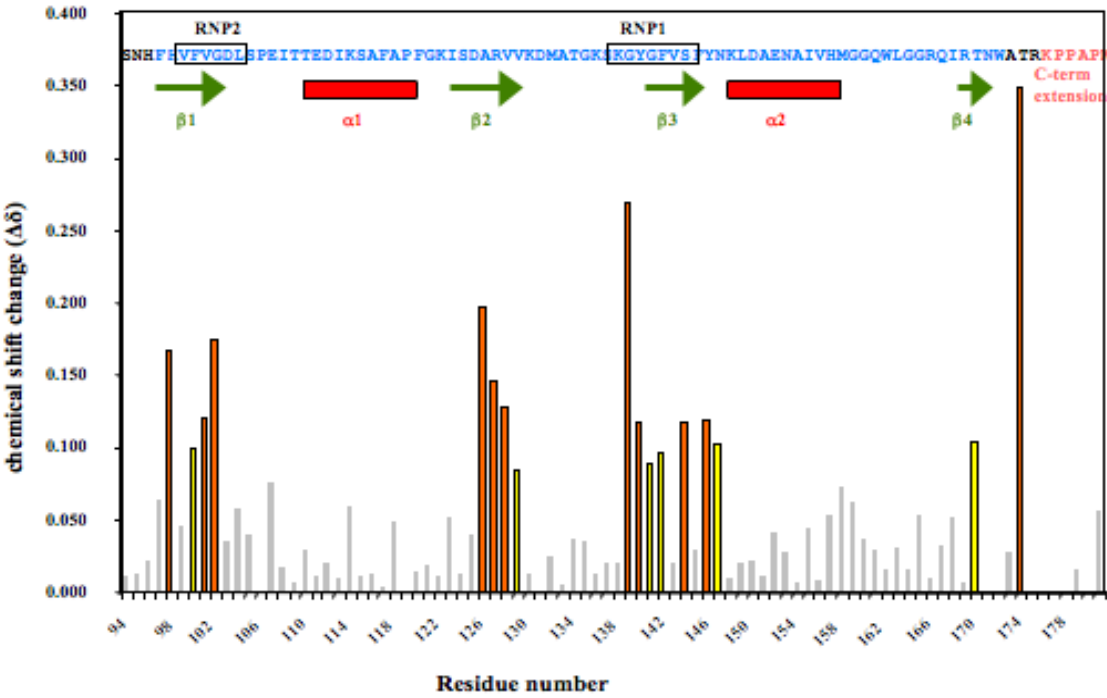
Figure 6. ARE-binding region on the TIAR RRM2. (Top) Chemical shift perturbation values were determined from the analysis of $(^{15}N,^1H)$-HSQC spectra of TIAR2l upon the addition of AU-rich RNA (The ratio of TIAR2l to RNA = 1:1.2, Concentration of TIAR2l = 300 μM). The chemical shift change was calculated as $\Delta\delta = \{(\delta^{15}N\times0.154)^2+(\delta^1H)^2\}^{1/2}$ and plotted against the amino acid sequence of TIAR2l. Top 20 residues showing significant perturbations or disappeared upon RNA-binding (N171, W172, R175, K176) are colored (orange > 0.12 ppm; yellow > 0.08 ppm) and they map to specific regions of TIAR2l secondary structure expected to be involved in RNA binding. D131 peak was overlapped after adding the RNA. (Bottom) Cartoon representation of the TIAR RRM2 structure (Imai et al., 2006; PDB 2dh7) with residues affected by RNA-binding colored: The residues which disappeared upon RNA-binding (in intermediate exchange) are colored in RED; The residues with greater than 0.12 ppm chemical shift perturbations are colored in ORANGE; The residues with greater than 0.08 ppm chemical shift perturbations are colored in YELLOW; And all the rest of the residues which showed minimal or no chemical shift perturbation upon RNA binding are colored in GRAY.

Interestingly, among the extension residues, K176 was the most significantly affected as it completely disappeared upon RNA binding (in intermediate exchange with the RNA). T174 and R175 were also significantly affected with Arg in intermediate exchange with the RNA. These results strongly support our SPR binding data and confirm that TIAR2 and the C-terminal extension region interact with the RNA target giving rise to the observed nanomolar affinity. Further studies are underway to explore and identify the residues to the N-terminus of RRM2 which may also be involved in strong interaction with ARE.

Discussion

Different TIAR RRMs have distinctive roles in RNA and DNA binding.

Previous studies have shown that TIAR strongly interacts with both RNA and DNA targets with nanomolar affinities (Dember et al. 1996; Kim et al. 2007; Suswam et al. 2005). In the current study, we further explore and compare the unique roles of different domains of TIAR in U-rich RNA and T-rich DNA binding by studying the kinetics and affinity of their interactions. Overall, TIAR domains bind both RNA and DNA targets with relatively similar kinetics and affinity (Table 1, 2). This is in contrast to another triple RRM-containing ARE-binding protein HuR that preferentially binds to RNA over DNA (Chapter 4). We confirm that RRM2 is the major binding domain as shown previously. But we also show the significant contribution of the six residues within the hinge region between RRM2 and RRM3 towards tight binding. RRM1 shows no binding to U-rich RNA but it binds T-rich DNA with micro molar affinity (Figure 2, 3).

The detailed kinetic analyses of separate TIAR RRMs binding U-rich RNA is shown in Table 1, and it reveals some very interesting 'hidden' information about their binding. The presence of six extension residues (KPPAPK) at C-terminus of RRM2 seems to have a remarkable effect on the dissociation rate constants, but not so much on the association rate constants of binding. All the TIAR domains containing the extension residues (TIAR2l, 12l, 123) have much slower dissociation rate constants of ~10^{-3} to 10^{-4} s^{-1} compared to ~10^{-1} s^{-1} for those without the extension (TIAR2s and 12s) (table 1). However, the association rate constants are quite similar for both TIAR2s and 2l (~10^3 to

10^4 $M^{-1}s^{-1}$) as well as for TIAR12s and 12l ($\sim 10^5$ to 10^6 $M^{-1}s^{-1}$). This interesting observation suggests to us that the extension residues are more likely to be involved in the stability of the TIAR-RNA interactions, but not so much in the initial electrostatic interactions.

In contrast, comparing TIAR12l vs TIAR2l reveals that they both have similar dissociation rate constants ($\sim 10^{-3}$ to 10^{-4} s^{-1}) but quite different association rate constants ($\sim 10^3$ for TIAR2l compared to 10^6 $M^{-1}s^{-1}$ for TIAR12l). Comparing TIAR12s vs TIAR2s also shows that they have similar dissociation rate constants ($\sim 10^{-1}$ s^{-1}) but different association rate constants ($\sim 10^4$ for TIAR2s compared to 10^5 $M^{-1}s^{-1}$ for TIAR12s). These results provide us with a clue that the RRM1 and/or the hinge region between RRM1 and 2 could potentially be involved in the initial electrostatic interactions with the U-rich RNA giving rise to the faster association rate constants, but not likely to be involved in the stability of the TIAR-RNA complex. It is also possible that the bivalency of TIAR12 constructs could contribute towards faster association rate constants as they have twice the chance of a productive initial interaction with the U-rich RNA via one RRM compared to the TIAR2 constructs. Although TIAR RRM1 alone does not show any binding to U-rich RNA, it is likely that it contributes to binding - though the possibility that the hinge region between RRM1 and RRM2 underlies our observation remains to be verified (currently under investigation). The role of the hinge region in ARE-binding kinetics and affinity has also been shown in previously studies involving Hu-proteins (Fialcowitz-White et al. 2007; Park et al. 2000). It was shown that the hinge region

between RRM2 and RRM3 of HuD protein affects the stability of its ARE-binding as the dissociation rate constant increased significantly in its absence whereas the association rate constant remained relatively similar (Park et al. 2000). In the case of HuR, the hinge region between RRM2 and RRM3 again contributed significantly to ARE-binding in a length dependent manner by increasing the RNA-binding affinity (> 30-fold) (Fialcowitz-White et al. 2007). The specific residue(s) within the hinge region of HuR/D proteins responsible for affecting the kinetics and affinity of their ARE-binding are yet to be identified.

The detailed kinetic analysis of separate TIAR RRMs binding T-rich DNA is shown in Table 2, and again it provides us with some crucial information about their binding: Comparing TIAR2l vs. TIAR2s, there is a dramatic difference in their dissociation rate constants ($\sim10^{-4}$ s^{-1} for TIAR2l compared to ~1 s^{-1} for TIAR2s) whereas the association rate constants are relatively similar ($\sim10^3$ to 10^4 $M^{-1}s^{-1}$). Comparing TIAR12s vs TIAR2s, they both have relatively similar association rate constants ($\sim10^4$ to 10^5 $M^{-1}s^{-1}$), but TIAR12s has a much slower dissociation rate constant than TIAR2s (~1 for TIAR2s compared to 10^{-2} s^{-1} for TIAR12s). The difference in their dissociation rate constants here is quite unique to DNA-binding and not seen in RNA-binding at all (Table 1: Both TIAR12s and TIAR2s have similar dissociation rate constants of $\sim10^{-1}$ s^{-1} when binding U-rich RNA). These data suggest that TIAR RRM1 may contribute to the stability of DNA binding, but not to the RNA binding.

Interactions involving TIAR12l and TIAR123 with T-rich DNA could not be fitted using simple 1:1 Langmuir binding model and instead they were analysed using 2-state (conformational change) model. This is by no means a proof of 2-state interactions, but an indication of more complicated binding events than simple 1:1 binding occurring on the surface of the chip and requires further investigation and optimisation (Rich and Myszka 2007, 2008).

The data presented here provide a fascinating insight into how TIAR might be interacting with ARE and DNA targets in vivo. They not only confirm TIAR RRM2 as a major RNA and DNA binding domain but also indicate the possible roles of the C-terminal extension in the stability of TIAR-RNA/DNA complexes formation and the region at N-terminus of RRM2 possibly in initial binding with the target RNA and DNA. Unlike their RNA binding, TIAR RRM1 can bind DNA although at μM affinity and may contribute to the stability of TIAR-DNA complex formation. This study also provides a detailed kinetic evidence underlying the previous report of TIAR being able to bind strongly to a single-stranded T-rich DNA, which may position TIAR to modulate transcription and help to localise TIAR to U-rich RNA once released from its DNA-binding site by active transcription for further processing, nucleocytoplasmic transport or post-transcriptional regulation (Suswam et al. 2005).

TIAR RRM2 as well as its C-terminal extension residues are significantly involved in ARE-binding.

The above findings clearly indicate that RRM2 and its C-terminal extension residues are the key contributors of the nanomolar affinity interactions observed between TIAR and its ARE-targets. Thus we employed NMR spectroscopy to identify and obtain further insight into the involvement of specific residues of TIAR RRM2 and its C-terminal extension in binding target RNA sequences in solution. This revealed involvement of specific residues of TIAR2l in forming complex with the 6-nt AU-rich RNA target (5' UUAUUU 3') (Figure 6). These include residues in RNP1 and 2, as well as the residues on beta sheets and β-α loop. These are typically expected classic RNA target-binding sites on the RRM as shown in many previous studies involving RRM family of proteins and their RNA targets (Auweter et al. 2006; Clery et al. 2008).

However they also include the three residues at the C-terminus of RRM2, T174, R175, and K176. This supports our SPR data and provides direct evidence for the involvement of these residues in the stable TIAR-RNA complex formation. Prolines at positions 177, 178, and 180 may also be involved in the interaction but this would not have been observed as they lack amide proton, therefore, no chemical shift can be observed. A179 and K181 however, were not perturbed suggesting that the interaction does not extend to this part of the hinge region. More interestingly, of the three residues at C-terminus of RRM2 involved in binding, two (T174 and R175) are included in all TIAR constructs containing RRM2. But K176 is only included the longer TIAR2 constructs used in our

SPR experiments (TIAR2l, TIAR12l, and TIAR123) which showed higher affinity interactions with U-rich RNA with slower dissociation rate constants than the shorter constructs (Figure 2). Thus K176 may be a key contact residue and play an important role in the stability of TIAR-RNA complex formation. This finding signifies the involvement of not only the key residues within the classically structured TIAR RRM2, but also the residues outside the structured motif in strong ARE-binding.

The involvement of the unstructured region outside the RRM in RNA-binding has also been documented in previous studies involving other RBPs (reviewed in Maris et al., 2005). TIA-1 RRM2, which shares 92 % sequence homology and an identical C-terminal extension with TIAR RRM2, has been investigated for its mode of interaction with the target RNA (Kuwasako et al. 2008). Chemical shift perturbation analyses of TIA-1 RRM2 with 5-nt U-rich RNA revealed that the cross-peaks strongly affected by the RNA-binding include β1 (H98), RNP2 (F100 and G102), β2 (A126, R127, V128, and V129), RNP1 (K138, G139, F142, and S144), β4 (T170, N171 and W172), and the C-terminal extension (A173, R175, and K176) (Kuwasako et al. 2008). Interestingly, they are almost identical as the cross-peaks of TIAR RRM2 strongly affected by the 6-nt AU-rich RNA binding (Figure 6) suggesting that they may have similar modes of interaction with AREs. This is not surprising given that their structures and sequences are highly homologous. But there were also differences between them. K138 and A173 in TIAR2l were not strongly affected by the AU-rich RNA binding. V101 (RNP2), Y140 and G141 (RNP1), and Y146 and N147 (β3-α2 loop) in TIAR2l were significantly

affected by the AU-rich RNA binding (Figure 6), but not by the U-rich RNA binding in TIA-1 RRM2 possibly due to their sequence specificity (6-nt AU- vs. 5-nt U-rich RNA). More importantly however, K176 at C-terminal extension of RRM2 was strongly affected by both U- and AU-rich RNA binding in TIA-1 and TIAR proteins respectively. Therefore, this positively charged residue, unique to RRM2 C-terminal extension of TIA-proteins, is likely to make a significant contribution towards high affinity interactions between TIA-proteins and their ARE targets.

Conclusion

TIAR is a multi-functional protein shuttling between nucleus and cytoplasm and plays an important role in regulation of gene expression interacting strongly with both RNA and DNA targets. This study reports the unique roles of individual domains of TIAR as well as the linker region between them in binding RNA and DNA targets by examining detailed kinetics and affinity of their interactions. TIAR RRM2 is the major binding domain for both RNA and DNA targets but the strong low nanomolar affinity observed between TIAR and its targets is only achieved in the presence of its C-terminal extension as well as RRM1. Kinetic analysis reveals that the extension residues may play an important role in the stability of the TIAR-RNA/DNA complexes. RRM1 however, may only contribute towards the stability of TIAR-DNA complexes. The specific role of the residues in the linker region at N-terminus of RRM2 in RNA/DNA binding remains to be solved. Further studies involving structural elucidation of TIAR-

RNA/DNA complexes will certainly help us to better understand the molecular mechanism of their interactions.

References

Auweter SD, Oberstrass FC, Allain FH (2006) Sequence-specific binding of single-stranded RNA: is there a code for recognition? Nucleic Acids Res 34:4943-59

Clery A, Blatter M, Allain FH (2008) RNA recognition motifs: boring? Not quite. Curr Opin Struct Biol 18:290-8

Dember LM, Kim ND, Liu KQ, Anderson P (1996) Individual RNA recognition motifs of TIA-1 and TIAR have different RNA binding specificities. J Biol Chem 271:2783-8

Fialcowitz-White EJ, Brewer BY, Ballin JD, Willis CD, Toth EA, Wilson GM (2007) Specific protein domains mediate cooperative assembly of HuR oligomers on AU-rich mRNA-destabilizing sequences. J Biol Chem 282:20948-59

Kim HS, Kuwano Y, Zhan M, Pullmann R, Jr., Mazan-Mamczarz K, Li H, Kedersha N, Anderson P, Wilce MC, Gorospe M, Wilce JA (2007) Elucidation of a C-rich signature motif in target mRNAs of RNA-binding protein TIAR. Mol Cell Biol 27:6806-17

Kuwasako K, Takahashi M, Tochio N, Abe C, Tsuda K, Inoue M, Terada T, Shirouzu M, Kobayashi N, Kigawa T, Taguchi S, Tanaka A, Hayashizaki Y, Guntert P, Muto Y, Yokoyama S (2008) Solution structure of the second RNA recognition motif (RRM) domain of murine T cell intracellular antigen-1 (TIA-1) and its RNA recognition mode. Biochemistry 47:6437-50

Maris C, Dominguez C, Allain FH (2005) The RNA recognition motif, a plastic RNA-binding platform to regulate post-transcriptional gene expression. Febs J 272:2118-31

Park S, Myszka DG, Yu M, Littler SJ, Laird-Offringa IA (2000) HuD RNA recognition motifs play distinct roles in the formation of a stable complex with AU-rich RNA. Mol Cell Biol 20:4765-72

Park-Lee S, Kim S, Laird-Offringa IA (2003) Characterization of the interaction between neuronal RNA-binding protein HuD and AU-rich RNA. J Biol Chem 278:39801-8

Rich RL, Myszka DG (2007) Survey of the year 2006 commercial optical biosensor literature. J Mol Recognit 20:300-66

Rich RL, Myszka DG (2008) Survey of the year 2007 commercial optical biosensor literature. J Mol Recognit 21:355-400

Suswam EA, Li YY, Mahtani H, King PH (2005) Novel DNA-binding properties of the RNA-binding protein TIAR. Nucleic Acids Res 33:4507-18

Crystallization trials of TIAR-RNA/-DNA complexes

Abstract

TIAR-RNA and TIAR-DNA interactions play important parts in post-transcriptional and transcriptional regulation of gene expression respectively. Determining the crystal structures of TIAR-RNA and/or -DNA complexes would help to explain the molecular mechanisms underlying their interactions. Crystallographic structure determination, however, depends on obtaining diffraction quality crystals of the complexes – a process which remains to be a major challenge. Here we report our attempts at crystallizing TIAR-RNA and TIAR-DNA complexes. This involved optimization of the length (6mer, 8mer, or 13mer) and composition (U-, AU-, or T-rich) of RNA or DNA targets, different domains of TIAR (TIAR RRM12l, TIAR RRM12s, or TIAR RRM2l), different molar ratios (protein : RNA/DNA = 1 : 0.8, 1 : 1 or 1 : 1.2), concentrations (5~20 mg/ml), temperatures (4 °C, 8 °C, or 20 °C), protein buffers (Tris or phosphate), and different crystallization robotics and screening conditions. Although crystals for the complex were not obtained from these trials, they identify potential obstacles and provide a direction for future trials.

Introduction

During the course of these investigations of TIAR it was of interest to attempt to determine the structure of the TIAR domains in complex with target oligonucleotide using X-ray crystallography. This method would provide high-resolution structural data that would reveal the details of the interactions between protein and oligonucleotide underlying their affinity and specificity (characterised using SPR and NMR - described in Chapters 4 and 5). X-ray crystallographic structure determination requires the production of crystals, however, and these are often not straightforward to produce, especially for complexes. A good understanding of the system of interest is required, the protein and oligonucleotide must be of extremely high purity, and the complex formed between them must be as stable and as homogeneous as possible. Even then, crystallization is never predictable, and there are many variables including complex concentration, the protein construct and oligonucleotide used, as well as the crystallization conditions employed, which could affect the crystal formation (Holbrook et al. 2001; Hollis 2007; Ke and Doudna 2004; Obayashi et al. 2007). To this end many commercial crystallization screens are available from several different companies (Hampton Research, Sigma, JB, and Qiagen) including those specially designed for protein-oligonucleotide complexes (Natrix, Hampton Research; Crystallization kit for DNA, Sigma). General trends and conditions used in successful crystallizations of protein-RNA/-DNA complexes have been summarized by Obayashi et al. and Hollis (Hollis 2007; Obayashi et al. 2007). One of the limiting factors of crystallization trials is the amount of protein-oligonucleotide complex available. Here the employment of crystallization robotics can greatly assist screening efforts. The two robotic systems used for this study were

Cartesian Honeybee Crystallization robot (Genomic Solutions) and CrystalMation (Rigaku). These automated systems allowed sub-µl sample volumes (as little as 100 nl/well in a 96 well plate) to be dispensed into crystallization trays consistently and rapidly, thus minimizing human errors and conserving precious complex samples. CrystalMation (Rigaku) in particular is a fully integrated crystallization system automating every step from screen making to online crystal trial imaging and analysis, thus making it less time consuming and allowing more thorough monitoring of potential crystal formation compared to manual screening.

In this Chapter the attempts at crystallizing TIAR12l, TIAR12s, and TIAR2l with various oligonucleotide targets is reported. Ultimately no crystals were achieved. This Chapter, however, serves to document what was attempted and may help guide future researchers in this pursuit.

Materials and Methods

Protein expression and purification

TIAR12l (residues 1-181), TIAR12s (residues 8-175) and TIAR2l (residues 94-181) were expressed and purified as described previously (Chapter 5) and concentrated to 5~20 mg/ml in Tris (50 mM Tris pH 8.0, 150 mM NaCl) or phosphate buffer (50 mM phosphate buffer pH 6, 100 mM NaCl).

Protein-oligonucleotide complex formation and crystal trials

RNA (6mer AU-rich: 5'UUAUUU3', 8mer U-rich: 5'UUUUUUUU3', 13mer U-rich: 5'UUUUUUUUUUUUU3', 13mer AU-rich: 5'AUUUAUUUAUUUA3') and

DNA (8mer T-rich: 5'TTTTTTTT3', 13mer T-rich: 5'TTTTTTTTTTTTT3') oligonucleotides were obtained from Dharmacon Research and SIGMA respectively and resuspended in matching buffer (Tris or Phosphate buffer) for the protein. RNA was incubated at 60 °C for 10 min, cooled on ice, and then combined with TIAR12l, TIAR12s, or TIAR2l protein at 1:1 or 1:1.2 molar ratio with slight excess of the RNA or DNA. Crystal trays were set up using either crystallization robots (Cartesian Honeybee Crystallization robot, Genomic Solutions or CrystalMation, Rigaku) or manually as hanging drops by the vapor diffusion method. Equal volumes (100 nl - 1 µl) of protein-RNA/-DNA complex solution and the reservoir solution were mixed and equilibrated over the reservoir solution at 20 °C, 8 °C, or 4 °C. All trays were monitored over the course of several days and weeks either using automated online imaging system (CrystalTrak, Rigaku) or manually by microscopic inspection.

Results

The TIAR constructs representing one and two domains of TIAR (TIAR2l, TIAR12l, and TIAR12s) (Figure 1) were prepared as described previously (Chapter 5), combined with their oligonucleotide targets, and used in crystal screening.
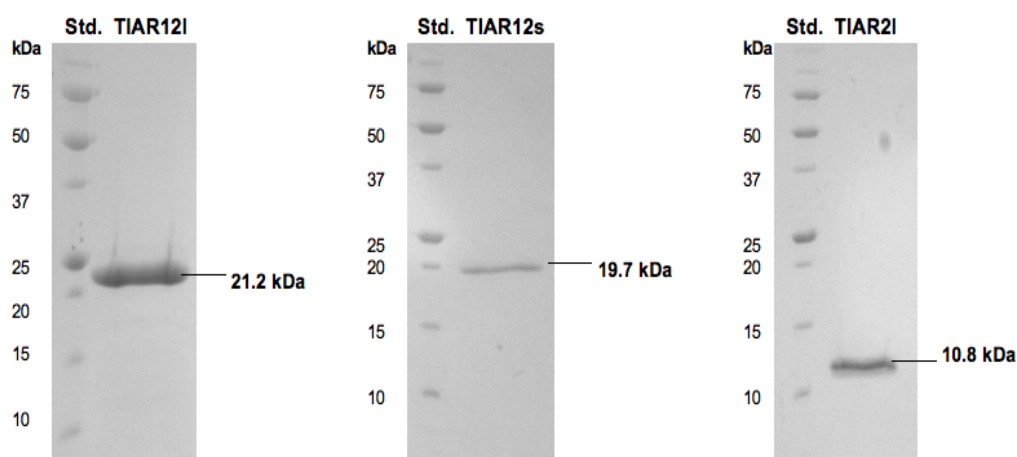
Figure 1. Recombinant proteins used in crystallization trials. The construction of plasmids to express recombinant proteins comprising RRM1 and 2 or RRM2 (TIAR12l, TIAR12s, and TIAR2l) was previously described (Chapter 5). Proteins were expressed in bacteria and purified to homogeneity as described in Materials and Methods, Chapter 5. Std., protein standard, with molecular mass (kDa) indicated.

TIAR12l (TIAR RRM12 with short C-terminal extension) was used as a major target of crystallization attempts as it has been shown to form the most stable complexes (binding with nanomolar affinities and slow dissociation rate constants) with both RNA (U-rich and AU-rich) and DNA (T-rich) targets (Chapter 4 and 5). TIAR2l (TIAR RRM2 with short C-terminal extension) was used as a crystallization target as RRM2 is the major binding domain and has also been shown to form stable complexes (although with much lower affinities than TIAR12l) with both RNA and DNA targets (Chapter 5). TIAR12s (TIAR RRM12), despite that it forms much less stable complexes with its targets with faster dissociation rate constants than TIAR12l or TIAR2l, was also included in the crystallization trials in case the C-terminal extension beyond the RRM2 region interfered with the crystallization process although less likely given the significant involvement of the C-terminal extension region in RNA- and DNA-binding as shown in Chapter 5. It is of note however, that

all three constructs contain extra 13 amino acid residues in their N-terminus, carried on from the expression vector (pGEX-KG2T) after the removal of the fusion tag, which are not involved in binding. Thus it is possible that the unstructured N-terminal extension region could potentially interfere with the crystallization of the complexes. Attempts were made to remove the extra residues by cloning TIAR constructs into a different expression vector (pGEX4T2), but it resulted in inefficient protease removal of the GST fusion tag, therefore insufficient protein yield required for crystallization trials.

The sequence (U-, AU-rich RNA and T-rich DNA) and length (6, 8, and 13mer) of the TIAR targets were chosen based on our studies (Chapter 4 and 5) as well as the previous structural and binding studies involving TIAR and other RRM-containing proteins with their target oligonucleotides (Auweter et al. 2006; Clery et al. 2008; Dember et al. 1996; Fialcowitz-White et al. 2007; Kumar et al. 2008; Kuwasako et al. 2008; Suswam et al. 2005; Wang and Tanaka Hall 2001). It was important to keep the length of the oligonucleotide targets to a minimum while maintaining strong and stable binding by TIAR proteins (especially for the U-rich RNA and T-rich DNA targets), as the longer the targets become, the more potential binding sites that they could provide for TIAR proteins resulting in heterogeneous population of the complexes, thus not ideal for crystallization. AU-rich RNAs (6mer for TIAR2l and 13mer for TIAR12l), derived from TNF-α mRNA, were specially designed to maximize stable 1:1 complex formation, while minimizing potential multiple binding by the TIAR proteins with the position of adenosine providing more specificity and homogeneity of the complex over U-rich RNA or T-rich DNA (Chapter 4) (Park-Lee

et al. 2003; Wang and Tanaka Hall 2001; Wilson et al. 2003). TIAR2l-6mer AU-rich RNA complex formation was also confirmed by NMR spectroscopy (Chapter 5), which showed that double-labeled TIAR2l formed a stable complex with different concentrations of AU-rich RNA, and remained in solution.

The prepared protein and oligonucleotide were then combined at 1:1 or 1:1.2 molar ratio (with slight excess of the oligonucleotides) as a starting point and as suggested previously (Hollis 2007; Sickmier et al. 2006; Wang and Tanaka Hall 2001). The precise molar ratio may not be critical for the initial screening although it could become more important in the optimization stage once the crystals are formed (Obayashi et al. 2007). The crystallization experiments of the complexes set up over the course of this study are summarized below:

TIAR12l-8mer U-rich RNA

Binding studies of TIAR with its oligonucleotide targets (described in Chapter 5) showed that TIAR12l bound with greater affinity to oligonucleotide than TIAR2l alone. The studies also showed that TIAR12l was capable of binding U-rich and AU-rich sequences of RNA as well as the single-stranded T-rich DNA. Since the crystal structure of another classic RRM-containing RBP HuD12 bound to target AU-rich sequence showed that the two RRMs were both involved in binding to 8 sequential single-stranded nucleotides (Wang and Tanaka Hall 2001), it was speculated that TIAR might interact with RNA in the similar way. Thus early efforts to produce crystals of TIAR in complex with RNA were focused on the TIAR12l construct with an 8mer U-rich RNA (Table 1 and 2).

Target oligonucleotide	5'UUUUUUUU3'
Molar ratio (protein:RNA)	1:1.2
Buffer	50 mM Tris pH 8.0, 150 mM NaCl
Temperature	20 °C
Crystallization robotics	Cartesian Honeybee Crystallization robot, Genomic Solutions
Protein concentration	10 mg/ml
Crystallization screens	Natrix (Hampton research), Crystallization kit for DNA (Sigma), Crystallization basic kit for proteins (Sigma), PEG/Ion screen (Hampton research), Crystallization low ionic kit for proteins (Sigma), Crystallization kit for protein-protein complexes (Sigma), Index screen (Hampton research), Wizard I/II (Emerald BioSystems), JB screens 1-10 (JB)
Summary	• No crystal was observed • Wizard I/II (Emerald BioSystems) and JB screens 1-10 (JB) resulted in the least changes compared to the other screens used. • White to brown precipitate formed in some wells (~25 %) after 2-3 days • No further change was observed

Table 1. A summary of crystallization conditions used for TIAR12l-8mer U-rich RNA complex.

TIAR12l-8mer U-/T-rich RNA/DNA

The above experiment resulted in no initial crystal formation and a low level of precipitation (less than 50 %) indicating that the concentration of the complex may not be sufficient enough to reach crystallization stage. Thus, it was repeated with higher protein concentration, both RNA and DNA targets, and 1:1 molar ratio although this may not be so critical for initial screening.

Target oligonucleotide	5'UUUUUUUU3', 5'TTTTTTTT3'
Molar ratio (protein:RNA)	1:1
Buffer	50 mM Tris pH 8.0, 150 mM NaCl
Temperature	20 °C
Crystallization robotics	CrystalMation, Rigaku
Protein concentration	18 mg/ml
Crystallization screens	Natrix (Hampton research), Crystallization kit for DNA (Sigma), Crystallization basic kit for proteins (Sigma), PEG/Ion screen (Hampton research), Crystallization low ionic kit for proteins (Sigma), Crystallization kit for protein-protein complexes (Sigma), Pro-complex suite (Qiagen)
Summary	• No crystal was observed. • Crystallization low ionic kit for proteins (Sigma) and Crystallization kit for protein-protein complexes (Sigma) did not result in much change compared to other screens.

|	
	• White to brown precipitate, oily drops, and phase separation was observed in ~40 % of wells (except for the wells from the screens mentioned above) after 3-7 days and remained as they were. • No further change was observed although some wells dried out or completely precipitated after a few months.

Table 2. A summary of crystallization conditions used for TIAR12l-8mer U-rich RNA and TIAR12l-8mer T-rich DNA complexes.

TIAR12l-13mer U-/AU-rich RNA

The above efforts to crystallize TIAR12l-8mer U-/T-rich oligonucleotides resulted in no crystals. Thus, here we used a higher protein concentration and the 13mer AU-rich RNA target as well as 13mer U-rich RNA in an attempt to increase the chance of crystallization. AU-rich RNA could potentially provide more specificity and homogeneity than U-rich RNA. Given our findings that the strong interaction between TIAR12l and its target RNA may occur in an open conformation with significant involvement of the RRM2 C-terminal extension region (Chapter 4 and 5), it was speculated that a longer RNA target may be required to form a stable complex with both RRMs as well as the extension region. The crystallization conditions are summarized in Table 3 and some of the wells are shown in Figure 2.

Target oligonucleotides	5'UUUUUUUUUUUUU3', 5'AUUUAUUUAUUUA3'
Molar ratio (protein:RNA)	1:1.2
Buffer	50 mM Tris pH 8.0, 150 mM NaCl
Temperature	20 °C
Crystallization robotics	CrystalMation, Rigaku
Protein concentration	27 mg/ml
Crystallization screens	Natrix (Hampton research), Crystallization kit for DNA (Sigma), Crystallization basic kit for proteins (Sigma), PEG/Ion screen (Hampton research), Pro-complex suite (Qiagen)
Summary	• No crystal was observed. • Brown precipitate and degradation was observed in many wells (>40%) after a few days (Figure 2). • No particular difference was observed between the complex with AU-rich RNA and U-rich RNA. • White precipitate, oily drops, and phase separation was also observed in some of the wells after 3-7 days (Figure 2).

Table 3. A summary of crystallization conditions used for TIAR12l-13mer U-rich and TIAR12l-13mer AU-rich RNA complexes.
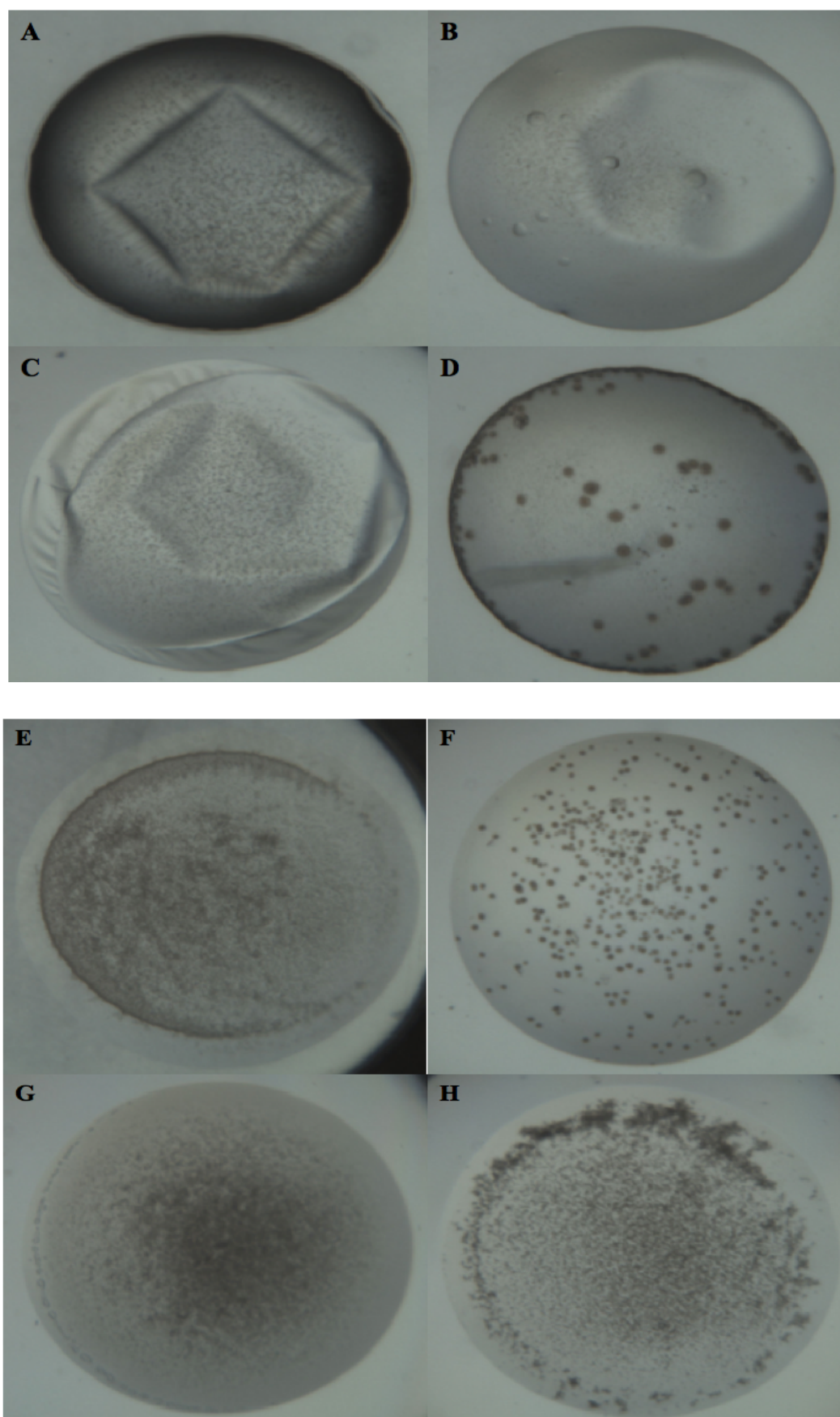
Figure 2. Precipitates and oily drops observed from TIAR12l-13mer U (A, C, D)-/AU (B, E, F, G, H)-rich RNA complexes. A. 0.1 M calcium acetate, 0.1 M sodium acetate pH 4.5, 10% (w/v) PEG 4000 **B.** 0.1 M magnesium acetate, 0.1 M sodium cacodylate pH 6.5, 15% (w/v) PEG 6000 **C.** 0.1 M sodium chloride, 0.1 M Tris pH 8, 15% (v/v) ethanol, 5% (v/v) MPD **D.** 0.2 M ammonium sulfate, 0.1 M sodium acetate pH 4.6, 25% (w/v) PEG 4000 **E.** 0.2 M sodium citrate, 0.1 M sodium cacodylate pH 6.5, 30% (v/v) 2-propanol **F.** 0.2 M ammonium sulfate, 30% (w/v) PEG 8000 **G.** 0.1 M HEPES sodium salt pH 7.5, 1.4 M sodium citrate **H.** 0.1 M sodium citrate pH 5.6, 20% (v/v) 2-propanol, 20% (w/v) PEG 4000.

TIAR12l-13mer AU-/T-rich RNA/DNA

The above experiments resulted in heavy brown precipitation (more than 40 %) within a few days indicating that the concentration of the complex may be too high. Thus, it was repeated with lower protein concentration, both RNA and DNA targets, two different temperatures, and two different molar ratios. The crystallization conditions are summarized in Table 4 and some examples of the wells with signs of precipitation and phase separation are shown in Figure 3.

Target oligonucleotide	5'TTTTTTTTTTTTT3', 5'AUUUAUUUAUUUA3'
Molar ratio (protein:RNA)	1:1 and 1:0.8 (slight excess of the protein)
Buffer	50 mM Tris pH 8.0, 150 mM NaCl
Temperature	20 °C and 4 °C
Crystallization robotics	Cartesian Honeybee Crystallization robot, Genomic Solutions
Protein concentration	16 mg/ml
Crystallization screens	Natrix (Hampton research), Crystallization kit for DNA (Sigma), Crystallization basic extension kit for proteins (Sigma), PEG grid (Sigma), Index (Hampton research),

	PACT suite (Qiagen), Pro-complex suite (Qiagen)
Summary	- No crystal was observed. - No particular difference was observed between the complex with AU-rich RNA and T-rich DNA. - Lower temperature, different molar ratios, and different crystal screens did not improve the chance of crystallization of the complex. - White to brown precipitate, oily drops, and phase separation was observed in many of the wells (>40%) after 3-7 days (Figure 3).

Table 4. A summary of crystallization conditions used for TIAR12l-13mer AU-rich RNA and TIAR12l-13mer T-rich DNA complexes.
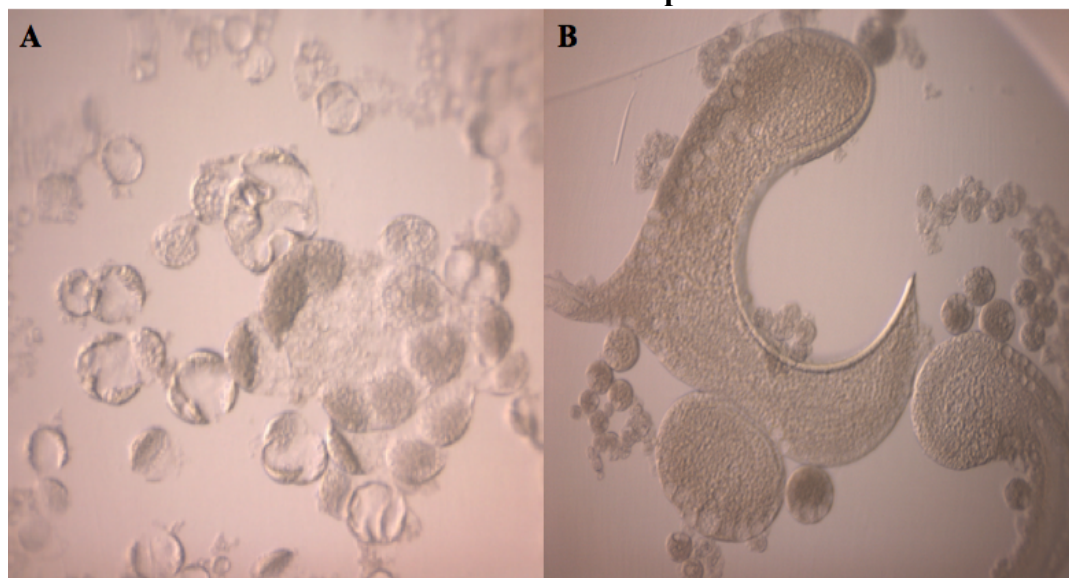
Figure 3. Precipitates, phase separation, and oily drops observed from TIAR12l-13mer AU-rich RNA complex after three days. A. 0.2 M calcium chloride dihydrate, 0.1 M BIS-TRIS pH 5.5, 45% (v/v) 2-methyl-2, 4 pentanediol **B.** 0.2 M calcium chloride dihydrate, 0.1 M BIS-TRIS pH 6.5, 45% (v/v) 2-methyl-2, 4 pentanediol.
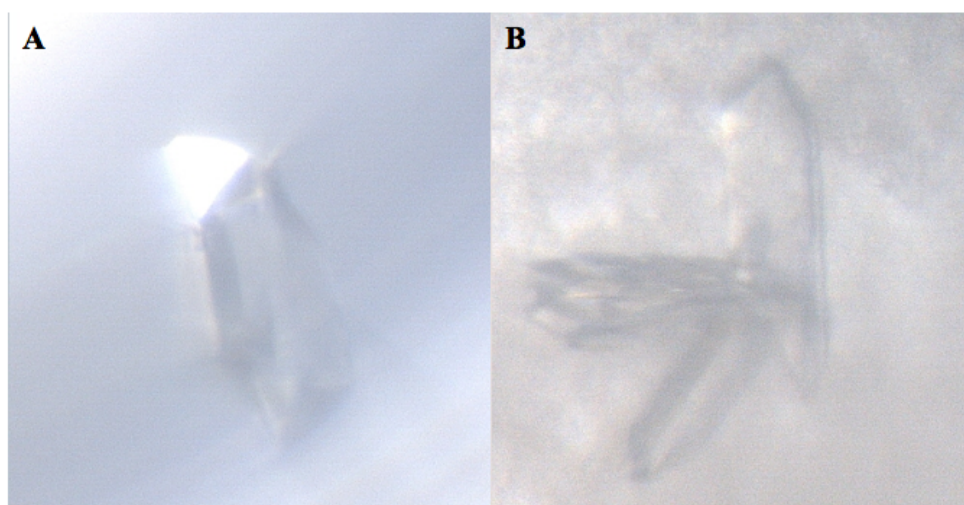
TIAR12l-13mer T-rich DNA

The above experiment was replicated in phosphate buffer (pH 6.0). The complex sample was prepared initially for our preliminary NMR experiment to investigate the role of the RRM2 C-terminal extension residues in oligonucleotide binding (preliminary data). Crystals were formed in some of the wells, but further testing and screening revealed that they were salt crystals. The crystallization conditions are summarized in Table 5 and some examples of the salt crystals formed are shown in Figure 4.

Target oligonucleotide	5'TTTTTTTTTTTTT3'
Molar ratio (protein:RNA)	1:1
Buffer	50 mM phosphate buffer pH 6.0, 100 mM NaCl
Temperature	20 °C
Crystallization method	Trays were set up by hand as hanging drops (vapour diffusion method)
Protein concentration	16 mg/ml
Crystallization screens	Natrix (Hampton research), Crystallization kit for DNA (Sigma), Crystallization low ionic kit for proteins (Sigma), Crystallization kit for protein-protein complexes (Sigma)
Summary	• Some crystals were formed and further screened around the conditions. However, X-ray diffraction experiments revealed that these were salt crystals (Figure 4).

	• White to brown precipitate, oily drops, and phase separation was observed in many of the wells (>40%) after 2-3 days.

Table 5. A summary of crystallization conditions used for TIAR12l-13mer T-rich DNA complex.

Figure 4. Salt crystals formed from the wells containing TIAR12l-13mer T-rich DNA complex after two to three days. A. 0.01 M magnesium chloride hexahydrate, 0.05 M HEPES sodium pH 7.0, 4.0 M lithium chloride **B.** 0.1 M ammonium acetate, 0.05 M HEPES sodium pH 7.0, 5% (w/v) PEG 8000.

TIAR12s-8mer T-rich DNA

Crystallization attempts were also made for TIAR12s (TIAR RRM12 without the C-terminal extension) in complex with T-rich DNA in case the C-terminal extension beyond the RRM2 region interfered with the crystallization process, despite the fact that they form much less stable complex than those involving TIAR12l or TIAR2l. The crystallization conditions are summarized in Table 6.

Target oligonucleotide	5'TTTTTTTT3'
Molar ratio (protein:RNA)	1:1.2
Buffer	50 mM Tris pH 8.0, 150 mM NaCl
Temperature	20 °C
Crystallization robotics	Cartesian Honeybee Crystallization robot, Genomic Solutions
Protein concentration	7 mg/ml
Crystallization screens	Natrix (Hampton research), Crystallization kit for DNA (Sigma), Crystallization basic kit for proteins (Sigma), PEG/Ion screen (Hampton research)
Summary	• No crystal was formed • White to brown precipitate formed in some wells (~25 %) after 2-3 days • No further change was observed

Table 6. A summary of crystallization conditions used for TIAR12s-8mer T-rich DNA complex.

TIAR2l-6mer AU-/8mer T-rich RNA/DNA

Since it was possible that RRM1 was not forming a stable interaction with the oligonucleotide targets, efforts to crystallize TIAR2l with oligonucleotides were also made (NMR studies showed that stable complexes could be formed). Crystals formed in some of the wells, but again X-ray diffraction experiments revealed that these were salt crystals. The crystallization conditions are summarized in Table 7 and some examples of the salt crystals formed are shown in Figure 5.

Target oligonucleotide	5'UUAUUU3', 5'TTTTTTTT3'
Molar ratio (protein:RNA)	1:1.2
Buffer	50 mM phosphate buffer pH 6.0, 100 mM NaCl (RNA) 50 mM Tris pH 8.0, 150 mM NaCl (DNA)
Temperature	20 °C and 8 °C
Crystallization method	CrystalMation, Rigaku
Protein concentration	10-15 mg/ml (for T-rich DNA) and 5 mg/ml (for AU-rich RNA)
Crystallization screens	Natrix (Hampton research), Crystallization kit for DNA (Sigma), Crystallization basic kit for proteins (Sigma), PEG/Ion screen (Hampton research), Index (Hampton research), SaltRx (Hampton research), Crystal screen HT (Hampton research)
Summary	• Some crystals formed from the wells containing TIAR2l-6mer AU-rich RNA complex. These were further screened around the conditions, put on the X-ray detector, but turned out to be all salt crystals (Figure 5). • No crystal was formed from the wells containing TIAR2l-8mer T-rich DNA complex and white to brown precipitate formed in some wells (~25 %) after 2-3 days. • White to brown precipitate, oily drops, and

	phase separation was observed in many of the wells (>40%) containing TIAR2l-6mer AU-rich RNA complex after 2-3 days.

Table 7. A summary of crystallization conditions used for TIAR2l-6mer AU-/8mer T-rich RNA/DNA complexes.
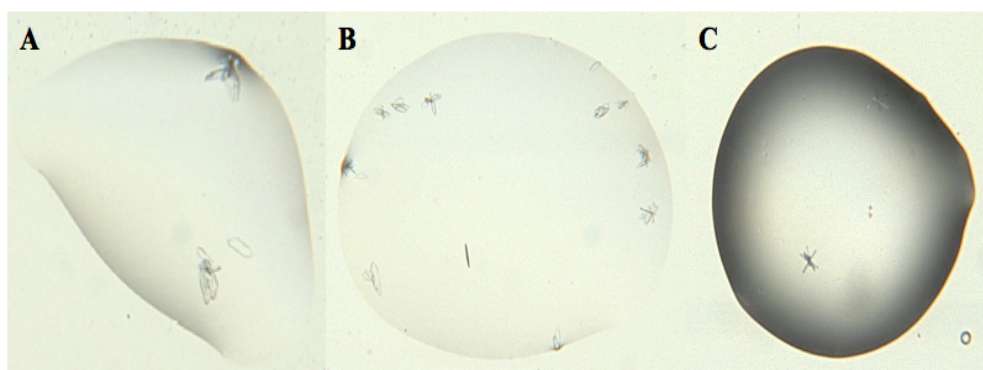
Figure 5. Salt crystals formed from the wells containing TIAR2l-6mer AU-rich RNA complex after two to three days. A. 0.2 M calcium chloride, 0.1 M sodium acetate pH 4.6, 20% (v/v) 2-propanol **B.** 0.02 M calcium chloride, 0.1 M sodium acetate pH 4.6, 30% (v/v) 2-methyl-2, 4-pentanediol **C.** 0.2 M lithium citrate, 20% (w/v) PEG 3350.

Discussion

After extensive efforts to grow crystals of TIAR12l, TIAR12s, and TIAR2l in complex with RNA and DNA oligonucleotides of varying length and sequences – there was no hint that we would be successful. Although purity levels were very high and complex formation appeared to be stable (from knowledge of affinities and NMR evidence in the case of TIAR2l-6mer AU-rich RNA) the complexes were not amenable to crystal formation. This may be for many reasons including 1) the way that RRM12l interacts with the oligonucleotides in a flexible and elongated shape as shown earlier by our SAXS analysis (Chapter 4) may not be favoring their crystallization and 2) the multiple binding positions available on the oligonucleotide could be leading to a heterogeneous population of the complexes.

The TIAR2l in complex with 6mer AU-rich RNA was anticipated to be a relatively inflexible and homogeneous sample. Although no crystals for this complex were achieved, it may be worthwhile to pursue this further in future trials under different conditions including different buffer (Tris or Hepes) as phosphate buffer led to salt crystals. It is possible that the presence of RNAse in the sample could lead to degradation of the unbound RNA in the complex solution. Although this was not evident during our NMR experiments involving TIAR2l-6mer AU-rich RNA complex and previous successful crystallization of protein-RNA complexes typically occurred within a week (summarized by Obayashi et al., 2007), continuous monitoring of the RNAse activity in the complex may be necessary over longer period of time in future trials.

Further optimization should also be made to remove the short N-terminal residues from the expression vector (either by using different expression vector system or treating the complex with protease to cleave any unbound or unstructured region) as this region could be interfering with the crystallization process. Another possibility for future crystallization trials is to crystallize TIAR alone first (as the X-ray crystal structure of TIA-1 RRM2 alone, which shares >90% homology with TIAR, has been elucidated), followed by soaking the target oligonucleotides into the protein crystals (Hollis 2007; Kumar et al. 2008). Whether this will result in successful crystallization of the complex remains to be tested.

The structure of the TIAR-oligonucleotide complex remains to be solved and is a worthwhile challenge as it can help us to understand the molecular mechanism underlying the interactions of TIAR with its oligonucleotide targets. Although no crystals were achieved from this study, it provides useful information for future researchers taking on this challenge, or suggests that this structure is better tackled using NMR spectroscopic techniques instead.

References

Auweter SD, Oberstrass FC, Allain FH (2006) Sequence-specific binding of single-stranded RNA: is there a code for recognition? Nucleic Acids Res 34:4943-59

Clery A, Blatter M, Allain FH (2008) RNA recognition motifs: boring? Not quite. Curr Opin Struct Biol 18:290-8

Dember LM, Kim ND, Liu KQ, Anderson P (1996) Individual RNA recognition motifs of TIA-1 and TIAR have different RNA binding specificities. J Biol Chem 271:2783-8

Fialcowitz-White EJ, Brewer BY, Ballin JD, Willis CD, Toth EA, Wilson GM (2007) Specific protein domains mediate cooperative assembly of HuR oligomers on AU-rich mRNA-destabilizing sequences. J Biol Chem 282:20948-59

Holbrook SR, Holbrook EL, Walukiewicz HE (2001) Crystallization of RNA. Cell. Mol. Life Sci. 58:234-243

Hollis T (2007) Crystallization of Protein-DNA Complexes. In: Doublie S (ed) Macromolecular Crystallography Protocols, vol 1. Humana Press, Totowa, NJ, pp 225-237

Ke A, Doudna JA (2004) Crystallization of RNA and RNA-protein complexes. Methods 34:408-414

Kumar AO, Swenson MC, Benning MM, Kielkopf CL (2008) Structure of the central RNA recognition motif of human TIA-1 at 1.95A resolution. Biochem Biophys Res Commun 367:813-9

Kuwasako K, Takahashi M, Tochio N, Abe C, Tsuda K, Inoue M, Terada T, Shirouzu M, Kobayashi N, Kigawa T, Taguchi S, Tanaka A, Hayashizaki Y, Guntert P, Muto Y, Yokoyama S (2008) Solution structure of the second RNA recognition motif (RRM) domain of murine T cell intracellular antigen-1 (TIA-1) and its RNA recognition mode. Biochemistry 47:6437-50

Obayashi E, Oubridge C, Krummel DP, Nagai K (2007) Crystallization of RNA-Protein Complexes. In: Doublie S (ed) Macromolecular Crystallography Protocols, vol 1. Humana press, Totowa, NJ, pp 259-276

Park-Lee S, Kim S, Laird-Offringa IA (2003) Characterization of the interaction between neuronal RNA-binding protein HuD and AU-rich RNA. J Biol Chem 278:39801-8

Sickmier EA, Frato KE, Shen H, Paranawithana SR, Green MR, Kielkopf CL (2006) Structural basis for polypyrimidine tract recognition by the essential pre-mRNA splicing factor U2AF65. Mol Cell 23:49-59

Suswam EA, Li YY, Mahtani H, King PH (2005) Novel DNA-binding properties of the RNA-binding protein TIAR. Nucleic Acids Res 33:4507-18

Wang X, Tanaka Hall TM (2001) Structural basis for recognition of AU-rich element RNA by the HuD protein. Nat Struct Biol 8:141-5

Wilson GM, Lu J, Sutphen K, Sun Y, Huynh Y, Brewer G (2003) Regulation of A + U-rich element-directed mRNA turnover involving reversible phosphorylation of AUF1. J Biol Chem 278:33029-38

Final Discussion and Conclusion

TIAR is a multi-functional RNA-binding protein which plays an important role in post-transcriptional regulation of gene expression, especially when the cells are under stress, by binding strongly to target RNA and leading to translational repression. TIAR also binds strongly to its single-stranded DNA targets and has shown to be involved in splicing. Despite its important roles, only limited characterization of its consensus RNA target sequence and the roles of the individual RRMs have been previously investigated. No investigation of the kinetics behind its high affinity interactions with its target sequences or the involvement of the regions other than the classic RRMs of the protein in binding were previously reported, and high-resolution structural information involving TIAR in complex with its oligonucleotide target still remains unavailable.

Thus, here we have addressed and explored these questions through an in depth biophysical and structural investigation into the RNA- and DNA-binding properties of TIAR in direct comparison to another potentially competing RNA-binding protein, HuR, in an attempt to better understand the mechanism behind its oligonucleotide binding, and therefore its versatile biological roles in regulation of gene expression in cells.

Firstly, a reliable *in vitro* system was needed for accurate measurements of protein-oligonucleotide interactions and Chapter 2 describes in detail why and how an SPR system using Biacore instrument was developed, optimized and used to determine the kinetics as well as the affinity of the interactions involving TIAR and its RNA targets. The Chapter particularly emphasizes the way in which the choice of

instrument and buffer components led to a stable, accurate, and robust SPR system. Examination of the rates of interactions of TIAR constructs and the oligonucleotide targets led to new discoveries of its distinguishing binding properties which would not have been apparent from measurements of affinity alone. These are described in Chapters 3, 4, and 5.

Whilst TIAR proteins have been reported previously to preferentially bind U-rich sequences (Dember et al., 1996), Chapter 3 describes the discovery of a new C-rich consensus motif for TIAR through our collaborator's *in vivo* and bioinformatics studies. This unexpected finding prompted us to investigate in detail the relative binding affinity and kinetics of TIAR to U-rich RNA compared with the new C-rich motif using our *in vitro* Biacore system described in Chapter 2. The kinetic and affinity results clearly showed lower but significant nanomolar binding of the C-rich motif by TIAR, confirming it as a novel TIAR target and demonstrating that TIAR-RNA interactions in post-transcriptional gene regulation are not restricted to AREs. Our findings then led to further functional assays that ultimately verified the biological effect of the C-rich motif in translational repression (Kim et al., 2007). Further studies are necessary to understand the precise mechanism of the C-rich RNA binding by TIAR as well as the roles of the C-rich motif-containing mRNA transcripts under different cellular environments.

Chapter 4 describes a comparison of the oligonucleotide-binding properties of TIAR and HuR. Both proteins target AREs and show similar trends by binding to their U-rich RNA target with higher affinities than their AU-rich RNA target. However

detailed kinetic analysis of their interactions revealed that this is likely to be influenced by the higher number of binding sites available on the U-rich RNA target than on the AU-rich RNA. Since both proteins, in fact, dissociate slower from the AU-rich RNA target than from the U-rich RNA it suggests that the AU-rich RNA is the preferred target sequence of TIAR and HuR. Further kinetic and affinity studies into their DNA-binding properties as well as SAXS analysis of their mode of interaction with the RNA in solution revealed striking differences in their oligonucleotide-binding properties, revealing that these triple RRM-containing proteins, despite their structural similarities, interact with their target oligonucleotides in fundamentally different ways.

Chapter 5 describes the investigation of the roles of individual domains of TIAR as well as the unstructured regions outside the RRMs in oligonucleotide binding. Interestingly, it was confirmed that the second domain (RRM2) of TIAR is the major RNA- and DNA-binding domain, but only in the presence of the flexible extension immediately C-terminal to the RRM2. The key residue(s) within the extension region responsible for the enhanced binding stability were identified using NMR, but require further confirmation through higher resolution structural studies and/or mutation studies of those identified residues. The unstructured N-terminal extension region of RRM2 may also be contributing towards the oligonucleotide binding, although this requires further investigation. RRM1 contributes towards the stability of TIAR binding with DNA but not with RNA, reflecting its possible role in splicing immediately following transcription.

Chapter 6 describes our extensive efforts to crystallize the TIAR-RNA complexes which could lead us to useful molecular insights into their binding interactions. Although no crystal was obtained, the work serves as a useful guideline for future researchers pursuing the same goal.

In conclusion, this thesis provides fascinating biophysical and structural insights into how TIAR may interact with its target oligonucleotides in cells and play a role in regulation of gene expression. It demonstrates the importance of kinetic analysis as well as the affinity analysis for investigating protein-RNA interactions. The structure of the TIAR-RNA/-DNA complex which could provide the crucial molecular insight behind TIAR's high affinity interactions still remains to be solved. Similar biophysical and structural investigation into other potentially competing RBPs such as AUF-1 or TTP, which are involved in destabilization of their target mRNAs, together with the knowledge and understanding gained from this thesis, will provide us with very useful systematic overview of how different ARE-binding proteins interact with their RNA targets and lead to critically different outcomes for the mRNAs. Such information would greatly help us towards a wider understanding of the complex interplay of protein-RNA interactions in gene regulation and how this can dictate the fate of the target mRNAs and their encoded proteins. The work presented in this thesis is all done *in vitro* and focuses specifically on the RNA-binding properties of TIAR in comparison to HuR, and not on the self-associating properties of the C-terminal glutamine-rich region of TIAR which is thought to be important in its role in stress granule formation. The study is thus a long way from revealing the far more complex protein-RNA interactions that take place in a cell.

Nevertheless, it provides insight into one aspect of the interactions that take place underlying the regulation of gene expression. The influence of other factors on these interactions in the cell including subcellular environment, proliferation status, tissue type, and interactions with other RBPs remains to be investigated.

General references

Anderson P, Kedersha N (2002) Visibly stressed: the role of eIF2, TIA-1, and stress granules in protein translation. Cell Stress Chaperones 7:213-21

Anderson P, Kedersha N (2007) On again, off again: the SRC-3 transcriptional coactivator moonlights as a translational corepressor. Mol Cell 25:796-7

Auweter SD, Oberstrass FC, Allain FH (2006) Sequence-specific binding of single-stranded RNA: is there a code for recognition? Nucleic Acids Res 34:4943-59

Aznarez I, Barash Y, Shai O, He D, Zielenski J, Tsui LC, Parkinson J, Frey BJ, Rommens JM, Blencowe BJ (2008) A systematic analysis of intronic sequences downstream of 5' splice sites reveals a widespread role for U-rich motifs and TIA1/TIAL1 proteins in alternative splicing regulation. Genome Res 18:1247-58

Bakheet T, Williams BR, Khabar KS (2006) ARED 3.0: the large and diverse AU-rich transcriptome. Nucleic Acids Res 34:D111-4

Barreau C, Paillard L, Osborne HB (2005) AU-rich elements and associated factors: are there unifying principles? Nucleic Acids Res 33:7138-50

Beck AR, Medley QG, O'Brien S, Anderson P, Streuli M (1996) Structure, tissue distribution and genomic organization of the murine RRM-type RNA binding proteins TIA-1 and TIAR. Nucleic Acids Res 24:3829-35

Beckel-Mitchener A, Miera A, Keller R, Perrone-Bizzozero N (2002) Poly(A) tail length-dependent stabilization of GAP-43 mRNA by the RNA-binding protein HuD. J Biol Chem 277:27996-28002

Brennan CM, Steitz JA (2001) HuR and mRNA stability. Cell Mol Life Sci 58:266-77

Caput D, Beutler B, Hartog K, Thayer R, Brown-Shimer S, Cerami A (1986) Identification of a common nucleotide sequence in the 3'-untranslated region of mRNA molecules specifying inflammatory mediators. Proc Natl Acad Sci U S A 83:1670-4

Chen CY, Gherzi R, Ong SE, Chan EL, Raijmakers R, Pruijn GJ, Stoecklin G, Moroni C, Mann M, Karin M (2001) AU binding proteins recruit the exosome to degrade ARE-containing mRNAs. Cell 107:451-64

Chen CY, Xu N, Shyu AB (1995) mRNA decay mediated by two distinct AU-rich elements from c-fos and granulocyte-macrophage colony-stimulating factor

transcripts: different deadenylation kinetics and uncoupling from translation. Mol Cell Biol 15:5777-88

Chen Y, Varani G (2005) Protein families and RNA recognition. Febs J 272:2088-97

Clery A, Blatter M, Allain FH (2008) RNA recognition motifs: boring? Not quite. Curr Opin Struct Biol 18:290-8

Dember LM, Kim ND, Liu KQ, Anderson P (1996) Individual RNA recognition motifs of TIA-1 and TIAR have different RNA binding specificities. J Biol Chem 271:2783-8

Eisinger-Mathason TS, Andrade J, Groehler AL, Clark DE, Muratore-Schroeder TL, Pasic L, Smith JA, Shabanowitz J, Hunt DF, Macara IG, Lannigan DA (2008) Codependent functions of RSK2 and the apoptosis-promoting factor TIA-1 in stress granule assembly and cell survival. Mol Cell 31:722-36

Enokizono Y, Konishi Y, Nagata K, Ouhashi K, Uesugi S, Ishikawa F, Katahira M (2005) Structure of hnRNP D complexed with single-stranded telomere DNA and unfolding of the quadruplex by heterogeneous nuclear ribonucleoprotein D. J Biol Chem 280:18862-70

Fan XC, Steitz JA (1998a) HNS, a nuclear-cytoplasmic shuttling sequence in HuR. Proc Natl Acad Sci U S A 95:15293-8

Fan XC, Steitz JA (1998b) Overexpression of HuR, a nuclear-cytoplasmic shuttling protein, increases the in vivo stability of ARE-containing mRNAs. Embo J 17:3448-60

Fialcowitz-White EJ, Brewer BY, Ballin JD, Willis CD, Toth EA, Wilson GM (2007) Specific protein domains mediate cooperative assembly of HuR oligomers on AU-rich mRNA-destabilizing sequences. J Biol Chem 282:20948-59

Forch P, Valcarcel J (2001) Molecular mechanisms of gene expression regulation by the apoptosis-promoting protein TIA-1. Apoptosis 6:463-8

Grosset C, Boniface R, Duchez P, Solanilla A, Cosson B, Ripoche J (2004) In vivo studies of translational repression mediated by the granulocyte-macrophage colony-stimulating factor AU-rich element. J Biol Chem 279:13354-62

Gueydan C, Droogmans L, Chalon P, Huez G, Caput D, Kruys V (1999) Identification of TIAR as a protein binding to the translational regulatory AU-rich element of tumor necrosis factor alpha mRNA. J Biol Chem 274:2322-6

Guhaniyogi J, Brewer G (2001) Regulation of mRNA stability in mammalian cells. Gene 265:11-23

Hinman MN, Lou H (2008) Diverse molecular functions of Hu proteins. Cell Mol Life Sci 65:3168-81

Hollams EM, Giles KM, Thomson AM, Leedman PJ (2002) MRNA stability and the control of gene expression: implications for human disease. Neurochem Res 27:957-80

Hudson BP, Martinez-Yamout MA, Dyson HJ, Wright PE (2004) Recognition of the mRNA AU-rich element by the zinc finger domain of TIS11d. Nat Struct Mol Biol 11:257-64

Izquierdo JM, Valcarcel J (2007) Two isoforms of the T-cell intracellular antigen 1 (TIA-1) splicing factor display distinct splicing regulation activities. Control of TIA-1 isoform ratio by TIA-1-related protein. J Biol Chem 282:19410-7

Kasashima K, Sakashita E, Saito K, Sakamoto H (2002) Complex formation of the neuron-specific ELAV-like Hu RNA-binding proteins. Nucleic Acids Res 30:4519-4526

Kawai T, Lal A, Yang X, Galban S, Mazan-Mamczarz K, Gorospe M (2006) Translational control of cytochrome c by RNA-binding proteins TIA-1 and HuR. Mol Cell Biol 26:3295-307

Kedersha N, Anderson P (2002) Stress granules: sites of mRNA triage that regulate mRNA stability and translatability. Biochem Soc Trans 30:963-9

Kedersha N, Stoecklin G, Ayodele M, Yacono P, Lykke-Andersen J, Fritzler MJ, Scheuner D, Kaufman RJ, Golan DE, Anderson P (2005) Stress granules and processing bodies are dynamically linked sites of mRNP remodeling. J Cell Biol 169:871-84

Kedersha NL, Gupta M, Li W, Miller I, Anderson P (1999) RNA-binding proteins TIA-1 and TIAR link the phosphorylation of eIF-2 alpha to the assembly of mammalian stress granules. J Cell Biol 147:1431-42

Keene JD (1999) Why is Hu where? Shuttling of early-response-gene messenger RNA subsets. Proc Natl Acad Sci U S A 96:5-7

Kim HH, Kuwano Y, Srikantan S, Lee EK, Martindale JL, Gorospe M (2009) HuR recruits let-7/RISC to repress c-Myc expression. Genes Dev 23:1743-8

Kullmann M, Gopfert U, Siewe B, Hengst L (2002) ELAV/Hu proteins inhibit p27 translation via an IRES element in the p27 5'UTR. Genes Dev 16:3087-99

Kumar AO, Swenson MC, Benning MM, Kielkopf CL (2008) Structure of the central RNA recognition motif of human TIA-1 at 1.95A resolution. Biochem Biophys Res Commun 367:813-9

Kuwasako K, Takahashi M, Tochio N, Abe C, Tsuda K, Inoue M, Terada T, Shirouzu M, Kobayashi N, Kigawa T, Taguchi S, Tanaka A, Hayashizaki Y, Guntert P, Muto Y, Yokoyama S (2008) Solution structure of the second RNA recognition motif (RRM) domain of murine T cell intracellular antigen-1 (TIA-1) and its RNA recognition mode. Biochemistry 47:6437-50

Lal A, Mazan-Mamczarz K, Kawai T, Yang X, Martindale JL, Gorospe M (2004) Concurrent versus individual binding of HuR and AUF1 to common labile target mRNAs. Embo J 23:3092-102

Le Guiner C, Lejeune F, Galiana D, Kister L, Breathnach R, Stevenin J, Del Gatto-Konczak F (2001) TIA-1 and TIAR activate splicing of alternative exons with weak 5' splice sites followed by a U-rich stretch on their own pre-mRNAs. J Biol Chem 276:40638-46

Liao B, Hu Y, Brewer G (2007) Competitive binding of AUF1 and TIAR to MYC mRNA controls its translation. Nat Struct Mol Biol 14:511-8

Loflin P, Chen CY, Shyu AB (1999) Unraveling a cytoplasmic role for hnRNP D in the in vivo mRNA destabilization directed by the AU-rich element. Genes Dev 13:1884-97

Lopez de Silanes I, Galban S, Martindale JL, Yang X, Mazan-Mamczarz K, Indig FE, Falco G, Zhan M, Gorospe M (2005) Identification and functional outcome of mRNAs associated with RNA-binding protein TIA-1. Mol Cell Biol 25:9520-31

Lopez de Silanes I, Zhan M, Lal A, Yang X, Gorospe M (2004) Identification of a target RNA motif for RNA-binding protein HuR. Proc Natl Acad Sci U S A 101:2987-92

Lu JY, Schneider RJ (2004) Tissue distribution of AU-rich mRNA-binding proteins involved in regulation of mRNA decay. J Biol Chem 279:12974-9

Ma WJ, Cheng S, Campbell C, Wright A, Furneaux H (1996) Cloning and characterization of HuR, a ubiquitously expressed Elav-like protein. J Biol Chem 271:8144-51

Ma WJ, Chung S, Furneaux H (1997) The Elav-like proteins bind to AU-rich elements and to the poly(A) tail of mRNA. Nucleic Acids Res 25:3564-9

Maris C, Dominguez C, Allain FH (2005) The RNA recognition motif, a plastic RNA-binding platform to regulate post-transcriptional gene expression. Febs J 272:2118-31

Masuda K, Abdelmohsen K, Gorospe M (2009) RNA-binding proteins implicated in the hypoxic response. J Cell Mol Med

Mazan-Mamczarz K, Kuwano Y, Zhan M, White EJ, Martindale JL, Lal A, Gorospe M (2009) Identification of a signature motif in target mRNAs of RNA-binding protein AUF1. Nucleic Acids Res 37:204-14

Mazan-Mamczarz K, Lal A, Martindale JL, Kawai T, Gorospe M (2006) Translational repression by RNA-binding protein TIAR. Mol Cell Biol 26:2716-27

Meng Z, King PH, Nabors LB, Jackson NL, Chen CY, Emanuel PD, Blume SW (2005) The ELAV RNA-stability factor HuR binds the 5'-untranslated region of the human IGF-IR transcript and differentially represses cap-dependent and IRES-mediated translation. Nucleic Acids Res 33:2962-79

Park S, Myszka DG, Yu M, Littler SJ, Laird-Offringa IA (2000) HuD RNA recognition motifs play distinct roles in the formation of a stable complex with AU-rich RNA. Mol Cell Biol 20:4765-72

Park-Lee S, Kim S, Laird-Offringa IA (2003) Characterization of the interaction between neuronal RNA-binding protein HuD and AU-rich RNA. J Biol Chem 278:39801-8

Phillips K, Kedersha N, Shen L, Blackshear PJ, Anderson P (2004) Arthritis suppressor genes TIA-1 and TTP dampen the expression of tumor necrosis factor alpha, cyclooxygenase 2, and inflammatory arthritis. Proc Natl Acad Sci U S A 101:2011-6

Piecyk M, Wax S, Beck AR, Kedersha N, Gupta M, Maritim B, Chen S, Gueydan C, Kruys V, Streuli M, Anderson P (2000) TIA-1 is a translational silencer that selectively regulates the expression of TNF-alpha. Embo J 19:4154-63

Prusiner SB (1989) Creutzfeldt-Jakob disease and scrapie prions. Alzheimer Dis Assoc Disord 3:52-78

Rivas-Aravena A, Ramdohr P, Vallejos M, Valiente-Echeverria F, Dormoy-Raclet V, Rodriguez F, Pino K, Holzmann C, Huidobro-Toro JP, Gallouzi IE, Lopez-Lastra M (2009) The Elav-like protein HuR exerts translational control of viral internal ribosome entry sites. Virology 392:178-85

Ross J (1995) mRNA stability in mammalian cells. Microbiol Rev 59:423-50

Shukla S, Dirksen WP, Joyce KM, Le Guiner-Blanvillain C, Breathnach R, Fisher SA (2004) TIA proteins are necessary but not sufficient for the tissue-specific splicing of the myosin phosphatase targeting subunit 1. J Biol Chem 279:13668-76

Suswam EA, Li YY, Mahtani H, King PH (2005) Novel DNA-binding properties of the RNA-binding protein TIAR. Nucleic Acids Res 33:4507-18

Tian Q, Streuli M, Saito H, Schlossman SF, Anderson P (1991) A polyadenylate binding protein localized to the granules of cytolytic lymphocytes induces DNA fragmentation in target cells. Cell 67:629-39

Wang X, Tanaka Hall TM (2001) Structural basis for recognition of AU-rich element RNA by the HuD protein. Nat Struct Biol 8:141-5

Wilkie GS, Dickson KS, Gray NK (2003) Regulation of mRNA translation by 5'- and 3'-UTR-binding factors. Trends Biochem Sci 28:182-8

Zhang W, Wagner BJ, Ehrenman K, Schaefer AW, DeMaria CT, Crater D, DeHaven K, Long L, Brewer G (1993) Purification, characterization, and cDNA cloning of an AU-rich element RNA-binding protein, AUF1. Mol Cell Biol 13:7652-65

Zhu H, Hasman RA, Young KM, Kedersha NL, Lou H (2003) U1 snRNP-dependent function of TIAR in the regulation of alternative RNA processing of the human calcitonin/CGRP pre-mRNA. Mol Cell Biol 23:5959-71